

NASA CR - 65837

Martin-CR-66-44 Copy No.

# LIGHTWEIGHT PRESSURIZATION SYSTEM FOR THE APOLLO SERVICE PROPULSION SYSTEM CONTRACT NAS9-3521

FINAL REPORT

JANUARY 1967

LIBRARY COPY

JAN 19 1967

MANNED SPACECRAFT CENTER  
HOUSTON, TEXAS

MARTIN COMPANY  
A DIVISION OF MARTIN MARIETTA CORPORATION  
Denver, Colorado

N68-11585

(ACCESSION NUMBER)

(THRU)

(PAGES)

NASA CR-65837

(NASA CR OR TMX OR AD NUMBER)

(PAGE)

(CATEGORY)

Martin-CR-66-44

LIGHTWEIGHT PRESSURIZATION SYSTEM  
FOR THE APOLLO SERVICE PROPULSION SYSTEM

Contract NAS9-3521

FINAL REPORT

January 1967

Prepared by

D. N. Gorman  
G. R. Page

Approved



C. D. Brown  
Program Manager

MARTIN COMPANY  
A DIVISION OF MARTIN MARIETTA CORPORATION  
Denver, Colorado

FOREWORD

This document is submitted in accordance with Article X, subparagraph D, of Contract NAS9-3521, dated 14 October 1964. The contract was performed under the cognizance of the National Aeronautics and Space Administration, Manned Spacecraft Center, Houston, Texas. The NASA Technical Representative was Mr. Zach D. Kirkland. The Martin Program Manager and Project Engineer are Mr. Charles D. Brown and Mr. David N. Gorman, respectively.

Other Martin Company personnel who contributed significantly to the technical execution of this contract are:

H. F. Brady	H. K. Merrill
R. A. Holtz	J. D. Montgomery
J. B. Keough	G. R. Page
B. K. Larkin	O. L. Scott
S. C. Lukens	J. A. Woytassek
J. S. Marino	

CONTENTS

	<u>Page</u>
Foreword . . . . .	ii
Contents . . . . .	iii
Summary . . . . .	xv
Symbols . . . . .	xvii and xviii
I. Introduction . . . . .	I-1 and I-2
II. Program Plan . . . . .	II-1
A. Phase I - Design and Analysis . . . . .	II-1
1. Survey of Pressurization Concepts and Related Systems . . . . .	II-1
2. Preliminary Study of Pressurization Systems . . . . .	II-1
3. Comparison of Candidate Pressurization Systems . . . . .	II-2
4. Detailed Design, Analysis, and Evalua- tion of Pressurization Systems Selected for Concentrated Study . . . . .	II-2
B. Phase II - Feasibility Demonstration . . . . .	II-2
1. Test Program . . . . .	II-3
2. Extended Mission Studies . . . . .	II-4
C. Lunar Excursion Module Pressurization Sys- tem Studies . . . . .	II-4
1. Analysis of Cascade Pressurization System for the Lunar Excursion Module Ascent and Descent Propulsion Systems. . . . .	II-4
2. Analysis of the Lunar Excursion Module Descent Propulsion Helium Storage Sub- system . . . . .	II-5 and II-6

III.	Phase I Results . . . . .	III-1
	A. Preliminary Study and Comparison of Sys- tem Concepts . . . . .	III-1
	1. Description of Candidate Systems . . . . .	III-1
	2. Preliminary Study and Analysis of Candidate Systems . . . . .	III-4
	3. Comparison of Candidate Pressurization Systems . . . . .	III-10
	B. Detailed Investigation of Selected Systems . . . . .	III-14
	1. Additional Study and Refinement of System Concepts . . . . .	III-15
	2. Finalized System Concepts . . . . .	III-18
	3. Problem Area Investigation . . . . .	III-19
	C. Selection of Recommended System . . . . .	III-28
	1. Criteria for Pressurization System Selection and Optimization . . . . .	III-28
	2. Comparison of the Three Candidate Systems . . . . .	III-29
	3. Selection of the Optimum Pressuriza- tion System . . . . .	III-36
IV.	Phase II Results . . . . .	IV-1
	A. Cascade System Loading Tests, Heat Ex- changer Tests, and Feasibility Demonstra- tion . . . . .	IV-1
	1. Test System . . . . .	IV-1
	2. Test Procedures . . . . .	IV-5
	3. Analysis and Evaluation of Results . . . . .	IV-10
	B. Cascade Pressurization System Primary Tank Support Structure and Tubing Heat Leak In- vestigation . . . . .	IV-41
	1. Test System . . . . .	IV-41
	2. Test Procedure . . . . .	IV-42
	3. Analysis and Evaluation of Results . . . . .	IV-43

C.	Apollo Service Propulsion System Cascade Pressurization System Extended in Mission Studies . . . . .	IV-49
1.	34-Day Mission . . . . .	IV-50
2.	90-Day Mission . . . . .	IV-51
3.	Optimum System for Extended Missions . . . . .	IV-52 and IV-53
V.	Advanced Lightweight Pressurization System Design Summary . . . . .	V-1 and V-2
VI.	Conclusions and Recommendations for Future Investigation . . . . .	VI-1
A.	Conclusions . . . . .	VI-1
1.	Optimum Pressurization System . . . . .	VI-1
2.	Weight Saving . . . . .	VI-1
3.	Pressurant Loading . . . . .	VI-1
4.	Cascade System Feasibility . . . . .	VI-1
5.	Extended Mission Capability . . . . .	VI-1
6.	Propellant Feedline Heat Exchanger . . . . .	VI-2
7.	Cascade System Size and Weight Predictions . . . . .	VI-2
B.	Recommendations for Future Investigation . . . . .	VI-2 and VI-3
	Appendix - Tables and Figures . . . . .	A-1
A.	Tables . . . . .	A-1 thru A-18
B.	Figures . . . . .	A-23 thru A-179

Table

1	Advanced Lightweight Pressurization System Design Mission Data . . . . .	A-1
2	Mission Duty Cycle for 34-Day Lunar Polar Orbit . . . . .	A-2
3	Mission Duty Cycle for 90-Day Earth Polar Orbit . . . . .	A-2
4	Merit Rating Summary . . . . .	A-3
5	Candidate System Ranking Based upon Prelimin- ary Analysis and Evaluation . . . . .	A-4
6	Analytical and Test Results Helium/Fuel Heat Exchanger . . . . .	A-5
7	Analytical and Test Results C. G. Products/ Fuel Heat Exchanger . . . . .	A-6
8	Potential Weight Reduction of the ALPS Candi- date Systems . . . . .	A-7
9	Results of System Reliability Studies . . . . .	A-7
10	Estimated Flight Qualified Component Costs . . . . .	A-8
11	Results of Helium Loading and Ten-Hour Hold Analysis Insulation Thickness = 2.0 Inches Helium Loading Temperature = 530°R . . . . .	A-9
12	Results of the Analytical Simulation for Stor- age Time up to Thirty Days . . . . .	A-10
13	System Comparison Summary . . . . .	A-11
14	List of Instrumentation - Cascade Gas Storage System . . . . .	A-13
15	Instrumentation List - Heat Exchanger System . . . . .	A-14
16	Measured System Chill-Down Time . . . . .	A-15
17	Helium Loading Results . . . . .	A-15
18	Liquid Hydrogen Consumption Cascade Feasibility Demonstration Tests . . . . .	A-16
19	Helium Loading Accuracies . . . . .	A-17
20	Nine-Day Mission Post-Test Analysis Burn Duration and Helium Mass Flow Rates . . . . .	A-18
21	Nine-Day Mission Abort Helium Usage & Residuals . . . . .	A-19

22	90 Day Mission Abort Helium Usage & Residuals . . . . .	A-19
23	Nine-Day Mission Helium Usage and Residuals . . . . .	A-19
24	Instrumentation List - Support Model Heat Leak Investigation . . . . .	A-20
25	System Design Parameters . . . . .	A-21
26	System Weight Statement . . . . .	A-22

Figure

1	System Number 0 and 1 . . . . .	A-23
2	System Number 1A . . . . .	A-24
3	System Number 2 . . . . .	A-25
4	System Number 4 . . . . .	A-26
5	System Number 5 . . . . .	A-27
6	System Number 7 . . . . .	A-28
7	System Number 8 . . . . .	A-29
8	ALPS Pressurant Usage Study . . . . .	A-30
9	ALPS Pressurant Usage Study . . . . .	A-31
10	ALPS Pressurant Usage Study . . . . .	A-32
11	Maximum Propellant Tank Pressure vs Pressurant Temperature Adiabatic Tank Walls . . . . .	A-33
12	System Weights for System 1 . . . . .	A-34
13	System Weights for System 1A . . . . .	A-35
14	System Weights for System 2 . . . . .	A-36
15	System Weights for System 4 . . . . .	A-37
16	System Weights for System 5 . . . . .	A-38
17	System Weights for System 8 . . . . .	A-39
18	Candidate System Weight Comparison . . . . .	A-40
19	System Weights for System 5 . . . . .	A-41
20	Pressurant Usage for System 8, Fuel Tank . . . . .	A-42
21	System 1 . . . . .	A-43
22	System 5 . . . . .	A-44
23	System 8 . . . . .	A-45

24	Helium Storage Test Schematic . . . . .	A-46
25a	Test and Calculated Data, Helium Storage Test 5 . . . . .	A-47
25b	Test and Calculated Data, Helium Storage Test 5 . . . . .	A-48
26	Test and Calculated Data, Helium Storage Test 5 . . . . .	A-49
27a	Test and Calculated Data, Helium Storage Test 6 . . . . .	A-50
27b	Test and Calculated Data, Helium Storage Test 6 . . . . .	A-51
28	Test and Calculated Data, Helium Storage Test 6 . . . . .	A-52
29	Feed Line Heat Exchanger . . . . .	A-53
30	Solenoid Valve Test System . . . . .	A-54
31	Feed Line Gas Cooler Test Schematic . . . . .	A-55
31a	Reactor RB2-100 Envelope . . . . .	A-56
32	System Weight for System 1 . . . . .	A-56a
33	System Weights for System 5 . . . . .	A-57
34	System Weights for System 8 . . . . .	A-58
35	Candidate System Weight Comparison . . . . .	A-59
36	Limit Operating Pressure vs Temperature . . . . .	A-60
37	Cascade Feasibility and Heat Exchanger Test Setup . . . . .	A-61
38	Cascade Feasibility and Heat Exchanger Test . . . . .	A-62
39	Primary Tank Pressure Vessel . . . . .	A-64
40	Primary Tank Pressure Vessel with LH <sub>2</sub> Jacket Hemisphere . . . . .	A-65
41	Completed Primary Tank Assembly . . . . .	A-66
42	Primary Storage Container Temperature Instru- mentation Locations . . . . .	A-67
43	Water Flow Loop with Propellant Feedline Heat Exchangers . . . . .	A-68
44	Feed Line Heat Exchanger . . . . .	A-69
45	Feed Line Heat Exchanger Photograph. . . . .	A-70

46	Cascade Feasibility Demonstration Helium Loading Pre-test Analysis $\text{LH}_2$ Boil-Off vs Loading Rate . . . . .	A-71
47	Cascade Feasibility Demonstration Helium Loading Pre-Test Analysis Loading Time vs Loading Rate . . . . .	A-72
48	Cascade Feasibility Demonstration Helium Loading Pre-test Analysis Maximum Helium Temperature vs Loading Rate . . . . .	A-73
49	Cascade Feasibility Demonstration Initial Operating Conditions for the Primary Sphere . . .	A-74
50	Cascade Feasibility Demonstration Heat Exchanger Performance Pre-test Analysis. . . .	A-75
51	Cascade Feasibility Demonstration Heat Exchanger Performance Pre-test Analysis . . .	A-76
52	Cascade Feasibility Demonstration Pre-test Analysis Heat Exchanger Performance . . . . .	A-77
53a	High-Pressure Heat Exchanger Posttest Analysis, Nine-Day Mission Abort, Run 1 . . . . .	A-78
53b	High-Pressure Heat Exchanger Posttest Analysis, Nine-Day Mission Abort, Run 1 . . . . .	A-79
54a	Low-Pressure Heat Exchanger Posttest Analysis, Nine-Day Mission Abort, Test Run 1 . . . . .	A-80
54b	Low-Pressure Heat Exchanger Posttest Analysis, Nine-Day Mission Abort, Test Run 1 . . . . .	A-81
55a	High-Pressure Heat Exchanger Posttest Analysis, Nine-Day Mission Abort, Test Run 2 . . .	A-82
55b	High-Pressure Heat Exchanger Posttest Analysis, Nine-Day Mission Abort, Test Run 2 . . .	A-83
56a	Low-Pressure Heat Exchanger Posttest Analysis, Nine-Day Mission Abort, Test Run 2 . . . . .	A-84
56b	Low-Pressure Heat Exchanger Posttest Analysis, Nine-Day Mission Abort, Test Run 2 . . . . .	A-85
57a	High-Pressure Heat Exchanger Posttest Analysis, 90-Day Mission Abort, Test Run 2 . . . .	A-86
57b	High-Pressure Heat Exchanger Posttest Analysis, 90-Day Mission Abort, Test Run 2 . . . .	A-87

58a	Low-Pressure Heat Exchanger Posttest Analysis, 90-Day Mission Abort, Test Run 2 . . . . .	A-88
58b	Low-Pressure Heat Exchanger Posttest Analysis, 90-Day Mission Abort, Test Run 2 . . . . .	A-89
59	Low-Pressure Heat Exchanger Pressure Drop - Water Side . . . . .	A-90
60a	Primary Storage Container Pretest Analysis, Nine-Day Mission Abort . . . . .	A-91
60b	Primary Storage Container Pretest Analysis, Nine-Day Mission Abort . . . . .	A-92
61a	Cascade Storage Container Pretest Analysis, Nine-Day Mission Abort . . . . .	A-93
61b	Cascade Storage Container Pretest Analysis, Nine-Day Mission Abort . . . . .	A-94
62a	Primary Storage Container Posttest Analysis, Nine-Day Mission Abort, Test Run 1 . . . . .	A-95
62b	Primary Storage Container Posttest Analysis, Nine-Day Mission Abort, Test Run 1 . . . . .	A-96
63a	Cascade Storage Container Posttest Analysis, Nine-Day Mission Abort, Test Run 1 . . . . .	A-97
63b	Cascade Storage Container Posttest Analysis, Nine-Day Mission Abort, Test Run 1 . . . . .	A-98
64a	Primary Storage Container Posttest Analysis, Nine-Day Mission . . . . .	A-99
64b	Primary Storage Container Posttest Analysis, Nine-Day Mission Abort, Test Run 2 . . . . .	A-100
65a	Cascade Storage Container Posttest Analysis, Nine-Day Mission Abort, Test Run 2 . . . . .	A-101
65b	Cascade Storage Container Posttest Analysis, Nine-Day Mission Abort, Test Run 2 . . . . .	A-102
66a	Primary Storage Container Pretest Analysis, 90-Day Mission Abort . . . . .	A-103
66b	Primary Storage Container Pretest Analysis, 90-Day Mission Abort . . . . .	A-104
67a	Cascade Storage Container Pretest Analysis, 90-Day Mission Abort . . . . .	A-105
67b	Cascade Storage Container Pretest Analysis, 90-Day Mission Abort . . . . .	A-106

68a	Primary Storage Container Posttest Analysis, 90-Day Mission Abort, Test Run 1 . . . . .	A-107
68b	Primary Storage Container Posttest Analysis, 90-Day Mission Abort, Test Run 1 . . . . .	A-108
68c	Primary Storage Container Posttest Analysis, 90-Day Mission Abort, Test Run 1 . . . . .	A-109
69a	Cascade Storage Container Posttest Analysis, 90-Day Mission Abort, Test Run 1 . . . . .	A-110
69b	Cascade Storage Container Posttest Analysis, 90-Day Mission Abort, Test Run 1 . . . . .	A-111
70a	Primary Storage Container Posttest Analysis, 90-Day Mission Abort, Test Run 2 . . . . .	A-112
70b	Primary Storage Container Posttest Analysis, 90-Day Mission Abort, Test Run 2 . . . . .	A-113
70c	Primary Storage Container Posttest Analysis, 90-Day Mission Abort, Test Run 2 . . . . .	A-114
71a	Cascade Storage Container Posttest Analysis, 90-Day Mission Abort, Test Run 2 . . . . .	A-115
71b	Cascade Storage Container Posttest Analysis, 90-Day Mission Abort, Test Run 2 . . . . .	A-116
72a	Primary Storage Container Pretest Analysis, Nine-Day Mission . . . . .	A-117
72b	Primary Storage Container Pretest Analysis, Nine-Day Mission . . . . .	A-118
73a	Primary Storage Container Pretest Analysis, Nine-Day Mission, Fourth Burn . . . . .	A-119
73b	Primary Storage Container Pretest Analysis, Nine-Day Mission, Fourth Burn . . . . .	A-120
74a	Primary Storage Container Pretest Analysis, Nine-Day Mission, Seventh Burn . . . . .	A-121
74b	Primary Storage Container Pretest Analysis, Nine-Day Mission, Seventh Burn . . . . .	A-122
75a	Cascade Storage Container Pretest Analysis, Nine-Day Mission . . . . .	A-123
75b	Cascade Storage Container Pretest Analysis, Nine-Day Mission . . . . .	A-124
75c	Cascade Storage Container Pretest Analysis, Nine-Day Mission . . . . .	A-125

76a	Cascade Storage Container Pretest Analysis, Nine-Day Mission, Fourth Burn . . . . .	A-126
76b	Cascade Storage Container Pretest Analysis, Nine-Day Mission, Fourth Burn . . . . .	A-127
77a	Cascade Storage Container Pretest Analysis, Nine-Day Mission, Seventh Burn . . . . .	A-128
77b	Cascade Storage Container Pretest Analysis, Nine-Day Mission, Seventh Burn . . . . .	A-129
78a	Primary Container Posttest Analysis, Nine-Day Mission, Test Run 1 . . . . .	A-130
78b	Primary Container Posttest Analysis, Nine-Day Mission, Test Run 1 . . . . .	A-131
78c	Primary Container Posttest Analysis, Nine-Day Mission, Test Run 1 . . . . .	A-132
79a	Primary Container Posttest Analysis, Nine-Day Mission, Test Run 1, Burn 4 . . . . .	A-133
79b	Primary Container Posttest Analysis, Nine-Day Mission, Test Run 1, Burn 4 . . . . .	A-134
80a	Primary Container Posttest Analysis, Nine-Day Mission, Test Run 1, Burn 7 . . . . .	A-135
80b	Primary Container Posttest Analysis, Nine-Day Mission, Test Run 1, Burn 7 . . . . .	A-136
81a	Cascade Container Posttest Analysis, Nine-Day Mission, Test Run 1 . . . . .	A-137
81b	Cascade Container Posttest Analysis, Nine-Day Mission, Test Run 1 . . . . .	A-138
81c	Cascade Container Posttest Analysis, Nine-Day Mission, Test Run 1 . . . . .	A-139
82a	Cascade Container Posttest Analysis, Nine-Day Mission, Test Run 1, Burn 4 . . . . .	A-140
82b	Cascade Container Posttest Analysis, Nine-Day Mission, Test Run 1, Burn 4 . . . . .	A-141
83a	Cascade Container Posttest Analysis, Nine-Day Mission, Test Run 1, Burn 7 . . . . .	A-142
83b	Cascade Container Posttest Analysis, Nine-Day Mission, Test Run 1, Burn 7 . . . . .	A-143
84a	Primary Container Posttest Analysis, Nine-Day Mission, Test Run 2 . . . . .	A-144

84b	Primary Container Posttest Analysis, Nine-Day Mission, Test Run 2 . . . . .	A-145
84c	Primary Container Posttest Analysis, Nine-Day Mission, Test Run 2 . . . . .	A-146
85a	Primary Container Posttest Analysis, Nine-Day Mission, Test Run 2, Burn 4 . . . . .	A-147
85b	Primary Container Posttest Analysis, Nine-Day Mission, Test Run 2, Burn 4 . . . . .	A-148
86a	Primary Container Posttest Analysis, Nine-Day Mission, Test Run 2, Burn 7 . . . . .	A-149
86b	Primary Container Posttest Analysis, Nine-Day Mission, Test Run 2, Burn 7 . . . . .	A-150
87a	Cascade Container Posttest Analysis, Nine-Day Mission, Test Run 2 . . . . .	A-151
87b	Cascade Container Posttest Analysis, Nine-Day Mission, Test Run 2 . . . . .	A-152
87c	Cascade Container Posttest Analysis, Nine-Day Mission, Test Run 2 . . . . .	A-153
88a	Cascade Container Posttest Analysis, Nine-Day Mission, Test Run 2, Burn 4 . . . . .	A-154
88b	Cascade Container Posttest Analysis, Nine-Day Mission, Test Run 2, Burn 4 . . . . .	A-155
89a	Cascade Container Posttest Analysis, Nine-Day Mission, Test Run 2, Burn 7 . . . . .	A-156
89b	Cascade Container Posttest Analysis, Nine-Day Mission, Test Run 2, Burn 7 . . . . .	A-157
90	Support Heat Leak Test Item . . . . .	A-158
91	Primary Tank Support Structure Heat Leak Test Fixture . . . . .	A-159
92	Primary Tank Support Structure Heat Leak Test Setup . . . . .	A-161
93	Support Structure Test Model . . . . .	A-162
94	Support Structure Attachment Boss . . . . .	A-163
95	Support Structure Anchor Points . . . . .	A-164
96	Support Structure Insulation . . . . .	A-165
97	Support Structure Model Ready for Installation . . . . .	A-166

98	Primary Tank Support Structure - Assembly Details . . . . .	A-167
99	Primary Support Model Heat Leak Rate Investi- gation, Thermocouple Locations . . . . .	A-168
100	Support Heat Leak Test Model after Removal of Supports and Dummy Tubes . . . . .	A-169
101	Primary Tank Support Structure Heat Leak Test Results . . . . .	A-170
102	Extended Mission - 34-Day Initial Maximum Heat Leak with Primary Tank Same as for 9 Day Mission . . . . .	A-171
103	Extended Mission - 34-Day Possible Insulation Variation for Systems with Sphere Same as 9 Day Mission No Liquid Hydrogen Carried in Jacket . . . . .	A-172
104	Extended Mission - 34 Day Possible Insulation Variation in Heat Leak for Systems with Sphere Same as 9 Day Mission Liquid Hydrogen Carried in Jacket . . . . .	A-173
105	Extended Mission - 34-Day Cascade Usage with Liquid Hydrogen Carried in the Jacket . . . . .	A-174
106	Extended Mission - 34-Day Increase in Total System Weight Liquid Hydrogen carried in Jacket. No Increase in Primary Tank Wall . . . . .	A-175
107	Extended Mission - 34-Day Increase in Total System Weight to Allow an Insulation Degrada- tion Factor of Ten No Liquid Hydrogen Carried in the Jacket Primary Tank Wall Increased . . . . .	A-176
108	Extended Mission - 34-Day Increase in Hard- ware Weight to Allow an Insulation Degradation Factor of Ten No Liquid Hydrogen Carried in the Jacket Primary Tank Wall Increased . . . . .	A-177
109	Extended Mission - 90-Day Possible Insulation Variation for System with Pressure Sphere Same as 9 Day Mission . . . . .	A-178
110	Primary Helium Tank Design . . . . .	A-179

### SUMMARY

The work reported herein was executed in two phases. Phase I entailed analytical and experimental investigation of several pressurization system concepts, which led to the selection of a system recommended for use in the Apollo service propulsion system (SPS). The major objective of Phase II was demonstration of the operating feasibility of the recommended system concept.

The initial task in Phase I was a survey of existing and envisioned pressurization system design concepts, of which seven were selected for preliminary analysis and study. Subsequently three of the seven concepts were subjected to more detailed analytical and experimental investigation. The systems studied in depth were (1) cryogenically stored helium, (2) cryogenically stored helium cascade, and (3) cryogenically stored helium combined with a hot-gas generator. Parametric analyses performed on these systems determined weight, reliability, and performance characteristics. Experimental investigations were conducted to determine pertinent operating characteristics of certain subsystems and components used in the three systems. Tests were run on a hydrazine catalytic gas generator, a coiled tube propellant feedline heat exchanger, and a helium solenoid valve.

The work of Phase I established the necessity of storing helium cryogenically to achieve significant weight reduction in the Apollo SPS pressurization system. Of the three final system candidates, the cryogenic helium cascade system was recommended as the optimum pressurization system for the Apollo SPS.

The system concept recommended at the conclusion of Phase I was subjected to test during Phase II, to demonstrate system feasibility. The feasibility test system consisted of a nonoptimized primary (cryogenic) helium storage tank assembly; a cascade (ambient) helium storage tank; propellant feedline heat exchangers (of the Apollo SPS type); and the necessary plumbing, valves, and regulation devices to simulate the Apollo SPS helium flow requirements. Actual Apollo mission duty cycles were simulated, and the results were compared with analytically derived performance data. Cascade system test results were in general better than predictions of the analytical model. However, it was determined that the present Apollo propellant feedline heat exchangers are not suitable for use at liquid hydrogen/helium temperatures because of a problem of propellant freezing.

SYMBOLS

- $A$  = cross sectional area of each support or line (sq ft)  
 $(C_p)_\ell$  = liquid specific heat capacity at constant pressure (joules/  
g $^{\circ}$ K)  
 $h_{Nuc}$  = nucleate pool boiling heat transfer coefficient (watts/cm $^2$  $^{\circ}$ K)  
 $k$  = thermal conductivity of support or line material (Btu/hr-ft- $^{\circ}$ R)  
 $k_a$  = apparent insulation thermal conductivity (Btu/hr-ft- $^{\circ}$ R)  
 $k_\ell$  = liquid thermal conductivity (watts/cm $^{\circ}$ K)  
 $\ell$  = length  
 $P$  = pressure of the boiling system (dynes/cm $^2$ )  
 $\dot{q}$  = heat leak rate through each support or line (Btu/hr)  
 $\dot{q}_I$  = heat transfer rate  
 $\dot{q}_{Tc}$  = calculated total heat transfer through all supports and  
lines (Btu/hr)  
 $\dot{q}_{Ti}$  = indicated total heat transfer through all the supports and  
lines (Btu/hr)  
 $\dot{q}_{Uc}$  = calculated heat transfer through the upper supports and  
lines (Btu/hr)  
 $\dot{q}_{Ui}$  = indicated heat transfer through the upper supports and  
lines (Btu/hr)  
 $r_{Co}$  = outside radius of the LH $_2$  container (ft)  
 $r_{Ii}$  = insulation inside radius (ft)  
 $r_{Io}$  = insulation outside radius (ft)

- $t_I$  = insulation thickness (ft)
- $\Delta T$  = temperature difference
- $\lambda$  = latent heat of evaporation at saturation (joules/g)
- $\mu_\ell$  = Newtonian viscosity of the liquid (g/cm-sec)
- $\rho_\ell$  = liquid density (g/cm<sup>3</sup>)
- $\rho_v$  = vapor density (g/cm<sup>3</sup>)
- $\sigma$  = surface tension between the liquid and its own vapor, calculated at T (dynes/cm)

## I. INTRODUCTION

This report describes the work performed during Phase I and Phase II of Contract NAS9-3521, Pressurization System for Use in the Apollo Service Propulsion System. This contract was executed under the direction of the NASA Manned Spacecraft Center, Houston, Texas.

The primary purpose of this contract was to develop an advanced lightweight pressurization system (ALPS) concept for use in the Apollo service propulsion system (SPS). The application of this system is for pressurization of the main SPS propellant tanks. The contract defined three major requirements that the finalized ALPS concept must fulfill:

- 1) It must be compatible with the current Apollo SPS;
- 2) It must offer substantial weight savings over the pressurization system currently in use;
- 3) It must be at least as reliable as the system currently in use.

Phase I required design, analytical, and experimental efforts devoted to various candidate system concepts, and culminated in the selection of an ALPS recommendation for the Apollo SPS application. The initial effort in Phase I was a survey of existing pressurization systems and system concepts. From this survey, several candidate concepts were selected for preliminary study. The preliminary studies concluded with the selection of three of the candidate systems to be subjected to more detailed design, analysis, and investigation. The detailed study effort included both analytical and experimental work to assist in system design and the investigation of problem areas. The final result of Phase I was the selection of a single system (a cryogenic helium cascade system) for the Apollo SPS.

The major purpose of Phase II was to establish the feasibility of the ALPS concept recommended at the conclusion of Phase I. This was accomplished largely through the testing of a nonoptimized ground operating model of the recommended system. The feasibility tests included demonstrations of pressurant loading time and accuracy and pressurant storage and expansion operational concept. In addition, tests were run to determine performance of the present Apollo type of propellant feedline heat exchanger

in the system, and to demonstrate the thermal performance of the pressurant storage tank support structure. Pretest and posttest analyses were performed for the purpose of comparison and evaluation of the analytical models used in Phase I of this contract. Also, as a part of Phase II, analyses were performed to determine the extent of modifications necessary to the recommended pressurization system concept for the execution of certain Apollo extended missions.

## II. PROGRAM PLAN

The basic requirements for the execution of this contract were defined by the contract statement of work\*. Those requirements, together with a description of the technical approaches and constraints related to their fulfillment, constitute the program plan. Constraints refers to the Apollo SPS mission, propellant, compatibility, and configuration data pertinent to the analysis and design of the propellant tank pressurization system.

The Apollo mission specified for ALPS design is described in Table 1. Some of the more important pressurization system design criteria, related to the reference mission, are also presented in Table 1. Other aspects of the program plan are discussed herein.

### A. PHASE I - DESIGN AND ANALYSIS

Phase I consisted primarily of an analytical study that considered the parametric analysis of various pertinent pressurization system candidate concepts and phenomena, the detailed study and optimization of certain selected candidate systems, and experimental investigations related to potential problem areas associated with the candidate systems. The major tasks included in this effort are discussed in the following subsections.

#### 1. Survey of Pressurization Concepts and Related Systems

This task entailed a survey of propellant tank pressurization concepts and systems that might be applicable to future use with the current Apollo SPS. The investigation included concepts involving technical considerations beyond, as well as within, present state of the art. The major considerations of the system survey were potentiality of weight savings and compatibility with Apollo SPS requirements.

#### 2. Preliminary Study of Pressurization Systems

Subsequent to the completion of the pressurization system survey, the candidate systems were subjected to preliminary design and analysis. The purpose of this effort was to provide

---

\*Contract NAS9-3521, Exhibit A, Statement of Work, Exhibit B, Statement of Work Redefinition.

a basis for comparative evaluation of the candidate systems, so that the concepts showing the least potential could be omitted from more detailed investigation. The present Apollo SPS pressurization system was also subjected to the preliminary analysis to provide a baseline reference for the comparison. Primary emphasis was directed toward the development of system comparisons in terms of weight, reliability, and compatibility with Apollo vehicle and mission requirements.

### 3. Comparison of Candidate Pressurization Systems

All candidate systems investigated during the preliminary study effort discussed above were subjected to a comparison study for the purpose of selecting the three systems most suitable for use in the Apollo SPS. The technique used for this comparison required a weighted numerical evaluation of the candidate systems, related to the results of the preliminary study effort. The numerical evaluation procedure was based on a comparison of relative merits of each candidate system, as measured by weight, reliability, and compatibility.

### 4. Detailed Design, Analysis, and Evaluation of Pressurization Systems Selected for Concentrated Study

The three selected candidate systems were subjected to a detailed investigation to produce more specific definition of design, subsystems, components, and operational requirements. The analyses were broadened to include consideration of thermal environment. Experimental investigations involving subsystem and component feasibility testing were performed to support some of the analytical results. This task also included generation of installation drawings for each of the systems under consideration, development of criteria for system selection, and selection of the optimum system for continued development in Phase II.

## B. PHASE II - FEASIBILITY DEMONSTRATION

The major purpose of Phase II was to demonstrate, by testing, the inherent feasibility of the ALPS concept recommended for the Apollo SPS at the conclusion of Phase I. Also included in Phase II were analyses of extended mission capabilities of the recommended system.

### 1. Test Program

The feasibility test program consisted of the following demonstrations.

- a. Loading - The time required to load the recommended pressurization system storage container was demonstrated. This time included system chill-down time as well as helium loading time. Also, the quantity of liquid hydrogen used for cooling was ascertained. Analytical predictions were performed to determine loading accuracy and the accuracy of analytical models used to establish the recommended loading procedure.
- b. Heat Exchanger Performance - Demonstration of the propellant feedline heat exchanger performance was accomplished in conjunction with system concept feasibility testing. Pressure drop and thermal characteristics of the heat exchangers were measured and compared with analytical data. Also, the susceptibility of freezing of the heat exchangers was determined. Demineralized water was used to simulate the propellant in these tests.
- c. Pressurant Storage and Expansion Concept - The feasibility of the storage and expansion concept recommended in Phase I of this contract was demonstrated using the following simulated mission duty cycles:

The nominal nine-day mission;

The nine-day mission abort operation (continuous 590-sec burn);

The 90-day mission abort operation (continuous 590-sec burn with full LH<sub>2</sub> jacket).

A nonoptimized, ground test model of the selected system concept was used in this demonstration. Coast period simulation was based on integrated primary tank heat leak for the model system being equal to integrated heat leak for the recommended optimum system. The engine burn periods were simulated on a real-time average flow rate basis. An objective of this demonstration was that the primary tank heat leak be less than 50 Btu/hr.

Pretest and posttest analyses were performed to establish the accuracy of the mathematical models in determining pressurant usage, pressurant residuals, pressure and temperature histories

of the pressurizing gas, and temperature history of the pressurant storage tank.

d. Support Structure Heat Leak Investigation - Tests were performed to determine the heat leak contribution of the various conduction paths into the primary helium tank. The test model used was a full-scale model of the upper support tripod and tubing arrangement used in the recommended system design. The lower support and tubing geometry is of similar design, so testing of the complete system was deemed unnecessary. The test model was constructed of the design material and included the necessary bosses and flanges required for the suspension system. A liquid hydrogen reservoir was located at the tank end of the model, and the opposite ends of the structure and tubing were maintained at ambient temperature. The entire test system was evacuated to below  $10^{-4}$  mm Hg.

## 2. Extended Mission Studies

The pressurization system recommended in Phase I was analyzed to determine modifications required to perform the following extended missions:

- 1) 34-day lunar polar orbit;
- 2) 90-day earth polar orbit.

The duty cycles for these missions are shown in Tables 2 and 3. These studies resulted in determination of the optimum system that would accomplish the above missions and the nominal nine-day design mission.

## C. LUNAR EXCURSION MODULE PRESSURIZATION SYSTEM STUDIES

This work was performed in concurrence with, but not as a part of, Phase II. The work plan is described below; however, the results of this work are presented in a separate final report.\*

### 1. Analysis of Cascade Pressurization System for the Lunar Excursion Module Ascent and Descent Propulsion Systems

The cascade pressurization concept as determined from Phase I was optimized for the propulsion requirements of the lunar

---

\*Lunar Excursion Module Pressurization System Studies, Final Report. Martin-CR-66-42. Martin Company, Denver, Colorado, June 1966.

excursion module (LEM) ascent and descent stages. This task was entirely analytical; neither detailed design drawings nor test data substantiation were required. A functional schematic diagram of each system was produced.

The ascent stage was designed for one mission duty cycle, and the descent stage was designed to accomplish three mission duty cycles. The four mission duty cycles used are as defined in Contract NAS9-3521.\*

The initial effort in this task was determination of propellant tank helium requirements for each stage and each mission. Prelaunch pressurizing gas was considered to be provided from a ground storage system; the cascade pressurization system was designed to supply only the pressurant required by the propellant tanks after launch.

Parametric analyses, varying primary container initial pressure and temperature, were then performed for each system and mission. These analyses included evaluations of primary storage container, cascade storage container, and propellant feedline heat exchanger operating characteristics. Cascade tank operating pressure and temperature were 4000 psia and ambient, respectively. Results of the parametric analyses were used to determine the optimum weight designs for the ascent and descent stage cascade systems.

## 2. Analysis of the Lunar Excursion Module Descent Propulsion Helium Storage Subsystem

The existing descent propulsion pressurization system was analyzed to determine mass, sizing, and operating characteristics of the helium storage subsystem. This task was entirely analytical; neither detailed design drawings nor test data substantiation were required.

The analysis considered the three descent stage mission duty cycles defined in Contract NAS9-3521.\* System sizing and optimization were compatible with all three duty cycles.

---

\*Contract NAS9-3521, Exhibit C, Statement of Work Continuation.

Parametric studies were performed to determine the optimum initial helium pressure and temperature, and the optimum helium operating pressure and temperature at the time of the first engine ignition. The optimum conditions are defined as those resulting in minimum subsystem mass. The optimization process progressed in the following manner.

Analyses using the time at the first engine ignition were performed to optimize (for minimum weight) helium operating pressure and temperature, and internal heat exchanger length. This portion of the mission is very short and is insensitive to the small heating rates encountered. Therefore, optimization of these operating conditions was performed independently of thermal design studies.

The long standby part of the mission was then analyzed to determine the optimum initial helium pressure and temperature and superinsulation thickness. The analysis was constructed so that the conditions at the end of the standby period matched the optimum conditions as determined in the preceding paragraph.

### III. PHASE I RESULTS

#### A. PRELIMINARY STUDY AND COMPARISON OF SYSTEM CONCEPTS

The Phase I work was initiated with a survey of propellant tank pressurization concepts and systems that could be applicable to future use with the current Apollo SPS. The investigation included concepts involving technical considerations beyond present state of the art. The major criteria for inclusion of systems in the survey were their potential for weight savings and compatibility with Apollo SPS mission and vehicle requirements. The survey produced nine basic system concepts for consideration. Of the nine systems surveyed, seven were selected as ALPS candidates, to be subjected to preliminary study, design, analysis, and comparison.

The purpose of this effort was to provide a basis for comparative evaluation of the candidate systems, so the candidates showing the least potential could be omitted from more detailed investigation. The present Apollo SPS pressurization system was also subjected to the preliminary analysis, to provide a baseline reference for the comparison. This system is designated as system 0 in this report. All other systems are designated by the numbers used in the original survey effort. A brief description of each system is included in the following subsections.

##### 1. Description of Candidate Systems

- a. System 0, Ambient Stored Helium - The present Apollo SPS pressurization system is shown schematically in Fig. 1. Helium stored at high pressure and ambient temperatures expands through propellant feedline heat exchangers before entering the propellant tanks. Purpose of the heat exchangers is to nullify the cooling effect of helium expansion from the storage container. The ambient stored helium system is a highly reliable pressurization system, due to system simplicity and absence of extreme (high or low) operating temperatures. This also is a relatively inexpensive system to design, develop, fabricate, and maintain -- again as a result of simplicity in concept and environment. The significant disadvantages of this system are its size and weight. Ambient storage of helium requires a considerable volume in relation to the overall system envelope. The containment of a large gas volume at high pressure results in extremely heavy storage containers.

- b. System 1, Cryogenic Stored Helium - This system is schematically identical to 0 (see Fig. 1). The only difference is in the helium storage environment. In a vehicle where cryogenic storage is possible, a considerable reduction in weight can be realized by storing the pressurant cryogenically, then heating it prior to entry into the propellant tanks. The system shown uses the main propellants to heat helium to near ambient temperature. Thus, the helium storage density is high, affording a relatively small container, while the tank entering density is low. Another advantage of storing the high-pressure gas at lower than ambient temperature is the strength/temperature relationships of the usable aluminum and titanium alloys, which show a very significant increase in strength with decreasing temperature. Storage container weight can thus be reduced in two ways -- container volume reduction and container material strength increase. The increased material strength at lower temperatures was used in the preliminary studies described in the following Subsection 2. However, in the detailed design and analysis (Section B) all pressurant storage containers were stressed for ambient temperature (530°R) allowables.
- c. System 1A - System 1A, shown in Fig. 2, is similar to System 1, but uses hydrogen to pressurize the fuel tank. This approach could possibly result in some weight saving since hydrogen is half the density of helium. Hydrogen was not considered as an oxidizer tank pressurant due to the potential explosion hazard of a hydrogen/nitrogen tetroxide vapor mixture.
- d. System 2, Cryogenic Stored, Heated Residual Helium - A method of reducing helium storage volume, and therefore storage weight, of the system previously discussed is to heat the storage container residual gas as shown in Fig. 3. The philosophy illustrated by this technique is that although initial helium storage conditions of low temperature and high pressure are conducive to minimum system weight, a final gas state of high temperature and low pressure within the storage container has the effect of reducing the mass of unusable residual helium and therefore the mass of the initial helium load. As shown in the figure, a gas generator may be incorporated as a heat source. Since heating of the storage container in this way may be comparatively low level, it is anticipated that auxiliary propellant feedline heat exchangers should be used to increase helium temperature to ambient.

- e. System 4, Cryogenic Stored, Heated Residual, Heated Helium - This system (Fig. 4) combines the use of residual pressurant heating with active helium heating in the supply line. It combines the potential advantages of low pressurant mass requirement and minimum pressurant storage residual. The gas generators, used for heating, could also be combined into a single unit, depending on the relative hot gas flow requirements to each heat exchanger and the resulting control problems encountered.
- f. System 5, Cascade Helium Storage, Propellant Feedline Heating - The cascade storage system (Fig. 5), like System 2, was conceived in an effort to reduce helium residual mass and the associated primary storage container size. This is done by replacing the cold helium flowing out of the primary container with warmer, less dense helium from an ambient temperature secondary container. The warm and cold gases in the primary container are separated by a flexible membrane. The membrane was later deleted, as discussed in Section B, Subsection 1. The main pressurant is expanded through propellant feedline heat exchangers to bring the temperature up to near ambient. The weight saved in the primary storage container must be compared to the weight added by the secondary container to determine desirability of the cascade concept.
- g. System 7, Main Tank Injection, Ambient Stored Helium - The main tank injection (MTI) system, shown in Fig. 6, represents one of the most advanced methods used in propellant tank pressurization. MTI is the process of generating pressurant gas within the confines of a propellant tank by injecting into the tank a reagent that reacts hypergolically with the propellant. Pressure control is accomplished by controlling the rate of reagent injection. The reagent is stored as a liquid at a pressure only slightly above propellant tank pressure. A very small, high-pressure helium bottle can be used for reagent pressurization. The high-density, low-pressure liquid reagent storage system represents a small fraction of the weight and volume of a gaseous helium pressurant storage container. System response is very high, even after extended shutdown periods. Ullage gas temperatures are relatively high, and the combustion product molecular weights are near  $21 \text{ lb}_m/\text{lb-mole}$  for the A-50 tank and  $30 \text{ lb}_m/\text{lb-mole}$  for the  $\text{N}_2\text{O}_4$  tank.

- h. System 8, Cryogenic Stored, Heated Helium/Gas Generator Products - The unique feature of this system (Fig. 7) is that fuel-rich gas generator combustion products are used to pressurize the fuel tank after serving as a helium gas heat source. This provides a free source of pressurant for the fuel tank, thereby decreasing the total system helium usage. It is not practical to consider the fuel-rich gas generator products as a pressurant for the oxidizer tank because a gas generator using  $N_2O_4/A-50$  must be operated at a very low oxidizer/fuel mixture ratio for stability and temperature reasons, and the resulting combustion products are reactive with the  $N_2O_4$ . Gas generator combustion products, having a molecular weight of  $16 \text{ lb}_m/\text{lb-mole}$  from a gas generator mixture ratio of 0.085, are used for fuel tank pressurization in the Titan II ICBM, Gemini launch vehicle, and Titan III core vehicle.

## 2. Preliminary Study and Analysis of Candidate Systems

The purpose of this effort was to determine the relative size, weight, operational characteristics, and component requirements of each candidate system to establish a realistic comparison of the advantages and disadvantages of the various candidates. These preliminary studies were performed using a common set of criteria for the analysis of all systems. These criteria were established in a manner to ensure a most efficient method of attaining the desired comparison of the candidate systems. The preliminary study and analyses were performed in accordance with the following stipulations:

- 1) Thermal effects of the environment were neglected -- outer surfaces of pressurant and propellant storage tanks were adiabatic;
- 2) Subsystem sizing was established on the basis of nominal vehicle requirements only and did not provide for helium usage margin;
- 3) All analyses were based on the design mission profile defined in Table 1;
- 4) The mass of tubing, insulation, support structure, and miscellaneous fittings was omitted. The mass analysis considered pressurant, pressurant storage containers, valves, pressure switches, gas generators

(and propellants), and heat exchangers. The material considered for pressure vessels was titanium 6Al-4V (ELI for cryogenic containers) alloy. All valves and pressure switches were considered as series-parallel redundant.

The present Apollo pressurization system was also analyzed using the above ground rules. Rather than use the actual mass, reliability numbers, etc, the Apollo system was reanalyzed to reflect the same criteria and techniques used in analyzing the candidate systems. In this way all systems were compared in the proper perspective.

The preliminary mass analysis and optimization of the candidate systems included parametric studies of three major variables -- temperature of stored gas pressurant entering the propellant tanks, initial pressurant temperature, and initial pressurant storage pressure.

- a. Propellant Tank Pressurant Usage - Since the mass of helium required to pressurize the propellant tanks is a function only of the temperature of the helium entering the tanks and the conditions within the tanks, it was convenient to make this analysis for all helium systems at one time. The mass of hydrogen required for fuel tank pressurization in System 1A was also determined at this time. An IBM 7094 computer program\* was used to calculate the pressurant masses required for fuel and oxidizer tanks, for several pressurant entering temperatures. The results are plotted in Fig. 8, 9, and 10. These figures also illustrate the effect of pressurant entering temperature on total mass of propellants vaporized during the mission.

Considering the fuel tank requirements (Fig. 8 and 9), it is noted that inlet temperature has almost no effect on pressurant mass, particularly above 500°R. Also, the effect on vaporized fuel is negligible, due to the comparatively low vapor pressure of the  $N_2H_4$ /UDMH mixture at operating temperatures. The oxidizer tank pressurant curve (Fig. 10) also shows only a very slight decrease in pressurant mass at temperatures above 500°R. Oxidizer vapor

---

\*Pressurization System for Use in the Apollo Service Propulsion System - Computer Program Utilization Manual. Martin-CR-66-39. Martin Company, Denver, Colorado, July 1966.

mass is much more sensitive to temperature, but this factor is of minor importance when compared to total pressurization system mass. It was concluded that with a stored-gas system for the Apollo SPS, no advantage is accrued by heating the pressurant to a level significantly above the nominal propellant temperature. System weight reductions must be effected through changes in pressurant storage technique rather than by increasing the pressurant entering temperature.

In addition to pressurant mass requirements, another effect of pressurant entering temperature was noted during the preliminary analysis. This is the influence of pressurant temperature on propellant storage tank pressure. With the onset of each vehicle coast period, the bulk propellants, ullage gases, and propellant tank walls will tend to attain uniform thermal equilibrium. If, at the end of a burn period, the tank ullage temperature is above ambient, the subsequent cooling will cause a decrease in propellant tank pressure. If the ullage temperature is below ambient at the end of the burn period, tank pressure will rise as equilibrium takes place. Figure 11 shows maximum tank pressures as a function of pressurant entering temperature. The data shown in this figure were taken from computer runs that analyzed the propellant tank thermodynamic histories over the design mission. The maximum operating pressure for the Apollo SPS is about  $225 \text{ lb}_f/\text{in.}^2$  absolute;\* therefore, entering gas temperature less than about  $300^\circ\text{R}$  would cause propellant tank venting in the course of a normal mission.

System mass is relatively unaffected by pressurant entering temperature, as long as the entering temperature is above  $300^\circ\text{R}$ . Therefore, ambient entering gas temperature was selected to minimize propellant tank pressure excursions. For purposes of this preliminary study, ambient temperature was taken as  $530^\circ\text{R}$ . Propellant tank pressurant usage was therefore fixed at  $29.3 \text{ lb}_m$  and  $34.7 \text{ lb}_m$  of helium for fuel and oxidizer tanks, respectively, and  $14.8 \text{ lb}_m$  of hydrogen for the System 1A fuel tank.

---

\*Actual design maximum pressures are 232 psia for Block I and 218 psia for Block II.

- b. Pressurant Storage - Gas storage container weight was optimized from the standpoint of initial pressure and initial temperature.\* Initial storage pressures considered were 1000, 2000, 3000, and 4000  $\text{lb}_f/\text{in.}^2$  absolute. In all cases, the final and/or minimum storage pressure was fixed at 400  $\text{lb}_f/\text{in.}^2$  absolute. Initial helium storage temperatures investigated were 37, 140, 300, and 530°R. In the case of hydrogen storage, the temperatures considered were 70, 140, 300, and 530°R; the minimum temperature of 70°R was chosen to prevent the hydrogen from condensing in the storage container. Only spherical geometry was considered. Although the outer surface of the container was considered adiabatic, heat transfer between the sphere wall and the pressurant was considered. Also, the sphere wall and pressurant were forced to thermal equilibrium during each coast period.

A mathematical model was used to simulate the helium expansion process.† The program was originally written for helium gas, but was also suitable for hydrogen gas with a slight revision of the equation of state used. Also included in this program are the equations for calculating the storage container mass, based on particular material properties, safety factors, and required dimensions. The sphere mass thus derived does not include any allowance for structural land areas or bosses that may be required.

- c. Pressurant Storage with Internal Heat Exchanger - For this study, a free convection heat exchanger was used in the helium storage tank operating only during propellant burn times. It was taken to be a single straight finned tube. The heat was supplied by hot-gas products of a gas generator burning main tank propellants. A constant flow rate of hot gas at a given fixed inlet temperature was supplied to the heat exchanger.

The size and weight of this system were obtained from a numerical computation of the helium storage vessel thermodynamics through a mission time, as was done on the basic helium system. The major modification to existing computer programs was the inclusion of the calculation of the heat flux from the heat exchanger.

---

\*This discussion is pertinent to the analysis of all high-pressure gas storage containers in all systems, with the exception of the primary storage tank in System 5.

†Ibid.

- d. Primary Helium Storage for Cascade System - This type of helium storage concept is used in System 5, shown in Fig. 5.

An IBM 1620 computer program was used to simulate the helium expansion process out of the primary container. This program also calculated the required flow of helium from the cascade container into the primary container simultaneously with the helium expansion process out of the primary container. The program first calculated the primary storage container mass based on the material properties, safety factors, and required volume. To simulate the expansion process, the program expanded a required amount of cold helium for each pressurization event. This single expansion continues until the primary storage container pressure drops to 300 psia. At that pressure and in order to maintain that pressure, ambient helium was expanded from the cascade container into the primary container simultaneously with the cold-gas expansion out of the primary container. Heat transfer between the primary container wall and both the hot and cold helium was considered. Also, the heat transfer between the hot and cold helium was considered. After each pressurization event, the primary container wall, hot helium and cold helium were forced into thermal equilibrium during each coast period.

- e. Propellant Feedline Heat Exchangers - The low pressure, feedline heat exchangers used in these systems are of the same basic geometry as the existing Apollo SPS heat exchangers, i.e., a single tube, counterflow coil enclosed within an expanded section of each propellant line. This analysis is analogous to a single straight section of tubing positioned normal to the flow of propellant (corrections are being included to simulate effects of coil). The desired inlet and outlet temperatures are inputs to the analysis, together with the tube diameter and pertinent thermal and physical properties of propellant, gas, and tubing material. The total length of tubing required to produce the required gas temperature change is computed, as is gas pressure drop, propellant temperature change, and total mass of the heat exchanger.

- f. Heat Exchanger/Gas Generator - An existing mathematical model, programed for use with the IBM 1620 computer, was used to predict heat exchanger and gas generator weight for various conditions of entrance and exit temperatures, pressures, and gas flow rates. The model was based on methods described by Kays and London.\* The basic configuration chosen for this analysis was a cross flow, finned tube unit with the fins exposed to the hot gas and the cold helium flowing inside the smooth tubing. This heat exchanger is typified by Kays and London, and the functional relationships they present were used to define the hot gas film coefficients.† Internal film coefficients for the cold gas were based upon the turbulent portion of Fig. 41.‡
- g. Auxiliary Liquid Propellant Storage - Systems 7 and 8 require storage of small quantities of propellants for the MTI process (System 7) and high-temperature gas generation (System 8). The quantities of liquids required were determined for each system through analysis of the respective processes. This, in conjunction with operating pressures, propellant density, and properties of the titanium 6Al-4V alloy, established the size and weight of each container.

The quantities of auxiliary propellants required in System 7 were determined by a detailed analysis of the MTI process for each of the main SPS propellant tanks. For System 8 the quantities of propellants were dictated by the hot-gas pressurization requirements of the SPS fuel tank.

- h. Results of Preliminary Weight Studies - After completion of the various subsystem studies, the subsystem and component weights were tabulated to produce comparative pressurization system weights for the ranges of pressurant storage temperatures and pressures considered. The weights for Systems 1, 1A, 2, 4, 5, and 8 are shown in Fig. 12 thru 17. The comparative weight for System 0, the present Apollo SPS pressurization system, is shown as the 530°R curve in Fig. 12. System 7, using liquid propellants stored at ambient temperature, was not applicable to the pressure/temperature optimization studies. The weight of System 7 is 307.6 lb<sub>m</sub>.

---

\*W. M. Kays and A. L. London: Compact Heat Exchangers. McGraw-Hill, 1958.

†Ibid., Figure 92.

‡Ibid.

### 3. Comparison of Candidate Pressurization Systems

The candidate pressurization systems included in the preliminary study effort were subjected to a comparison study for the purpose of selecting the three systems most suitable for use in the Apollo SPS. The three selected systems were then analyzed and investigated in greater detail, as discussed in Section B. The methods used in this comparison and selection effort are discussed in this subsection.

The technique used for the comparison required a numerical evaluation of the candidate systems, related to the results of the preliminary study effort. The numerical evaluation procedure devised was based on a comparison of certain relative merits of each candidate system, as measured by the pertinent, common characteristics among all systems. Each characteristic was assigned a weighting factor that was an indication of the importance of the particular characteristic in regard to the entire evaluation. The following characteristics were considered, with the indicated weighting factors:

- 1) Mass -- 1/2;
- 2) Reliability -- 1/4;
- 3) Compatibility and adaptability -- 1/4.

A merit rating number, composed of contributions from each of the above items, was computed for each candidate system. Each constituent in the merit number was defined as a ratio so its maximum value would be 1 (unity) prior to multiplication by the proportional weighting factor. Therefore, the maximum value for the total merit rating number is also 1. The contributing factors are discussed individually.

- a. Mass - Since the major objective of this contract was to develop a pressurization system that is lighter than the current Apollo SPS pressurization system, mass was the most important consideration in the merit rating evaluation. The effect of mass on the overall merit rating was defined as the ratio of mass of the lightest system to mass of the particular candidate system:

$$(N_m)_m = \frac{\text{mass of lightest system}}{\text{mass of candidate system}}.$$

The value of  $(N_m)_m$  will attain 1 as an upper limit, and may approach 0 as the lower boundary.

The values for system mass used in this evaluation are comparative rather than absolute. Sizing of systems during the preliminary study effort was only on the basis of nominal vehicle requirements, and did not consider the effects of pressurant leakage, contingent system operation, or other design perturbations that would cause arbitrarily established variations in pressurant usage. Also, the mass of tubing, insulation, support structure, etc has been omitted. Such items as loaded pressurant, pressurant storage containers, valves, pressure switches, gas generators, and heat exchangers were included in system mass estimates. This applies also to the present Apollo SPS pressurization system mass figure used in this comparison study. Rather than use the actual system mass, the system was reweighed to reflect the same criteria and technique as established above for the candidate systems. In this way, all systems were compared in the proper perspective.

- b. Reliability - Reliability was the second key criterion affecting pressurization system selection. Man-rating of the final selected system will be an ultimate necessity, so a favorable preliminary reliability characteristic was mandatory. It is ineffective to compare a ratio of reliability numbers directly, because variations usually occur only beyond the second significant digit. A ratio of failure rates is a much more sensitive method of comparison. Therefore, the contribution of reliability to the merit rating number was defined as:

$$(N_{m.R}) = \frac{1.0 - \text{Reliability number for present system}}{1.0 - \text{Reliability number for candidate system}}$$

Reliability numbers were calculated on the basis of generic failure rates established for the individual components associated with each candidate system. Environmental and mission dependent effects were considered where applicable. The reliability analysis, like the mass analysis, excluded from consideration certain items not directly related to this comparison effort. Vent relief valves, pressurant fill valves, and filters were omitted.

These components are common to all systems studied, and in general do not contribute to airborne (in-flight) system operation. Items that received attention in the reliability analysis included flow control valves, check valves, pressure switches, heat exchangers, gas generators, pressurant storage containers, lines, and fittings.

- c. Compatibility and Adaptability - In this evaluation, compatibility is a term used to indicate the capability of each candidate in conforming to the constraints imposed by the Apollo SPS vehicle and mission. This included such considerations as environment, geometry, operational characteristics, and logistics. In general, compatibility is a measure of the ease and potential of making any given pressurization system an operational part of the Apollo SPS. The adaptability portion of this criteria indicated a consideration of the degree of development problems associated with each system. A state-of-the-art system using off-the-shelf hardware would get a higher rating than a more advanced concept for which an extensive component development program would be required. The total contribution of compatibility and adaptability to the merit rating was:

$$(N_m)_c = (X),$$

where (X) is a number chosen as follows:

(X) = 0 indicates a definite incompatibility with the SPS;

(X) = 0.25 indicates the candidate system could probably be used with the SPS, but extensive development would be required, along with probable changes in SPS existing design;

(X) = 0.50 indicates the candidate can be used with the SPS, after moderate development effort and with few concessions in existing design or operation;

(X) = 0.75 indicates the candidate can be used with the SPS, and requires a minimum of development effort and minimum interference with existing SPS operation;

(X) = 1.0 indicates no development effort required and the candidate is completely compatible with existing SPS design.

The final merit rating number was computed as the sum of each of the three contributors:

$$N_m = 1/2 (N_m)_m + 1/4 (N_m)_R + 1/4 (N_m)_c.$$

The systems with the highest merit rating were considered to be the most promising candidates, and the systems rated lowest were considered to be least worthy of further consideration.

Pertinent results of the candidate pressurization system comparison study are shown in Table 4. The overall merit rating numbers of candidate systems range from a low of 0.5583 to a high of 0.8426. Merit rating of the current Apollo SPS pressurization system is 0.6393. The total possible range of merit rating numbers is from 0 to 1. Candidates with the higher merit ratings were considered to be more desirable for the Apollo SPS application.

To more clearly illustrate the comparison of total system masses for the candidate and the current Apollo SPS pressurization systems, curves shown in Fig. 18 were prepared. For the stored-gas systems (1, 1A, 2, 4, 5 and 8), the curves represent total system mass as a function of initial storage temperature -- at the optimum storage pressure. Systems 0 and 7 are shown as point values, since they operate only at ambient temperature.

The relative ranking of the candidate systems (present Apollo system included) according to numerical merit rating is given in Table 5. System 5 has the highest overall rating, by a significant margin. As noted in Fig. 18 it was also potentially the lightest of all candidate systems. System 1 ranks second, and System 1A is a close third.

Systems 1 and 1A are very similar in concept. Figure 18 reveals that these two systems are also extremely comparable in mass. However System 1A depends on two separate working fluids, whereas System 1 uses only helium. Therefore System 1A was excluded from further consideration because of complexity considerations.

Systems 5, 1, and 8 were the three top candidates in the numerical evaluation. Figure 18 also shows that these three systems have the highest weight-saving potential over the widest temperature range of all candidate systems.

Based on this comparison, Systems 5, 1, and 8 were selected as candidates for more detailed design and analysis.

#### B. DETAILED INVESTIGATION OF SELECTED SYSTEMS

The three candidate pressurization systems selected for concentrated study were defined and evaluated in detail to determine the advantages and disadvantages of each system. The results of the detailed evaluation were used in a comprehensive comparison of the candidate systems. From this comparison, the system offering the greatest overall advantages for use in the Apollo SPS was selected. The methods and criteria used in the system evaluation and the results obtained are discussed in this section.

The detailed studies are discussed in relation to the following major categories:

- 1) Additional study and refinement of system concepts;
- 2) Problem area investigation,
  - a) Helium storage tests,
  - b) Propellant feedline heat exchanger tests,
  - c) Pulsed mode pressurization control tests,
  - d) Gas generator/propellant feedline gas cooler tests;
- 3) Optimum system selection.

The thermodynamic analyses used in these detailed studies incorporated the methods and models of the preliminary studies, with consideration of the thermal effects of the system environment added. Final pressurant storage container sizing included a 5% contingency factor to allow for leakage and loading tolerances. Also, the system mass estimated in this section reflects the effects of all identifiable components required for complete flight systems.

### 1. Additional Study and Refinement of System Concepts

One early accomplishment of the detailed design and analysis effort was the review of the basic concepts for the purpose of incorporating possible improvements. Several potentially attractive modifications were considered that affected all three candidate systems. Certain modifications involving Systems 5 and 8 were adopted. Others -- undesirable primarily because they increased system mass -- were discarded.

The modifications studies and used are discussed briefly in this subsection.

- a. System 5 - The original concept of System 5 included a flexible membrane (bladder) within the primary helium tank. The purpose of the bladder is to retain the warm cascade gas within the primary tank, so that all available energy heats the primary gas (and tank) rather than escaping into the propellant tanks, where it would be relatively ineffective. In removing the bladder, it was recognized that some of the warm gas would exit from the primary tank and exert some detrimental effect on system mass. However it was determined that by suitable diffusion of the entering cascade gas, nearly perfect mixing could be attained.

The analysis of the bladderless primary tank was based on the premise that the entering cascade gas instantaneously and thoroughly mixed with the resident primary tank gas. Otherwise, the mathematical model used in the thermodynamic and sizing analysis was the same as that for the system with a bladder.

The results of the analysis are shown in Fig. 19. These weights were generated by the same rules used during the preliminary study and are to be interpreted as comparative rather than absolute figures. The results show an increase in the minimum system weight for all three storage temperatures. Figure 19 also shows that the minimum weight points were shifted toward slightly higher storage pressure, although the effect is barely discernible.

In consideration of the bladderless version of System 5, the following observations were immediately apparent:

Development cost and schedule uncertainties would necessarily be less than for the original concept of System 5 (with a primary tank bladder);

Reliability is higher than for the original concept of System 5;

System weight is slightly higher than for the original version.

The only disadvantage in removing the bladder from System 5 was the increase in system weight. As noted in Fig. 19, the weight increase at an initial storage pressure of 4000 psia amounts to less than 25 lb<sub>m</sub>. The development and reliability factors were recognized as being more important than the system weight difference; therefore, the use of a bladder in the primary helium storage tank was not considered in further examination of System 5.

- b. System 8 - System 8 was modified in two aspects after the preliminary studies were completed. The first modification was the replacement of the original gas-to-gas heat exchanger (for heating the helium and cooling the gas generator products) with two liquid-to-gas propellant feedline heat exchangers. The other modification entailed replacing the bipropellant gas generator with a monopropellant unit.

In the early stages of the detailed analysis, it was found that a basic energy unbalance would prevent the use of a direct gas-to-gas heat exchanger. The energy that must be lost by the hot-gas generator products to achieve the maximum tank entering temperature of 600°R far exceeded the amount of energy required to heat the cold helium to that same temperature. It was then decided to analyze the use of separate propellant feedline heat exchangers -- one to heat the helium to near ambient temperature, and the other to cool the hot gas generator exhaust products to an acceptable temperature (600°R). The operating parameters for the System 8 unit were identical to those for the System 1 helium/oxidizer heat exchangers that had already been analyzed in the System 1 studies. Therefore,

only the hot gas/fuel heat exchanger was significant. Subsequent analysis of this unit provided data compatible with existing design requirements and indicated heat exchanger weights would be in the same range as weights for the helium/oxidizer units.

The use of a hydrazine monopropellant gas generator was considered for System 8 because:

System complexity (both component and operating) would be significantly reduced, since only one propellant supply subsystem would be required;

The combustion products are cleaner. Only hydrogen, nitrogen, and ammonia are produced in the  $N_2H_4$  decomposition process, all of which are compatible with the system and do not form sludge or any type of solid precipitate. The  $N_2O_4$ /Aerozine 50 reaction produces -- in addition to the constituents listed above -- water, vapor, and various carbon compounds that are known to produce liquid and solid contaminants detrimental to consistent system performance;

The  $N_2H_4$  monopropellant unit is capable of generating gases at lower temperatures than the bipropellant units.

Consultation with two companies prominent in the field of developing the  $N_2H_4$  gas-generator concept (Rocket Research Corporation, and Sundstrand Aviation Company) revealed that hydrazine gas generators are now within state-of-the-art technology and could offer greater advantages than a bipropellant system for the Apollo SPS application. This is substantiated in the fact that such units are now flying on two different space vehicle systems (Mariner and Ranger). Figure 20 shows the estimated fuel tank pressurant usage requirements for  $N_2H_4$  combustion products. These curves compare very favorably with the required usage of 89.6 lb<sub>m</sub> (at tank inlet temperature of 600°R and propellant temperature of 530°R) predicted for bipropellant gas-generator products.

It was concluded that in all respects the  $N_2H_4$  monopropellant gas generator was more appropriate for System 8 application than the  $N_2O_4$ /Aerozine 50 unit.

## 2. Finalized System Concepts

The finalized concepts of Systems 1, 5, and 8 are discussed in this subsection.

- a. System 1 - System 1 is shown schematically in Fig. 21. This system is the least complex of the three candidates in terms of concept and operation. Helium stored at high pressure and low temperature is the pressurant. The flow of helium is controlled by solenoid valves energized by pressure switches that sense propellant tank pressures. The helium is heated while en route to the propellant tanks by heat exchangers that use the propellants as heat sources. The helium storage system consists of a pressure vessel surrounded by a lightweight, rigid jacket wrapped with NRC-2 superinsulation. The purpose of the jacket is to contain a coolant to maintain the pressure vessel and stored helium at the proper temperature during the prelaunch hold period. Residual coolant in the jacket at launch time is vented and does not cause a weight penalty. The propellant tank pressure switches and the solenoid valves are grouped into series/parallel units to attain high reliability. The orifice shown just downstream of each set of solenoid valves is used to trim the maximum helium mass flow rate for test convenience. They would not be necessary in the flight design. Propellant retention screens are used at the pressurization line outlet in each propellant tank to prevent liquids from backflowing through the lines. It is not necessary to prevent propellant vapors from entering the pressurization lines, since the solenoid valves preclude the possibility of mixing of the vapors from fuel and oxidizer tanks.
- b. System 5 - System 5 is shown in Fig. 22, and is functionally identical to System 1 with the exception that a cascade helium tank and associated valving and pressure switches have been added. The cascade tank contains ambient temperature helium used to heat the primary storage system during latter stages of the mission. This increases the final temperature of the primary helium,

thus reducing the mass of helium that must be loaded initially. The total volume of loaded helium (primary plus cascade) is also less than for System 1, which means a reduction in helium tankage mass.

Operation of the cascade arrangement is as follows. Helium for propellant tank pressurization is at all times extracted from the primary tank. When pressure within the primary tank falls below a minimum set level (in this case, 400 psia), the solenoid valves are energized and admit helium into the primary tank. Pressure in the primary tank is then controlled at 400 psia by the pressure switch/solenoid valve arrangement during the remainder of the mission. The pressure switches on the primary storage tank are arranged in series/parallel redundancy, as are the solenoid valves between cascade and primary tanks.

- c. System 8 - System 8 (Fig. 23) consists of two separate types of pressurization systems. A cold stored helium system, identical in operation to System 1, pressurizes the oxidizer tank. The fuel tank is pressurized by exhaust gases from a hydrazine monopropellant gas generator. The fuel tank pressurant is composed of hydrogen, nitrogen, and ammonia. Helium from the main supply tank is used to pressurize the hydrazine tank by a quad redundant pressure switch/solenoid valve arrangement. A flexible bladder is used in the hydrazine tank to permit zero gravity operation. Hydrazine flows through a set of shutoff valves (series/parallel redundant) to the gas generator. The gas generator uses a spontaneous catalyst (Shell 405) to decompose the hydrazine at a temperature of about 1960°R. The gases are cooled in the feedline heat exchanger before entering the fuel tank. The gas generator propellant shutoff valves are operated by series/parallel redundant pressure switches on the main fuel tank.

### 3. Problem Area Investigation

Further information was required for the evaluation program; the information needed fell in two categories:

- 1) Performance data for components and subsystems;
- 2) Feasibility of certain system concepts.

Both analytical and experimental studies were performed to obtain the required information. Where applicable, experimental results were compared with analytical predictions.

The Phase I test program was concerned with establishing the basic characteristics of several subsystems and components that might be used in a pressurization system for the Apollo SPS. The general purpose of the program was to obtain empirical data on several candidate subsystems to establish feasibility and to validate the analytical models used for the candidate systems. The experimental investigations covered the following basic areas of concern:

- 1) Thermodynamics of a cryogenic helium storage container;
- 2) Propellant feedline heat exchanger characteristics;
- 3) Operation of a solenoid valve as used in a propellant tank pressure control system;
- 4) Operation of a gas generator/feedline heat exchanger system as a fuel tank pressurization source.

The experimental test program is discussed in the following paragraphs. Additional details on equipment (instrumentation), procedures, and conduction of individual tests are available.\*

- a. Helium Storage Tests - The objective of this test was to acquire data on the thermodynamic characteristics of helium stored at low temperatures (about 140°R), including the effects of expansion of helium from the container and external heating of the container during simulated burn/coast periods.

The test fixture, shown schematically in Fig. 24, consisted of an insulated storage sphere, an insulated vacuum tank or chamber in which the storage sphere was mounted, and a liquid nitrogen/helium heat exchanger. The stainless steel sphere had an internal volume of 3.94 cu ft and weighed 1230 lb with the temperature rake installed. The sphere was covered with foil-backed fiberglass insulation having an installed thickness of 1/2 to 9/16 in. Isolation of the storage sphere mounting tabs

---

\*Pressurization System for Use in the Apollo Service Propulsion System - Monthly Progress Report. Martin-CR-64-82 (Issue 8). Martin Company, Denver, Colorado, June 1965.

from the vacuum chamber supports was accomplished with 15/16-in.-thick Teflon shims. The helium heat exchanger consisted of 60 ft of steel tubing (with a diameter of 1/4 in. and a wall thickness of 0.035 in.) immersed in liquid nitrogen. Strategically positioned thermocouples and pressure transducers were used to monitor temperature and pressure.

The insulated storage sphere was precooled by filling it with liquid nitrogen at ambient pressure (12 psia). The liquid nitrogen was then drained from the sphere by pressurization with cold helium, and the sphere was evacuated to scavenge the residual helium/nitrogen gas mixture. After establishment of a satisfactory vacuum in the cold sphere, helium loading was initiated. Helium was loaded through the helium heat exchanger at a rate consistent with maintaining a sphere inlet temperature of approximately 160°R. Loading was continued until the sphere was charged to 3000 psia, at which time the test run began. The sphere was maintained in a locked-up condition until an adequate gas temperature rise (15 to 20 deg) had been observed. The gas pressure was then vented to successively lower pressure levels (2500, 2000, 1500, 1000, and 500 psia). At each pressure level, the sphere was locked up for the required temperature rise period. Pertinent temperatures and pressures were recorded continuously during the entire test run.

Of the six helium storage sphere tests that were executed, the last two -- Runs 5 and 6 -- were considered successful for comparison to analytical simulation. The first four runs were performed to check out and troubleshoot the test system.

The analytical simulation of the helium storage tests was performed with the IBM 7094 gas expansion computer programs (also used for the pressurant storage analysis on the three candidate systems). One modification was made to the basic gas expansion program to simulate the helium storage tests. This modification was the addition of venting at given rates from an established pressure level to the next desired pressure level.

The results of the evaluation and comparison of the test results with the analytical simulation for Tests 5 and 6, respectively, are shown in Fig. 25a, 25b, 26, 27a, 27b,

and 28. These figures show almost identical results for both tests. The calculated temperature rise rates of the helium and sphere wall temperature are very close to the temperature rise rates experienced during a large portion of both tests. The only exceptions occur at the start of the first and second coast periods for both tests. These exceptions are due to a tendency of the calculated helium temperature to approach and stay about 1 to 2 deg below the calculated wall temperature. Due to this tendency, the calculated helium temperature increased at a much faster rate than the test helium temperature during the short time immediately following venting. This tendency also explains the large difference in calculated and test helium pressure during the first and second coast periods. The start of the first coast period in both tests clearly shows that the calculated helium temperature increased rapidly to within 2 degrees of the calculated wall temperature and then began the gradual temperature rise while the test helium temperature rise was gradual during the entire coast. Except for the small deviations mentioned above, the calculated helium pressures, helium temperatures, and wall temperatures compared favorably with the helium pressures, average helium temperatures, and average wall temperatures experienced during the two tests when instrumentation accuracy is considered. The accuracy of the thermocouples at the temperatures experienced during the tests was  $\pm 8^\circ\text{F}$ . The accuracy of the pressure transducer was  $\pm 50$  psi. Therefore, on the basis of this evaluation and comparison, the computer program did provide a good simulation of actual conditions, within the accuracy of the measurements.

- b. Propellant Feedline Heat Exchanger Tests - The objective of this test was to determine the operating characteristics of a propellant feedline heat exchanger similar to that of the Apollo SPS, using ambient temperature  $\text{N}_2\text{H}_4/\text{UDMH}$  fuel to heat  $160^\circ\text{R}$  helium.

A detailed drawing of the heat exchanger is shown in Fig. 29.  $\text{N}_2\text{H}_4/\text{UDMH}$  fuel was supplied to the heat exchanger from a facility supply tank. The fuel outlet end of the heat exchanger was fitted with one thickness of 100-mesh stainless steel screen to serve as an ice-catcher. Static pressure bosses were provided upstream and downstream of the screen to provide for measurement of pressure drop

across the screen. The screen and pressure taps were provided to determine whether freezing of the fuel occurred as a result of transferring heat to the cold helium. Helium was supplied to the heat exchanger inlet at approximately liquid nitrogen temperature. Pressures and temperatures were measured at the propellant and helium inlets and exits. Also, the propellant and helium flow rates were continuously controlled and measured.

A total of five propellant feedline heat exchanger test runs were performed. The first three were checkout runs, and the last two were data runs. Tests 4 and 5 were the only runs that were evaluated and compared with analytical data.

Runs 4 and 5 each consisted of alternating periods of operation (simulated sustained flight) and shutdown (simulated coasting). Helium mass flows of 0.05 to 0.07 lb/sec, and propellant flows of 180 to 190 gpm were used.

Analytical simulation was accomplished with the gas-to-liquid heat exchanger computer program used for the previous analyses of candidate systems. The test data input to the program were helium inlet and outlet temperatures, fuel inlet temperature, helium and fuel flow rates, and helium inlet pressure. Also input were the physical and thermodynamic properties of helium and propellant, and the test heat exchanger configuration, i.e., tube inside and outside diameters, length and wall thickness, and feedline cross sectional area. The computer program calculated the heat exchanger length, helium pressure drop, and fuel temperature drop.

The analytical simulation was conducted for the steady-state portions of Tests 4 and 5 only. For Test 4, the 6-min steady-state run is designated as Test 4-A, and the two 2-min runs are designated as Test 4-B and Test 4-C. For Test 5, the 6-min, 2-min, and two 3-min steady-state runs are designated as Tests 5-A, 5-B, 5-C, and 5-D, respectively. The results of the evaluation and comparison for these tests are shown in Table 6.

On the basis of this comparison, it was deduced that the analytical model will give quite conservative values for heat exchanger sizes. The primary source of disagreement between the calculated and actual heat exchanger

length was the equation used to predict the heat transfer coefficient across the inside gas film. The computer program used an equation for a straight tube with moderate temperature rise while in actuality the tube was a helical coil with high gas temperature rise. Use of the correction for a helical coil increases the inside film coefficient by about 30 to 40% for the actual exchanger dimensions and results in a decrease in the predicted lengths. This effect was incorporated into the computer program along with other refinements, i.e., temperature at which properties were evaluated and more precise exponents. Much closer agreement between predicted and measured values should result; however, the analytical model will still be maintained on the slightly conservative side.

- c. Pulse-Mode Pressurization Control Tests - The objective of this test was to obtain empirical information on a pulse-mode pressure control subsystem that might be incorporated into a propellant tank pressurization system. It was desired that the subsystem control the ullage pressure in a simulated propellant tank within a narrow band when supplied 140 to 160°R helium from a stored source. Further, the subsystem had to function properly at helium flow rates from zero (coasting flight) to values associated with full-thrust sustained flight.

The test fixture was composed of the 4-cu-ft, insulated storage sphere (same unit used in the helium storage test), a Sterer 3/4-in. solenoid-operated shutoff valve (P/N 28370), a Hydra Electric 155-psig pressure switch and a 10½-cu-ft accumulator sphere (simulated minimum propellant tank-top ullage). A 0.020-in.-diameter, sharp-edged orifices was installed downstream of the Sterer shutoff valve to reduce its flow capacity to the desired range. A remotely operated throttling valve was installed in the discharge line from the accumulator sphere to permit adjustment of helium mass flow rate to the desired values of 0.06 to 0.10 lb/sec. Remotely controlled shutoff valves were installed at appropriate points in the system to permit fast-response starting and stopping of the helium flow from the accumulator and to isolate the Sterer valve for purposes of leak checking. A schematic diagram of the system is shown in Fig. 30.

The power supply to the Sterer valve was controlled by the pressure switch, with provisions for manual override on the control console. The pressure switch was wired to send 28 vdc to the valve whenever the accumulator pressure dropped below the  $155 \pm 1$  psig set-point, thus calling for the valve to open. The Sterer valve was mounted in a small vacuum chamber having uninsulated walls. A vacuum pump was provided to evacuate the chamber to approximately 0.2 psia.

A series of three runs was made with the stored helium gas source at an initial condition of 160°R and 2000 psia (maximum working pressure allowed for the pilot-operated shutoff valve used). Each run included an initial pressurization of the simulated tank-top ullage to a lockup condition, followed by either a sustained pressurization run (full duration burn) or an interrupted run (burning and coasting).

Operation of the pulse-mode subsystem was satisfactory during all test runs, and acceptable data were obtained on the dynamic characteristics of the subsystem and its components at helium mass flows up to 0.07 lb/sec.

Maximum response time was 65 msec on opening and 50 msec on closing. Minimum response time was 45 msec on opening and 35 msec on closing. The control system operation was entirely successful under all conditions tested. The valve was tested for leakage at various temperatures between ambient and 140°R; no leakage was detected.

- d. Gas Generator/Propellant Feedline Gas Cooler Tests - The objective of this test was to determine the operating characteristics of a pressurization subsystem comprising a hydrazine decomposition chamber (hot-gas generator) supplying pressurant gases and a propellant feedline gas cooler.

The test fixture used in this test was a modification of the fixture used for the feedline heat exchanger test. The heat exchanger (gas cooler) was the same unit and the  $N_2H_4$ /UDMH propellant circuit was unchanged. The gas generation and flow system consisted of a hydrazine supply tank having a capacity of 1.2 cu ft (75 lb of hydrazine); a 1/2-in. solenoid-operated shutoff valve in the

hydrazine line at the gas generator inlet; a Rocket Research Company, Model RB2-100, reaction chamber (hot-gas generator of the hydrazine decomposition type) mounted on the gas inlet side of the gas cooler; and a gas discharge throttling system composed of a fixed-exit orifice in parallel with a remotely operated throttle valve. The gas throttling system was developed when it became apparent that the gas generator was subject to destructive detonation if allowed to discharge into an inadvertently closed system. The provision of a fixed orifice in the gas discharge system forestalled the possibility of operating the gas generator with a closed exit. A remotely controlled gas sample collector system was provided to permit collection of a gas sample during the run. The system is shown in Fig. 31 and 31a.

The test run was started by initiating propellant flow and firing the gas generator simultaneously, using the previously established valve settings. No adjustments were made during the run. The system was allowed to run for approximately 6 min. During the latter part of the run, the sampling system was closed to trap a sample of gas. At the end of the 6-min burn, the fuel flow and the gas generator were shut off simultaneously to simulate the start of a coast period. The surface temperature of the gas-cooler tube was monitored on shutdown to detect any excessive temperature rise (above 450°F). After a simulated coast period of 10 min, during which the low-rate,  $\text{GN}_2$  purge flowed through the gas-cooler circuit,

a 2-min burn was made in the same manner as the preceding 6-min burn. Following another 10-min coast period, a final 2-min burn was made. After approximately 1 min of the final 2-min burn had elapsed, a short period of simulated pulse-mode operation was performed by closing and opening the gas generator hydrazine supply valve at frequencies of from 1 to 0.25 cps. The propellant flow was continuous during pulse-mode operation of the gas generator. Following completion of the test run, the gas sample bottle isolation hand valves were closed, and the sample bottle was removed from the system.

There were four hot gas to fuel feedline heat exchanger tests attempted. Of these four, the last two, Tests 3 and 4, were successful. Analytical simulation was conducted for the steady-state portions of Tests 3 and 4 only.

The analytical simulation was accomplished with the same gas-to-liquid heat exchanger computer program that was used for the helium-to-fuel heat exchanger simulation. The same type of input parameters were required; output data were also the same. Values for the input parameters were taken from test data representative of the steady-state operation during Tests 3 and 4. Burns during Test 3 consisted of a 6-min run, a 2-min run, and a 2-min pulse-mode run. Test 4 was identical to Test 3 except a higher gas flow rate was used. The 6-min and 2-min steady-state runs for Test 3 are referred to as Tests 3-A and 3-B, respectively. The 6-min and 2-min steady-state runs from Test 4 are similarly referred to as Tests 4-A and 4-B, respectively.

The results of the evaluation and comparison of these tests are shown in Table 7. These results are similar for all four tests. The results show that the computed data are higher than the test data for the three parameters (heat exchanger length, hot-gas pressure drop, and fuel temperature rise) that were compared. The percentage difference between the computed data and test data is much greater than that observed in the previous comparisons, i.e., the comparisons on the helium-to-fuel heat exchanger. Two reasons exist for this increase between predicted and actual values. The first is due to the previously discussed need for improving the computer program equations for calculating heat transfer film coefficients, and the second is due to the unknown chemical composition of the gas generation products. The necessary changes in the computer program have since been incorporated. Since the gas analysis from the gas generator tests were unsatisfactory, the chemical composition used in the analytical simulation was 59% hydrogen, 32% nitrogen, and 9% ammonia (% by mole). This composition was estimated for the gas generator exit temperature range experienced during the tests. A successful sample and analysis of the gas generator products would have given the actual chemical composition from which the physical and thermodynamic properties of the gas generator products could have been obtained. Use of the actual physical and thermodynamic properties in the computer program would help bring the predicted values closer to the actual test conditions. However, the greatest improvement will be obtained by revising the heat transfer equations in the analytical model to obtain predictions only slightly conservative in nature.

## C. SELECTION OF RECOMMENDED SYSTEM

The most important facet of the entire Phase I work was the selection of the most promising pressurization system for the feasibility test program to be executed during Phase II. Seven system concepts were subjected to preliminary study, analysis, and evaluation. Subsequently, a numerical comparison and evaluation of the seven systems resulted in selection of the three most promising systems for more detailed design, analysis, and evaluation. This detailed study effort included experimental as well as analytical investigations and resulted in the selection discussed in this section.

1. Criteria for Pressurization System Selection and Optimization

The basis for system selection has already been reported.\* In accordance with that report, the following criteria were considered in the prototype system selection:

- 1) Mass;
- 2) Envelope;
- 3) Reliability;
- 4) Minimization of system startup time;
- 5) Minimization of pressurization system leakage;
- 6) Minimization of propellant tank venting;
- 7) Cost;
- 8) Component availability;
- 9) Complexity;
- 10) Ground system requirements;
- 11) Storage time up to 30 days.

All three systems are discussed in terms of each of the selection criteria in the following subsection.

---

\*System Selection Summary for Advanced Lightweight Pressurization System. Martin-CR-65-6. Martin Company, Denver, Colorado, January 1965.

## 2. Comparison of the Three Candidate Systems

- a. Mass - A basic requirement in developing a new pressurization system for the Apollo SPS is a significant reduction in mass, as compared to the present system. Therefore, minimum mass was considered as the most important single criterion for system selection. The existing Apollo SPS pressurization system mass was calculated to be 880 lb<sub>m</sub> for purposes of comparison. This calculation was based on the data in Table 1, and used the same analytical techniques as were used in deriving masses of the candidate systems. Masses for the three candidate systems are plotted in Fig. 32, 33, and 34.

During the course of the Phase I work, calculations indicated that the 10-hr hold capability for helium storage at 37°R could be provided by a reasonable size of liquid hydrogen jacket surrounding the helium pressure vessel. It was later determined that the heating rates from the ground environment were of such magnitude that it was practical to load only enough liquid hydrogen to support a 1-hr prelaunch hold period. It then became necessary to include a vacuum jacket around the superinsulation for the systems stored at 37°R. This ensured maximum thermal performance of the superinsulation, reducing the ground heating rate to levels equivalent to the flight conditions. This design change is discussed further in Chapter V. Neither the vacuum jacket weights nor the coolant weights are included in Fig. 32, 33, and 34.

The storage of helium at either 37°R or 140°R offers considerable mass reductions over the present Apollo system. The savings in mass dissipates rather rapidly at initial storage temperatures above 140°R; therefore, temperatures above 140°R were excluded from further consideration. Initial storage temperatures between 37 and 140°R are excluded, as will be discussed in Subsection j. Total mass of each of the three candidate systems at 37 and 140°R have been plotted as a function of initial helium storage pressure in Fig. 35. It is observed that System 5 at 37°R is clearly the optimum system from the minimum mass aspect. Considering the present system optimized mass of 880 lb<sub>m</sub>, System 5 offers a potential reduction of 535 lb<sub>m</sub>.

Table 8 illustrates the potential reduction in mass for each of the candidate systems, at 37 and 140°R initial storage temperatures.

- b. Envelope - All three candidate systems were designed to conform to the geometry limitations of the existing Apollo SPS. Furthermore, there is little discernible difference in the overall envelope of all three candidate systems. Therefore, this criterion had no influence on final system selection.
- c. Reliability - Final reliability analyses were completed for the three candidate systems and for the present Apollo SPS pressurization system. Results of these analyses are tabulated in Table 9. The effects of all components were considered in this effort. This included vent-relief valves, fill-line disconnect, filters, lines, and fittings that were omitted from earlier analyses. Therefore, the reliability numbers given reflect realistic evaluations of the systems. It was noted that the greatest probable sources of failure in all systems are the lines and fittings. This is because such unreliable individual components as valves, regulators, and pressure switches have been assembled into redundant units, considerably diminishing the possibility of total functional failures. To eliminate the possibility that the effect of lines and fittings could obscure other important comparative features of candidate system reliability, an analysis was made that omitted lines and fittings from consideration. These results, presented in Table 9, show that System 1 is slightly higher in reliability than the present Apollo system and System 8 is slightly lower.
- d. Minimization of System Startup Time - The pressurization system selected should add no appreciable complexity to the Apollo SPS start sequence nor impose time lags that necessitate anticipation of start operations. All three candidate systems were equally advantageous in this respect. None required more than a single command to initiate operation, and all were instantly responsive (within the 20- to 50-msec time required to actuate a normal solenoid valve). This criterion was therefore not influential in selection of the optimum system.

- e. Minimization of Pressurization System Leakage - Since all candidate systems contain the same types of components, the comparison of leakage characteristics of the systems was resolved by a count of all pressurized gas lines that have the potential of leaking gas from the system. The system with the greatest number of such lines was considered the least desirable. On this basis, System 1 with 21 lines was the minimum leak system, System 8 with 24 lines was second best, and System 5 with 29 lines ranked third. Since most of the lines will be welded together in the flight system, it is not considered that the criterion of leakage has a strong influence on system selection.
- f. Minimization of Propellant Tank Venting - Extensive propellant tank thermodynamic analyses were performed using the design mission profiles and heating data as supplied by NASA-MSC. These studies indicated that the maximum operating pressures of the propellant tank would not be exceeded during the mission, regardless of which candidate pressurization system was used. Since propellant tank venting is not indicated, all three candidate systems are considered to be equally acceptable.
- g. Cost - The estimated hardware cost figures for each candidate system are presented in Table 10. The tabulations include both development and purchase costs for the components. These estimates are based on actual costs incurred during the Titan III transtage procurement program, modified to reflect the variations in component requirements and applications. Therefore, the costs are believed to be representative of man-rated, flight-qualified hardware. However, this information is presented for purposes of comparison only and should not be construed as firm prices.

System 1 is definitely the least expensive of the three, and System 8 is the most expensive (by about 50%). System 5 is about in the middle, 15% above System 1 in development and qualification costs, and 30% higher in purchase costs per vehicle.
- h. Availability - All systems can be developed in approximately 21 months. No development span differences exist among the systems.

- i. Complexity - Complexity, as related to system selection, has two connotations:

The extent to which a candidate system affects the design and operation of other existing Apollo SPS subsystems;

The inherent complexity of the pressurization system itself, as determined by the total number of components.

The only existing subsystem affected by any of the candidate systems is the electrical power supply. It is estimated that the solenoid valves used will require power at rates of 0.5 kw for System 1 and 0.75 kw for Systems 5 and 8. Electrical power is used only during periods of main engine operation, so the total power requirements are about 0.083 kw-hr for System 1, and 0.125 kw-hr for Systems 5 and 8. Voltage required is 28 vdc for all three systems.

System 1 has 27 working components, System 5 has 38, and System 8 has 39. Evaluation of both aspects of complexity, therefore, indicates that System 1 is the most desirable with Systems 5 and 8 about equal.

- j. Ground System Requirements - Ground system requirements are established by a helium loading time, a 10-hr hold capability, and a minimum change to the present ground system requirements. The three candidate systems were compared on the basis of these three requirements. The following is a summary of the comparison of the three candidate systems.

Helium Loading Time Requirement - Helium loading time was estimated for the three candidate systems at two storage conditions (Table 11). The loading rate for each case was adjusted to ensure that the allowable working pressure of the pressure vessel would not be exceeded. The helium loading time was defined as the sum of the actual loading time and the time required to cool the helium and the sphere to the storage conditions. For a 140°R storage temperature and 4000 psia storage pressure, the loading times were about the same. System 8 had the least time required for loading and System 1 the most. The difference between

System 8 and System 1 loading time, however, was only 3 min. For a 37°R storage temperature and a 2000 psia storage pressure, the helium loading time for System 5 was greater than the loading times for Systems 1 and 8. The loading time for System 8 was only 3 min less than for System 1. On the basis of this comparison, System 8 has the best loading time (by a slight amount) for both storage conditions. The amount of coolant ( $\text{LN}_2$  or  $\text{LH}_2$ ) required to cool the helium and helium sphere down to the storage conditions during and after the loading process was also evaluated. For a 140°R storage temperature and 4000 psia storage pressure, System 8 required 349 lb<sub>m</sub> of  $\text{LN}_2$  less than System 1 and 96 lb<sub>m</sub> less than System 5. For a 37°R storage temperature and a 2000 psia storage pressure, System 5 used less  $\text{LH}_2$  coolant than either Systems 1 or 8. System 8 has the more desirable helium loading requirements for the 140°R, 4000 psia storage conditions while System 5 is more advantageous at storage conditions of 37°R and 2000 psia.

10-Hour Hold Capability - The capability of each candidate system to maintain a given storage condition for 10 hr was evaluated. The amount of coolant ( $\text{LN}_2$  or  $\text{LH}_2$ ) required to maintain the given storage conditions was calculated for each candidate system. For a 140°R storage temperature and a 4000 psia storage pressure, System 8 required the least amount of  $\text{LN}_2$ . System 5 required about 8 lb<sub>m</sub> more  $\text{LN}_2$  than System 8, and System 1 required about 28 lb<sub>m</sub> more  $\text{LN}_2$  than System 8. For storage at 37°R and 2000 psia, System 5 required the least amount of  $\text{LH}_2$ .\* System 8 required 6 lb<sub>m</sub> more  $\text{LH}_2$  than System 5, and System 1 required 25 lb<sub>m</sub> more  $\text{LH}_2$  than System 5. For a 10-hr hold capability, System 8 is more desirable for 140°R storage temperature and 4000 psia storage pressure, and System 5 is more desirable for 37°R storage temperature and 2000 psia storage pressure.

---

\*It was subsequently determined that ground hold capability could not be provided by  $\text{LH}_2$  boiloff. See Chapter V.

Other GSE Requirements - In addition to helium,  $\text{LN}_2$ , and  $\text{LH}_2$  requirements discussed above, System 8 also requires 98.4 lb<sub>m</sub> of hydrazine to service the gas generator propellant tank. This is not a large amount but it does require an additional ground supply system that is not needed for Systems 1 and 5. It is concluded that Systems 1 and 5 have the same types of ground servicing requirements. System 8 also has the same requirements plus the additional requirement of a hydrazine supply. The time required to load the system does not vary significantly -- the minimum being 76 min for System 8 at 37°R and 2000 psia and the maximum being 133 min for System 5 at the same storage conditions.

- k. Storage Time up to Thirty Days - At the conclusion of detailed design and analysis of the three candidate systems, each system was subjected to an analytical simulation of a 30-day mission, considering two 30-day mission profiles. The first considered a mission identical to the existing 9-day design with the addition of a 21-day coast at the end of the fourth burn period (lunar orbit insertion). This mission profile is referred to as Mission Plan A. The second, referred to as Mission Plan B, was a 30-day earth orbital coasting with 50% propellant mass loaded followed by a single main-engine burn to propellant depletion. The three systems were subjected to the analytical simulation of the two 30-day missions to determine which system was most adaptable to additional missions. The results of this analytical simulation for the three candidate systems are discussed below.

Thirty-Day Mission Plan A - The analytical simulation for Mission Plan A used the identical pressurant storage system configuration as the system designed for the 9-day mission. The amount of helium loaded and used was also the same as that required for the 9-day mission. The primary question that the analytical simulation answered was whether the pressure in the helium sphere would exceed the limit operating pressure during the extended fourth coast. Table 12 shows the maximum helium pressures obtained during Mission Plan A simulation, the helium temperature at the maximum pressure, the limit operating pressure at maximum conditions minus maximum pressure,

and the time at which maximum pressure was obtained. The results show that the maximum pressures obtained for all three candidate systems at all the storage pressures and temperatures were considerably lower than the limit operating pressure for each sphere. These maximum pressures all occurred at the end of the first coast. Figure 36 shows the limit operating pressures as a function of temperature. On the basis of these results, all three systems are equally adaptable to the 30-day Mission Plan A.

Thirty-Day Mission Plan B - The analytical simulation for Mission Plan B also used the identical pressurant storage system configuration as the system designed for the 9-day mission. The helium usage requirement changed since the propellant loaded was 50% of the propellant loaded for the 9-day mission. The helium usage was smaller than that for the 9-day mission. Due to the decrease in helium usage, the helium loaded and the storage pressures were also smaller than the values used in the 9-day mission since identical sphere volumes were used. Again, the primary question that the analytical simulation answered was whether the pressure in the helium sphere would exceed the limit operating pressure during the 30-day coast period. Table 12 shows the results of the analytical simulation for Mission Plan B. The maximum helium pressures obtained at the end of the 30-day coast were considerably below the limit operating pressures for each sphere; therefore, the three candidate systems are adaptable to the 30-day Mission Plan B. System 5 is more desirable than Systems 1 and 8 for a helium storage temperature of 140°R since the difference between the limit operating pressure and maximum pressure is greater for System 5 than for either Systems 1 or 8. For a storage temperature of 37°R, System 1 is slightly more desirable than System 5 since the difference between limit operating and maximum pressures for System 1 is approximately 65 psi greater than for System 5.

### 3. Selection of the Optimum Pressurization System

The pertinent results of the system evaluation effort are summarized in Table 13. Examination of this table reveals that significant differences in the three candidate systems are seen in only three areas -- mass, cost, and complexity (as measured by total number of components). The criterion of minimum system mass is definitely in favor of System 5, with Systems 8 and 1 following in that order. The mass savings are 535 lb<sub>m</sub> for System 5, 426 lb<sub>m</sub> for System 8, and 370 lb<sub>m</sub> for System 1, as compared to the calculated optimum mass of 880 lb<sub>m</sub> for the existing Apollo system. Component development and qualification costs are minimum for System 1, System 5 is about 17% higher, and System 8 is about 28% higher than System 1. Hardware costs per vehicle are again minimum for System 1, with System 5 20% higher, and System 8 43% higher. System 1 is the least complex by component count, with Systems 5 and 8 being equal. However, the additional components required in System 5 are combined in various series/parallel redundant units that, when related to the important criterion of reliability, impose only a very small penalty on the system. It is noted that Systems 1 and 5 are compatible with the present Apollo system reliability, while System 8 is less reliable than the present system. It is concluded that the greater saving in mass afforded by System 5 is more significant than the small variations found in evaluation of the other criteria. Martin Company, therefore, selects System 5, with helium pressurant stored at 37°R, to fulfill the requirements of an ALPS for the current Apollo SPS.

#### IV. PHASE II RESULTS

##### A. CASCADE SYSTEM LOADING TESTS, HEAT EXCHANGER TESTS, AND FEASIBILITY DEMONSTRATION

###### 1. Test System

The test system used for the cascade system loading tests, heat exchanger tests, and the cascade system feasibility demonstrations is shown in Fig. 37 and 38. For the purpose of simplifying the description of the test system, the system may be divided into interdependent subsystems, namely, the cascade gas storage/expansion system and the heat exchanger system.

- a. Cascade Gas Storage/Expansion System - This system comprised a primary gas storage container, a cascade gas storage container, and a pressure-regulating system operating between the two containers.

The cascade storage container, shown in the left center of Fig. 37, was an uninsulated sphere (24-in. inside diameter x 1.88-in. wall, Type 304 stainless steel) having a storage volume of 3.94 cu ft. The cascade storage container was equipped with the instrumentation listed in Table 14. The sphere was also equipped with a helium gas fill valve (CHFV), a vent valve (CVV) and a relief valve/rupture disc safety package.

The gas discharge line from the cascade storage container was routed to a pressure regulator that consisted of an Annin Domotor throttling valve (RV-3) positioned by pneumatic signals from a Mason-Neilan pressure controller (C-3). The function of this system was to regulate the gas flow from the cascade storage container as required to maintain the pressure in the primary storage container at approximately 400 psia. The pressure regulator was provided with a command closed feature and a controller isolation valve to protect the Mason-Neilan controller from pressures above its allowable working pressure. A cascade gas flow measurement station was provided between the outlet of the cascade gas flow regulator and the inlet of the primary storage container. The flow measurement system consisted of two turbine-type flowmeters in tandem, plus the required pressure and temperature instrumentation for calculating mass flow rate. The instrumentation is listed in Table 14.

Gas from the cascade storage/pressure regulating system was conducted to the primary storage container through approximately 12 ft of 1/2-in.-diameter, stainless steel tubing. The primary helium storage container was a composite of a high-pressure gas storage sphere, a low-pressure liquid hydrogen jacket, and approximately 1 in. (80 layers) of NRC-2 superinsulation around the liquid hydrogen jacket. The construction of the primary storage container is shown in Fig. 39 thru 41. The container temperature instrumentation locations are shown in Fig. 42.

An existing Titan III transtage sphere of 6Al-4V titanium (32.32 in. inside diameter by 0.38-in. wall) was used as the primary helium pressure vessel. The volume of the sphere was 10.25 cu ft. The liquid hydrogen jacket (Fig. 40) was a sphere made of Type 304 stainless steel, having an inside diameter of 38 in. and a wall thickness of 0.078 in.

The primary helium storage container was installed in a 48-in.-diameter vacuum chamber, as shown in the lower left corner of Fig. 37. A vacuum system, consisting of a 3-in. roughing pump and a 6-in. diffusion pump, was provided to maintain the chamber pressure at or below  $10^{-4}$  mm Hg absolute.

The 1/2-in. cascade gas transfer line was connected to the top (1-in.) inlet port of the primary sphere. A combination vertical/horizontal gas temperature rake was inserted into the primary sphere through the 1-in. inlet tube also. The 1/2-in. gas outlet tube was routed from the bottom port of the storage sphere up through the annulus of the hydrogen jacket to exit coaxially with the jacket vent tube. The gas outlet tube was routed through a pneumatically operated stop valve (HSV) to the inlets of the two feedline heat exchangers. The gas outlet tubing was insulated with 1-in.-thick fiberglass insulation to prevent excessive heating of the helium gas while en route to the heat exchanger inlets. A helium loading line was connected to the outlet line for the purpose of loading the primary storage container with helium. An admission valve (PHFV) was provided in the fill line, together with an orifice to limit loading flow rate to a maximum of 0.1 lb/sec.

A vacuum-jacketed liquid hydrogen fill line was provided to transfer liquid hydrogen to the primary storage sphere from a 1500-gal. mobile dewar. Adapters were provided to permit filling either the primary gas storage sphere or its jacket with liquid hydrogen. The primary storage container liquid hydrogen jacket was equipped with a thermistor liquid-level indicating system that signaled the operator's console when the thermistor was immersed in liquid hydrogen, signifying that the liquid hydrogen jacket was full. The 1500-gal. liquid hydrogen supply dewar was not provided with a liquid-level indicating system.

A valved crossover line was provided between the primary container gas outlet line and the liquid hydrogen jacket vent, to permit expelling the liquid hydrogen from the jacket with cold helium.

A vent line was provided to conduct evolved hydrogen gas from the storage sphere or its jacket to a hydrogen vent stack. The vent line was equipped with a remotely operated valve and a hand valve to divert the venting hydrogen gas to the flow measurement system, as required for the primary storage container heat leak rate test. The hydrogen gas flow measurement system consisted of a water-bath gas heater and a Rockwell positive-displacement (bellows) type gas meter. The purpose of the water bath was to raise the temperature of the hydrogen gas to approximately ambient to increase the volumetric flow rate to a value consistent with the design rating of the gas meter, and to decrease the magnitude of the temperature correction to standard-state conditions. The inlet to the gas meter was instrumented for gas pressure and temperature.

- b. Propellant Feedline Heat Exchanger System - Two feedline heat exchangers of identical geometry were installed in series in a tap water flow system having a flow capability of 270 gpm. The installation of the heat exchangers is shown in Fig. 43. The geometry of the heat exchangers is shown in Fig. 44 and 45. The center body shown was not included in the configuration at the inception of testing; however, it was added to alleviate an icing condition on the tube coil that was discovered early in the test program. Both of the heat exchangers were equipped with view ports through which the surfaces of the tube coils were photographed during test runs.

The upstream heat exchanger (upper left in Fig. 43) was designated the high-pressure heat exchanger. Helium gas at primary container storage conditions was delivered directly to the heat exchanger gas inlet. The high-pressure, ambient temperature gas from the heat exchanger outlet was then routed to a pressure regulator consisting of an Annin Domotor throttling valve controlled by a Mason-Neilan pressure controller. The function of the pressure-regulating system was to maintain a constant pressure of 175 psia in the gas flow control/measurement system located downstream of the controller. An accumulator (1.5-cu-ft K-bottle) was connected into the system at the regulator outlet to attenuate the pressure surges produced by the regulator action.

The flow control/measurement system consisted of two turbine flowmeters in tandem (for increased data reliability), and a flow control orifice placed downstream of the flow measurement station. The orifice was sized to flow 0.058 lb/sec of helium at inlet conditions of 175 psia and 500°R. A small vernier valve was provided in parallel with the orifice to trim the flow to the desired value. The gas exhausting from the system was conducted through a stop valve (OSV) to the facility helium recovery system.

The downstream heat exchanger was designated the low-pressure heat exchanger. A regulator/controller system, identical to that described for the high-pressure heat exchanger, was provided in the gas supply line from the primary storage container. The pressure controller was set to maintain 175 psia at the flow measurement/control station in the heat exchanger gas outlet line. A 1.5-cu ft K-bottle accumulator was connected into the gas supply line between the regulator outlet and the heat exchanger inlet, servicing the same purpose as previously described for the high-pressure heat exchanger control. The flow measurement and control section in the heat exchanger gas outlet line duplicated that described for the high-pressure heat exchanger.

Instrumentation was provided on both heat exchangers to acquire data on helium and water mass flow rates and pressure and temperature differentials for both the water and gas circuits. The instrumentation functions are listed in Table 15.

## 2. Test Procedures

The cascade feasibility demonstration and heat exchanger test program consisted of the following tests:

- 1) Primary container heat leakage rate;
- 2) Nine-day mission abort sequence;
- 3) 90-day mission abort sequence;
- 4) Nine-day design mission.

The test procedures for each of these tests are described in this subsection.

- a. Primary Container Heat Leak Determination - This initial phase of the program was a determination of the heating rate of the primary storage sphere, combined with an immersion calibration of the gas temperature instrumentation.

With the vacuum chamber pressure at approximately  $10^{-5}$  mm Hg, the primary storage sphere was first filled with liquid nitrogen to obtain an end-to-end calibration of the thermocouple and thermistor data acquisition system at the equilibrium liquid nitrogen boiling condition. The liquid nitrogen was then expelled with helium gas until the sphere wall and gas temperatures indicated that no liquid nitrogen remained in the system.

Following the liquid nitrogen draining, the primary sphere was filled with liquid hydrogen. When the insulation temperatures indicated attainment of equilibrium conditions, the immersed gas temperature instrumentation was calibrated. At this time the liquid hydrogen supply to the primary container was shut off, and the evolving hydrogen gas was routed through the flow measurement system. Flow measurement data and temperatures of the storage sphere and insulation were then recorded at 30-min. intervals for approximately 12 hr. The pressure in the vacuum chamber was between  $10^{-4}$  and  $10^{-5}$  mm HG during the measurement period. The rates of liquid hydrogen mass boil-off were used to calculate the heat leakage rate. Four heat leakage rate runs were made, the first two of which were invalidated by bypass leakage of gas through a perforated burst disc in the  $H_2$  vent system.

- b. Nine-Day Mission Abort Sequence - Prior to conducting this first section of the cascade feasibility and heat exchanger test program, the test fixture was exercised with ambient temperature helium to set the heat exchanger pressure regulators under dynamic conditions, and also to trim the gas flow control orifice verniers for the desired flow rate. In addition, the low-pressure heat exchanger shell pressure drop was determined over a range of water flow rates, with the gas tubing coil removed.

The nine-day mission abort sequence was preceded by a helium loading operation. The primary storage container was first pressurized to approximately 140 psig with ambient temperature helium to prevent possible leakage of air into the system during liquid hydrogen jacket filling. The primary container jacket was then filled, during which time the helium pressure in the storage container decayed to approximately atmospheric pressure. The supply pressure to the primary container helium fill valve (PHFV) was then set at 800 to 1000 psig. Helium fill was initiated by opening PHFV and leaving it open (orificed for 0.1 lb/sec maximum flow rate) until the liquid hydrogen liquid-level light extinguished, indicating that the full-jacket condition was not being maintained, or until the jacket pressure increased to within 10 psi of the liquid hydrogen supply pressure. The PHFV was opened and closed as required to load helium as rapidly as the above liquid-level and jacket-pressure constraints would permit. After approximately 35 min, the rate of acceptance of the primary sphere had attenuated to the point where PHFV was left open and the helium fill proceeded at a constant pressure of 800 to 1000 psig. The jacket was maintained in a filled condition (intermittent level indicator light) by a constant makeup flow of liquid hydrogen. Helium loading was continued until the terminal gas temperature of 36°R was reached.

The cascade storage container was pressurized to the desired loading condition (3500 to 4500 psig, 510°R) at a convenient time during the primary container loading period. When the primary container terminal conditions were reached the helium and liquid hydrogen fill valves were closed, thus completing the loading procedure. The liquid hydrogen supply dewar was weighed on a platform scale ( $\pm 10$  lb) before and after loading, to obtain the liquid hydrogen usage for the loading. An alternative method of topping the liquid hydrogen jacket was developed in the latter

part of the test program, which resulted in a significant reduction in liquid hydrogen usage. This method maintained the liquid hydrogen level even with the top of the storage sphere by monitoring the top jacket wall and sphere wall thermocouples for evidence of intermittent immersion. Maintenance of a gas space in the top of the jacket is believed to have significantly reduced carry-over of liquid into the vent, without adversely affecting helium loading time.

The nine-day mission abort sequence was initiated by emptying the liquid hydrogen from the jacket of the primary storage container. This was accomplished by opening the liquid hydrogen fill line bypass valve (BPV) to the  $H_2$  vent stack and displacing the liquid hydrogen out of the jacket by bleeding 36°R helium gas from the storage sphere into the jacket with the jacket vent valve (VV) closed. The amount of helium bled from the primary container was approximately 0.5% of the mass loaded. The liquid hydrogen displaced from the jacket was back-flowed through the liquid hydrogen fill line, and discharged through BPV to boil off en route to the  $H_2$  vent stack. The use of 36°R helium to pressure drain the jacket caused no significant perturbation to the stabilized jacket, sphere, and gas temperatures.

The nine-day mission abort sequence was run by first establishing rated water flow through the heat exchangers, then opening the gas outflow stop valves (OSV) to initiate a continuous 590-sec gas flow. When the pressure in the primary storage container reached approximately 500 psig, the cascade pressure regulating system was armed to admit pneumatic operating pressure to the regulator valve (RV-3) and to open the C-3 controller sensing line to the cascade gas transfer line. When the primary storage container had decayed to approximately 400 psia (the set-point for the cascade pressure-regulating system), the regulator opened to initiate cascading operation. At the end of the desired 590-sec burn time, the OSV valves were closed to terminate gas outflow. Continuous data recordings of the functions listed in Tables 14 and 15 were made during the burn.

The procedure of initiating water flow through the heat exchangers prior to gas flow was used because the start transient of the water flow system could not be sufficiently predicted to ensure that full water flow would be established in time to prevent a rapid icing condition on the heat exchanger tube coils. The icing condition was shown to cause abnormally low gas temperatures at the heat exchanger gas outlets and, consequently, also at the downstream gas flow control orifice. This condition caused a significant increase in the gas mass flow rate through the system. This condition was considered unacceptable to the performance of a valid cascade system demonstration; therefore, full water flow was verified prior to initiation of gas flow to ensure that the design gas flow rate would be maintained throughout the burn.

- c. 90-Day Mission Abort Sequence - The 90-day mission abort sequence was conducted using the same procedure as that described for the 9-day mission abort sequence, with the exception that the liquid hydrogen jacket was not drained prior to the run.
- d. Nine-Day Design Mission - The nine-day design mission was preceded by a loading sequence as described for the nine-day mission abort sequence. The completion of the loading sequence was designated  $T = 0$  hours for the nine-day design mission, with the primary storage container loaded to design conditions (approximately 875 psig and 35°R) and the cascade container loaded to near-design loading. The mission then proceeded according to the following schedule.

Elapsed Time (hr)	Event
0.0	Start mission (coast)
9.6	Burn for 13.0 sec
17.2	Burn for 13.0 sec
24.8	Burn for 13.0 sec
32.5	Burn for 390.2 sec
34.2	Burn for 20.2 sec
53.6	Burn for 10.2 sec
56.3	Burn for 121.0 sec
68.0	Burn for 3.2 sec
79.6	Burn for 3.2 sec
91.2	Burn for 3.2 sec

This mission duty cycle was based on coast times that were calculated to permit the same amount of primary container gas heating as that predicted for the nine-day design mission with a flight-configuration primary container. Since the test primary container heat leakage rate was approximately 2.4 times greater than the flight container value, the durations of the coast periods were proportionately shorter.

The procedure for conducting coasts was to calibrate and run the data recorders once each hour. The recorders were run for a period of approximately 30 sec each time, after which the recorders were turned off. All data acquisition channels remained activated to eliminate the possibility of warmup drift.

During coast periods, the cascade and primary containers were locked off by closing the RV-3 regulator and HSV valves, respectively, to prevent possible tubing system leaks from invalidating the desired constant stored mass condition. Prior to each burn, the gas outflow system downstream of the HSV primary container outlet stop valve was pressurized with ambient-temperature helium to a level equal to the primary container. Immediately before starting the burn, the PHFV system pressurization valve was closed, and the HSV was opened to place the primary container on the line with the outflow system.

The burns (gas outflow) were initiated by opening the outflow stop valves (OSV). The burns were terminated by closing the HSV valve at the primary container gas outlet. The OSV valves were closed prior to the outflow system prepressurization procedure described above.

Two significant procedural changes were made for nine-day mission Run 2, based on fixture performance observed during Run 1. During Run 1, it was noted that the relatively slow response of the cascade pressure regulator (RV-3) at burn termination was permitting a significant flow of cascade container gas into the primary container after the gas flow out of the primary container had been terminated. In addition, during some of the shorter burns, the expected cascading operation did not occur because of the hysteresis (deadband) and response time of the cascade container outlet pressure regulating system. To alleviate the low response effects, a shutoff valve (CSV) was installed in the cascade container outlet line, immediately upstream of the regulator valve, as shown in Fig. 38. This modification was made prior to nine-day mission Run 2.

The CSV was used in two ways to improve fixture performance. First, it was used to shut off cascade flow sharply at the same time that primary flow was shut off (simultaneous closure of CSV and HSV). Second, prior to the short burns (8 and 9, lasting 3.2 sec) that required cascading, the CSV was first opened momentarily to provide cascade gas flow until the primary gas pressure increased to a value slightly above the cascade pressure regulator setting. With the CSV closed, the regulator valve (RV-3) subsequently closed under a zero cascade flow condition. The short burn was then conducted with no cascade flow, since the cascading operation had been conducted separately just prior to the burn. During the performance of both nine-day mission runs, full flow of water was verified through the heat exchangers prior to initiation of gas flow, for the reasons given under procedures for the nine-day mission abort sequence. In addition as an extra precaution against the adverse conditions caused by heat exchanger icing, the maximum available water flow rate of 240 to 260 gpm was used instead of the design flow rate of 115 gpm.

### 3. Analysis and Evaluation of Results

Pretest and posttest analyses were conducted during the feasibility demonstration of the cascade pressurization system concept. The purpose of the analyses was to evaluate the analytical models and techniques used in Phase I. The pretest and posttest method of analysis is described for the pressurant loading demonstration, heat exchanger demonstration and pressurant storage, and expansion concept demonstration. Evaluation and comparison of the test results and analytical results were made and are discussed in this subsection.

- a. Pressurant Loading Demonstration - The primary tank pressurant loading procedure was demonstrated prior to and in conjunction with the pressurant storage feasibility tests. The helium loading procedure established the time required to load the test pressurant storage container. This time included the time required to accomplish the following functions:

- 1) Precooling the system;
- 2) Loading the required mass of pressurant to the specified conditions.

Pretest and posttest analyses were conducted to determine the loading accuracy and the accuracy of the analytical model used to establish the recommended loading procedure in the liquid hydrogen range. These pretest and posttest analyses and an evaluation and comparison of the test results are discussed in the following paragraphs.

Pretest Analysis - The helium loading pretest analysis was conducted for the as-designed test system. The anticipated initial conditions in the primary container were 500°F and 12 psia for the helium temperature and pressure, respectively. The final loaded condition for this analysis was 37°R and 816 psia for the helium temperature and pressure, respectively, and a helium loaded mass of 68.3 lb<sub>m</sub>. The helium supply temperature and pressure of 500°R and 1500 psia was assumed for this analysis. The ambient temperature was anticipated to be 500°R. This analysis involved calculating the time required for sphere and jacket chill down and for loading helium to the specified initial conditions.

The sphere and jacket chilldown analysis assumed a maximum liquid hydrogen usage, i.e., the heat extracted from the sphere and jacket went only into boiloff of hydrogen with no sensible heat going into gaseous hydrogen. The assumption was made because of the relatively high maximum liquid hydrogen flow rate of 0.3 lb<sub>m</sub>/sec. This maximum flow rate was calculated as the maximum hydrogen flow rate through the vent system and at a maximum allowable jacket pressure of 40 psia. The required chilldown time was determined by calculating the total mass of the primary tank assembly and then calculating the mass of liquid hydrogen required to reduce the temperature of this mass from ambient to 37°R. The required mass of liquid hydrogen was then divided by the maximum liquid hydrogen mass flow rate of 0.3 lb<sub>m</sub>/sec.

An IBM 7094 computer program\* was used to conduct the helium loading pretest analysis. This analysis assumed that the system chilldown had been completed. The helium loading pretest analysis established a helium loading rate for the test system. The helium loading rate was established by analyzing the loading operation at several helium flow rates and then determining which flow rate gave the most desirable loading performance. Evaluation of the loading performance centered about the following three parameters:

---

\*Martin-CR-66-39. op. cit.

- 1) Maximum helium temperature obtained during the loading operation;
- 2) The time required for loading;
- 3) The total liquid hydrogen boiloff during loading.

Posttest Analysis - An adequate posttest analysis to recalculate the system chilldown could not be performed. This analysis was not conducted because instrumentation was not available to monitor the liquid hydrogen mass flow rates during the liquid hydrogen fill operations. These actual liquid hydrogen mass flow rates were necessary to calculate a system chilldown time. Therefore the precool pretest analysis was used in comparison with test results.

The helium loading posttest analysis was conducted using the loading computer program, and the following were used as input parameters:

- 1) The helium temperature and pressure were 500°R and 12 psia, respectively, prior to the start of chilldown;
- 2) The helium mass loading rate was 0.1 lb<sub>m</sub> sec;
- 3) The regulator setting was 875 psia;
- 4) The regulator tolerance was  $\pm 20$  psi;
- 5) The loaded helium mass was 74.5 lb<sub>m</sub>;
- 6) Final temperature tolerance was +0.5°R;
- 7) Liquid hydrogen temperature was 35°R;
- 8) Helium supply temperature was 500°R;
- 9) Ambient temperature was 500°R.

The loading procedure followed in the posttest analysis used a constant helium loading rate. The analysis also assumed that the heat extracted from the loaded helium went directly into vaporization of the liquid hydrogen. It was assumed that the liquid hydrogen jacket was always full and that both the liquid hydrogen and container wall were at a constant temperature of 35°R. At the start of the loading operation, helium was loaded at a constant rate

until the helium pressure reached the upper limit of the pressure regulator setting. Helium flow was then stopped, and the pressure was allowed to decrease to the lower limit of the regulator setting. This loading process continued until the required amount of helium was loaded into the container. When the required helium loaded mass was obtained, the helium temperature was allowed to decrease until it was within the temperature tolerance set for the required final helium temperature ( $35.5^{\circ}\text{R}$ ). At this point the loading operation was considered to be complete.

Evaluation and Comparison of Results - In pretest analysis, the time required for system chilldown was calculated to be approximately 5 min, and the predicted liquid hydrogen usage (liquid hydrogen boiled off) was  $63 \text{ lb}_m$ . This calculated time was for a maximum liquid hydrogen flow rate of  $0.3 \text{ lb}_m/\text{sec}$  and would therefore give a minimum time required for system chilldown.

The results of the helium loading analysis are presented in a plot of the three parameters discussed above as a function of helium loading rate. The analysis was conducted for four helium loading rates -- 0.30, 0.20, 0.15, and  $0.10 \text{ lb}_m/\text{sec}$ . The loading rates were selected because the values would keep helium temperatures below  $1000^{\circ}\text{R}$  and still obtain a reasonable loading time. These results are presented in Fig. 46, thru 48. After examination of these results, the most desirable loading rate was determined to be  $0.10 \text{ lb}_m/\text{sec}$ . This loading rate resulted in the lowest maximum temperature and liquid hydrogen usage. However, the loading time is only 9.5% greater than the loading time at a loading rate of  $0.30 \text{ lb}_m/\text{sec}$ .

The system chilldown times measured during four tests are shown in Table 16. The times measured in the last three tests listed in Table 16 show good agreement. These three times were approximately four times larger than the chilldown time of 5 min calculated in the pretest analysis.

The times required to load helium to liquid hydrogen temperatures are shown in Table 17 for the pretest analysis, posttest analysis, and also four test runs. This table also shows the final loaded conditions for each loading run. It was necessary to conduct only one posttest analysis for comparison with the four test data points. The reason for this is the similarity of initial conditions for the test runs.

The analytical results of the pretest and posttest analyses were not consistent. The posttest analysis calculated a shorter loading time than the pretest analysis even though more mass was loaded. This time difference was probably due to the higher loaded pressure obtained and the large pressure regulator tolerance. There were also inconsistencies observed in the test results. It was possible that the inconsistencies could be attributed to human factor deviations resulting from the loading procedure that was followed (see Subsection 2). The results of the posttest analysis, Run 2, did not agree with either of the nine- or 90-day mission abort test Run 1. It was possible that the disagreement was due to the large pressure regulator tolerance used in the analytical simulation.

A comparison of analytical and test values of liquid hydrogen usage for primary tank loading is shown in Table 18. The values included the hydrogen used for system chilldown as well as that used for loading the helium. Only two points were analyzed, because the loaded conditions for all the runs were very close to one or the other of those two conditions. There is considerable difference in predicted and actual values of hydrogen usage. This difference was expected, due to the nature of the mathematical model used and the fact that the loading process was completely manually controlled. The mathematical model considered only the hydrogen usage due to cooling the helium and heat leak into the primary tank; the effects of heat leak into the liquid hydrogen transfer line and liquid loss through the vent line were excluded from the calculations. It is significant that the hydrogen usage for the two nine-day mission runs was approximately half of the usage for the previous runs. This was due to the variation in loading procedure discussed in Subsection 2.b. An automatic loading process could probably be more repeatable and also more efficient.

Loading Accuracy at Liquid Hydrogen Temperature - An evaluation of the accuracy with which a specified mass of helium can be loaded into the primary tank at liquid hydrogen temperature was performed.

Figure 49 illustrates the mass of helium in the primary storage container as a function of temperature and pressure. The Apollo SPS design loading of 68.3 lb<sub>m</sub> was established as the desired primary tank load for the feasibility test program. The loaded helium should attain an equilibrium temperature equal to the boiling point of hydrogen, which was 35.0 to 35.1°R at the Denver test site; the atmospheric pressure during all loading exercises was 11.75±0.1 psia. This would indicate that the initial primary tank pressure should be 760 psia. Prior to testing, the effect of temperature stratification within the liquid hydrogen (and in the helium) on the accuracy of attaining a uniform equilibrium temperature was unknown. It was, therefore, necessary to consider a temperature tolerance in the selection of the initial helium pressure. A tolerance of 4°R was considered reasonable for these tests, since there was only one thermistor measuring temperature to ± 1°R and the nine thermocouples throughout the tank were accurate to only ± 5°R. Considering an initial maximum possible temperature of 39°R, a pressure of 875 psia was established to ensure a minimum initial helium mass of 68.3 lb<sub>m</sub> in the primary tank. In observing Figure 49, it is noted that if the tank is accurately loaded at a uniform equilibrium temperature of 35°R and a pressure of 875 psia, it will contain 74.5 lb<sub>m</sub> of helium.

In studying the reduced data from the primary tank thermocouple array, no indications of stratification were observed at the loaded condition for any of the six test runs. Therefore, the helium temperature indicated by the centrally located thermistor -- the most accurate temperature sensor in the primary tank at ± 1°R -- was in fact representative of the entire helium mass in the tank. Table 19 summarizes the measured primary tank loaded conditions for each test run. The mass loaded was referenced to 74.5 lb<sub>m</sub> to obtain the

loading inaccuracy. Note that the temperature tolerance is given as  $\pm 1$  rather than  $\pm 1$ ; this reflects the fact that the actual helium temperatures could not have been below the hydrogen boiling point of 35°R, since the hydrogen jacket was vented to the atmosphere. Therefore, the thermistor must

have, at all times, operated in the lower half of its tolerance band. The columns designated as nominal in Table 19 illustrate the loaded mass and loading inaccuracy as derived from the measured temperature and pressure values, disregarding the instrumentation tolerances. The upper and lower limits for helium mass loaded were then calculated, considering the possible temperature and pressure extremes as dictated by the tolerances. The minimum temperature considered was 35.0°R, which was the minimum possible hydrogen boiling point encountered during testing. The loading inaccuracies which included instrumentation tolerances were determined by comparing the maximum deviation of helium mass loaded to the reference value of 74.5 lb<sub>m</sub>. The average inaccuracy values were calculated as the arithmetic mean of the absolute values for each run.

It is noted that the initial pressures were 10 to 42 psia greater than the desired value of 875 psia. Inability to establish the initial pressure more closely to the specified value was due to the relatively insensitive direct readout provided. The primary tank pressure signal was set up on a multichannel Sanborn Recorder, with a sensitivity of 40 psia per mm of stylus deflection. Provision of a more sensitive direct pressure readout capability will permit the initial tank pressure to be established more accurately, and will therefore result in better overall loading accuracies.

- b. Heat Exchanger Performance - Heat exchanger tests were conducted in conjunction with the cascade system feasibility tests to determine:
- 1) Heat exchanger performance characteristics at liquid hydrogen temperature;
  - 2) The extent of propellant freezing;
  - 3) The accuracy of the pressure drop and thermal analyses on both the pressurant and propellant side of the heat exchanger.

These tests were conducted with one heat exchanger located upstream and another heat exchanger located downstream of the pressure regulation equipment. Demineralized water was used to simulate the propellant during these tests. Pretest and posttest analyses were conducted to determine the accuracy of the analytical techniques used in Phase I at the liquid hydrogen temperature region. These pre- and post-test analyses are discussed in the following paragraphs together with an evaluation and comparison of the test results.

Heat Exchanger Pretest Analysis - This analysis was conducted to predict the performance of two high and low-pressure test heat exchangers. The two heat exchanger configurations are identical. Each configuration consists of a 19.5-ft-long coiled tube (0.5-in. outside diameter by 0.049-in. 304 stainless steel). The mean coil diameter is 4.75 in., and the shell inside diameter is 6.357 in.

An IBM 7094 computer program\* was used to conduct the pretest analysis. The performance of both high and low-pressure heat exchangers was evaluated at a constant helium inlet temperature of 37°R. The inlet temperature of the demineralized water was assumed to be constant at 500°R for both high- and low-pressure heat exchangers. The mass flow rate of the water was 16 lb<sub>m</sub>/sec, and the helium mass flow rate was constant at 0.0579 lb<sub>m</sub>/sec. The performance of the low-pressure heat exchanger was evaluated for an exit pressure heat exchanger was evaluated for an exit pressure of 175 psia. The high-pressure heat exchanger performance was evaluated for helium inlet pressures of 400 psia to 1200 psia. This pressure range corresponds to the operating pressure region that was predicted for the primary sphere.

---

\*Martin-CR-66-39. op. cit.

Heat Exchanger Posttest Analysis - This analysis was conducted to simulate the performance of the high- and low-pressure test heat exchangers during three of the test mission profiles. The three test mission profiles were the nine-day abort, test Runs 1 and 2, and 90-day abort, test Run 2. The 90-day abort test Run 1 was not simulated due to incomplete test data.

The heat exchanger tests were simulated by using the test data as input parameters to the analytical model. The following test data were used as input parameters:

Helium inlet temperature;

Helium mass flow rate;

Helium exit pressure;

Water inlet temperature;

Water mass flow rate.

The test heat exchanger configuration was also a program input. The following parameters were calculated by the computer program:

Helium outlet temperature;

Helium pressure drop;

Water outlet temperature;

Water pressure drop.

These calculated parameters were then compared with the corresponding test data parameters as a function of mission time for both high- and low-pressure heat exchangers and for each of the three abort missions.

Evaluation and Comparison of Results - The results of the pretest analysis for both high- and low-pressure heat exchangers are shown in Fig. 50, 51, and 52. A comparison of the results of the pretest analysis and the test results could not be made since some of the anticipated heat exchanger inlet conditions were not of the same magnitude as the actual test inlet conditions. The actual helium inlet temperatures ranged from 100 to 230°R during most of the

tests, as compared to the assumed helium inlet temperature of 37°R. This difference was due to the helium warming after leaving the primary container and before entering the heat exchanger. The actual water mass flow rate ranged from 33.92 to 36.43 lb<sub>m</sub>/sec as compared to the assumed water mass flow rate of 16 lb<sub>m</sub>/sec. The water mass flow rate was increased from the anticipated value to the actual value to reduce or eliminate the freezing problem that was encountered during the initial test runs. The actual water inlet temperature ranged from 509 to 513°R compared with the anticipated inlet temperature of 500°R. The anticipated helium mass flow rate was 0.0579 lb<sub>m</sub>/sec. The actual helium mass flow rates ranged from 0.0557 to 0.0646 lb<sub>m</sub>/sec.

The results of both high- and low-pressure heat exchanger tests and posttest analyses are presented in Fig. 53a, 53b, 54a, 54b, 55a, 55b, 56a, 56b, 57a, 57b, 58a, and 58b for each of the three test missions. These figures show plots of the calculated and test values for helium outlet temperature, helium pressure drop, and water pressure drop. The water outlet temperatures were not plotted since there was less than 0.5°R deviation during the entire test mission. Instead the arithmetic average for both the calculated and test values are given. The helium outlet pressures and inlet temperatures are also plotted as a function of test mission time.

The deviation between the calculated and test values for helium outlet temperatures varied. Initially the deviations were small and then increased with time for all the high- and low-pressure heat exchanger tests. The calculated helium outlet temperatures were in every case nearly constant whereas the test helium outlet temperatures decreased with time in every test run. This decrease was due to the heat exchanger localized freezing. The heat exchanger freezing was verified by films taken during each test. In general the comparison between the calculated and test helium outlet temperatures was favorable considering that the computer program cannot simulate the freezing that occurred during the tests.

The calculated and test helium pressure drop results did not compare as favorably as the helium outlet temperature comparison. The deviation between the calculated and test pressure drop values was large and inconsistent for every

test run except one -- the low-pressure heat exchanger for 90-day mission abort Run 2. In general the actual helium pressure drop was less than the analysis predicted. The inaccuracy of the helium pressure drop calculation could be due to the analytical techniques used in the heat exchanger computer program. The computer program calculates the helium pressure drop at the mean helium conditions, i.e., the log mean helium temperature and average pressure of the inlet and outlet conditions. A more accurate technique would be to divide the heat exchanger into small segments and calculate the pressure drop across each segment and sum these pressure drop values over the total length of the heat exchanger.

The results of the calculated and test values for the water outlet temperatures compared very favorably. The average water outlet temperatures were used for the comparison since both the calculated and test water outlet temperatures were approximately constant throughout each test run. In all cases the water temperature drop, both calculated and test values, was never greater than  $1^{\circ}\text{R}$ , and the deviation between the calculated and test values was very small.

The deviation between the calculated and test water pressure drop was very consistent in all test cases. The test water pressure drop was approximately 10 psid, and the calculated pressure drop was approximately 2.5 psi below the test values. The computer program considered water pressure drop due to the shell inlet and outlet and the heat exchanger coils. The model did not account for the heat exchanger center body that was located inside the heat exchanger coil to reduce the heat exchanger freezing (see Subsection 1). Figure 59 illustrates the results of water flow tests performed on one heat exchanger, and shows that approximately 1 to 1.2 psi pressure drop was due to the heat exchanger center body. By subtracting this amount from the test water pressure drop values, the comparison between the calculated and test results becomes more favorable. It is noted in Fig. 59 that three of the data points for the heat exchanger without the center body fall slightly below those for the shell-only configuration. This discrepancy is due to normal scatter of the test data and illustrates that the helium coil has insignificant effect on the liquid side pressure drop.

- c. Pressurant Storage and Expansion Concept Demonstration - Tests were conducted to demonstrate the feasibility of the cascade pressurant storage and expulsion concept. These tests were conducted for the following simulated mission duty cycles:

The nominal nine-day mission duty cycle;

The nine-day mission abort operation (continuous 590-sec burn);

The 90-day mission abort operation (continuous 590-sec burn with full liquid hydrogen jacket.)

The tests were conducted with a preprototype system, and the mission duty cycle was so simulated that the total amount of heat transferred to the primary storage container during the simulated coast periods was equal to the predicted heat transfer during the actual coast periods. The burn periods were simulated in real time. Pretest and posttest analyses were conducted to determine the accuracy of the analytical techniques and models used in Phase I. An evaluation and comparison of the analytical results with the test results was conducted to establish the following:

Cascade helium usage;

Primary and cascade helium residuals;

Helium pressure and temperature histories for both the primary and cascade containers;

Temperature histories for both the primary and cascade storage containers.

Prior to initiation of feasibility tests, the actual heat leak into the primary storage container was determined. The method of measurement was discussed in Subsections 1 and 2. Two test runs were performed, resulting in heat leak rates of 31 and 32 Btu/hr. These two figures were averaged to 31.5 Btu/hr for the measured rate. This compares favorably with a pretest calculated rate of 27 Btu/hr. Using the value of 31.5 Btu/hr for the primary tank heat leak, the effective thermal conductivity of the installed NRC-2 superinsulation was analytically deduced to be  $1.12 \times 10^{-4}$  Btu/hr-ft-°R.

This subsection describes pertinent analysis and evaluation of remaining test results.

Pretest Analysis - The pretest analysis consisted of simulating the helium expansion processes of both the primary and cascade storage containers for the nine-day abort, 90-day abort, and nine-day design missions. This analysis was performed for a primary container heat leak of 31.5 Btu/hr, which corresponds to the average of the heat leak rates, 31 and 32 Btu/hr, that were measured in the heat leak calibration tests for the actual test system configuration. The initial helium temperature and pressure in the primary container were 35°R and 875 psia, respectively, for the three missions. The helium loaded mass was calculated to be 74.5 lb<sub>m</sub> for the initial conditions and test sphere volume. The initial helium temperature corresponds to the saturation temperature for liquid hydrogen at Denver ambient pressure. The initial helium pressure was the pressure in the primary sphere for the minimum allowable helium loaded mass of 68.3 lb<sub>m</sub> and a temperature of 39°R. This initial pressure allowed for a 4°R uncertainty in the helium temperature measurements with assurance of attaining the minimum allowable helium loaded mass. The initial helium temperature and pressure in the cascade container were 520°R (anticipated ambient temperature) and 4354 psia, respectively, for the three missions. The cascade helium loaded mass was calculated to be 10.45 lb<sub>m</sub> for the initial conditions and cascade test sphere volume. The initial pressure corresponds to the pressure obtained from an adiabatic wall expansion in the cascade container to a minimum pressure of 450 psia and for a helium-expelled mass of 9.25 lb<sub>m</sub>. This helium-expelled mass corresponds to the helium usage obtained for a nine-day mission abort with the primary container at 37°R and 816 psia initial conditions and a heat leak of 27 Btu/hr. The 27 Btu/hr heat leak was the initial predicted heat leak for the test system configuration. The pretest analysis for each mission is discussed in the following paragraphs.

Nine-Day Mission Abort - The abort operation for the nine-day design mission was simulated by a single 590.2-sec helium expansion from the primary container, commencing with an empty liquid hydrogen jacket. This simulation also used a minimum primary container pressure of 400 psia and assumed a cascade helium entering temperature of 450°R. The primary helium mass flow rate was 0.1157 lb<sub>m</sub>/sec. This helium mass flow rate was considered constant and was determined by dividing the minimum allowable helium loaded mass by the helium outflow time of 590.2 sec. The primary container expansion process was simulated by using the cascade pressurization computer program.

After reviewing the results of the primary sphere pretest analysis, the cascade pretest analysis was initiated. The cascade container expansion for the nine-day mission abort was simulated by a single 437.2-sec adiabatic expansion. This adiabatic expansion began at the initial conditions previously discussed. The cascade helium flow rate was assumed to be constant at  $0.0153 \text{ lb}_m/\text{sec}$ . This flow rate was calculated by dividing the cascade helium usage by the total helium outflow time both of which were determined in the primary container pretest analysis. An adiabatic wall expansion was assumed in this pretest analysis. This expansion process was simulated by using the helium expansion computer program\*.

90-Day Mission Abort - The abort operation for the 90-day lunar polar orbit mission was simulated by a single 590.2-sec expansion from the primary container commencing with a full liquid hydrogen jacket. The initial conditions in the primary tank were identical to the nine-day mission abort. The helium mass flow rate and cascade helium entering temperature were also the same values used in the nine-day mission abort.

To simulate this mission with the existing cascade pressurization computer program, two types of helium expansion processes were assumed. The first expansion process was for an isothermal wall at liquid hydrogen temperature. The second expansion process was adiabatic with respect to the helium. The mission was simulated for both assumed expansion processes, and the results were compared. For the first and second assumed expansion process, the cascade helium usage was  $9.25 \text{ lb}_m$  and  $16.02 \text{ lb}_m$ , respectively. Because of this large variation in helium usage, a great degree of uncertainty existed as to which of the assumed expansion processes best simulated the actual process, and the possibility of obtaining a significant error with either assumption, or both was greatly increased.

To simulate the actual expansion process more accurately, it became necessary to investigate the heat transfer between the sphere wall and the liquid hydrogen. After reviewing several technical publications dealing with heat transfer to boiling liquid, an empirical equation that described the nucleate pool boiling phenomena was selected†.

---

\*Martin-CR-66-39. op. cit.

†E. G. Brentari, P. J. Giarranano, and R. V. Smith: Boiling Heat Transfer for Oxygen, Nitrogen, Hydrogen, and Helium. National Bureau of Standards Technical Note 317. U.S. Government Printing Office, Washington, D.C., 1965.

This equation described the nucleate pool boiling heat transfer coefficient as:

$$h_{\text{Nuc}} = 8.54 \times 10^{-10} \left[ \frac{(C_p)_\ell}{\lambda \rho_v} \right]^{1.5} \left[ \frac{(k_\ell)(\rho_\ell)^{1.28}(P)^{1.75}}{(\sigma^{0.906})(\mu_\ell)^{0.626}} \right] (\Delta T)^{1.5},$$

where

$h_{\text{Nuc}}$  = nucleate pool boiling heat transfer coefficient  
(watts / cm<sup>2</sup> °K);

$(C_p)_\ell$  = liquid specific heat capacity at constant pressure  
(joules/g °K);

$\lambda$  = latent heat of vaporization at saturation (joules/g);

$\rho_v$  = vapor density (g / cm<sup>3</sup>);

$\rho_\ell$  = liquid density (g / cm<sup>3</sup>);

$k_\ell$  = liquid thermal conductivity (watts/cm °K);

$P$  = pressure of the boiling system (dynes / cm<sup>2</sup>);

$\sigma$  = surface tension between the liquid and its own vapor, evaluated at T (dynes/cm);

$\mu_\ell$  = Newtonian viscosity of the liquid (g/cm-sec);

$\Delta T$  = temperature difference between wall and liquid (°K).

This equation was programed into the existing cascade pressurization computer program. The computer program was also modified to calculate inside and outside wall temperatures whenever the jacket was full of liquid hydrogen. This change became necessary because of the high temperature gradient that exists across the sphere wall, during the 90-day mission abort.

The cascade container pretest analysis was initiated after completion of the primary container pretest analysis. Again it was assumed that the expansion was adiabatic with respect to the sphere wall. The initial conditions were the same as the cascade container conditions used in the nine-day abort. From the results of the primary container pretest analysis, the cascade helium outflow time was determined to be 425.2 sec and the helium mass flow rate was 0.0179 lb<sub>m</sub> sec. The helium expansion computer program was used to simulate the cascade container expansion process.

Nine-Day Design Mission - The initial conditions, helium outflow rates, minimum pressure, and cascade helium entering temperature that were used in the two previous analyses were also used in this analysis. This analysis assumed that the helium and wall temperatures reached a thermal equilibrium during each coast period. The analysis also assumed instantaneous mixing between the helium in the primary sphere and the cascade helium entering the primary sphere. The effective thermal conductivity used for the sphere insulation was  $1.12 \times 10^{-4}$  Btu/hr-ft-°R. This value was determined from the heat leak calibration tests. The cascade pressurization computer program was used to simulate the nine-day mission.

The cascade container pretest analysis for the nine-day design mission was performed by using the helium expansion computer program. This cascade container pretest analysis assumed an adiabatic external wall and that the helium and wall temperature reached a thermal equilibrium condition during each coast period. The cascade helium outflow times and mass outflow rates for this pretest analysis were established in the primary container pretest analysis. The initial conditions in the cascade container were the same as the initial conditions in the two previous cascade container pretest analysis.

Posttest Analysis - The posttest analysis consisted of simulating the test runs that were conducted to demonstrate the cascade pressurant storage and expansion concept. Posttest analyses were conducted for six test runs, two test runs for each of the three simulated mission duty cycles previously described. These posttest analyses were conducted by first simulating the primary container expansion tests, and then, after reviewing those results, simulating the cascade using the results of the primary container posttest analysis.

This method of analysis was also followed in the pretest analysis. In the posttest analysis, however, the actual test initial conditions, burn times, and insulation surface temperatures were used.

The basic analytical assumptions made in these analyses were identical to the assumptions made in the pretest analyses and other previous analyses. These analyses assumed that instantaneous mixing occurred between the cascade helium entering and the helium in the primary container. The posttest analyses did not consider helium stratification in either container. The helium mass outflow rates were assumed constant in both the primary and cascade containers. No tolerances were included in the pressure regulator setting in the primary container. The heat transfer between helium and container wall was considered to be natural free convection in both the primary and cascade containers. The cascade container expansion process was assumed to be adiabatic with respect to the container wall external surface. The heat transferred through the primary container insulation, supports and lines was assumed to be transferred directly into the pressure vessel and helium. During the simulated coast periods, the helium and container wall were assumed to reach a thermal equilibrium condition in both containers. The cascade helium flow rate entering the primary container was assumed to be constant.

The actual test initial conditions were obtained by establishing from the test data an initial helium pressure and temperature and container wall temperature. The initial helium temperature was taken from the thermistor temperature reading since the thermistor measurement was considered the more accurate of all the temperature measurements. The initial container wall temperature was determined from thermocouple measurements.

The average value (as a function of time) of the four actual outside insulation temperatures was used to calculate the heat leak rates through the insulation. The maximum spread in the four temperatures was typically less than 6°R, although the spread did increase to about 40°R during the ninth and tenth burns. The same average temperature was used to calculate heat leak rates through the tank supports and lines since the structure temperatures were not recorded. The insulation effective thermal conductivity was  $1.12 \times 10^{-4}$  Btu/hr-ft-°R, which was determined for the test system configuration during the heat leak calibration tests.

In simulating the primary container test runs, the most critical test parameter was the helium mass outflow rate. Slight variations in the helium mass flow rates made significant variations in calculated parameters, particularly in the cascade helium usage. For the nine-day and 90-day test simulation runs, the actual flow rate history was integrated, and the result divided by the outflow time to obtain the average value. The cascade helium flow rates used for the cascade container expansion simulation were established using the same method followed in the pretest analysis.

The posttest analyses considered the temperature of the cascade helium entering the primary container to be the average of the maximum and minimum temperatures measured in the cascade container during each test run. This consideration was consistent with previous analytical evaluations. These analyses also considered the regulated helium pressure to be the average of all the test helium pressures obtained after the start of cascade helium flow. The pressure undershoot due to the slow regulator response was not included in the average regulated pressure value.

More detailed discussion of the posttest analyses for each of the simulated duty cycles are discussed in the following paragraphs. Included in the discussions are the initial conditions and other input parameters used to simulate each test run.

Nine-Day Mission Abort - Posttest analyses were conducted for the primary container using the cascade pressurization computer program to simulate the primary container expansion process for the two test runs, Run 1 and Run 2. Run 1 had an initial primary helium pressure of 917 psia and an initial helium and container wall temperatures of 34.6°R and 53°R, respectively. The integrated helium mass flow rate was calculated to be 0.12035 lb<sub>m</sub>/sec. The average regulated pressure after start of cascade helium flow was 422 psia. The average cascade helium inlet temperature was 498°R. The initial primary container conditions used in the simulation of test Run 2 were 894 psia for helium pressure and 34.4°R and 40.5°R for helium and wall temperatures, respectively. The integrated helium mass flow rate for Run 2 was 0.11949 lb<sub>m</sub>/sec. The average regulated

helium pressure after the start of cascade helium flow was 417 psia. The average cascade helium inlet temperature was 501°R. The outside insulation surface temperatures were 530°R and 519°R for Run 1 and Run 2, respectively.

After reviewing the results of the primary container posttest analysis, the cascade container posttest analysis was conducted using the helium expansion computer program. From the results of the primary container posttest analysis, the cascade helium usage and outflow time were established for each test run. The cascade helium mass outflow was calculated by dividing the helium usage by the total outflow time. This same analytical technique was used in the pretest analysis. These helium mass outflow rates were 0.0150 and 0.0155 lb<sub>m</sub>/sec for Run 1 and Run 2, respectively. The initial conditions in the cascade container were 4448 psia helium pressure and 527°R helium and wall temperatures for Run 1. Run 2 had initial conditions of 4341 psia helium pressure and 527°R helium and wall temperature.

90-Day Mission Abort - For the two 90-day mission abort test runs conducted, primary container posttest analyses were performed using the cascade pressurization computer program with the program modifications previously discussed. Other assumptions particular to this type mission that were discussed in the pretest analysis were also used in the posttest analysis.

The initial conditions in the primary container were 907 psia helium pressure and 34.2°R helium and wall temperature for Run 1. The integrated helium mass flow rate for Run 1 was 0.1198 lb<sub>m</sub>/sec, and the total burn time was 600 sec. The cascade helium entering temperature was 450°R in Run 1, and the pressure regulator setting was 424 psia.

For the second 90-day mission abort test run, the initial conditions were 895 psia helium pressure and 34.45°R helium and wall temperature in the primary container. This test run also had a 600-sec burn, and the integrated helium mass outflow was 0.11814 lb<sub>m</sub>/sec. The cascade helium entering temperature was 495°R, and the regulator setting was 428 psia. A liquid hydrogen temperature of 35°R was used in the simulation of both runs.

After completion of the primary container posttest analysis, the cascade container posttest analysis was initiated to simulate the expansion process from the cascade container into the primary container. From the results of the primary container posttest analysis, the cascade helium usage and outflow times were established. Cascade helium flow rates were established for each burn during which cascade helium was expelled. This was done in the same manner as previously discussed. The cascade helium usage and outflow times for these analyses are presented and discussed under Evaluation and Comparison of Results.

The cascade container initial conditions for the first test run were 4521 psia helium pressure and 515.5°R helium and container wall temperature. The second test run had cascade container initial conditions of 3541 psia helium pressure, 510°R helium temperature, and 509°R wall temperature.

Evaluation and Comparison of Results - Evaluation and comparison of the pretest and posttest analytical results with the test results were conducted to determine the accuracy of the analytical techniques and computer programs used in Phase I. The calculated and test pressure and temperature histories for both the primary and cascade helium were compared. The same comparison was made for the container wall temperature histories of both containers. Primary and cascade helium residuals and cascade helium usage requirements were also compared. The three simulated mission duty cycles were evaluated and compared and are discussed in the following paragraphs.

Nine-Day Mission Abort - The results of the primary container pretest analysis are presented as helium pressure and temperature histories and the temperature history of the container wall. These pressure and temperature history curves are shown in Fig. 60a and 60b. The curves show that cascade helium flow begins 153 sec after start of primary helium flow. The helium and sphere wall temperature histories were approximately identical until about 300 sec after start of mission. At this time the helium temperature began to increase at a faster rate up to a final maximum temperature of 112°R. The final maximum sphere wall temperature was 96.5°R. The cascade helium usage for this analysis was 6.68 lb<sub>m</sub>. The total helium residual in the primary container was 12.9 lb<sub>m</sub>.

After the primary container posttest analysis was completed the cascade container posttest analysis was performed. Identical steps used in the previous pretest and posttest analysis for determining cascade helium flow rates were followed after establishing cascade helium usage and total outflow times. The cascade helium outflow rates for Run 1 and Run 2 were 0.01926 and 0.01789 lb<sub>m</sub> sec, respectively.

The initial conditions in the cascade container for the first run were 4361 psia helium pressure and 489°R helium and wall temperature. The second run had an initial helium pressure of 4319 psia and a helium and wall temperature of 523°R.

Nine-Day Mission - The posttest analyses were conducted after the completion of two test runs that simulated the nine-day mission duty cycle. These analyses were conducted using the same method of analysis and the computer programs that were used in the pretest analysis. The difference between the pretest and posttest analyses was that actual test conditions were used as input parameters in the posttest analysis, and, in the pretest analysis, the anticipated values were used.

Primary container expansion posttest analysis was conducted to simulate the two test runs. The same coast periods used in the pretest analysis were used. The burn duration times and corresponding helium flow rates for both test runs are shown in Table 20.

The initial conditions in the primary container for Run 1 were 885 psia helium pressure, 35°R helium temperature, and 30°R container wall temperature. The cascade helium entering temperature was 483°R, and the regulator setting was 428 psia. Insulation outside surface temperatures varied throughout the run from a minimum of 496 to 519°R.

For the second test run, the initial conditions in the primary container were 896 psia helium pressure, 34.8°R helium temperature, and 38.5°R wall temperature. A cascade entering temperature of 497°R was used, and the pressure regulator setting was 430 psia. The measured outside insulation surface temperatures varied from a minimum of 498 to a maximum of 513°R.

The results of the cascade container pretest analysis are presented for the same temperature and pressure histories that were presented in the primary container pretest analysis. The cascade sphere pressure and temperature history curves are shown in Fig. 61a and 61b. The curves show all parameters are constant until the start of cascade flow at  $T + 153$  sec. At this time both the helium pressure and temperature dropped to final values of 1260 psia and  $465^{\circ}\text{R}$ , respectively. The wall temperature shows a more gradual drop in temperature from its initial value to  $509^{\circ}\text{R}$ . This wall temperature drop was gradual because of the large cascade container mass of  $1240 \text{ lb}_m$ . The helium residual in the cascade container was approximately  $3.8 \text{ lb}_m$ .

The results of the primary container tests and posttest analyses for Runs 1 and 2 are shown in helium pressure, helium temperature, and container wall temperature history curves, Fig. 62a, 62b, 64a, and 64b. Table 21 shows the test and analytical results of the cascade helium usage and residuals of the primary container in both test runs.

The pressure history curves show that cascade helium flow began at  $T + 159$  sec for Run 1 and  $T + 157$  sec for Run 2. The calculated cascade flow start times were  $T + 151$  sec and  $T + 146$  sec for Runs 1 and 2, respectively. The pressure histories were similar with the exception of the pressure undershoot seen in the test pressure history. This pressure undershoot was due to the slow response time of the test regulator and accounts for the large deviation in the cascade flow start times. If the pressure undershoot had not occurred the cascade flow start times would have been  $T + 148$  sec and  $T + 142$  sec for Runs 1 and 2, respectively. Neglecting the pressure undershoot, the maximum deviations between the test and calculated helium pressure were approximately 3.5% and 2.5% for Runs 1 and 2, respectively.

The calculated and test helium temperature histories were similar until about  $T + 200$  sec in both runs. At this point the deviations between the calculated and test helium temperatures became significant. It should be pointed out that each test helium temperature point was a corrected average of nine out of the ten temperature measurements obtained; one temperature was consistently 50 to  $60^{\circ}\text{R}$  higher

than the nine other measurements. The corrected average helium test temperature was calculated by calculating the average of the nine good temperatures and then correcting this average value by a temperature correction factor. This temperature correction factor was obtained at the initial conditions and was determined by correcting the average value of the nine temperatures to the value of the thermistor measurement. The correction factor was in all cases 1 to 2°R. This temperature correction procedure was used to determine the temperature histories for all of the test results. Since the temperature measurements were placed to represent equal radial volumes, the corrected average temperature can also be considered to represent equal volumes. This temperature averaging procedure does not always represent the true average temperature of the helium mass in the container. The stratification that resulted when the warm cascade helium began flowing into the primary container was significant. The helium temperature difference between the top and bottom temperature measurements ranged between 50 to 350°R depending on the amount of cascade helium in the container. Because of the stratification that occurred, the helium density varied considerably throughout the tank. The mathematical model used in the analysis considered instantaneous and perfect mixing of the warm incoming cascade helium with the resident cold helium in the primary tank. This supposition results in helium leaving the primary tank at a higher temperature than it would if stratification exists; therefore, the primary tank retains less energy and exhibits lower helium temperatures than it would with stratification. All six test runs reflect the stratification effect of higher average primary tank temperatures than those predicted by the continuous mixing mathematical model.

The container wall temperature histories for the two test runs showed only a slight decrease until  $T + 300$  sec. At this time the wall temperature increased in both tests. The calculated wall temperature in both cases dropped to approximately the calculated helium temperature. These two temperatures remained approximately equal (the calculated wall temperature was about 0.2 to 0.4°R higher than the helium temperature) until about  $T + 350$  sec, at which time the deviation between the two became noticeable. The most apparent reason for the large deviation between the calculated and tested container wall temperature in both

runs was that the calculated heat transfer rate between the wall and helium was larger than the actual wall-to-helium heat transfer rate. This would account for the almost immediate drop of the calculated wall temperature to the calculated helium temperature.

Table 21 shows the test and calculated values for the cascade helium usage and the primary helium residual for Runs 1 and 2. The cascade helium usage test values were obtained by subtracting the initial calculated helium mass from the final calculated mass. The calculated helium usage was calculated by the analytical model. The cascade helium usage was less than predicted by 15.5% in Run 1 and 24.5% in Run 2. These deviations were primarily due to the analytical model not accounting for the helium stratification that occurs during the test and the analytical model assuming the cascade entering temperature to be constant. The first reason was probably the most significant. The primary helium residual test values were obtained by adding the test cascade helium usage value to the difference between the primary helium loaded and the primary helium expelled. The primary helium expelled was determined by integrating the test flow rates over the total outflow time.

The results of the cascade container tests and posttest analyses are presented in Fig. 63a, 63b, 65a, and 65b. The pressure histories were similar in both runs, and showed that the calculated helium pressure was less than the test value. The calculated helium pressure curves indicated a more rapid drop in pressure than the test helium pressure curves immediately after the start of helium outflow. However about halfway through the expansion, the slope of the calculated pressure curve was about the same as the test pressure curve in both test runs. The deviations between the calculated and test final helium pressure were -20 and -30% for Runs 1 and 2, respectively. The deviations were primarily due to the calculated helium expelled mass being greater than it was for the test run and the helium mass flow rate being assumed constant in the calculated case as compared to the variable mass flow rate experienced during the tests.

The test helium mass residuals calculated from the equation of state at the final test helium temperature and pressure were 4.90 and 4.51 lb<sub>m</sub> for Runs 1 and 2, respectively. The calculated residuals were 3.93 and 3.26 lb<sub>m</sub> for Runs 1 and 2, respectively.

90-Day Mission Abort - The results of the primary container pretest analysis for the 90-day mission abort are presented as helium pressure and temperature histories. These results are shown in Fig. 66a and 66b. The helium pressure and temperature decreased from the start of helium outflow until the start of cascade flow (T + 165 sec). At this time the pressure reached 400 psia and remained constant for the duration of the outflow period. The helium temperature dropped to a minimum of 27.2°R at the start of cascade flow and then increased to a final maximum temperature of 105°R. The inside wall temperature followed the helium temperature closely and slightly higher until T + 300 sec. At this time the three temperatures were equal to the liquid hydrogen temperature of 35°R, which was held constant during the entire mission. The inside wall temperature then increased to a final maximum of 81.7°R. The outside wall temperature had only a slight deviation from the liquid hydrogen temperature. The greatest deviation occurred at the final conditions where the outside wall temperature reached 36.6°R. This final condition produced a temperature difference across the wall of 45.1°R. The cascade helium usage for this analysis was 7.56 lb<sub>m</sub>, and the total primary tank residual helium mass was 13.77 lb<sub>m</sub>.

Figures 67a and 67b show the results of the cascade container pretest analysis for the 90-day mission abort. These results show that the helium temperature and pressure drop from their initial values of 520°R and 4354 psia to their final values of 453.5°R and 933 psia. The wall temperature dropped only 12°R due to the large container mass. The helium residual mass was 2.89 lb<sub>m</sub> for this analysis.

The test results and posttest analysis results for the primary container 90-day mission abort simulation Runs 1 and 2 are presented as pressure and temperature histories in Fig. 68a, 68b, 68c, 70a, 70b, and 70c. The test helium pressure and temperature histories were obtained using the same methods that were described in the nine-day mission abort test results discussion. The test wall temperature history was for the outside wall; the inside wall

temperature of the container was not measured during these tests. The helium pressure histories were similar to the pressure histories discussed in the nine-day mission abort results. The test pressure was less than the calculated pressure up to the start of cascade helium flow. The test helium pressure undershoot existed in both runs. The maximum pressure deviations between the calculated and test values were 7.5 and 5.5% for Runs 1 and 2, respectively. The helium temperature histories for both the test and analytical cases were similar to the temperature histories discussed in the nine-day mission abort results. The maximum helium temperatures, both test and calculated, at the end of the 90-day abort mission were less than the maximum temperature obtained at the end of the nine-day mission. The result was anticipated, since, in the 90-day abort mission, heat was transferred from the helium to the liquid hydrogen; whereas, in the nine-day mission, the primary tank cascade process was nearly adiabatic. The stratification effect discussed on page IV-31 is again observed in the comparison of actual and calculated primary tank temperatures. However, prior to the start of cascade helium flow, the calculated and test helium temperatures compared very well in both runs. The maximum deviation was approximately -1% for both Run 1 and Run 2. The comparison between the calculated and test outside wall temperature was as favorable as the helium temperature comparison. The deviation between the calculated and test outside wall temperatures was +1% or less for both test runs. The temperature histories indicated that the outside wall temperatures were very nearly constant and approximately equal to the liquid hydrogen temperature throughout both of the test runs.

Table 22 shows the cascade helium usage and the primary helium residuals calculated for both the analytical and test cases in Runs 1 and 2. The cascade helium usage results were obtained in the same manner discussed in the nine-day mission abort results. The cascade helium usage calculated was 20 and 15.6% higher than the test values for Runs 1 and 2, respectively. The calculated helium mass residuals in the primary container were also higher than the test values by 11 and 8.7% for Runs 1 and 2, respectively. The reasons for these deviations were the same as discussed on Page IV-33 in the nine-day mission abort results. The cascade helium usages for the 90-day

mission abort runs were slightly higher than the values given for the nine-day mission abort. These higher helium usage values in the 90-day mission abort runs were due to the heat transferred out of the helium.

The 90-day mission abort results of the cascade container tests and posttest analyses for Runs 1 and 2 are also presented as pressure and temperature history curves, Fig. 69a, 69b, 71a, and 71b. These pressure and temperature history curves showed results similar to those discussed for the nine-day mission abort results. The calculated helium pressure was again less than the test helium pressure during both test runs. The profiles were approximately the same as were observed in the previous results. The calculated final helium pressure was 33 and 30% below the test helium pressures in Run 1 and Run 2, respectively. The temperature histories for both the calculated and test temperatures were similar in Runs 1 and 2. The calculated helium temperatures initially were less than the test temperatures until about  $T + 360$  sec at which time the calculated values became greater than the test values. The maximum deviations were +2.5% in Run 1 and -1.6% in Run 2. The test temperatures for the cascade container wall in Run 2 were not plotted due to erroneous temperature test data. Run 1 cascade wall temperature histories were similar to previous results. The calculated wall temperature was always less than the test wall temperature. The maximum deviation occurred at the end of the test run, and this value was approximately 1%. For Run 1 the cascade helium residual mass was  $3.84 \text{ lb}_m$  for the final test conditions, and the calculated value was  $2.55 \text{ lb}_m$ . The test helium residual mass was  $3.39 \text{ lb}_m$ , and the calculated value was  $2.40 \text{ lb}_m$  for Run 2.

Nine-Day Mission - The results of the nine-day design mission primary container pretest analysis are presented as temperature and pressure histories (Fig. 72a, 72b, 73a, 73b, 74a, and 74b) for the helium and sphere wall. Figures 72a and 72b show the primary sphere helium pressure and temperature histories and the wall temperature history over the entire mission time. The analysis predicted a maximum helium pressure at the start of the fourth burn to be 1207 psia. Helium pressure dropped from 400 to 365 psia at the start of the seventh coast and increased to 400 psia at the start of the eighth burn. The drop in

pressure was due to the drop in helium temperature; which was due to the helium and sphere wall reaching a thermal equilibrium condition during the seventh coast. At the end of the seventh burn, the helium and wall temperatures were 117.8 and 100.7°R, respectively. The calculated equilibrium temperature for the helium and sphere wall was 109°R, which produced an 8.8°R drop in helium temperature. Cascade helium flow began during the fourth burn and occurred during the fifth, seventh, and eighth burns. The maximum helium temperature of 136°R occurred at the end of the ninth coast. Figures 73a, 73b, 74a, and 74b show the primary helium pressure and temperature histories and the wall temperature history for the fourth and seventh burns -- the two longest. The total cascade helium usage was 5.08 lb<sub>m</sub>, and the total cascade helium outflow was 279.6 sec. The primary container helium residual mass was 11.28 lb<sub>m</sub> for this analysis.

The results of the cascade container pretest analysis are presented in Fig. 75a, 75b, 75c, 76a, 76b, 77a, and 77b. Figures 75a, 75b, and 75c present the cascade helium pressure and temperature histories and wall temperature history for the total mission time. These curves show the minimum helium pressure and temperature of 1900 psia and 455°R, respectively, occurring at the end of the seventh burn. Also shown is where the helium and sphere wall temperatures reached a thermal equilibrium during each coast period. Figures 76a, 76b, 77a, and 77b show the histories for the same parameters discussed above for each burn when helium outflow occurred. The helium residual mass in the cascade container for this analysis was 5.37 lb<sub>m</sub>.

The results of the primary container expansion during the two test runs that simulated the nominal nine-day mission duty cycle and the results of the computer program test simulation for the primary container expansion and same mission are shown in Fig. 78a, 78b, 78c, 79a, 79b, 80a, 80b, 84a, 84b, 84c, 85a, 85b, 86a, and 86b. These figures present the pressure and temperature histories that occurred during the tests and that were calculated by the analytical model for test Runs 1 and 2. Figures 78a, 78b, 78c, 84a, 84b, and 84c present the helium pressure and temperature histories and the container wall temperature history for the complete test mission profiles of Run 1 and Run 2. Figures 79a, 79b, 80a, 80b, 85a, 85b, 86a,

and 86b present the same pressure and temperature histories for the fourth and seventh burns. These burn periods were of longer duration than any in the mission.

In general the helium pressure histories were similar throughout the entire mission for both runs. The calculated pressures compared a little more favorably with the test pressures in Run 2 than in Run 1. In both runs the calculated pressures compared very well with the test pressures during the preliminary coast period. After the first coast period, the difference between the calculated and test pressures began to increase with each coast period until the end of the third coast where the calculated pressure was higher than the test values for Runs 1 and 2, respectively. During the fourth burn, the helium pressure dropped to approximately 430 psia in both runs. Between the end of the fourth burn and the end of the seventh burn, the calculated and test helium pressure compared satisfactorily. After the end of the seventh burn, the calculated helium pressure decreased in both runs. This calculated helium pressure drop was due to the helium temperature increasing above the wall temperature during the seventh burn and then decreasing when the thermal equilibrium condition between the helium and wall was calculated during the coast period. This pressure drop was also calculated after the eighth and ninth burns. Prior to the start of the eighth burn and through the end of Run 1, the deviation between the calculated and test helium pressure increased significantly. This increase was due to the primary helium pressure dropping below 400 psia, which initiated cascade helium flow into the primary container prior to the start of primary helium flow. The pressure in the primary sphere increased rapidly over 500 psia due to the slow shutdown response of the regulator. The test procedure was revised prior to Run 2, to require deactivating the regulation system after each burn. The success of the revision was reflected in the good helium pressure comparison that resulted in Run 2 during the eighth, ninth, and tenth burns. In both Run 1 and Run 2, the pressure histories compared slightly better during the fourth burn than during the seventh. The pressure undershoot was approximately 40 psi during the fourth burn of Runs 1 and 2 as compared to a 50-psi undershoot during the seventh.

In general the temperature profiles, both calculated and test, were similar in Runs 1 and 2. The comparison between the calculated and test helium temperatures was good prior to the start of cascade helium flow. After the start of cascade helium flow during the fourth burn, the stratification effect drove the helium temperature up rapidly -- as discussed on page IV-31. The test container wall temperature histories were very inconsistent and irregular prior to the start of the fourth burn in both runs.

Table 23 shows the cascade helium usage and the primary helium residuals that were calculated for both the analytical and test cases in Runs 1 and 2. The cascade helium usage values were obtained in the same manner that was discussed in the nine-day mission abort results. During Run 1, cascade helium flow occurred during the fourth and seventh burns, the seventh coast, the eighth burn, and the eighth coast. In Run 2, cascade helium flow occurred during the fourth and seventh burns and for about 5 min prior to the start of the eighth burn (so that primary tank pressure would be up to 400 psia). The analytical model predicted cascade helium flow during the fourth, fifth, seventh, eighth, and ninth burns for Run 1 and Run 2. The calculated helium usage was less than the test helium usage during Runs 1 and 2. In Run 1, this deviation between the calculated and test usage values was significant; this was due to the slow response of the test regulator during the cascade flow that occurred during the eighth burn. Instead of terminating the cascade flow when the primary tank pressure exceeded 400 psia, the regulator remained open until the primary tank pressure reached about 505 psia (Fig. 78a). This caused the final primary tank pressure to be about 495 psia, rather than the predicted 428 psia. In Run 2, the calculated cascade helium usage was only 0.105 lb<sub>m</sub> less than the test value; a similar end pressure discrepancy was noted (Fig. 84c), but was of a much smaller magnitude. When the effects of the primary tank pressure deviations were considered in the analysis, a much better data correlation resulted. The primary container helium residuals were obtained using the same methods used in the nine-day mission abort results. The calculated primary helium residual masses were originally less than the test values in both Run 1 and Run 2. However, after considering the pressure overshoot problem, the calculated residuals were much closer to the test values. It is

noted that more cascade helium was used in Run 1 than in Run 2. This resulted from a larger total mass of helium being extracted from the primary tank during Run 1 (72.48 lb<sub>m</sub>) than was extracted during Run 2 (70.10 lb<sub>m</sub>), due to a slight shift in flow rate from one run to the next.

The test results and analytical results for the cascade container expansion during the nine-day mission simulation are presented in Fig. 81a, 81b, 81c, 82a, 82b, 83a, 83b, 87a, 87b, 87c, 88a, 88b, 89a, and 89b. The test and calculated helium pressure and temperature histories and container wall temperature history are presented for the complete test mission profile in Fig. 81a, 81b, and 81c for Run 1 and in Fig. 87a, 87b, and 87c for Run 2. Figures 82a, 82b, 83a, 83b, 88a, 88b, 89a, and 89b present the same pressure and temperature histories for the fourth and seventh burns.

Cascade tank pressure and temperature remained constant until outflow began during the fourth burn. After the fourth burn, the calculated cascade helium pressure and temperature and cascade container wall temperature were in good agreement with the test results during the time between the end of the fifth burn and the end of the seventh burn for both Run 1 and Run 2. The deviations between the calculated and test helium pressure were much greater between the end of the seventh burn and the end of the mission. The helium and wall temperature deviations were not as large as the pressure deviation during this time period. In Run 1, the calculated cascade helium residual mass was 3.63 lb<sub>m</sub>, and the test value was

2.065 lb<sub>m</sub>. This was due to the fact that the actual primary tank end pressure was 495 psia, rather than the predicted value of 428 psia. Cause of the higher final pressure was slow response of the cascade regulation device. In Run 2, the difference between the calculated and test cascade helium residuals was less than in Run 1; the test value was 3.29 lb<sub>m</sub>, and the calculated value was 3.33 lb<sub>m</sub>.

## B. CASCADE PRESSURIZATION SYSTEM PRIMARY TANK SUPPORT STRUCTURE AND TUBING HEAT LEAK INVESTIGATION

### 1. Test System

The support structure and tubing heat leak test fixture is depicted schematically in Fig. 90 and 91 and pictorially in Fig. 92.

Details of the support structure and tubing test model are shown in Fig. 93 thru 97. The test model consisted of three Type 304 stainless steel support tubes 30 in. long, with an outside diameter of 0.750 in. and a wall thickness of 0.035 in. The anchor ends of the support tubes were flattened and bent as shown in Fig. 95. The other end of the support tubes was provided with a Type 304 stainless steel clevis bolted to the support bracket as shown in Fig. 94. The support bracket was assembled to the simulated primary storage container hub and liquid hydrogen heat sink tank in the manner shown in Fig. 98. Two dummy gas tubes to simulate the cascade helium inlet and hydrogen vent lines (Type 304 stainless steel, 0.500 in. outside diameter, 0.035 in. wall thickness) were connected to the simulated primary container hub as shown in Fig. 93 and 98. The tubes were routed to ambient temperature anchor points as shown in Fig. 95, in a manner to provide the desired developed tube lengths of 51 and 56 in.

The liquid hydrogen heat sink tank had a capacity of 1 lb of liquid hydrogen, and it was fitted with a fill tube (Type 304 stainless steel, 0.500 in. outside diameter) and a vent tube (Type 304 stainless steel, 1 in. outside diameter). The fill and vent tubes were conducted through the vacuum chamber bottom dome. The liquid hydrogen tank was equipped with a two-thermistor probe. The thermistors were located approximately 1 1/2 in. from the bottom of the liquid hydrogen tank and 1 1/2 in. from the top of the tank. The lower thermistor was used to record liquid hydrogen temperature, and the upper thermistor was connected to the liquid level indicator on the operator's console. The entire support structure, dummy gas tubes, and liquid hydrogen tank were insulated with 100 layers of NRC-2 superinsulation, with a packing density of approximately 250 layers per in. The liquid hydrogen tank fill and vent tubes were wrapped with 2 layers of NRC-2 superinsulation. The insulated test model is shown in Fig. 97. The model was instrumented for acquisition of the functions listed in Table 24 and shown in Fig. 100.

The support heat leak test model was installed in a vacuum chamber that was situated in a water bath (Fig. 91 and 92). A water circulating pump was provided to circulate water from the tank up to the water cascade distribution ring at the top of the vacuum tank, to provide a uniform chamber wall temperature. The water bath was maintained at 50 to 55°F by a small constant supply flow of 80°F water from the facility supply.

The 1/2-in. liquid hydrogen supply line to the test model liquid hydrogen tank was connected to a 1000-liter mobile liquid hydrogen dewar through a 3/4-in. vacuum-insulated flexible metal hose and approximately 8 ft of 3/4-in. stainless steel tubing insulated with 1 in. of fiberglass insulation (helium purged). The dewar supply hose was equipped with a shutoff hand valve and a helium purge tee.

The 1-in. H<sub>2</sub> vent line from the liquid hydrogen tank was routed to the gas flowmeter through an ambient-temperature water bath, and also directly to the H<sub>2</sub> vent system through a remotely operated vent valve. This system was the same system used for the primary storage container heat leakage rate test.

## 2. Test Procedure

The support structure heat leak test run was performed with the structure installed in the vacuum chamber as described in Subsection 1. The vacuum chamber was evacuated to a pressure of  $10^{-5}$  mm Hg and maintained at that pressure for approximately 8 hr to permit the insulation to out-gas before the main vacuum pump valve was closed. The vacuum chamber walls were maintained at 515 to 520°R by circulating water over the chamber into the bath tank.

After purging the liquid hydrogen heat sink tank and connected supply and vent system with helium gas, liquid hydrogen was introduced into the heat sink tank. The tank was topped periodically until stabilized conditions were attained, as evidenced by the structure temperature histories. The structure was allowed to stabilize for approximately 24 hr. The heat sink tank was refilled before starting the measurement run.

The measurement run was begun by closing the H<sub>2</sub> vent valve and opening the gas meter inlet valve to route the evolving hydrogen gas through the meter. As additional insurance against bypass leakage through the vent system relief system, the vent system

isolation hand valve was closed. Recordings of all the instrumentation functions listed in Table 24 were taken at 30-min intervals until a marked reduction in gas evolution rate indicated exhaustion of the liquid hydrogen. This point occurred approximately 25 hr after the measurement period was begun. The heat leakage rate into the heat sink tank was determined by using the mass flow rate of the evolving  $H_2$  gas (calculated from the meter volumetric rate and the gas pressure and temperature at the meter), and the liquid hydrogen latent heat of vaporization.

Following the test run, the vacuum chamber was opened and the structure supports and dummy tubes were removed, leaving only the liquid hydrogen heat sink tank, supported by its fill and vent tubes as shown in Fig. 100. The superinsulation was carefully refolded over the base (simulated container boss and mount bracket) of the heat sink tank.

The vacuum chamber was reclosed and evacuated to between  $10^{-5}$  and  $10^{-4}$  mm Hg pressure, and the water cascade system set to maintain the chamber walls at 510 to 520°R, thus duplicating the previous test run environment. A tare run was then conducted, using the same procedure as the test run to determine the heat leak contribution of the test fixture. The measurement period (time to liquid hydrogen exhaustion) was approximately 49 hr.

To obtain the net heat leakage rate attributable to the support structure and tubing only, the data sampling times were generalized on a percentage-of-run-time basis. This technique allowed comparison of data at points in the two runs where the liquid hydrogen liquid level was approximately identical.

### 3. Analysis and Evaluation of Results

The analyses conducted during the demonstration of the total heat transfer through the pressurant storage tank support structure were divided into pretest and posttest analyses. The purpose for these analyses was to evaluate and verify the analytical techniques used in Phase I for calculating heat transfer through pressurant storage support structure at liquid hydrogen temperatures. The analytical techniques were evaluated and verified by comparing the analytical results with the results of the tests that evaluated the heat transfer through the upper lines and supporting structure. A complete description of the test system and test procedures for evaluating the support structure heat leak was presented in the two previous subsections of this report. A description of the method of analyses for the pretest and posttest analyses is presented in the following paragraphs followed by an evaluation and comparison of the results.

- a. Pretest Analysis - The pretest analysis was conducted to predict the heating rates for the test model system. This test model system represented a full-scale model of the upper tripod support structure and connecting tubing for the Phase I-designed SPS primary helium storage tank. Using anticipated environmental conditions, the pretest analysis calculated the heat leak through:

- 1) Design system tank supports, helium inlet line, and liquid hydrogen vent line;
- 2) Test system liquid hydrogen fill and vent lines;
- 3) Test system liquid hydrogen container insulation.

The anticipated environmental conditions for the pretest analysis were an ambient temperature of 530°R and an ambient pressure of 12 psia. At this ambient pressure, the saturation temperature of liquid hydrogen is approximately 35°R. The anticipated temperature difference between ambient conditions and the liquid hydrogen container was 495°R.

The heat leaks through the design system tank supports, helium inlet line, and liquid hydrogen vent line were calculated using the following expression:

$$\dot{q} = \frac{A k \Delta T}{\ell} ,$$

where

$\dot{q}$  = heat leak rate through each support or line (Btu/hr);

A = cross sectional area of each support or line (sq ft);

k = thermal conductivity of support or line material (Btu/hr-ft-°R);

$\Delta T$  = temperature difference (495°R);

$\ell$  = total length of each support or line (ft).

This analysis assumed a constant thermal conductivity for each support and line at the mean temperature between the cold and warm ends. The analysis did not consider heat transfer through the supports and lines in a radial direction, i.e., heat transfer through support and line insulation.

The heat transfer rate through the test system liquid hydrogen fill and vent lines was calculated using the same expression and assumptions that were used to calculate heat leaks through the design system supports and lines.

The liquid hydrogen container was insulated with 1 in. of NRC-2 superinsulation. Heat transfer rates through the insulation located on the side, top, and bottom of the cylindrical container were calculated. The heat transfer rate through insulation located on the container side was calculated using the following equation:

$$\dot{q}_I = \frac{2\pi k_a \ell \Delta T}{\ln \left( r_{I_o} / r_{I_i} \right)},$$

where

$\dot{q}_I$  = heat transfer rate through insulation on container side (Btu/hr);

$\Delta T$  = temperature difference (495°R);

$r_{I_o}$  = insulation outside radius (ft);

$r_{I_i}$  = insulation inside radius (ft);

$k_a$  = apparent insulation thermal conductivity (Btu/hr-ft-°R);

$\ell$  = length of liquid hydrogen container (ft).

The total heat transfer rate through both the top and bottom of the container was calculated using the following equation:

$$q_I = \frac{2 r_{C_o}^2 k_a T}{t_I},$$

where

$q_I$  = total heat transfer rate through both top and bottom (Btu/hr);

2 = number accounting for consideration of the top and bottom;

$r_{C_o}$  = outside radius of the  $LH_2$  container (ft);

$k_a$  = apparent insulation thermal conductivity (Btu/hr-ft-°R);

$t_I$  = insulation thickness (ft);

The apparent insulation thermal conductivity used in this analysis was  $1.12 \times 10^{-4}$  Btu/hr-ft-°R. This value was obtained from the results of the heat leak calibration tests described in Section A, Subsection 3.

- b. **Posttest Analysis** - The posttest analysis was conducted using the same method of analysis that was used in the pretest analysis. However, instead of using the anticipated ambient conditions, this analysis used the average temperature of the vacuum tank wall and the average liquid hydrogen temperature for calculating the temperature difference,  $\Delta T$ . The average temperatures of the vacuum tank and liquid hydrogen were 515.0 and 35.5°R, respectively, during the heat leak tests. Other than using a temperature difference of 479.5°R, the posttest analysis was conducted using the same values that were used in the pretest analysis.
- c. **Evaluation and Comparison of Results** - The calculated heat leak rate for the upper primary tank support structure in the pretest and posttest analysis were 3.16 and 3.06 Btu/hr, respectively. The difference between the two calculated values was directly proportional to the two different values for temperature difference that were used. The test results for the upper tank supports and tubing heat leak evaluation tests are presented in Fig. 101. In this figure, the indicated heat leaks were plotted as a

function of percentage of elapsed time for test Run 1 and for the test fixture tare run. In test Run 1, the liquid hydrogen boiloff rate was measured for the complete test system, and, in the tare run, the boiloff rate was measured for the test system without the design system upper supports and tubing. The net indicated heat leak for the design system supports and tubing represents the difference between the two measured flow rates. The indicated heat leaks were plotted as a function of percentage of elapsed time to compare the results at equal liquid volumes. The measured liquid hydrogen boiloff rates decreased with time during each test because, as the volume of liquid hydrogen decreased, the volume of hydrogen vapor increased; therefore, more heat was transferred into the vapor and less into the liquid. This decrease in boiloff rate was not constant in either test until approximately 60% of the elapsed time, which indicates that an unstable condition existed prior to this time period. A stable condition existed when the measured liquid hydrogen boiloff rates were due only to heat transferred into the container. The primary reasons for the increased boiloff rates during the unstable conditions were:

- 1) The residual boiloff in the liquid hydrogen fill line;
- 2) The boiloff due to the superheated liquid hydrogen present in the container after liquid hydrogen flow was discontinued.

After liquid hydrogen flow was stopped, the container pressure dropped from the dewar pressure (32 psia) to ambient pressure (12 psia). This pressure drop produced a corresponding drop in the liquid saturation temperature of approximately 7°R and produced the superheated liquid condition. The dashed lines in Fig. 101 represent the extrapolation of stable conditions and produced net indicated heat leak for the upper supports and tubing of 3.75 Btu/hr at the start of the tests. At the 95% of elapsed time, the net indicated heat leak value was 3.15 Btu/hr. The maximum deviation between the calculated heat leak value and the net indicated obtained from the test results was -16.0 and -18.4% for the pretest and posttest analysis, respectively, and this deviation occurred at the start of the tests. At 95% of elapsed time, the deviations were +0.32% for the pretest analysis and -3.0% for the posttest analysis.

The total heat transfer into the primary pressurant storage container, i.e., heat transferred through both the upper and lower tank supports and tubing, was evaluated by the following equation:

$$q_{T_i} = q_{T_c} \frac{q_{U_i}}{q_{U_c}},$$

where

$q_{T_i}$  = indicated total heat transfer through all the supports and lines (Btu/hr);

$q_{T_c}$  = calculated total heat transfer through all supports and lines (Btu/hr);

$q_{U_i}$  = indicated heat transfer through the upper supports and lines (Btu/hr);

$q_{U_c}$  = calculated heat transfer through the upper supports and lines (Btu/hr).

The value for  $q_{T_c}$  was 5.78 Btu/hr, and the value for  $q_{U_c}$  was 3.06 Btu/hr, which was calculated in the posttest analysis. The values for  $q_{U_i}$  range from 3.75 Btu/hr at a run time equal to zero to 3.15 Btu/hr at 95% of elapsed time. The evaluation for  $q_{T_i}$  was also conducted for the same time periods, and this evaluation produced  $q_{T_i}$  values of 7.08 Btu/hr at time equal to zero and 5.95 Btu/hr at 95% of elapsed run time.

### C. APOLLO SERVICE PROPULSION SYSTEM CASCADE PRESSURIZATION SYSTEM EXTENDED IN MISSION STUDIES

Extended mission studies were performed using the profiles shown in Tables 2 and 3 for a 34-day lunar and a 90-day earth polar orbit.

The pressurant usages for the two missions were determined by using the minimum allowable propellant temperature of 500°R and a pressurant inlet temperature of 475°R. The 34-day mission required a full propellant load, while the 90-day mission propellant was off loaded 70%. The helium pressurant usage for the 34-day and 90-day missions are 64.94 and 17.56 lb<sub>m</sub>, respectively.

In the study an effort was made to design a system that would limit the increase in the present weight of the SPS design system. The longer duration missions have no effect on the operating characteristics of the cascade helium sphere, since it is stored at ambient temperature.

The primary sphere, which is stored initially at 37°R, could absorb too much heat and exceed the design working stress due to the excessive rise in temperature and pressure.

Three basic approaches were pursued in the investigation of extended mission capability:

- 1) Reduction of primary tank heating rate;
- 2) Reduction of the effects of primary tank heating;
- 3) Increase of the primary tank strength to accommodate the increased heating and higher pressure.

Primary tank heating rate can be reduced by increasing the number of NRC-2 insulation sheets and by decreasing the amount of conductive heating. The latter method was approached by considering the use of titanium alloy 6Al-4V for the lines and supports connecting to the primary tank. Titanium 6Al-4V was not used in the basic Phase I system design due to the unavailability of tubing in the required sizes at that time. However, producers of titanium mill products are continuing to develop methods of forming 6Al-4V tubing, so it is considered that the proper sizes may become available in the near future.

Methods of reducing the effects of primary tank heating considered were off loading helium and launching with a full jacket load of liquid hydrogen.

The only method considered for increasing the primary tank strength was by increasing the wall thickness.

#### 1. 34-Day Mission

Shown in Fig. 102 is the maximum heat leak that can be tolerated in the primary sphere for the 34-day mission with the present SPS primary tank design. The heat leaks shown were the initial values, which were with a gas temperature of 37°R. These values will decrease slightly with increasing gas temperatures. The system with stainless steel lines and supports could tolerate a larger initial heat leak since the heat leak was reduced more with increasing temperatures than systems with titanium 6Al-4V.

Since the heat leak into the system is somewhat uncertain due to the variation in thermal performance that exists with multilayer insulation, the system capabilities were plotted as a function of an insulation degradation factor as seen in Fig. 103 and 104. The degradation factor is the ratio of actual expected heating rate through the installed insulation to the ideal heating rate as derived from published thermal performance data. A degradation factor of 5 is considered nominal. The tops of the lines in Fig. 103 and 104 represent a measure of the maximum heating rates allowable; the bottoms of the lines represent the minimum heating rates allowable. If no liquid hydrogen is carried in the jacket, the maximum heat leak allowable to make the mission is below the nominal value considered, as seen in Fig. 103. Therefore, none of these systems is capable of making the 34-day mission. Figure 104 shows that, with liquid hydrogen carried in the jacket, the maximum allowable heat leak exceeds the nominal value for most systems and provides various degrees of performance margin. The minimum heat leak values for these systems were controlled by the maximum possible cascade usage from the SPS design system. Figure 105 shows cascade usage as a function of the time at which the liquid hydrogen is completely boiled off. If the liquid hydrogen is dumped before 600 hr, the maximum available cascade gas is not exceeded. This allows any system shown in Fig. 104 to adequately perform the mission even if the heat leak is at a minimum (corresponding to the minimum attainable value of insulation thermal conductivity). Since dumping the residual liquid hydrogen before 425 hr would reduce the maximum allowable heat leak, the jacket should be emptied between 425 and 600 hr.

With liquid hydrogen carried in the jacket, the system for the 34-day mission would have a launch weight increase over the SPS cascade design system as shown in Fig. 106. Of this value, 29.8 lb is liquid hydrogen that would be boiled off or dumped before the eighth burn. The increase in hardware weight of this system for the SPS design system is tabulated below.

Lines and Supports Insulation Thickness (in.)	Weight Increase (lb <sub>m</sub> )	
	304 Stainless	Ti 6Al-4V
2	0	-2.29
3	6.92	4.63
3 1/2	10.77	8.48

If liquid hydrogen cannot be carried in the jacket, the primary tank wall thickness will have to be increased. The system weights for the 34-day mission with the increase in primary sphere wall and off loading of helium are shown in Fig. 107. The systems were designed to allow for a heat leak variation of ten times the nominal value for the insulation, allowing for a reasonable margin. The hardware weight increase in SPS design system is shown in Fig. 108.

## 2. 90-Day Mission

In the study of the 90-day mission it was found that it is difficult to design a system that would not increase the SPS design system mass without an increase in primary tank storage temperature. However, with an initial storage temperature of 140°R, the existing Phase I system design will easily make the 90-day mission. Figure 109 shows the allowable range of insulation degradation factor for performance of the 90-day mission. When loading to an initial pressure of 1400 to 1600 psia, a very large initial heat leak can be tolerated since the gas temperature can rise to ambient after the first burn without exceeding the design working stress of the primary tank. The material of the lines and supports and the thickness of insulation will not affect the ability of this design to accomplish the mission. The reduction in total system weight for the 90-day mission is tabulated:

Lines and Supports Initial Pressure (psia)	Reduction in Weight ( $lb_m$ )	
	304 Stainless	Ti 6Al-4V
1400	49.97	52.26
1600	47.40	49.69
1800	44.93	47.22
2000	42.59	44.88

These weight savings are due almost entirely to the reduced helium loading required to accomplish this mission. If titanium supports and lines are used, the weight saving is an additional 2.3  $lb_m$ .

### 3. Optimum System for Extended Missions

In the selection of the optimum cascade system for extended mission use, the following observations are pertinent:

- 1) The 90-day mission can be accommodated by the present system design; therefore, the optimum system is determined by performance for the 34-day mission;
- 2) To ensure sufficient heating rate margin without strengthening the primary pressure vessel, it is necessary to launch with liquid hydrogen in the annular jacket;
- 3) Optimum initial primary tank pressure is minimum allowable to maintain required helium mass loaded (1400 psia).

It is noted that the minimum weight modification to permit the required extended mission capability is to change support tubing and lines to titanium alloy and launch with a full load of liquid hydrogen (Fig. 106). This alternative is even more attractive when the following facts are considered:

- 1) The weight penalty incurred by launching with liquid hydrogen affects only the system for a 34-day mission; no structural weight increases need be built into each system, regardless of mission;

- 2) Most of the weight penalty (the mass of liquid hydrogen loaded -- 30 lb<sub>m</sub>) will be eliminated during the first 600 hr of the mission. Therefore, the mean effective weight penalty is less than half of that indicated in Fig. 106.

The required size of tubing in titanium 6Al-4V is not yet available. Furthermore, it is noted from Fig. 104 that a high degree of heat leak margin can be had when stainless steel support and lines are used. Also, the difference in weight between stainless steel and the titanium alloy is less than 2.5 lb<sub>m</sub>. It is, therefore, recommended that the stainless steel supports and lines be retained in the design for extended missions.

Considering Fig. 104, it is observed that 3 in. of insulation (at an initial pressure of 1400 psia and for stainless steel supports and lines) provides a comfortable margin in insulation degradation factor on both sides of the nominal value expected. It is now determined that the only modifications necessary to the presently designed system to accommodate the extended missions are:

- 1) Increase the insulation thickness from 2 to 3 in.;
- 2) Provide for continuous venting of hydrogen vapor in proportion to the boiloff rate (34-day mission only).

This modification will add about 7.0 lb<sub>m</sub> of hardware weight to the designed system -- 4.0 lb<sub>m</sub> insulation and 3.0 lb<sub>m</sub> for hydrogen vent system.

## V. ADVANCED LIGHTWEIGHT PRESSURIZATION SYSTEM DESIGN SUMMARY

The purpose of this chapter is to present some of the more detailed design aspects of the cryogenic helium cascade pressurization system selected for the Apollo SPS. Also discussed herein are certain design modifications that have been included since the completion of Phase I.

The finalized primary tank design concept is shown in Figure 110. It is noted that the NRC-2 superinsulation has been replaced by two discrete radiation shields, enclosed within a rigid vacuum jacket that contains the entire assembly. The discrete shield design, which has been under considerable development by the Pioneer Central Division of Bendix Corporation, offers several distinct advantages over the use of multilayer foil types of superinsulation.

- 1) Fabrication Simplicity - The rigid radiation shields are much easier to fabricate and assemble satisfactorily than a multilayer foil insulation system;
- 2) Repeatability of Performance - Much more stringent control of surface finishes and thermal radiation characteristics can be maintained with a rigid radiation shield than with multilayer foil. Also, since only two shields are required rather than approximately 150, the attainment and maintenance of optimum vacuum conditions is greatly improved. This results in much better performance repeatability from unit to unit and as a function of time;
- 3) Ground Hold Capability - The discrete shield design includes a rigid vacuum jacket surrounding the shields. Therefore, the prelaunch (ground environment) heat leak is essentially the same as the space environment value. Subsequent to the completion of Phase I, it was found that the calculations to coolant requirements for a 10-hr ground hold capability at 37°R were in error. In reality, the Phase I design has capability for only a 1-hr ground hold without replenishing the coolant (liquid hydrogen). This problem, which was caused by the increased heating rate resulting from the required helium purge of the exposed NRC-2 while on the ground, is eliminated with the discrete shield vacuum jacket design.

The liquid hydrogen jacket (commercially pure titanium) is dimpled at several locations, and spot-welded to the pressure vessel. The resulting annular space for the containment of liquid hydrogen is approximately 1 in. The contained volume of the annulus is approximately 1.6 cu ft.

The pressure vessel/hydrogen jacket assembly is suspended within the vacuum jacket by means of six radial bumpers (only two are shown). The bumper arrangement, developed by Bendix Corporation, is designed for a minimum conductive heat leak into the cryogenically stored helium. Also, the bumpers provide structural suspension for the internal helium and hydrogen lines. The two radiation shields are suspended between the liquid hydrogen jacket and the vacuum jacket by means of attachments to the inner lines. Two brackets, which support the entire assembly at the locations of the six radial bumpers, provide bosses for attachment to the SPS structure. The vacuum jacket and internal lines, as well as the liquid hydrogen jacket, are constructed of commercially pure titanium. This eliminates the necessity and unreliability of joining titanium with a dissimilar base metal.

Although only two radiation shields are required for the heat leak rate acceptable for the nominal nine-day design mission, the addition of more shields and/or vapor cooling provides readily attainable capability for greatly reducing the heat leak to acceptable levels required for some of the extended missions. For instance, by vapor cooling the two shields now in the system, the system would have operational capability for the two extended missions reported in Chapter IV, Section C.

The nominal heat leak for the primary tank as shown in Figure 110 is about 15 Btu/hr. The system will perform satisfactorily for a heat leak range of 3 to 30 Btu/hr.

Some of the more pertinent design parameters are defined in Table 24. A complete weight statement is given in Table 25.

## VI. CONCLUSIONS AND RECOMMENDATIONS FOR FUTURE INVESTIGATION

### A. CONCLUSIONS

A study of the data produced during the execution of this contract reveals several important conditions. These are discussed in this section.

#### 1. Optimum Pressurization System

The cryogenic helium cascade system is the optimum propellant tank pressurization system for the Apollo SPS.

#### 2. Weight Saving

Use of the cryogenic helium cascade system in place of the present ambient stored helium system will reduce the Apollo SPS weight by 515 lb<sub>m</sub>.

#### 3. Pressurant Loading

The use of a liquid hydrogen cooling jacket surrounding the cascade system primary tank pressure vessel greatly facilitates the helium loading operation. Three major advantages of this technique are apparent:

- 1) Loading time is minimum;
- 2) Initial conditions are reliably repeatable;
- 3) Required ground support equipment is minimized.

#### 4. Cascade System Feasibility

Demonstration of the cascade system operating principles and characteristics by test has established the feasibility of this system concept.

#### 5. Extended Mission Capability

Extended mission capability is readily attainable in the cascade system. This is provided by slight modification of the thermal protection system and does not require changes in basic system configuration or sizing.

#### 6. Propellant Feedline Heat Exchanger

Propellant feedline heat exchangers provide a lightweight, reliable means of heating the cryogenic helium to ambient temperature prior to entry into the propellant tanks. However, the single tube coil Apollo SPS type of heat exchanger is not suited to use with 37°R helium. A multiple-finned tube design, similar to the LEM descent stage heat exchanger, is necessary to prevent localized freezing of the propellant.

#### 7. Cascade System Size and Weight Predictions

The mathematical model used to predict size, weight, and operating characteristics of the cascade storage system proved to be very accurate in predicting system performance for the two 9-day, 10-burn mission test runs. Actual cascade helium usage was 0 and 6% greater than predicted for Runs 1 and 2, respectively. However, the actual cascade helium usage for the four single-burn mission abort runs was 15 to 25% less than calculated. The reason for the conservative calculations was the high degree of temperature stratification in the primary tank throughout the duration of the abort runs -- the mathematical model considers that the primary tank helium exists at a uniform, but variable, temperature at all times. Some stratification did occur during early cascading in the two 9-day mission runs, but was almost completely damped out during the subsequent coast periods. This validation of the mathematical model by comparison with test data indicates that the size and weight of the cascade system for the Apollo SPS and design mission were properly evaluated.

One method of increasing the weight saving afforded by the cascade system would be to lower the specified minimum helium supply pressure to a value close to the propellant tank operating pressure. This change would result in a reduction in cascade helium usage.

### B. RECOMMENDATIONS FOR FUTURE INVESTIGATION

The results of this contract work illustrate the capability of the cryogenic helium cascade system to perform the necessary propellant tank pressurization function for the Apollo SPS. Furthermore, it has been shown that the replacement of the present ambient stored helium SPS pressurization system with this

cascade system will result in a vehicle weight reduction of 515 lb<sub>m</sub>.

It is recommended that the inherent advantages of the cascade system be developed further in the form of a flightweight system design, fabrication, and qualification program. The flightweight system should be developed for the present lunar landing mission and should include capabilities for performing the presently envisioned Apollo extended mission duty cycles. Reduction of basic Apollo vehicle weight for the extended mission applications is extremely important due to the increased weight of life support, instrumentation, and various other additional equipment anticipated.

It is also suggested that the helium cascade pressurization system concept be considered for other propulsion systems wherein minimum weight is an essential criterion. Analytical studies of cascade systems for the LEM ascent and descent stages indicate substantial weight savings can be effected, as compared to ambient helium pressurization of those stages.

The cascade pressurization system operates at maximum efficiency when the cascade helium flow is metered as required to just maintain the minimum primary tank pressure. This necessitates the use of helium regulation components between the cascade and primary tanks. An alternative method of metering the cascade flow is by replacing the regulation components with a fixed area orifice. This arrangement would result in a nonoptimum cascade flow profile, but would greatly reduce system complexity, and increase reliability. It is recommended that an investigation of this alternative method of cascade flow control be performed to determine the pertinent weight and performance characteristics. This investigation should include experimental verification of the analytic predictions.

Martin-CR-66-44

APPENDIX

TABLES AND FIGURES

## A. TABLES

TABLE 1

ADVANCED LIGHTWEIGHT PRESSURIZATION  
SYSTEM DESIGN MISSION DATA

<u>EVENT</u>	<u>TIME FROM LIFT OFF</u>	<u>DURATION</u>
Launch	00.00 Hrs	
Earth Orbit Injection	.20	
Translunar Orbit Injection	4.70	
First Translunar Midcourse Correction	22.79	13.00 Sec
Second Translunar Midcourse Correction	40.79	13.00
Third Translunar Midcourse Correction	58.79	13.00
Lunar Orbit Insertion	76.79	390.2
First Lunar Orbit Plane Change	80.88	20.20
Second Lunar Orbit Plane Change	127.38	10.20
Trans-earth Orbit Injection	133.38	121.0
First Trans-earth Midcourse Correction	160.92	3.20
Second Trans-earth Midcourse Correction	188.42	3.20
Third Trans-earth Midcourse Correction	215.92	<u>3.20</u>
		Total 590.2 Sec

-----  
Prelaunch Hold Time - 10.0 hours

Mixture Ratio (Nominal) = 2.00

<u>Propellant Tankage:</u>	<u>Oxidizer</u>	<u>Fuel</u>
Total Volume (maximum)	321.0 ft <sup>3</sup>	255.6 ft <sup>3</sup>
Ullage (minimum)	12.2 ft <sup>3</sup>	9.3 ft <sup>3</sup>
Operating Pressure (nominal)	175 psia	175 psia
Propellant Temperature (limits)	40-80°F	40-80°F
Propellant Tank Temperature (maximum)	600°R	600°R

TABLE 2  
MISSION DUTY CYCLE FOR 34-DAY LUNAR POLAR ORBIT

<u>Function</u>	<u>Firing Duration (sec)</u>	<u>Time from Launch (hrs)</u>
Launch	-	0
Mid-Course Correction 1	17.1	12.5
Mid-Course Correction 2	5.6	44.7
Mid-Course Correction 3	5.6	67.9
Lunar Polar Orbit Injection	250.5	69.3
Guidance Correction	1.7	70.0
Guidance Correction	1.7	71.0
Guidance Correction	1.7	72.0
Guidance Correction	1.7	73.0
Transearth Injection 1	156.0	745.0
Transearth Injection 2	113.0	746.0
Mid-Course Correction 1	5.5	763.8
Mid-Course Correction 2	1.8	811.0
Mid-Course Correction 3	1.8	836.1

TABLE 3  
MISSION DUTY CYCLE FOR 90-DAY EARTH POLAR ORBIT

<u>Function</u>	<u>Firing Duration (sec)</u>	<u>Time from Launch (hrs)</u>
Launch	-	0
Orbit Injection	140.0	1.1
Orbit Deboost	18.0	2162.0

TABLE 4  
MERIT RATING SUMMARY

SYSTEM	MASS (lb <sub>m</sub> )	(N <sub>m</sub> ) <sub>m</sub>	RELIABILITY	(N <sub>m</sub> ) <sub>R</sub>	(N <sub>m</sub> ) <sub>c</sub>	MERIT RATING
0	700	.2786	.999451	1.0000	1.00	.6393
1	291	.6701	.999374	.8770	.90	.7794
1A	298	.6544	.999373	.8756	.80	.7461
2	242	.8058	.999142	.6399	.50	.6879
4	290	.6724	.999076	.5942	.45	.5973
5	195	1.0000	.999181	.6703	.70	.8426
7	308	.6331	.999284	.7668	.20	.5583
8	272	.7169	.999268	.7500	.60	.6960

TABLE 5  
CANDIDATE SYSTEM RANKING BASED UPON  
PRELIMINARY ANALYSIS AND EVALUATION

Rank	System	Merit Rating
1	5	.8426
2	1	.7794
3	1A	.7461
4	8	.6960
5	2	.6879
6	0	.6393
7	4	.5973
8	7	.5583

TABLE 6  
Analytical and Test Results  
Helium/Fuel Heat Exchanger

TEST RUN	HELIUM OUTLET TEMPERATURE, °R	TEST VALUES			CALCULATED VALUES		
		LENGTH, FT.	HELIUM $\Delta P$ , PSIA	FUEL $\Delta T$ , °R	LENGTH, FT.	HELIUM $\Delta P$ , PSIA	FUEL $\Delta T$ , °R
4-A	496	19.5	51.0	1.90	24.6	48.5	1.74
4-B	499	19.5	51.0	1.90	25.8	52.0	1.80
4-C	499	19.5	51.0	1.90	25.9	52.5	1.83
5-A	518	19.5	47.5	1.30	28.0	38.5	1.49
5-B	521	19.5	34.5	1.20	30.2	42.5	1.55
5-C	521	19.5	34.5	1.10	30.4	42.5	1.47
5-D	520	19.5	34.8	1.20	29.3	41.3	1.46

TABLE 7  
ANALYTICAL AND TEST RESULTS  
G. G. PRODUCTS/FUEL HEAT EXCHANGER

TEST RUN	HELIUM OUTLET TEMP., °R	TEST VALUES			CALCULATED VALUES		
		LENGTH, FT.	HELIUM $\Delta P$ , PSIA	FUEL $\Delta T$ , °R	LENGTH, FT.	HELIUM $\Delta P$ , PSIA	FUEL $\Delta T$ , °R
3-A	544	19.5	62.0	3.8	28.4	132	4.47
3-B	545	19.5	60.0	3.5	28.3	135	4.54
4-A	563	19.5	146.0	1.9	31.5	242	6.11
4-B	556	19.5	144.0	4.0	34.4	260	6.10

Table 8  
Potential Weight Reduction of the ALPS Candidate Systems

Candidate System	Helium Storage Temperature (°R)	Helium Storage Pressure (psia)	Potential Weight Reduction (lbm)
1	140.0	4000.0	341.0
5	140.0	4000.0	380.0
8	140.0	4000.0	398.0
1	37.0	2000.0	369.0
5	37.0	2000.0	535.0
8	37.0	2000.0	426.0

Table 9  
Results of System Reliability Studies

System	Total Reliability	Reliability Without Lines and Fittings
1	.999862	.999990
5	.999780	.999946
8	.999714	.999860
Apollo	.999733	.999948

Table 10  
Estimated Flight Qualified Component Costs  
(For System Comparison Only)  
System 1

<u>Component</u>	<u>No. of Each</u>	<u>Dev. &amp; Quali- fication Costs</u>	<u>Hardware Costs Per Vehicle</u>
Solenoid Valve	8	\$117,500	\$22,400
Pressure Switch	2 Quads	100,000	7,200
Disconnect	5	-	2,500
Heat Exchanger	2	100,000	8,000
Filter	1	45,400	318
Jacketed Helium Tank	1	250,000	30,000
Relief Valve	3	200,000	22,500
Lines & Fittings	-	-	5,000
TOTAL . . . . .		\$812,900	\$97,918

System 5

<u>Component</u>	<u>No. of Each</u>	<u>Dev. &amp; Quali- fication Costs</u>	<u>Hardware Costs Per Vehicle</u>
Solenoid Valve	12	\$117,500	\$33,600
Pressure Switch	3 Quads	100,000	10,800
Disconnect	6	-	3,000
Heat Exchanger	2	100,000	8,000
Filter	1	45,400	318
Jacketed Helium Tank	1	250,000	30,000
Helium Tank	1	132,000	12,000
Relief Valve	3	200,000	22,500
Lines & Fittings	-	-	5,000
TOTAL . . . . .		\$944,900	\$125,218

System 8

<u>Component</u>	<u>No. of Each</u>	<u>Dev. &amp; Quali- fication Costs</u>	<u>Hardware Costs Per Vehicle</u>
Solenoid Valve	12	\$117,500	\$33,600
Pressure Switch	3 Quads	100,000	10,800
Disconnect	6	-	3,000
Heat Exchanger	2	100,000	8,000
Filter	2	45,400	636
Jacketed Helium Tank	1	250,000	30,000
Positive Expulsion Tank	1	200,000	10,000
Gas Generator	1	400,000	20,000
Relief Valve	4	200,000	30,000
Lines & Fittings	-	-	5,000
TOTAL . . . . .		\$1,412,900	\$151,036

Table 11  
Results of Helium Loading and Ten-Hour Hold Analysis  
Insulation Thickness = 2.0 Inches  
Helium Loading Temperature = 530°R

Candidate System	Helium Storage Temp. (°R)	Helium Storage Press. (psia)	Mass of Helium Loaded (lbm)	Helium Loading Rate (lbm/sec)	Estimated Loading Time (minutes)	Wt. of LN <sub>2</sub> or LH <sub>2</sub> Required for Loading (lbm)	Wt. of LN <sub>2</sub> Required for 10 Hour Hold (lbm)
1	140	4000	106.89	.02969	104	(LN <sub>2</sub> ) 766	(LN <sub>2</sub> ) 88.4
5	140	4000	71.70	.0199	101.5	(LN <sub>2</sub> ) 513	(LN <sub>2</sub> ) 68.8
8	140	4000	58.14	.0161	101	(LN <sub>2</sub> ) 417	(LN <sub>2</sub> ) 60.3
1	37	2000	189.30	.0523	79	(LH <sub>2</sub> ) 665	(LH <sub>2</sub> ) 55.0*
5	37	2000	71.70	.0100	133	(LH <sub>2</sub> ) 258	(LH <sub>2</sub> ) 30.0*
8	37	2000	96.90	.0269	76	(LH <sub>2</sub> ) 349	(LH <sub>2</sub> ) 36.0*

\*See Section V.

Table 12  
Results of the Analytical Simulation for Storage Time up to Thirty Days

Mission Plan	Candidate System	Helium Storage Temp.	Helium Storage Press.	Heating Rate at Max. Press. $\frac{\text{Btu}}{\text{hr}}$	Maximum Helium Press.	Helium Temp. at Max. Press.	Limit Operating Pressure Minus Max. Pressure	Mission Time for Maximum Pressure
A	1	140.0°R	4000 psia	3.0564	4022.0	140.73°R	2478.0 psia	End of 1st Coast
	5	140.0°R	4000	2.664	4030.02	141.00	2469.98	End of 1st Coast
	8	140.0	4000	2.5488	4033.75	141.12	2466.25	End of 1st Coast
	1	37.0	2000	3.8376	2034.37	37.61	1735.63	End of 1st Coast
	5	37.0	2000	2.916	2072.07	38.28	1697.93	End of 1st Coast
	8	37.0	2000	3.1572	2055.24	37.98	1714.76	End of 1st Coast
B	1	140.0	2500	2.8224	3072.06	170.29	3127.94	End of 1st Coast
	5	140.0	1500	2.340	2133.57	196.31	3796.43	End of 1st Coast
	8	140.0	2500	2.2752	3345.92	184.84	2704.08	End of 1st Coast
	1	37.0	1250	3.6612	2182.57	60.33	1477.43	End of 1st Coast
	5	37.0	550	2.520	1968.19	112.64	1411.81	End of 1st Coast
	8	37.0	1320	2.9448	2821.71	73.09	778.29	End of 1st Coast

Table 13- System Comparison Summary

Comparison Category	Apollo	System 1	System 5	System 8	Remarks
1. Mass	880 lbm	510.13 lbm	344.65 lbm	454.49 lbm	Calculated Optimum weights for each system. All within Apollo limitations.
2. Envelope	- NO SIGNIFICANT DIFFERENCE -				
3. Reliability	0.999733	0.999862	0.999780	0.999714	
4. System Start-up Time	- NO SIGNIFICANT DIFFERENCE -				All systems startup time in milliseconds.
5. System Leakage	- NO SIGNIFICANT DIFFERENCE -				With major portion of system using welded joints leakage becomes insignificant.
6. Propellant Tank Venting	NONE	NONE	NONE	NONE	No venting required from systems studied.
7. Cost Ratios Dev. & Qual. Cost/Veh.	1.0 1.0	0.9 1.40	1.05 1.68	1.15 2.00	Cost ratios of systems studied to existing Apollo system.
8. System Availability	Current	21 mo.	21 mo.	21 mo.	Hardware Development Time
9. Complexity Additional Pwr. Reqmt. Rate Total No. of working components	None None 22	0.5 KW 0.083 KWH 27	0.75 KW 0.125 KWH 38	0.75 KW 0.125 KWH 39	Power Requirements Above Existing Apollo System

Table 13 - System Comparison Summary

Comparison Category	Apollo	System 1	System 5	System 8	Remarks
10. Grd. System Requirements He. Ld. Time 10 hr. hold	Unknown None	79 min. 55 lbm*	133 min. 30 lbm*	76 min. 36 lbm*	Calculated - not verified by test Amount of coolant (LH <sub>2</sub> ) required to maintain storage conditions (calculated). Equipment required to load 98# of hydrazine for G. G. propellant tank.
Other	- NO DIFFERENCE -			Hydrazine Loading	
11. 30 Day Storage Capability Plan A Plan B	- NO SIGNIFICANT DIFFERENCE - NO SIGNIFICANT DIFFERENCE				All Systems Adaptable All Systems Adaptable

\*See Section V .

TABLE 14  
LIST OF INSTRUMENTATION - CASCADE GAS STORAGE SYSTEM

Symbol	Function	Type	Range	Accuracy
T <sub>pg</sub> <sup>-0</sup>	Temperature, Primary Sphere Gas, Reference	Thermistor	30°R-60°R	± 1°R
T <sub>pg</sub> <sup>-1</sup> thru T <sub>pg</sub> <sup>-5</sup>	Temp., Primary Sphere Gas, Vertical Axis	Cu/Cn	20°R-200°R	± 5°R*
T <sub>pg</sub> <sup>-6</sup> thru T <sub>pg</sub> <sup>-9</sup>	Temp., Primary Sphere Gas, Horizontal Axis	Cu/Cn	20°R-200°R	± 5°R*
T <sub>ps</sub> <sup>-1</sup> thru T <sub>ps</sub> <sup>-3</sup>	Temp., Primary Sphere Wall	Cu/Cn	20°R-200°R	± 10°R
T <sub>pii</sub> <sup>-1</sup> thru T <sub>pii</sub> <sup>-4</sup>	Temp., Pri. Sphere Insulation, Inner Surf.	Cu/Cn	20°R-200°R	± 10°R
T <sub>pio</sub> <sup>-1</sup> thru T <sub>pio</sub> <sup>-4</sup>	Temp., Pri. Sphere Insulation, Outer Surf.	Cu/Cn	460°R-560°R	± 4°R
T <sub>cst</sub> , T <sub>csm</sub> , T <sub>csb</sub>	Temp., Cascade Sphere Gas; Top, Middle, Bottom	Cu/Cn	460°R-560°R	± 4°R
T <sub>csw</sub>	Temperature, Cascade Sphere Wall	Cu/Cn	460°R-560°R	± 4°R
T <sub>po</sub>	Temperature, Primary Sphere Outlet Gas	Cu/Cn	20°R-200°R	± 10°R
T <sub>csl</sub>	Temperature, Gas in Cascade Transfer Line	Cu/Cn	460°R-560°R	± 4°R
T <sub>lpg</sub>	Temperature, H <sub>2</sub> at Rockwell LPG Meter	Cu/Cn	460°R-560°R	± 4°R
P <sub>pg</sub>	Pressure, Primary Sphere Gas	Strain Gage Transducer	0-2000 psig	± 20 psi
P <sub>csg</sub>	Pressure, Cascade Sphere Gas		0-6000 psig	± 60 psi
P <sub>csl</sub>	Pressure, Gas in Cascade Transfer Line		0-500 psig	± 10 psi
P <sub>j</sub>	Pressure, LH <sub>2</sub> Jacket	Bourdon Gage	0-30 psig	± 0.6 psi
P <sub>lpg</sub>	Pressure, H <sub>2</sub> Gas at Rockwell LPG Meter	Bourdon Gage	0-30 psig	± 0.3 psi
Q <sub>cg</sub>	Flow Rate, Cascade Gas	Turbine Meter	0-20 CFM	± 1%
V	Flow, H <sub>2</sub> Vent Gas	Rockwell Meter	0-100 SCFH	± 1%

\* Accuracies based on end-to-end calibration by immersion in LN<sub>2</sub> and LH<sub>2</sub>.

TABLE 15  
INSTRUMENTATION LIST - HEAT EXCHANGER SYSTEM

<u>SYMBOL</u>	<u>FUNCTION</u>	<u>TYPE</u>	<u>RANGE</u>	<u>ACCURACY</u>
TLpgi	Temp. - L. P. Heat Exchanger Gas, Inlet	Cu/CN	20°R - 200°R	± 10°R
Thpgi	Temp. - H. P. Heat Exchanger Gas Inlet	Cu/CN	20°R - 200°R	± 10°R
TLpgo	Temp. - L. P. Heat Exchanger Gas, Outlet	Cu/CN	460°R - 560°R	± 4°R
Thpgo	Temp. - H. P. Heat Exchanger Gas, Outlet	Cu/CN	460°R - 560°R	± 4°R
Thpgf	Temp. - H. P. H. E. Gas at Flow Meter	Cu/CN	460°R - 560°R	± 4°R
Thpwi	Temp. - H. P. H. E. Water, Inlet	Plat. Resist.	460°R - 520°R	± 0.1°R
TLpwi	Temp. - L. P. H. E. Water, Inlet	Plat. Resist.	460°R - 520°R	± 0.1°R
TLpwo	Temp. - L. P. H. E. Water, Outlet	Plat. Resist.	460°R - 520°R	± 0.1°R
Phpgo	Press. - H. P. H. E. Gas, Outlet	↑	0 - 3000 Psig	± 60 Psi
Plpgo	Press. - L. P. H. E. Gas, Outlet		0 - 200 Psig	± 4 Psi
Phpgf	Press. - H. P. H. E. Gas at Flow Meter	Strain	0 - 200 Psig	± 4 Psi
Plpgf	Press. - L. P. H. E. Gas at Flow Meter	Gauge	0 - 300 Psig	± 6 Psi
Phpwi	Press. - Water at Inlet to H.P.H.E.	Type	0 - 100 Psig	± 2 Psi
Δ Phpg	Differential Press. - H.P.H.E. Gas	Transducer	0 - 50 Psi	± 1 Psi
Δ Plpg	Differential Press. - L.P.H.E. Gas		0 - 50 Psi	± 1 Psi
Δ Phpw	Differential Press. - H.P.H.E. Water		0 - 50 Psi	± 1 Psi
Δ Plpw	Differential Press. - L.P.H.E. Water		0 - 50 Psi	± 1 Psi
Qhpgu	Flow Rate - H.P.H.E. Gas, Upstream Meter		10 - 120 CFM	± 2%
Qhpgd	Flow Rate - H.P.H.E. Gas, Downstream Meter	Cox	6 - 60 CFM	± 2%
Qlpgu	Flow Rate - L.P.H.E. Gas, Upstream Meter	Turbine	6 - 60 CFM	± 2%
Qlpgd	Flow Rate - L.P.H.E. Gas, Downstream Meter	Meter	6 - 60 CFM	± 2%
Qw	Flow Rate - Heat Exchanger Water	↓	30 - 300 GPM	± 2%

TABLE 16

## Measured System Chill-Down Time

<u>Test</u>	<u>Time</u>
Nine-Day Mission Abort, Run #1	15.0 min.
Nine-Day Mission Abort, Run #2	19.8 min.
Nine-Day Mission Abort, Run #1	21.0 min
Nine-Day Mission Abort, Run #2	19.8 min.

TABLE 17

## HELIUM LOADING RESULTS

LOADING RUN	LOADING TIME	LOADED CONDITIONS		
		HELIUM PRESSURE	HELIUM TEMP.	HELIUM MASS
Pre-Test Analysis	3.95 hrs.	838 Psia	37.8°R	68.3 lb <sub>m</sub>
Post-Test Analysis	3.13 hrs.	1033 Psia	35.5°R	81.0 lb <sub>m</sub>
Nine-Day Mission Abort, Run #1	6.10 hrs.	1034 Psia	35.7°R	81.31 lb <sub>m</sub>
Nine-Day Mission Abort, Run #2	4.67 hrs.	992 Psia	35.5°R	79.3 lb <sub>m</sub>
Ninety-Day Mission Abort, Run #1	4.95 hrs.	1026 Psia	35.5°R	80.69 lb <sub>m</sub>
Ninety-Day Mission Abort, Run #2	6.52 hrs.	992 Psia	35.4°R	79.5 lb <sub>m</sub>

TABLE 18  
LIQUID HYDROGEN CONSUMPTION  
 Cascade Feasibility Demonstration Tests

TEST RUN	REMARKS	LH <sub>2</sub> USED (lbm)	
		ACTUAL	ANALYTICAL
Check Run No. 1	Jacket maintained at flooded condition. Level indicator maintained "covered" at all times.	480	351
9-Day Mission Abort Run No. 1	Same as above.	560	374
9-Day Mission Abort Run No. 2	Same as above.	530	351
90-Day Mission Abort Run No. 1	Same as above.	490	374
90-Day Mission Abort Run No. 2	Jacket level maintained at level indicator thermistor (intermittent "covered" light)	470	351
9-Day Mission Run No. 1	Loaded twice, due to solid nitrogen plug in fill line. Jacket filled only to top of primary sphere.	490	351
9-Day Mission Run No. 2	Jacket filled only to top of primary sphere.	250	351

Table 19 Helium Loading Accuracies

Run No.	Temperature °R	Pressure PSIA	Nominal		With Instrumentation Tolerances	
			Mass Loaded lb <sub>m</sub>	Loading Inaccuracy %	Mass Loaded lb <sub>m</sub>	Loading Inaccuracy %
9-Day Abort						
1	+1 34.6 -0	917 ± 20	77.21	+3.64	74.6-77.5	+4.03
2	+1 34.4 -0	894 ± 20	76.40	+2.55	73.6-76.4	+2.55
90-Day Abort						
1	+1 34.2 -0	907 ± 20	77.36	+3.84	74.8-77.0	+3.36
2	+1 34.4 -0	895 ± 20	76.38	+2.52	73.6-76.4	+2.58
9-Day Mission						
1	+1 35.0 -0	885 ± 20	75.00	+0.67	73.0-76.5	+2.01
2	+1 34.8 -0	896 ±	75.88	+1.85	72.7-76.0	-2.42
Average Inaccuracy			2.51			2.83

TABLE 20  
NINE-DAY MISSION POST-TEST ANALYSIS BURN DURATION  
AND HELIUM MASS FLOW RATES

TEST RUN	BURN PERIOD	BURN DURATION	HELIUM MASS FLOW RATE
1	First	13.5 sec	0.107 lbm/sec
	Second	14.8 sec	0.106 lbm/sec
	Third	14.5	0.109 lbm/sec
	Fourth	390.0	0.128 lbm/sec
	Fifth	21.5	0.107 lbm/sec
	Sixth	12.0	0.096 lbm/sec
	Seventh	120.0	0.112 lbm/sec
	Eighth	5.0	0.079 lbm/sec
	Ninth	3.0	0.085 lbm/sec
	Tenth	4.7	0.088 lbm/sec
2	First	14.0	0.111 lbm/sec
	Second	11.7	0.094 lbm/sec
	Third	14.4	0.109 lbm/sec
	Fourth	388.2	0.1228 lbm/sec
	Fifth	20.0	0.109 lbm/sec
	Sixth	12.2	0.102 lbm/sec
	Seventh	119.7	0.115 lbm/sec
	Eighth	4.5	0.080 lbm/sec
	Ninth	3.8	0.091 lbm/sec
	Tenth	4.4	0.079 lbm/sec

TABLE 21  
9 Day Mission Abort Helium Usage & Residuals

TEST RUN	CASCADE HELIUM USAGE		PRIMARY HELIUM RESIDUAL		MEASURED PRIMARY TANK OUTFLOW
	TEST	CALCULATED	TEST	CALCULATED	
1	5.70 lbm	6.59 lbm	11.90 lbm	12.76 lbm	71.01 lbm
2	5.61 lbm	6.98 lbm	10.31 lbm	11.68 lbm	71.70 lbm

TABLE 22  
90 Day Mission Abort Helium Usage & Residuals

TEST Run	CASCADE HELIUM USAGE		PRIMARY HELIUM RESIDUAL		MEASURED PRIMARY TANK OUTFLOW
	TEST	CALCULATED	TEST	CALCULATED	
1	7.09 lbm	8.47 lbm	12.46 lbm	13.84 lbm	72.00 lbm
2	6.86 lbm	7.93 lbm	12.33 lbm	13.42 lbm	70.89 lbm

TABLE 23  
9-Day Mission Helium Usage and Residuals

TEST RUN	CASCADE HELIUM USAGE		PRIMARY HELIUM RESIDUAL		MEASURED PRIMARY TANK OUTFLOW
	TEST	CALCULATED	TEST	CALCULATED	
1	8.908 lbm	7.379 lbm	11.43 lbm	9.90 lbm	72.48 lbm
		8.90* lbm		11.42* lbm	
2	5.668 lbm	5.563 lbm	11.45 lbm	11.34 lbm	70.10 lbm
		6.00* lbm		11.78* lbm	
*After correction for final primary tank pressure.					

TABLE 24  
Instrumentation List - Support Model Heat Leak Investigation

<u>Symbol</u>	<u>Function</u>	<u>Type</u>	<u>Range</u>	<u>Accuracy</u>
T <sub>wt</sub>	Temperature, vacuum chamber wall, top.	Cu/Cn	460°R - 560°R	± 4°R
T <sub>wm</sub>	Temperature, vacuum chamber wall, middle.	Cu/Cn	460°R - 560°R	± 4°R
T <sub>wb</sub>	Temperature, vacuum chamber wall, bottom.	Cu/Cn	460°R - 560°R	± 4°R
T <sub>1</sub>	Temperature, #1 support anchor.	Cu/Cn	460°R - 560°R	± 4°R
T <sub>2</sub>	Temperature, anchor end, 51" dummy tube.	Cu/Cn	460°R - 560°R	± 4°R
T <sub>3</sub>	Temperature, dummy tube, 22/51 station.	Cu/Cn	360°R - 560°R	± 4°R
T <sub>4</sub>	Temperature, dummy tube insulation outer surface.	Cu/Cn	460°R - 560°R	± 4°R
T <sub>5</sub>	Temperature, support tube, 13/30 station.	Cu/Cn	360°R - 560°R	± 4°R
T <sub>6</sub>	Temperature, support tube insulation outer surface.	Cu/Cn	460°R - 560°R	± 4°R
T <sub>7</sub>	Temperature, #2 support anchor.	Cu/Cn	460°R - 560°R	± 4°R
T <sub>8</sub>	Temperature, anchor end, 56" dummy tube.	Cu/Cn	460°R - 560°R	± 4°R
T <sub>9</sub>	Temperature, #3 support anchor.	Cu/Cn	460°R - 560°R	± 4°R
T <sub>lh2</sub>	Temperature, liquid hydrogen in tank.	Thermistor	30°R - 60°R	± 1°R
T <sub>lpg</sub>	Temperature, H <sub>2</sub> gas at meter inlet.	Cu/Cn	460°R - 560°R	± 4°R
P <sub>lpg</sub>	Pressure, H <sub>2</sub> gas at meter inlet.	Bourdon Gage	0-30 psig	± 0.6 psi
P <sub>o</sub>	Pressure, vacuum chamber.	Phillips Gage	10 <sup>-7</sup> - 10 <sup>-1</sup> mm Hg	± 10%
Pt	Pressure, H <sub>2</sub> gas in LH <sub>2</sub> tank.	Bourdon Gage	0-30 psig	± 0.6 psi
V	Flow, H <sub>2</sub> vent gas.	Rockwell Meter	0-100 SCFH	± 1%

Martin-CR-66-44

TABLE 25  
System Design Parameters

Primary Storage Container

Pressure Vessel Internal Volume	6.8 ft <sup>3</sup>
Pressure Vessel Internal Diameter	28.3 in.
Initial Helium Temperature	37.0 °R
Initial Helium Pressure	2000 Psia
Minimum Design Pressure	400 Psia
Pressure Vessel Material	Titanium 6AL-4V, ELI Grade
Pressure Vessel Working Stress	78,800
Allowable Heat Leak	3 to 30 $\frac{\text{Btu}}{\text{Hr}}$
Required Usable Helium Mass	68.3 lbm

Cascade Storage Container

Internal Volume	2.75 ft <sup>3</sup>
Internal Diameter	21.0 in.
Helium Temperature	530 °R
Initial Helium Pressure	4000 Psia
Minimum Design Pressure	450 Psia
Material	Titanium 6AL-4V, Heat Treated
Working Stress	110,000 Psia
Required Usable Helium Mass	5.5 lbm

TABLE 26  
System Weight Statement

<u>Item</u>	<u>Weight (lbm)</u>
Primary Tank Assembly	
Pressure Vessel	71.7
LH <sub>2</sub> Jacket	9.5
Vacuum Jacket	16.2
Internal Suspension and Tubing	4.0
Radiation Shielding	8.0
Primary Tank Assembly Sub-Total	<u>109.4</u>
Cascade Tank Assembly	50.1
Heat Exchangers	34.0
Valves, Fittings, Supports, & Miscellaneous	93.2
Primary Tank Helium	71.7
Cascade Tank Helium	<u>6.7</u>
Total Pressurization System Weight	365.1 lbm

## B. FIGURES

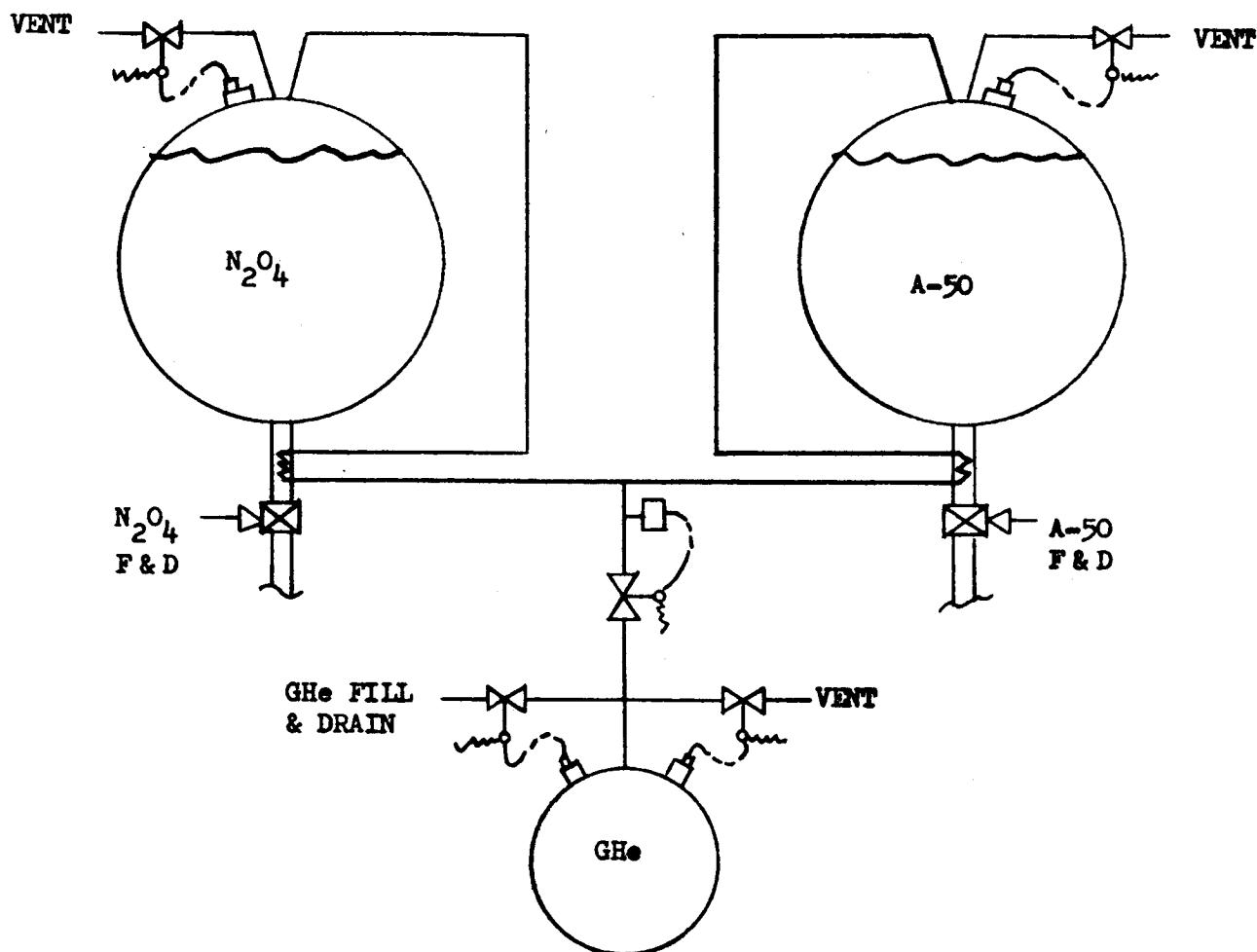


FIGURE 1 SYSTEM NUMBER 0 AND 1

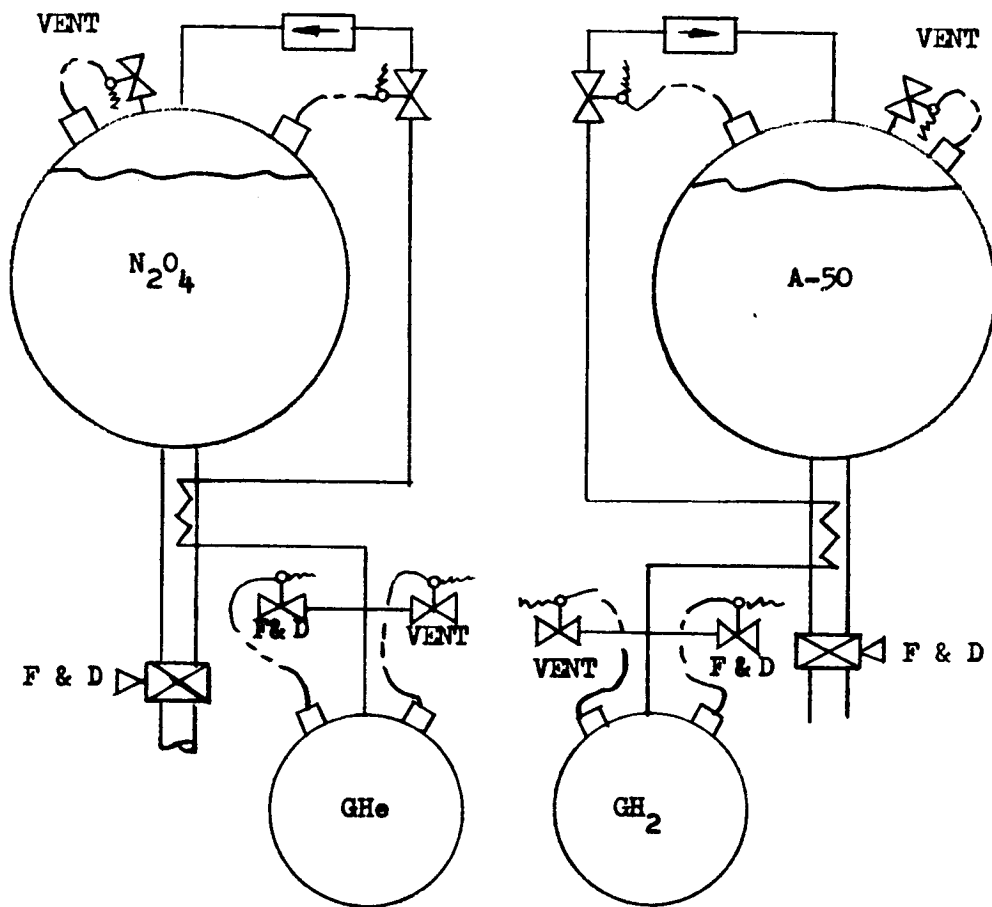


FIGURE 2 SYSTEM NUMBER 1A

Martin-CR-66-44

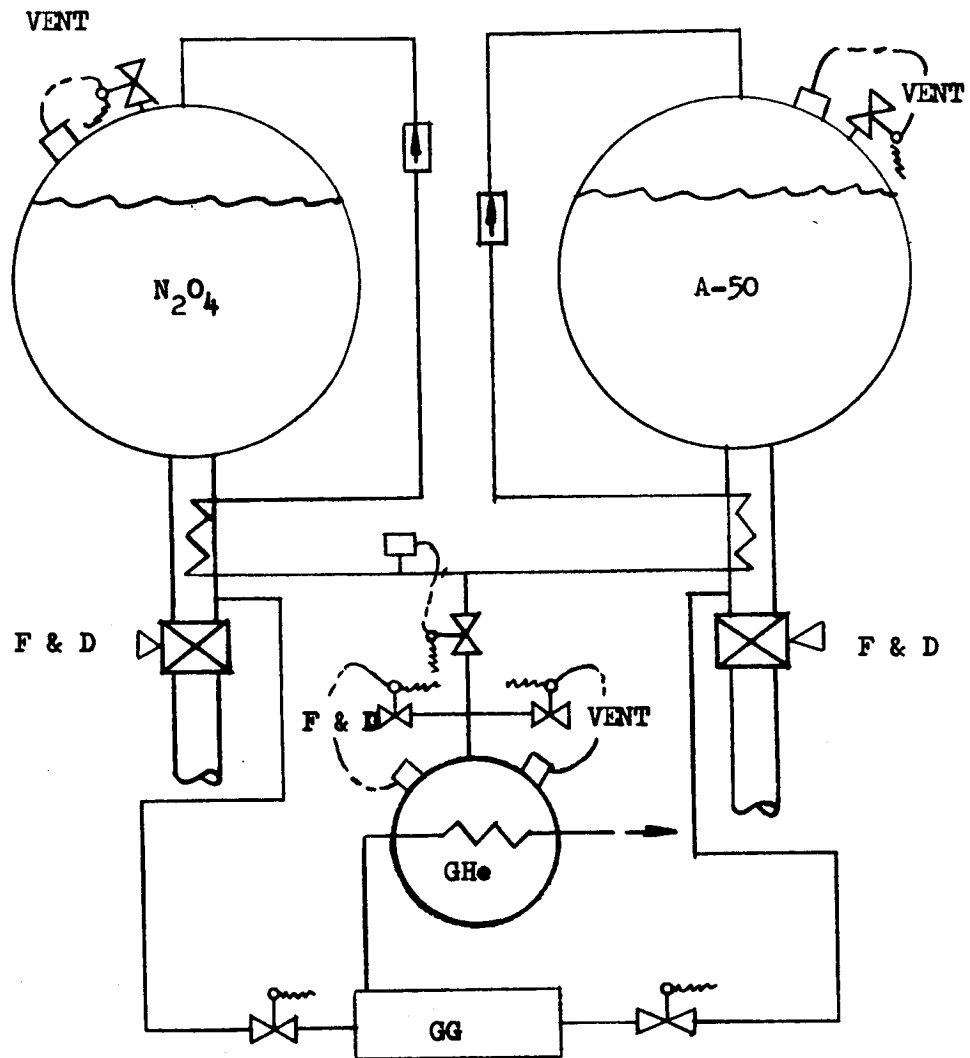


FIGURE 3 SYSTEM NUMBER 2

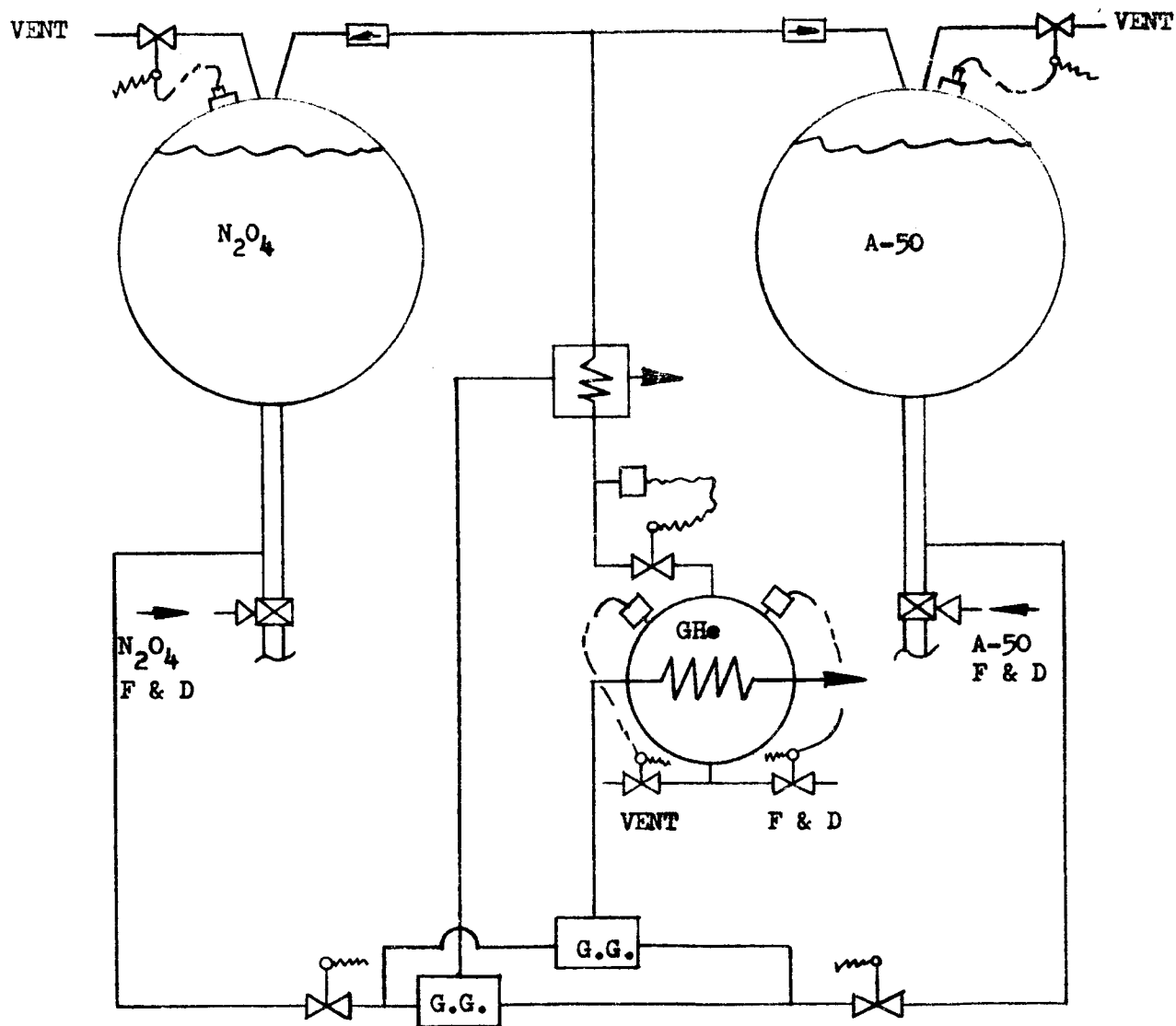


FIGURE 4 SYSTEM NUMBER 4

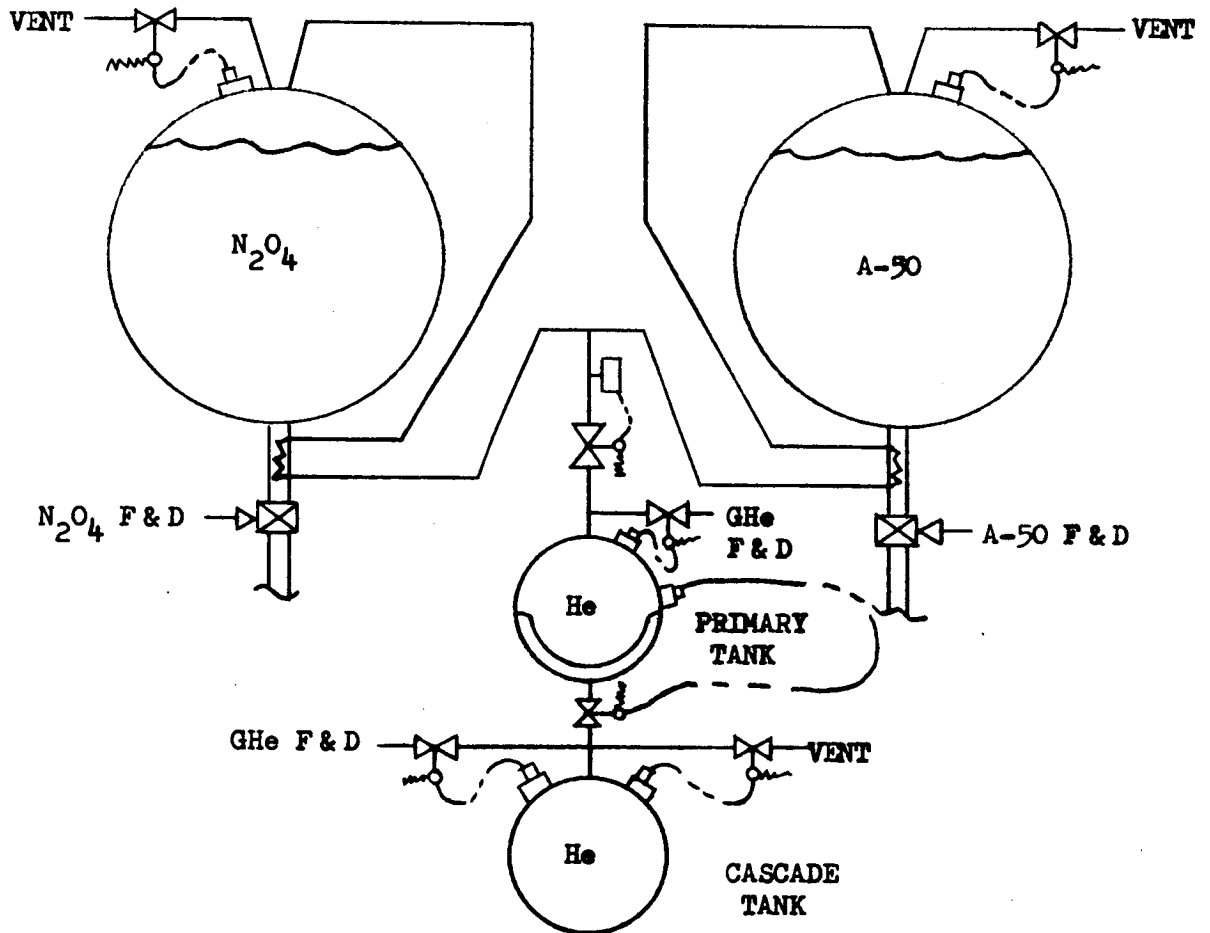


FIGURE 5 SYSTEM NUMBER 5

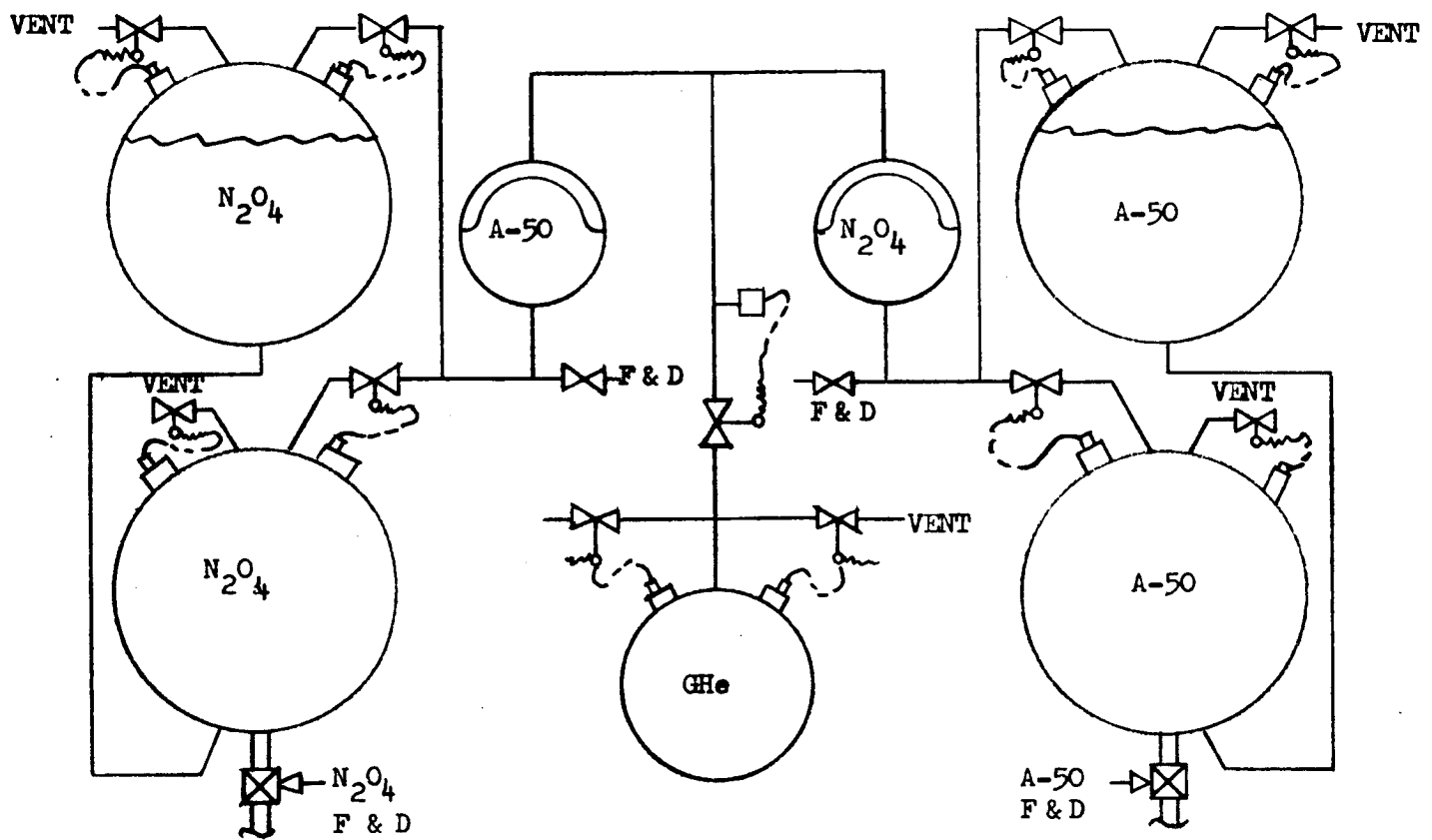


FIGURE 6 SYSTEM NUMBER 7

Martin-CR-66-44

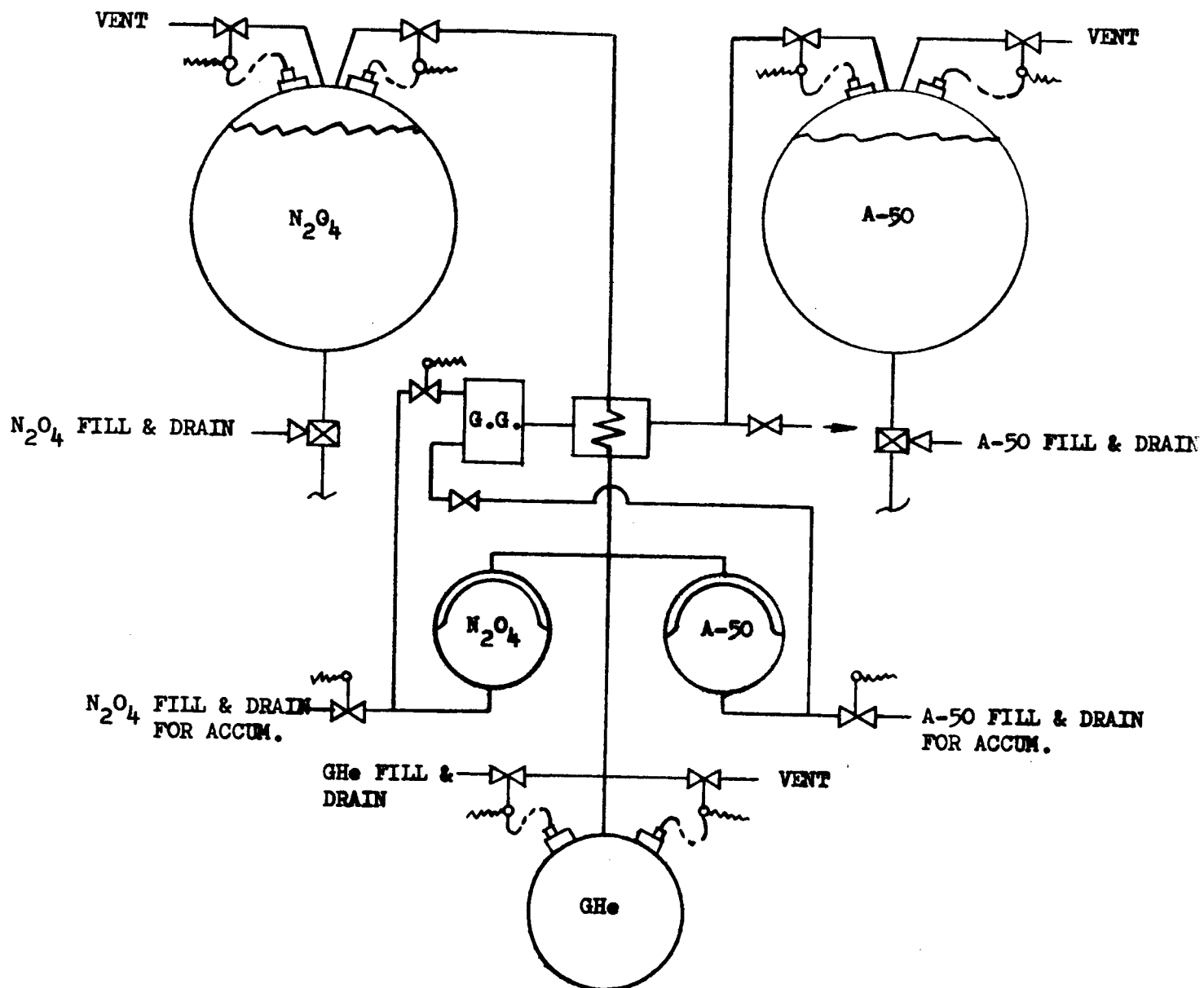
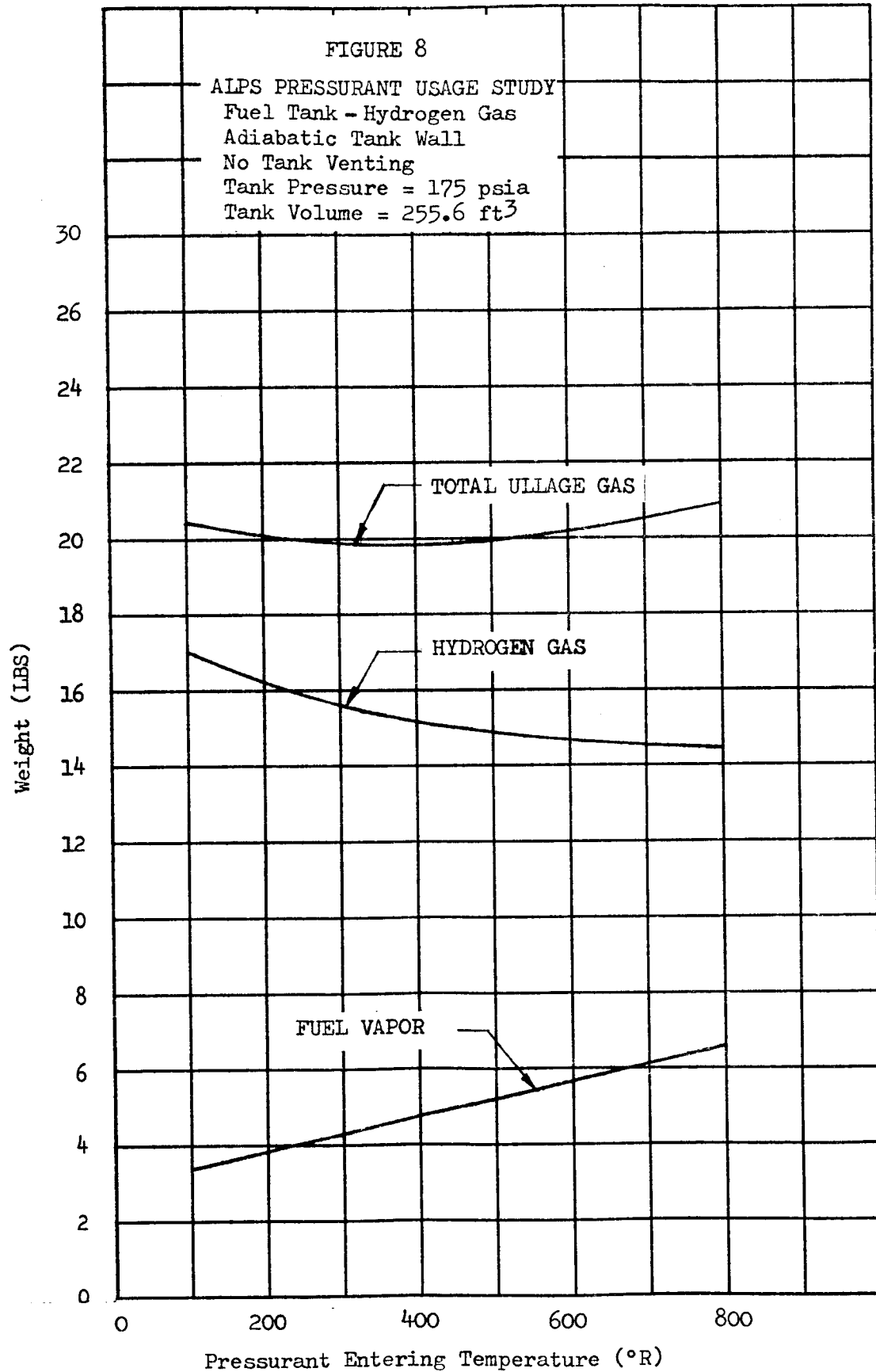
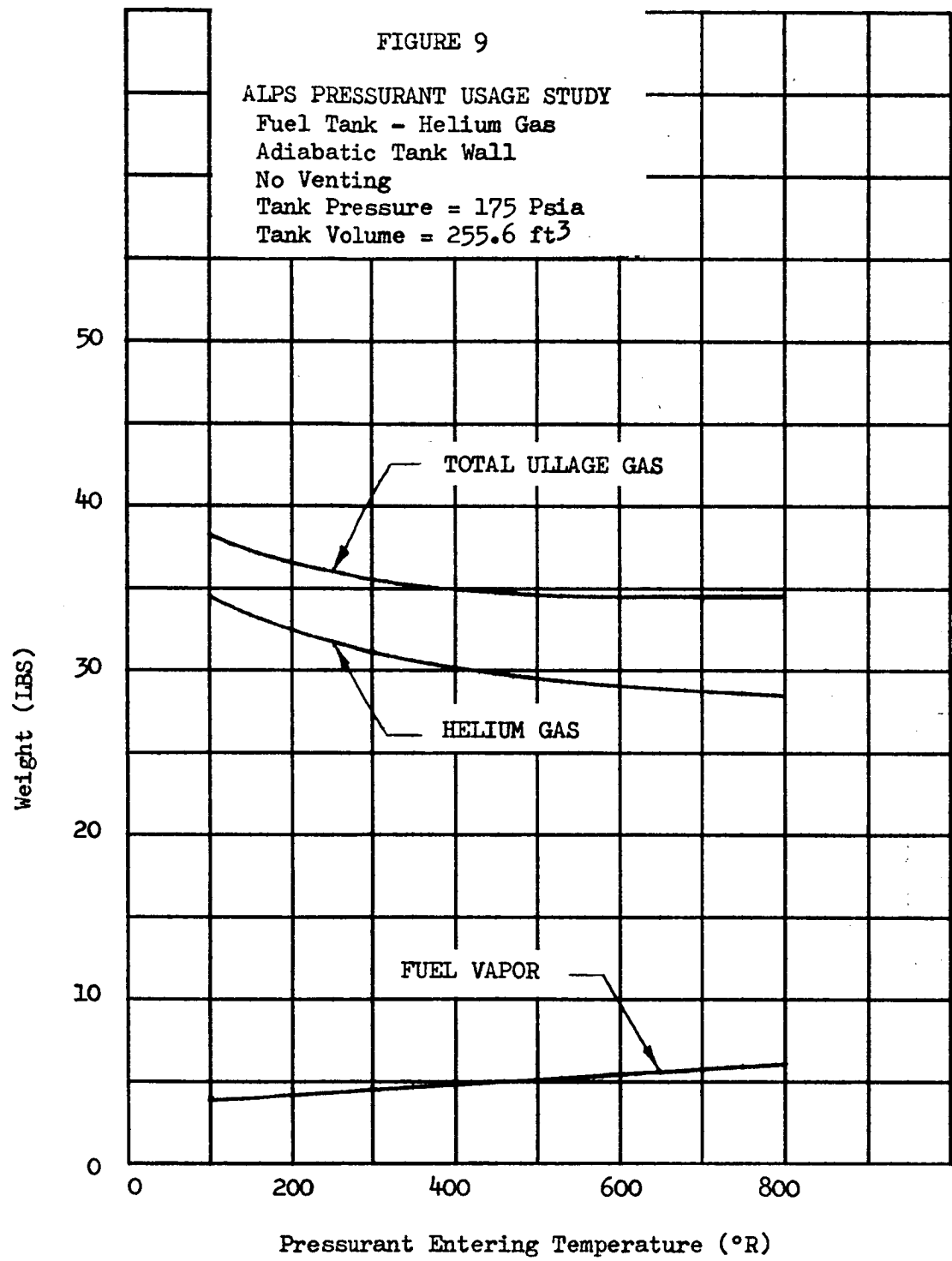


FIGURE 7 SYSTEM NUMBER 8

Martin-CR-66-44





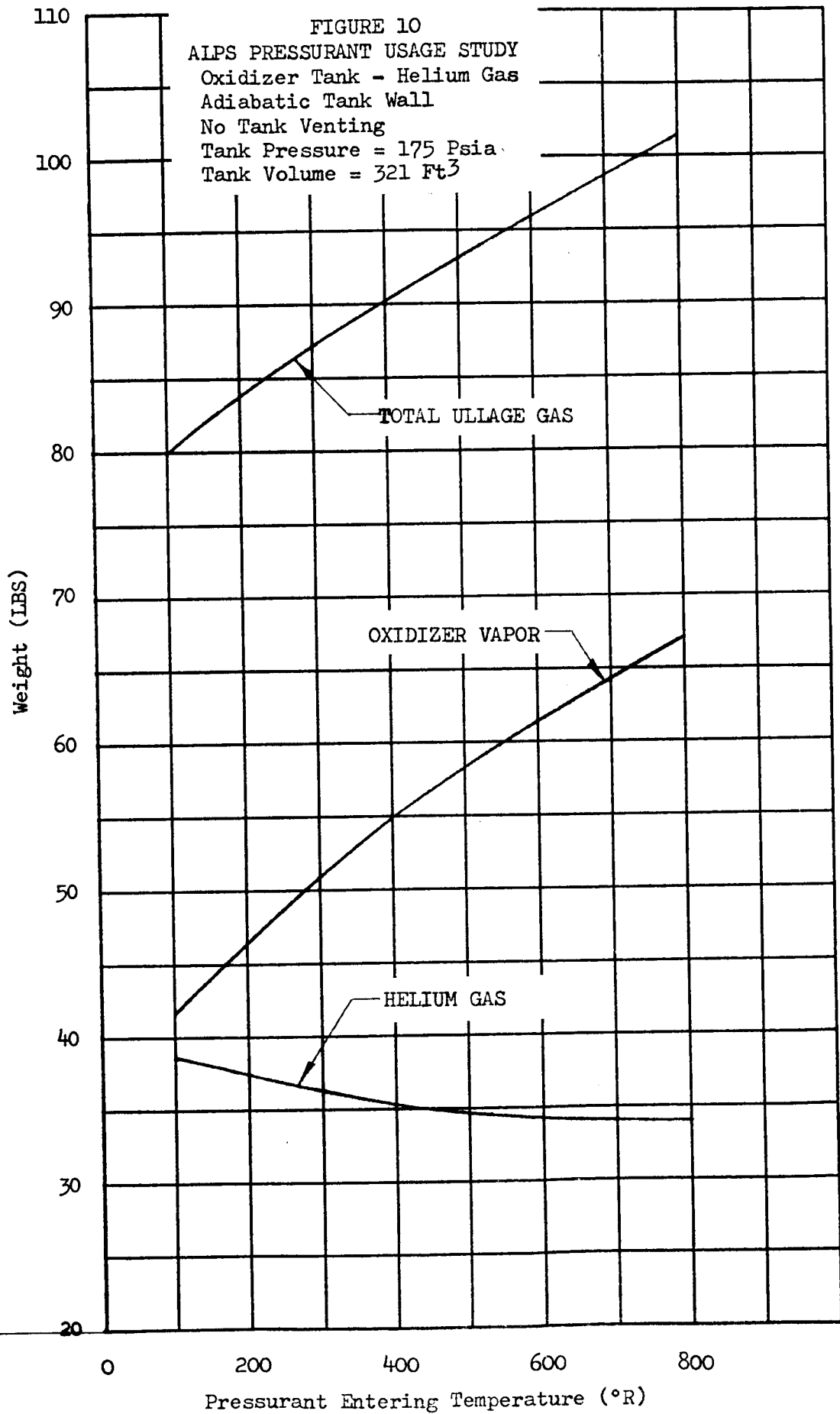
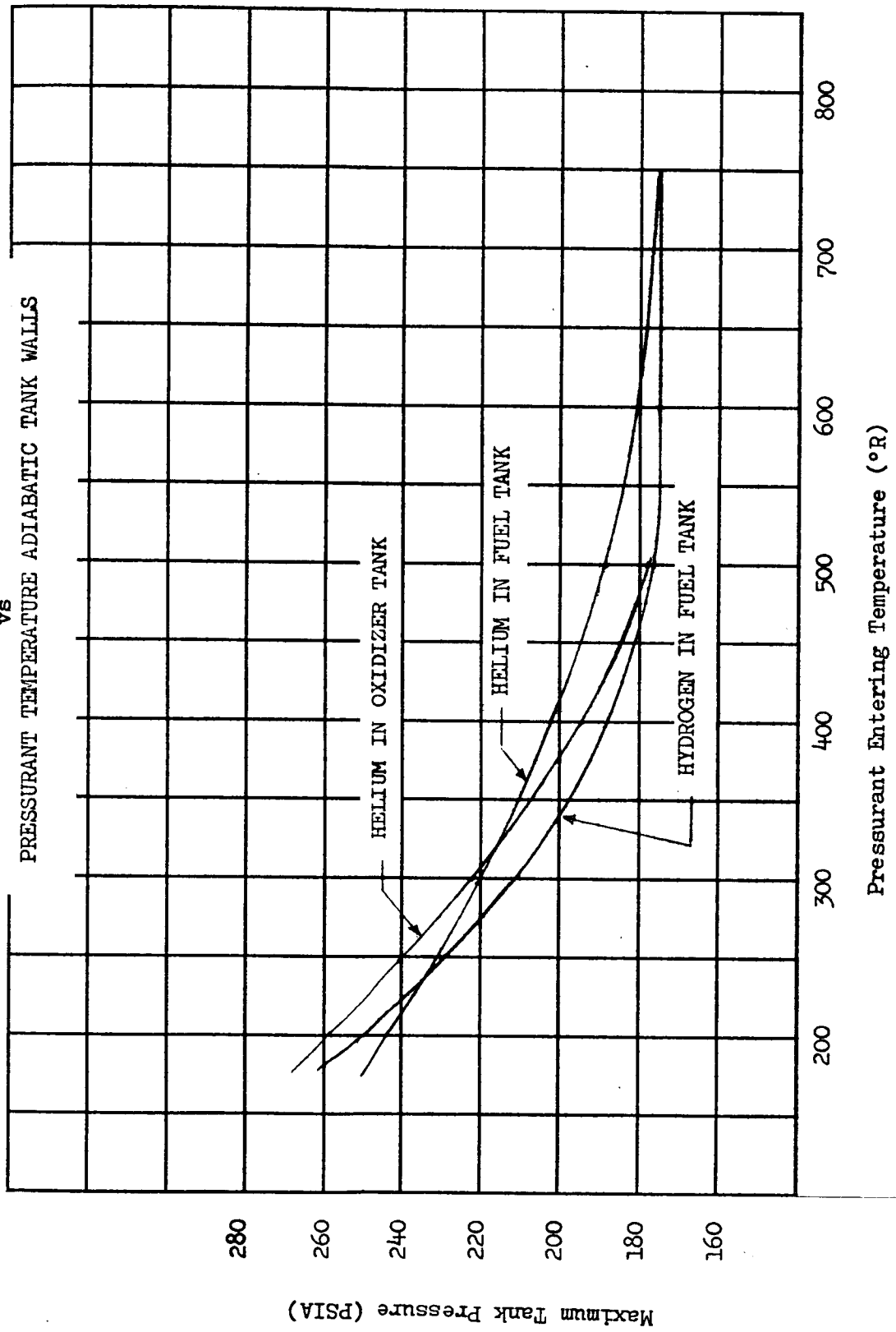
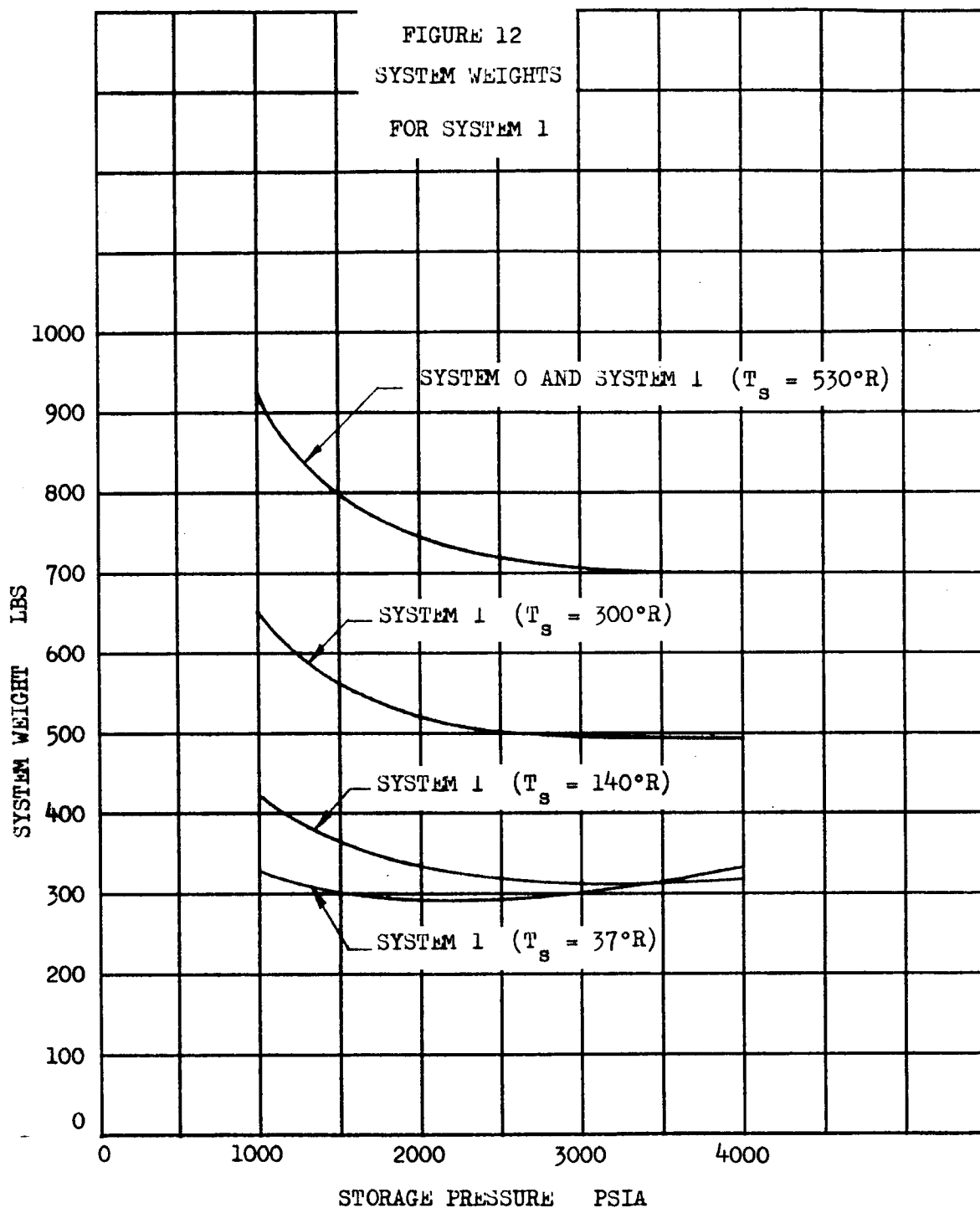
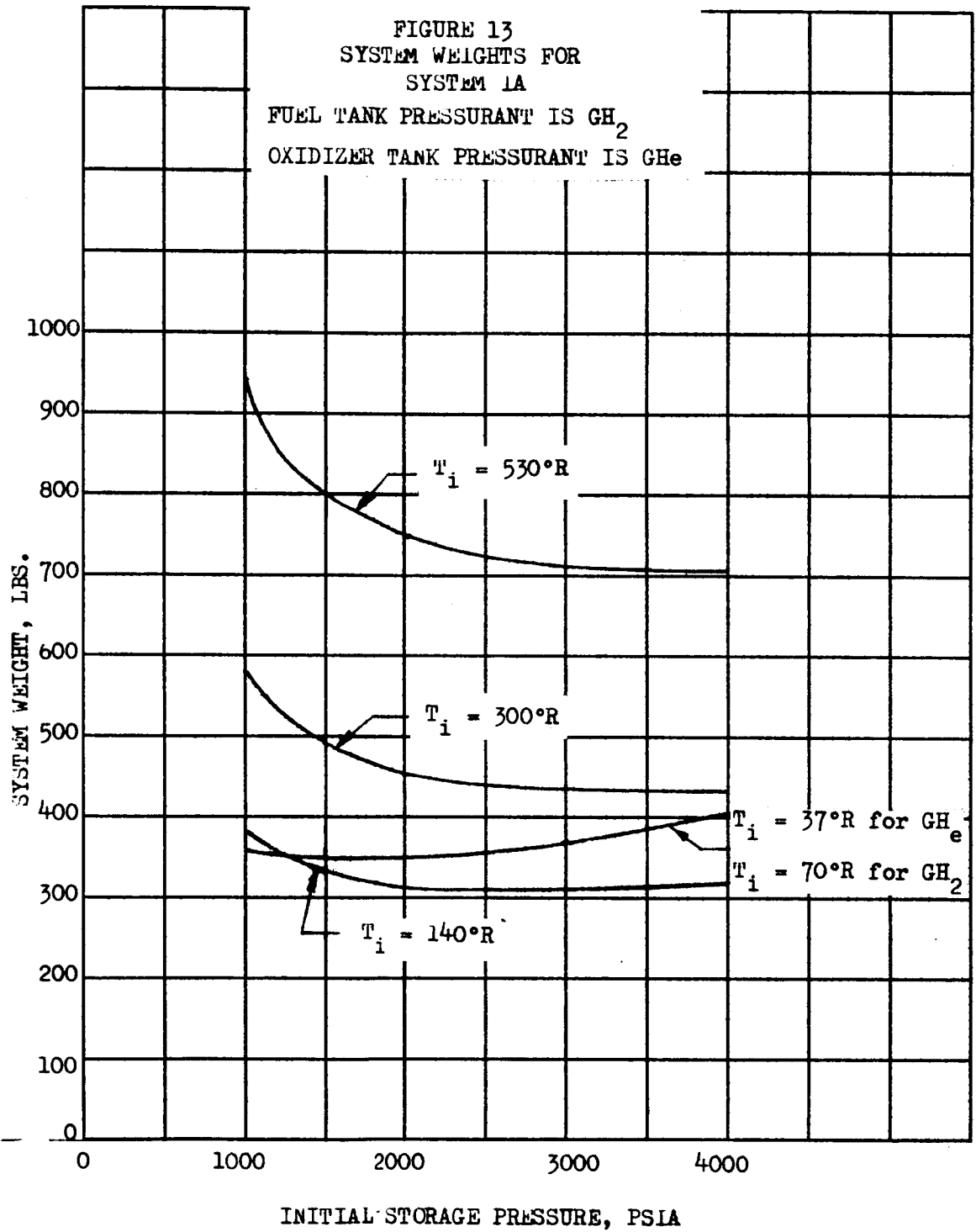


FIGURE 11  
MAXIMUM PROPELLANT TANK PRESSURE  
vs  
PRESSURANT TEMPERATURE ADIABATIC TANK WALLS







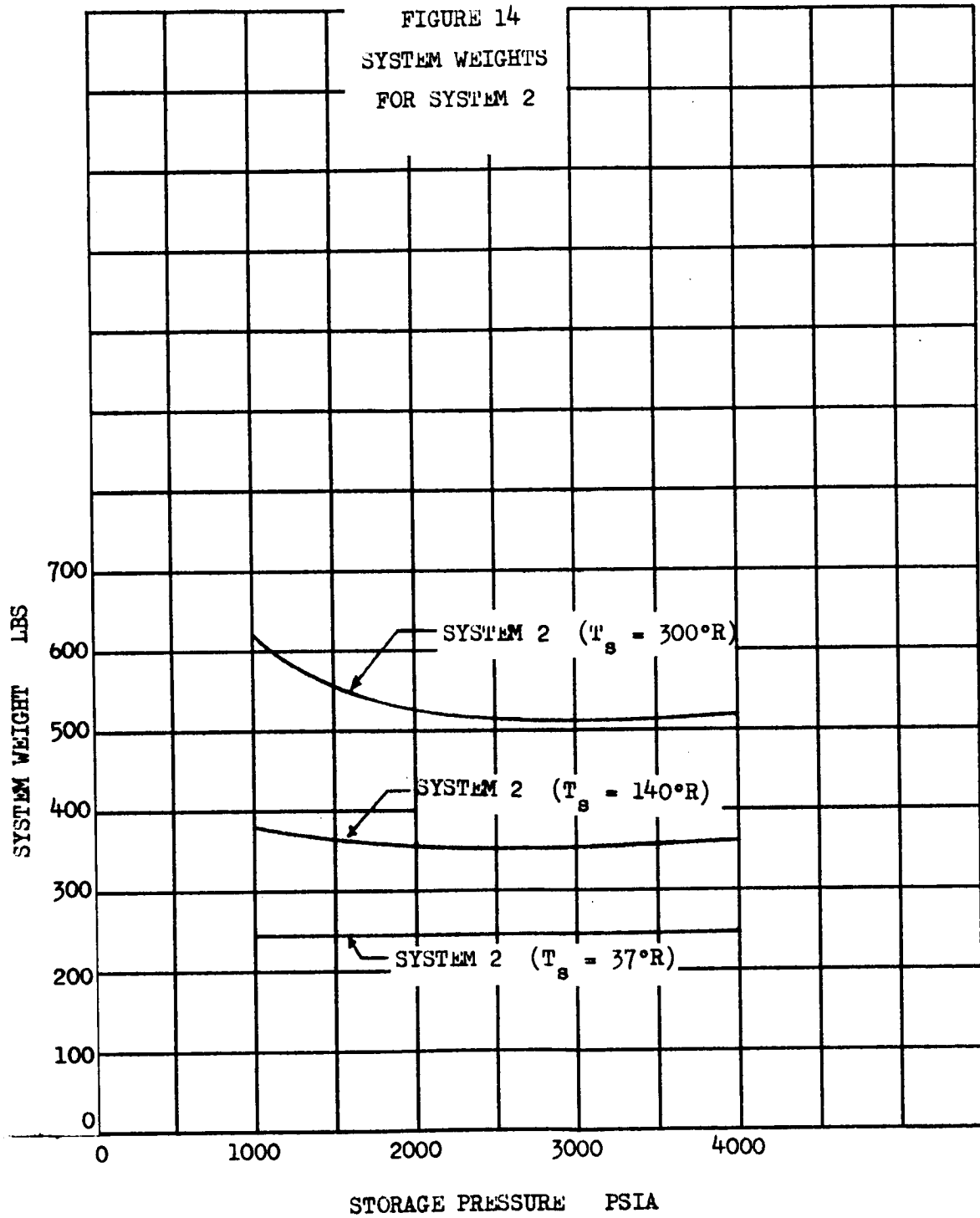
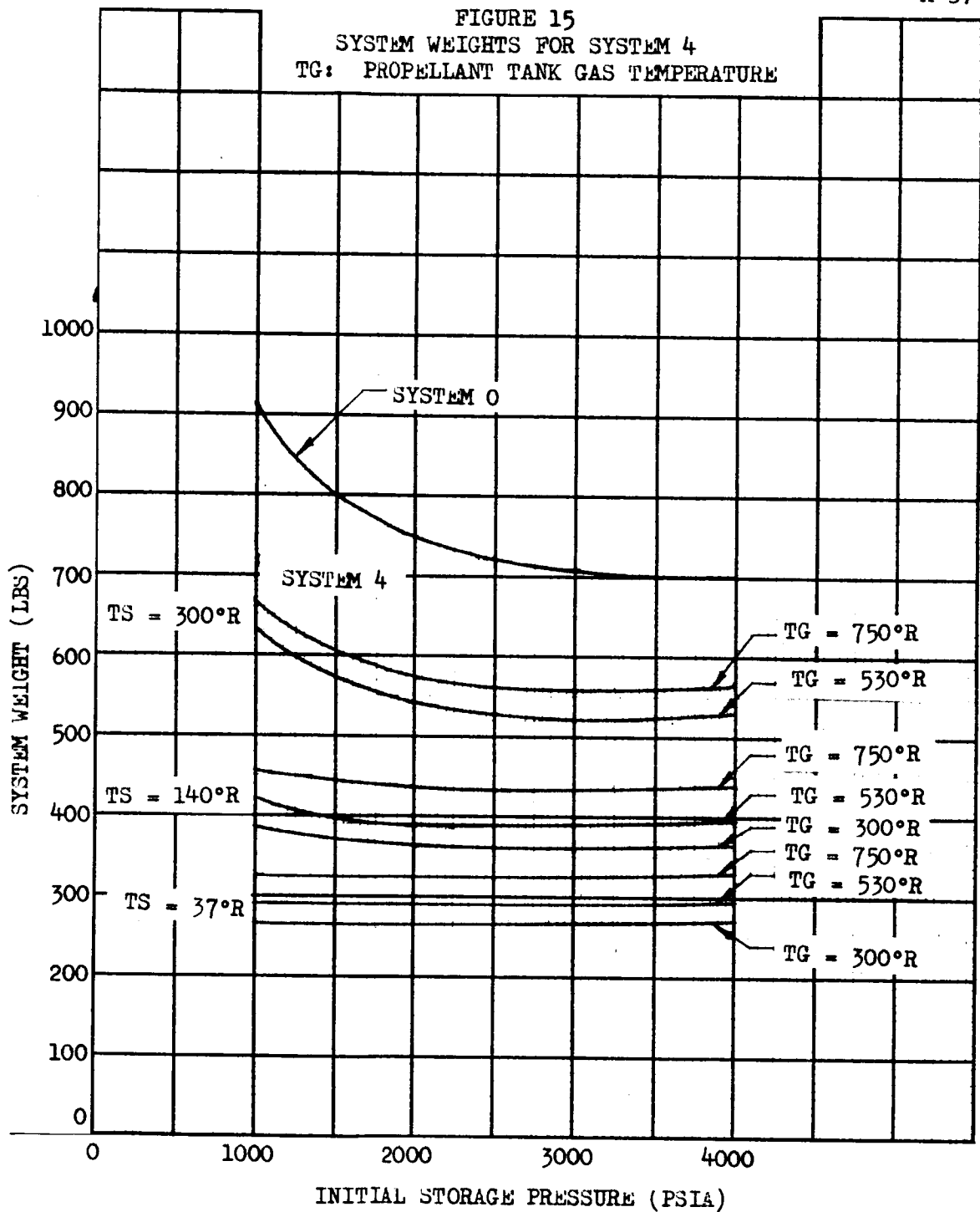


FIGURE 15  
SYSTEM WEIGHTS FOR SYSTEM 4  
TG: PROPELLANT TANK GAS TEMPERATURE



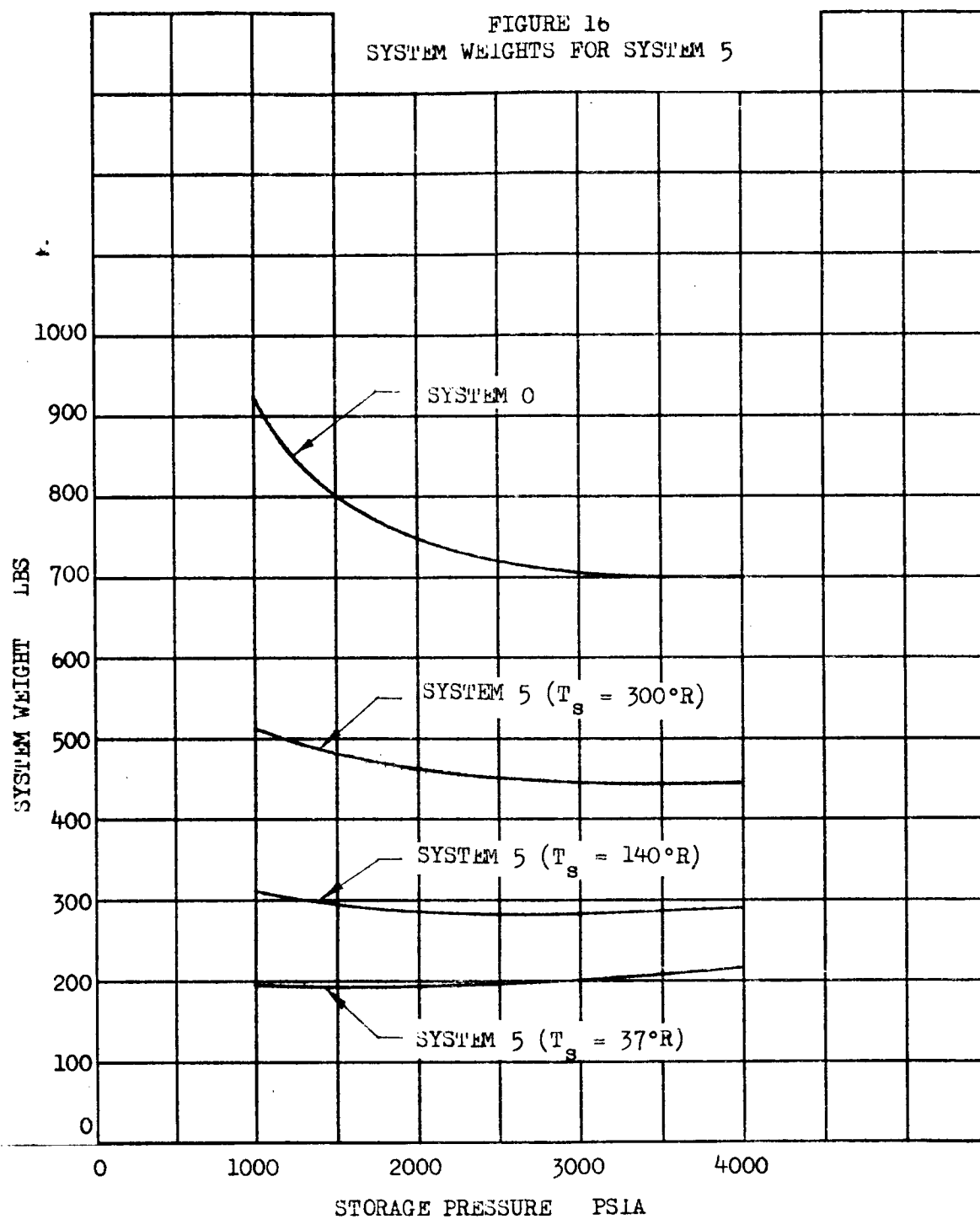
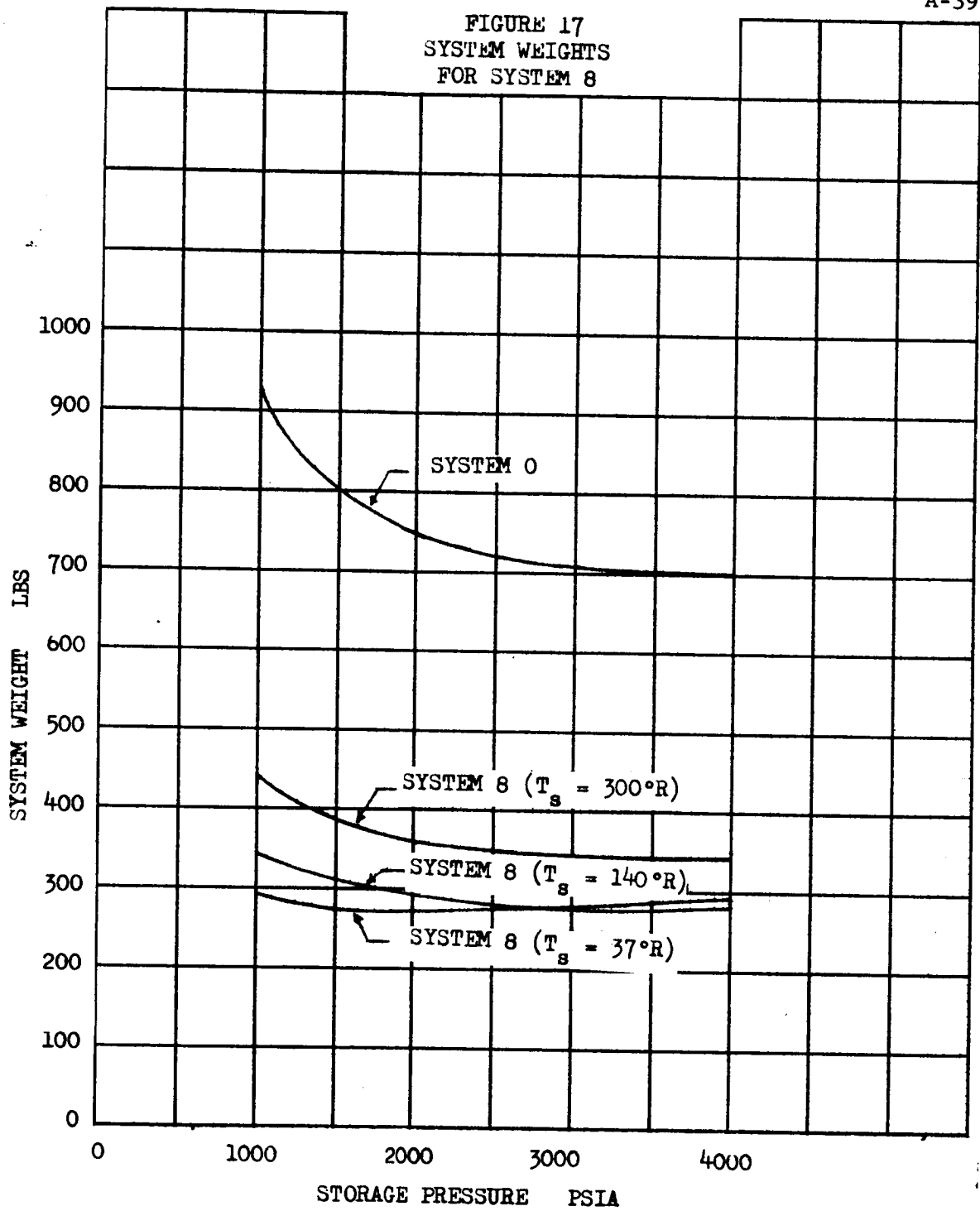
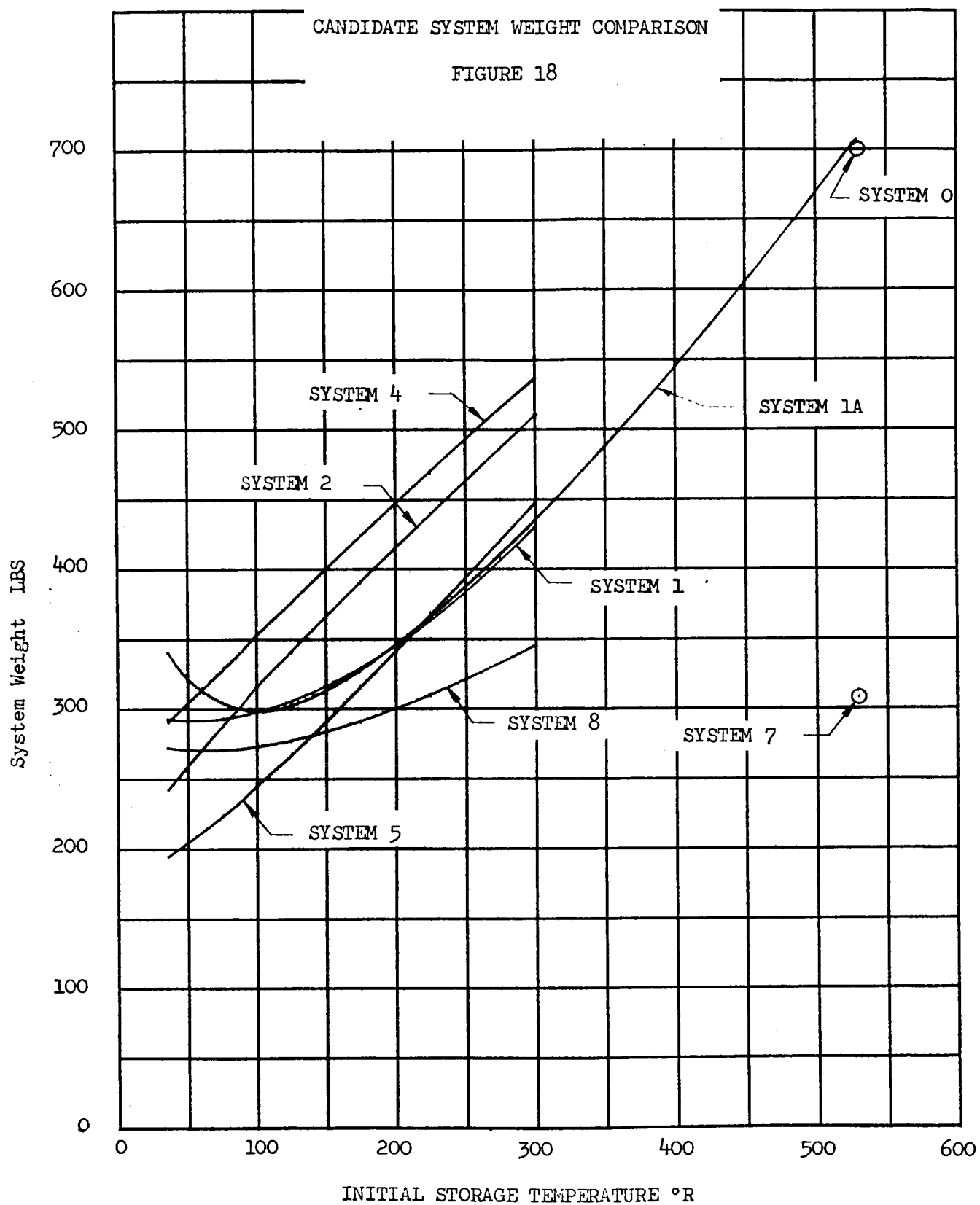


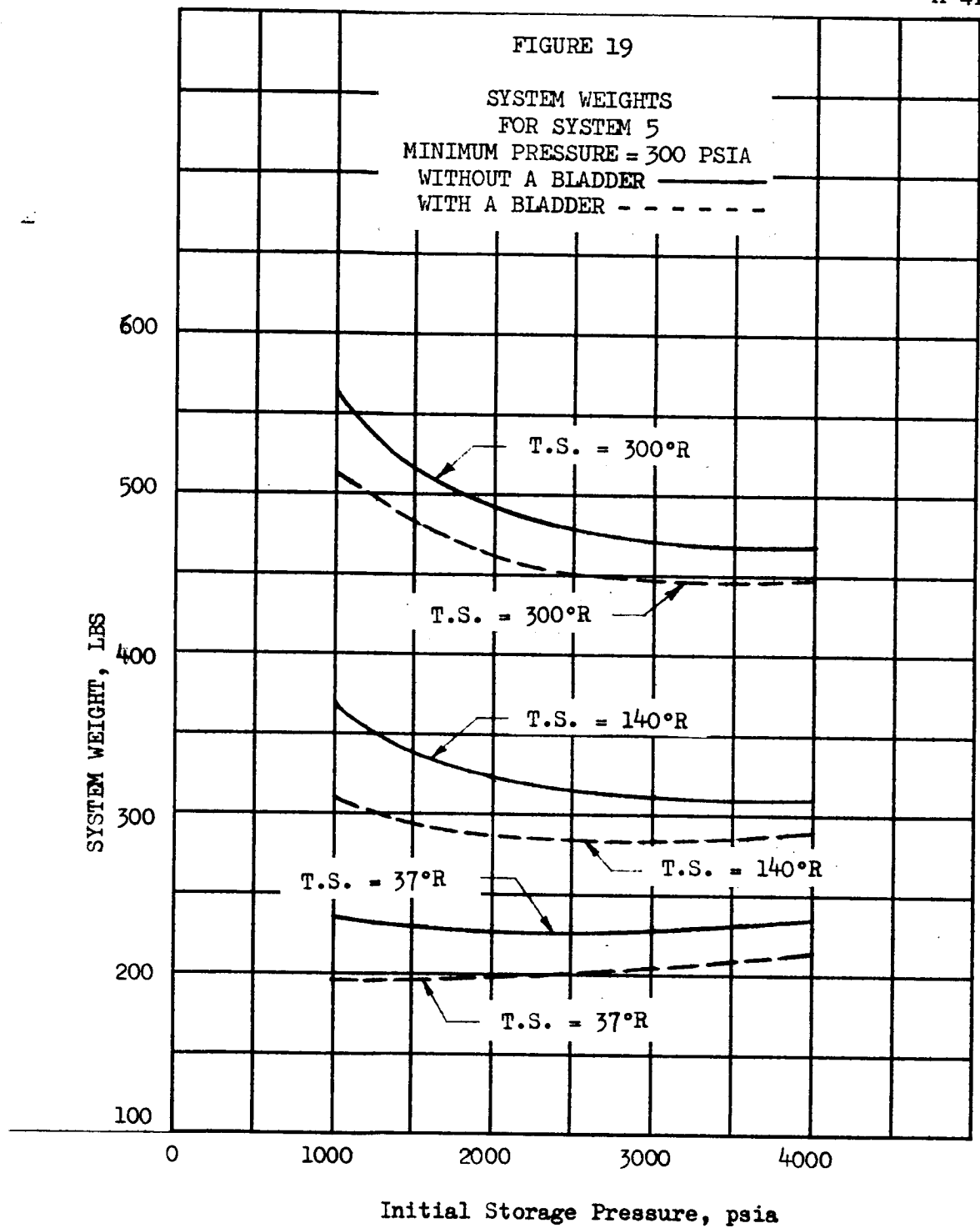
FIGURE 17  
SYSTEM WEIGHTS  
FOR SYSTEM 8

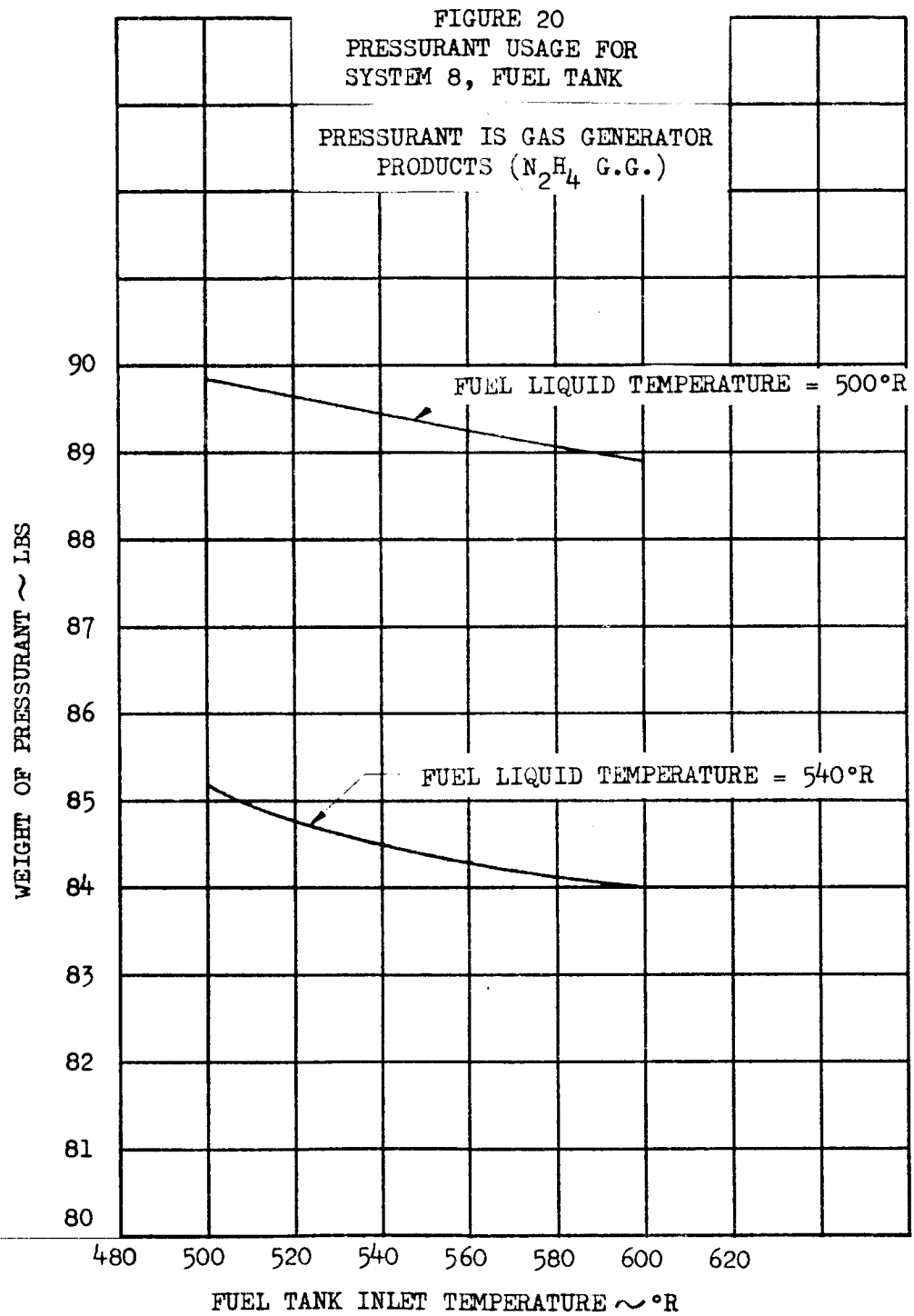


## CANDIDATE SYSTEM WEIGHT COMPARISON

FIGURE 18







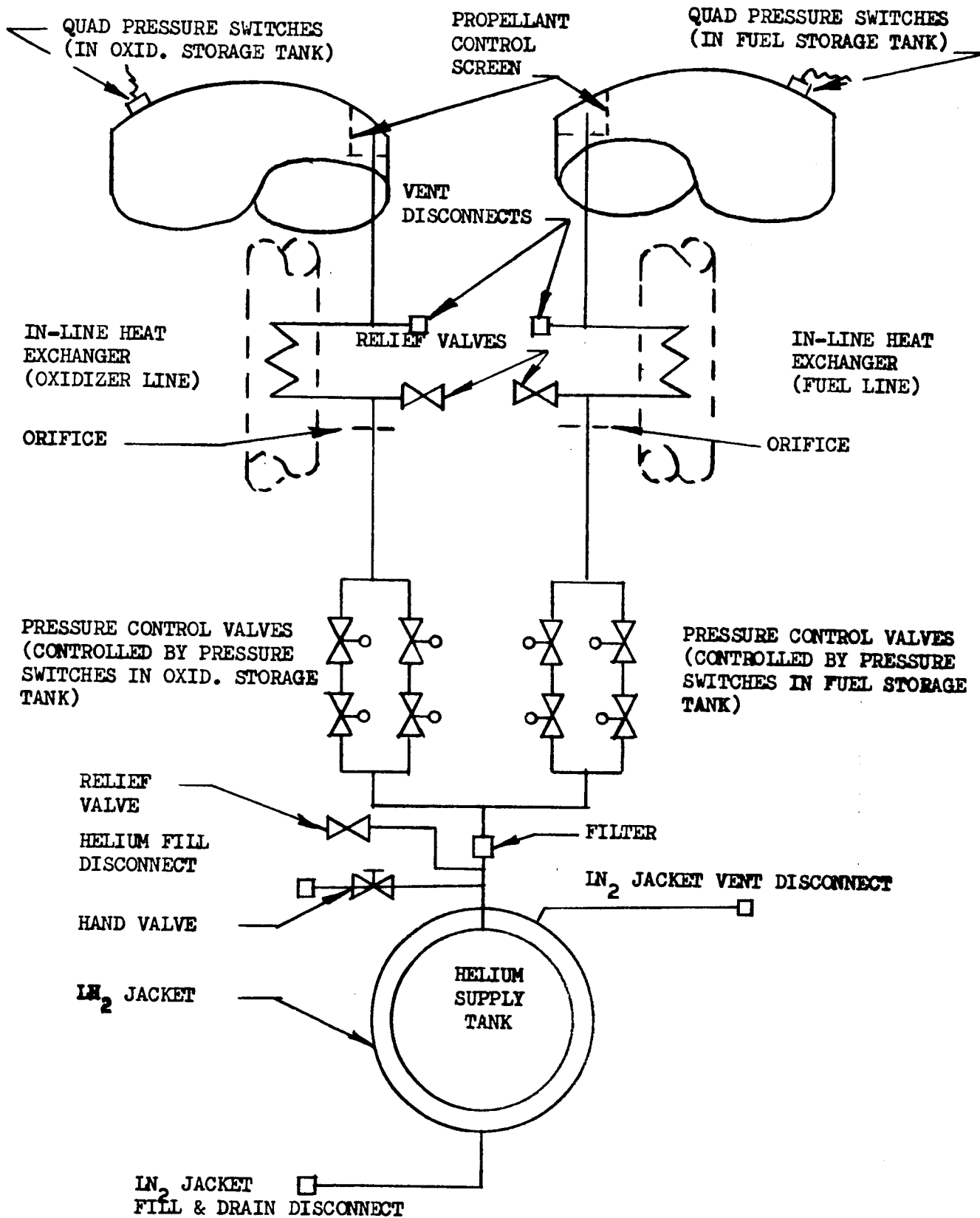


FIGURE 21 - SYSTEM 1

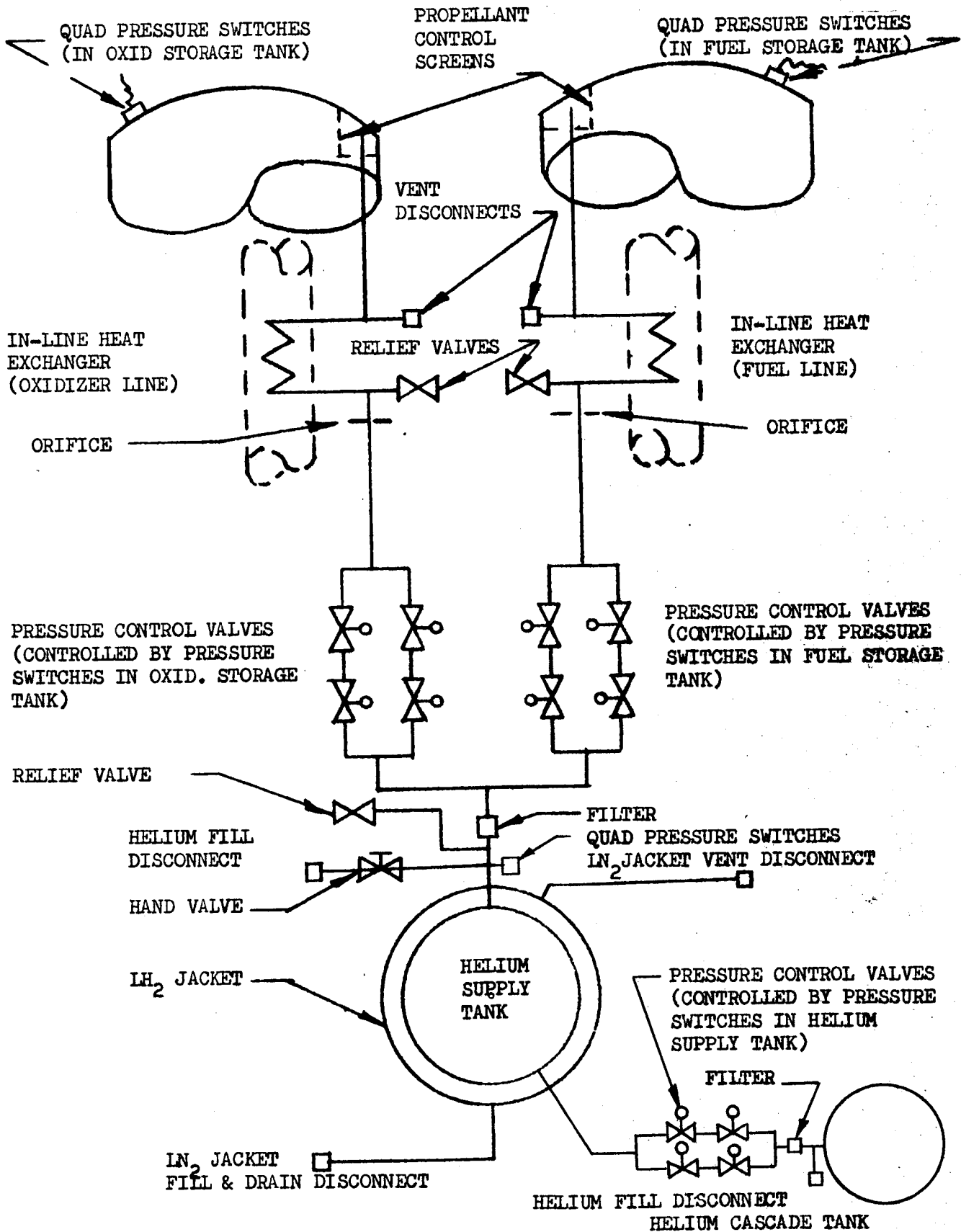


FIGURE 22 - SYSTEM 5

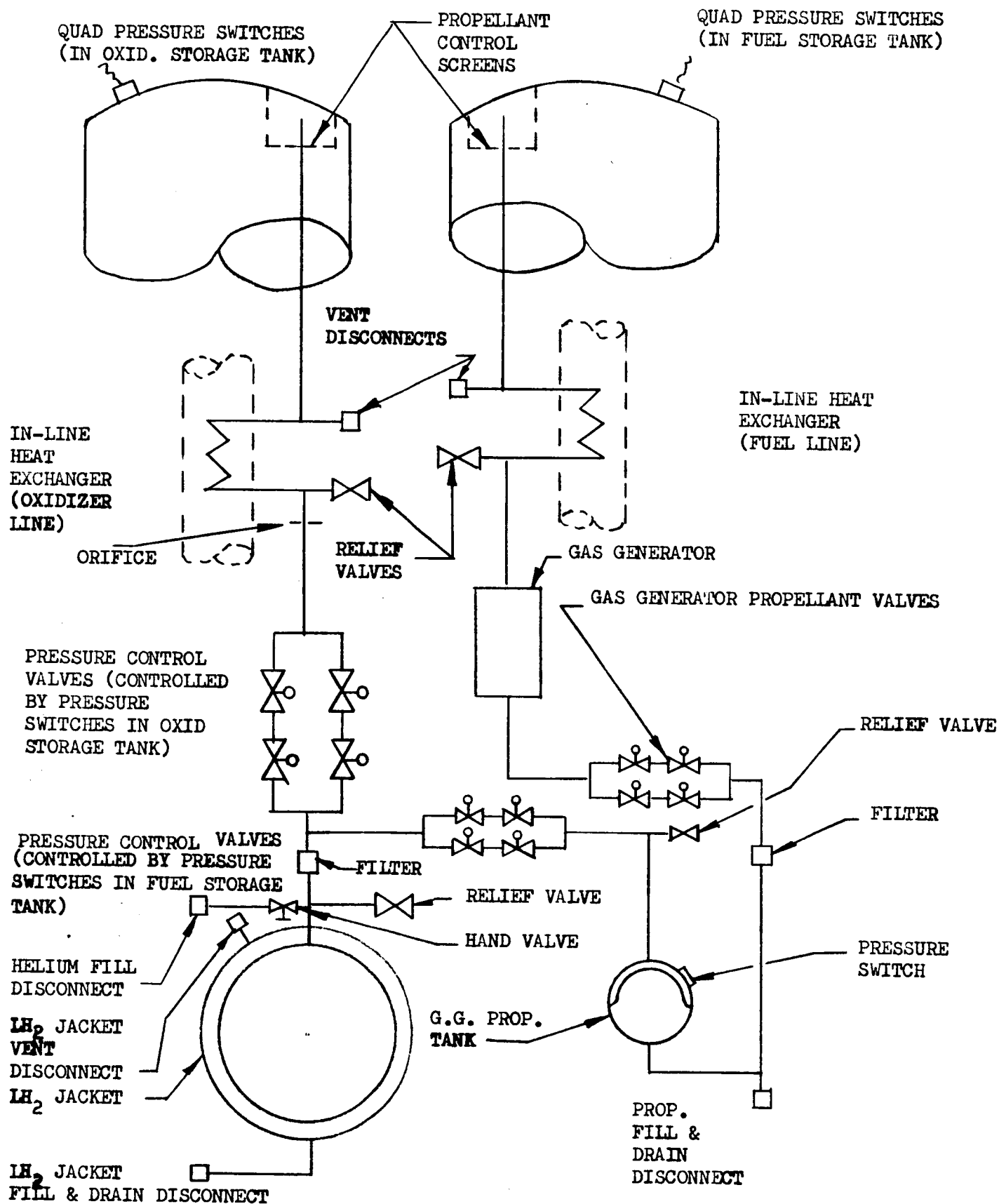
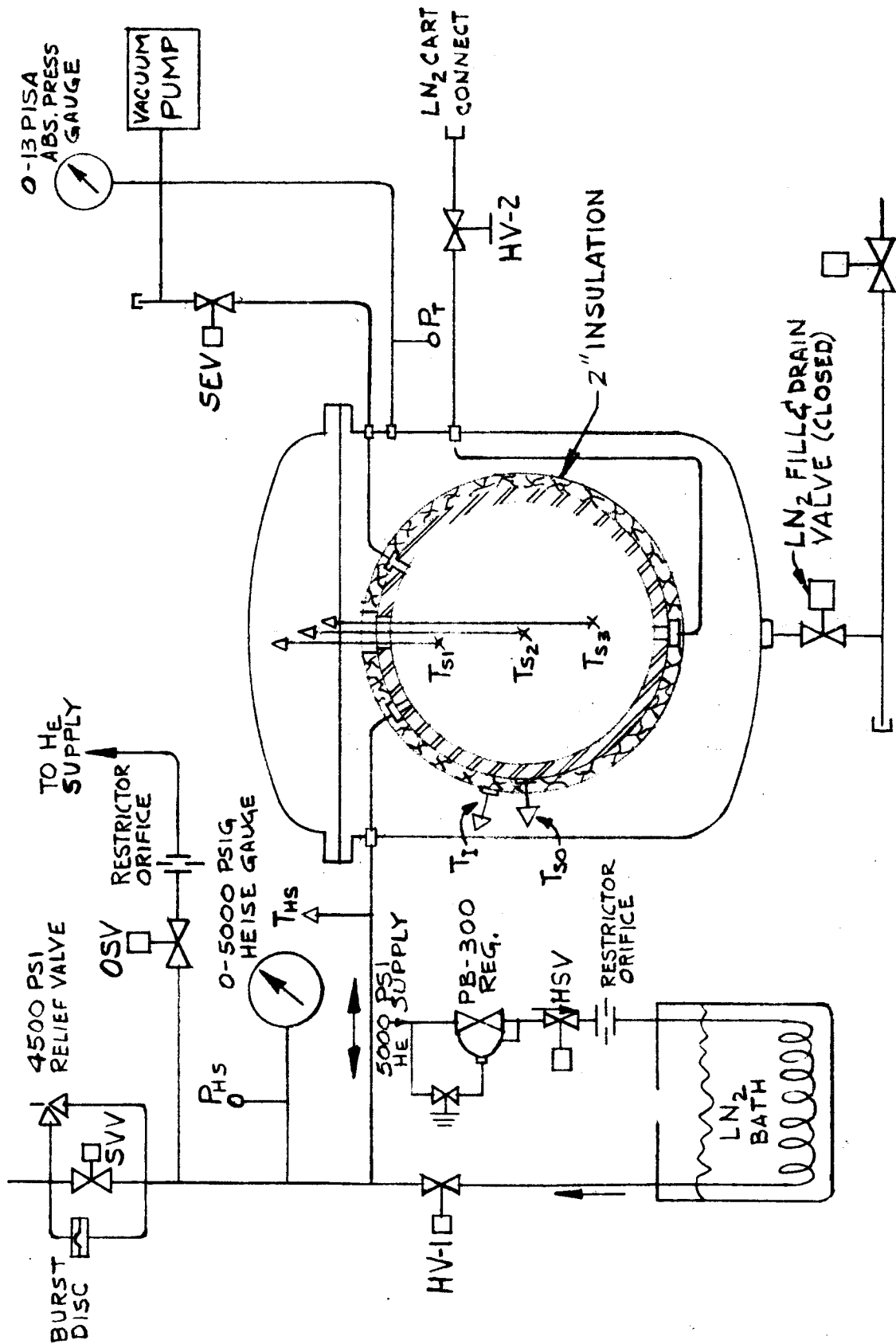


FIGURE 23 - SYSTEM 8

FIGURE 24 HELIUM STORAGE TEST SCHEMATIC



Martin-CR-66-44

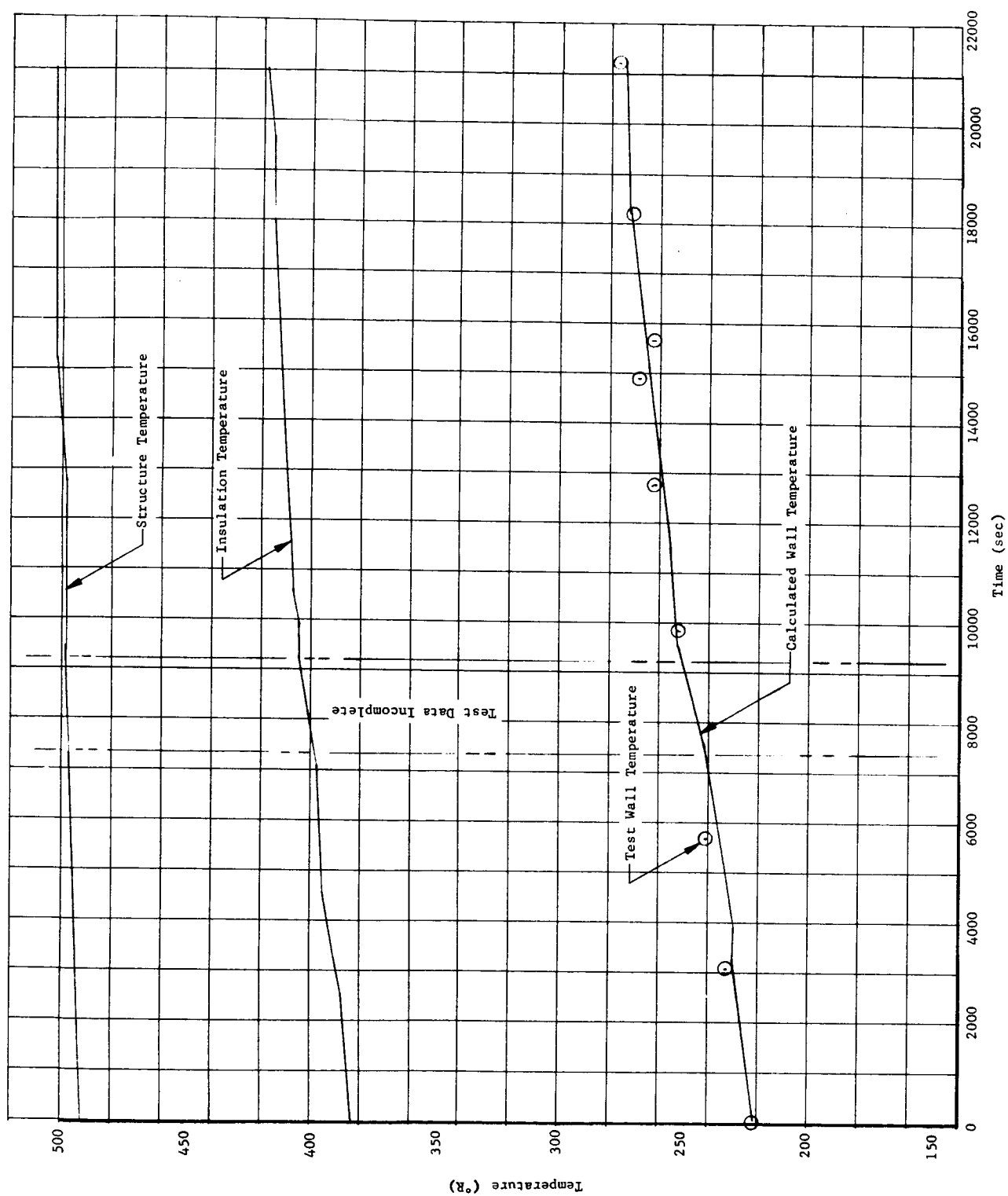


Fig. 25a Test and Calculated Data, Helium Storage Test 5

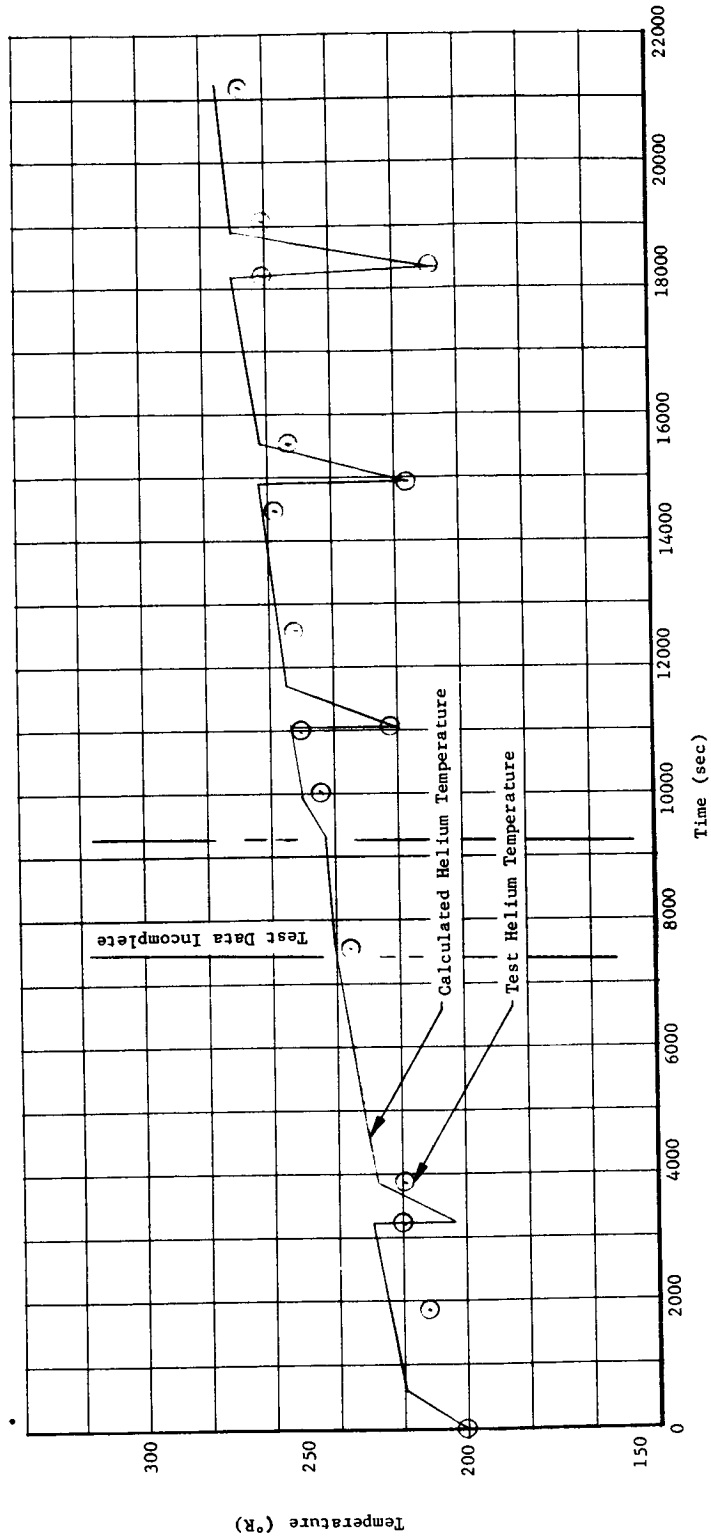


Fig. 25b Test and Calculated Data, Helium Storage Test 5

Martin-CR-66-44

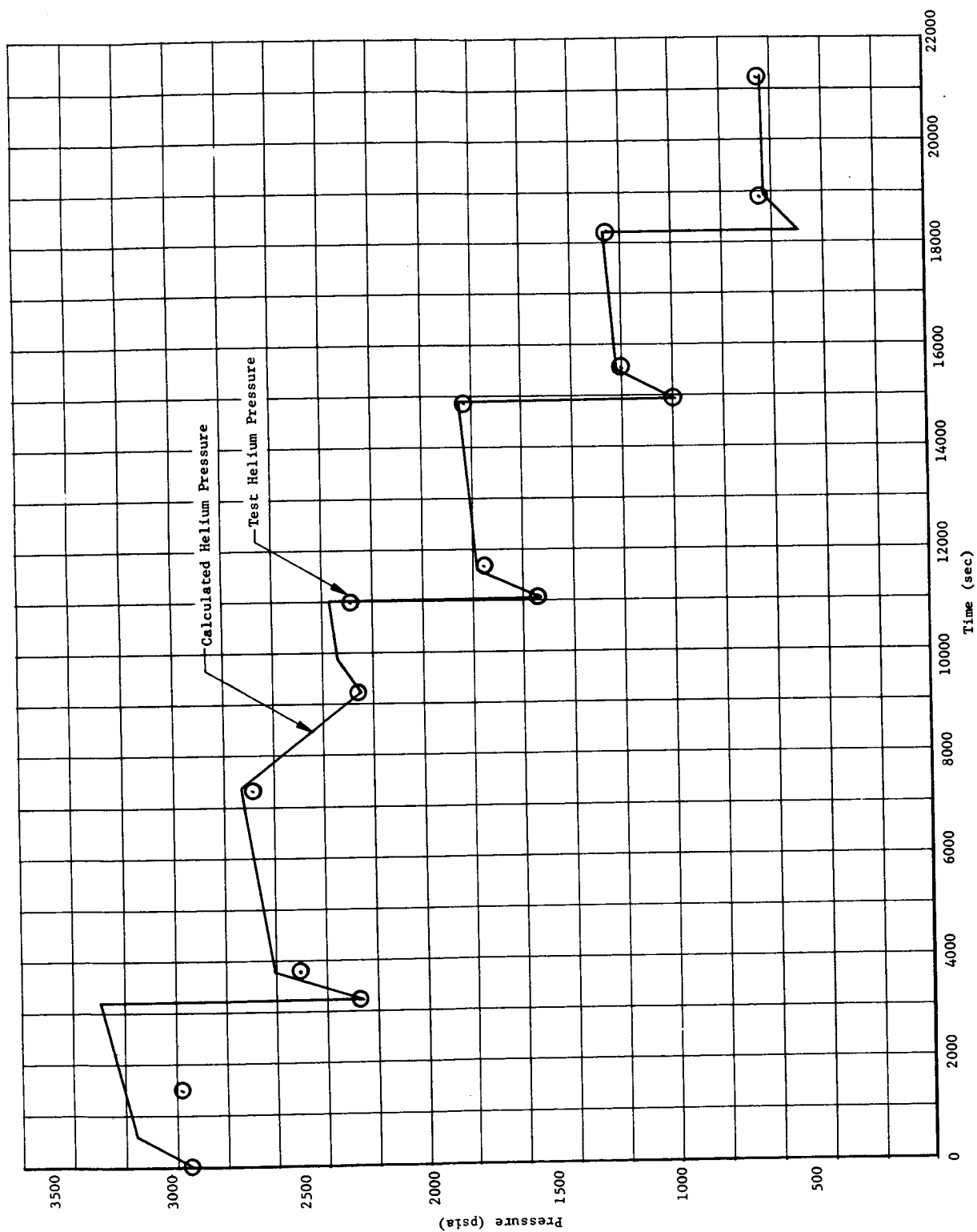


Fig. 26 Test and Calculated Data, Helium Storage Test 5

Martin-CR-66-44

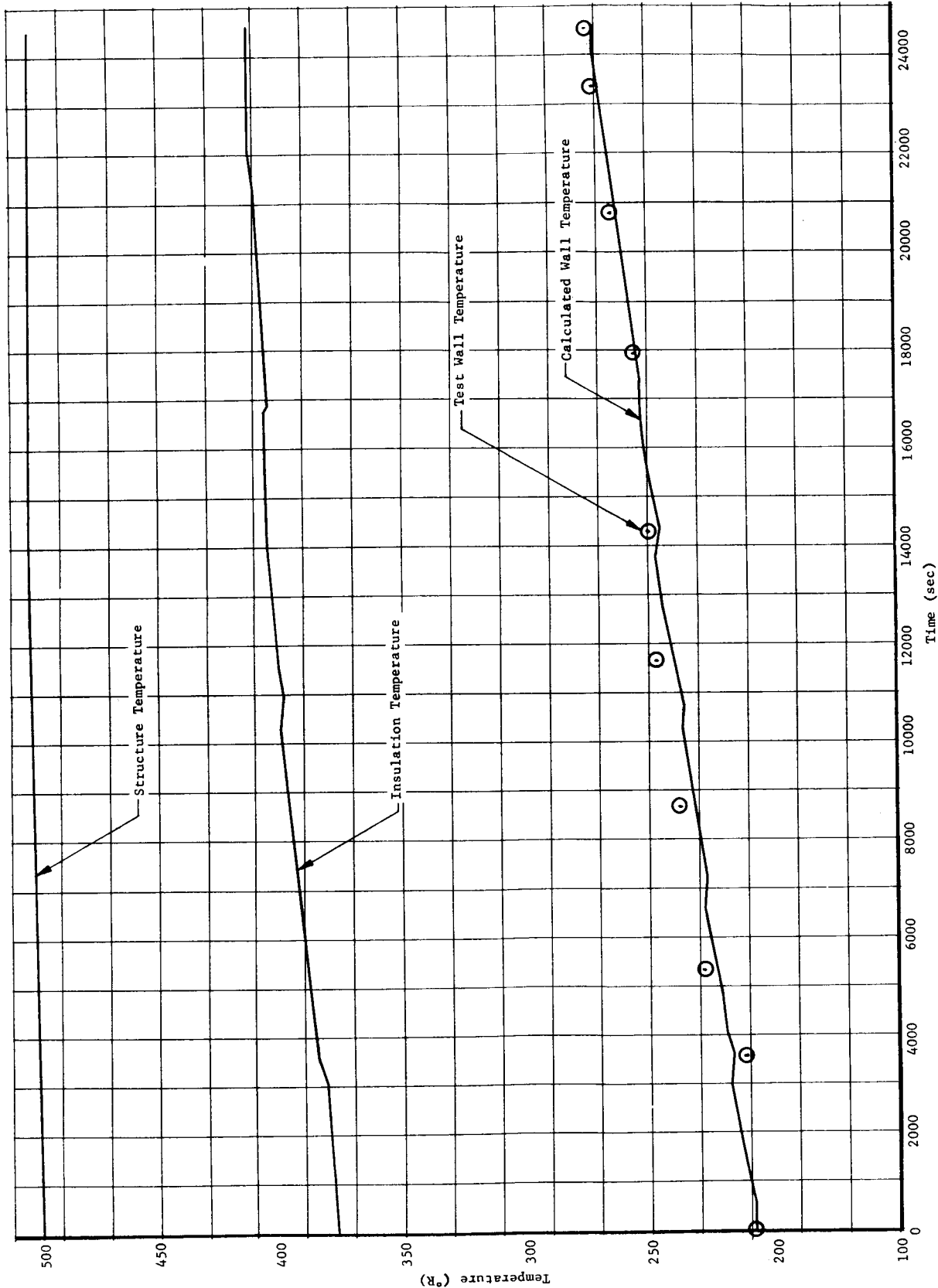


Fig. 27a Test and Calculated Data, Helium Storage Test 6

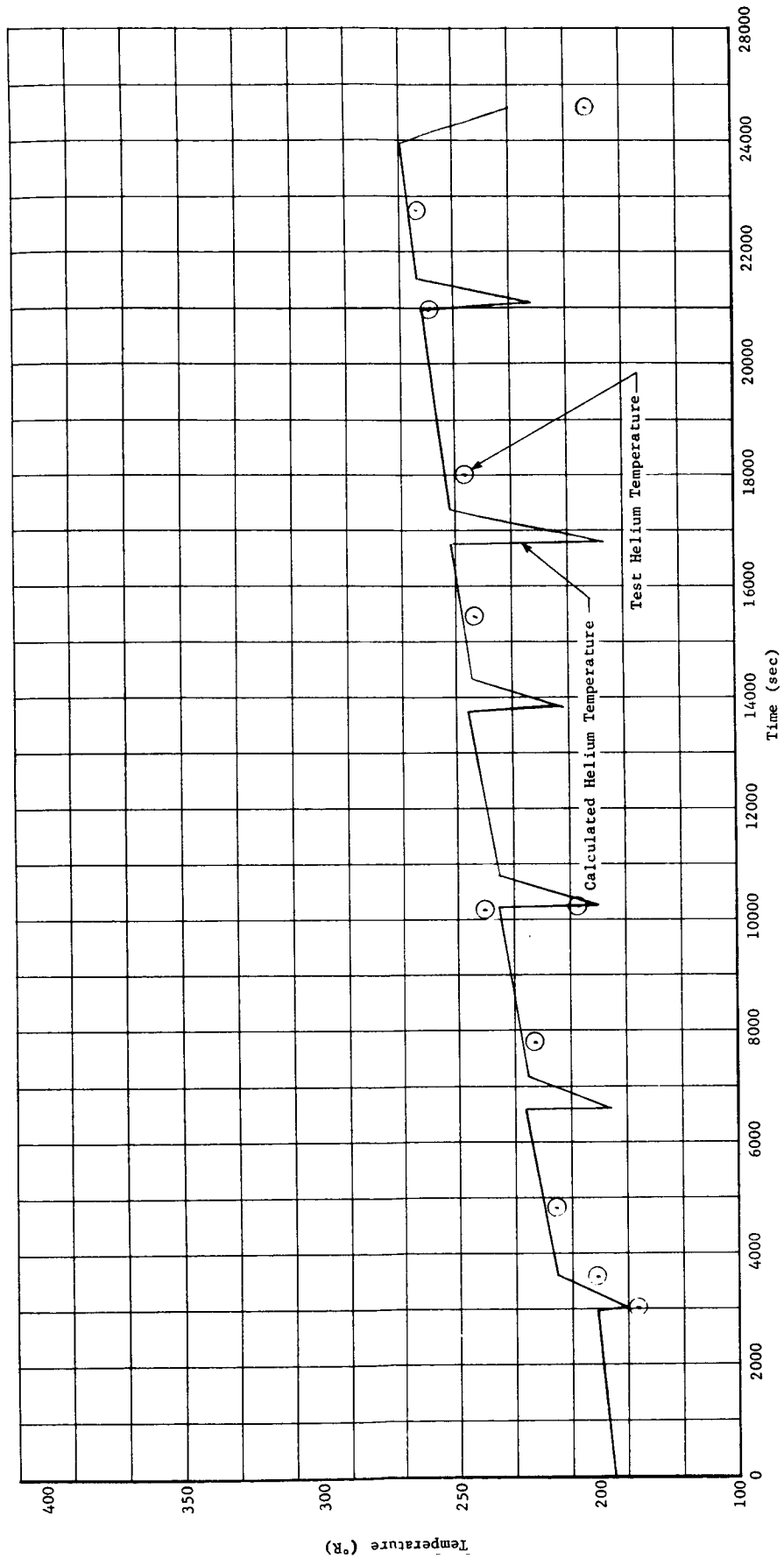


Fig. 27b Test and Calculated Data, Helium Storage Test 6

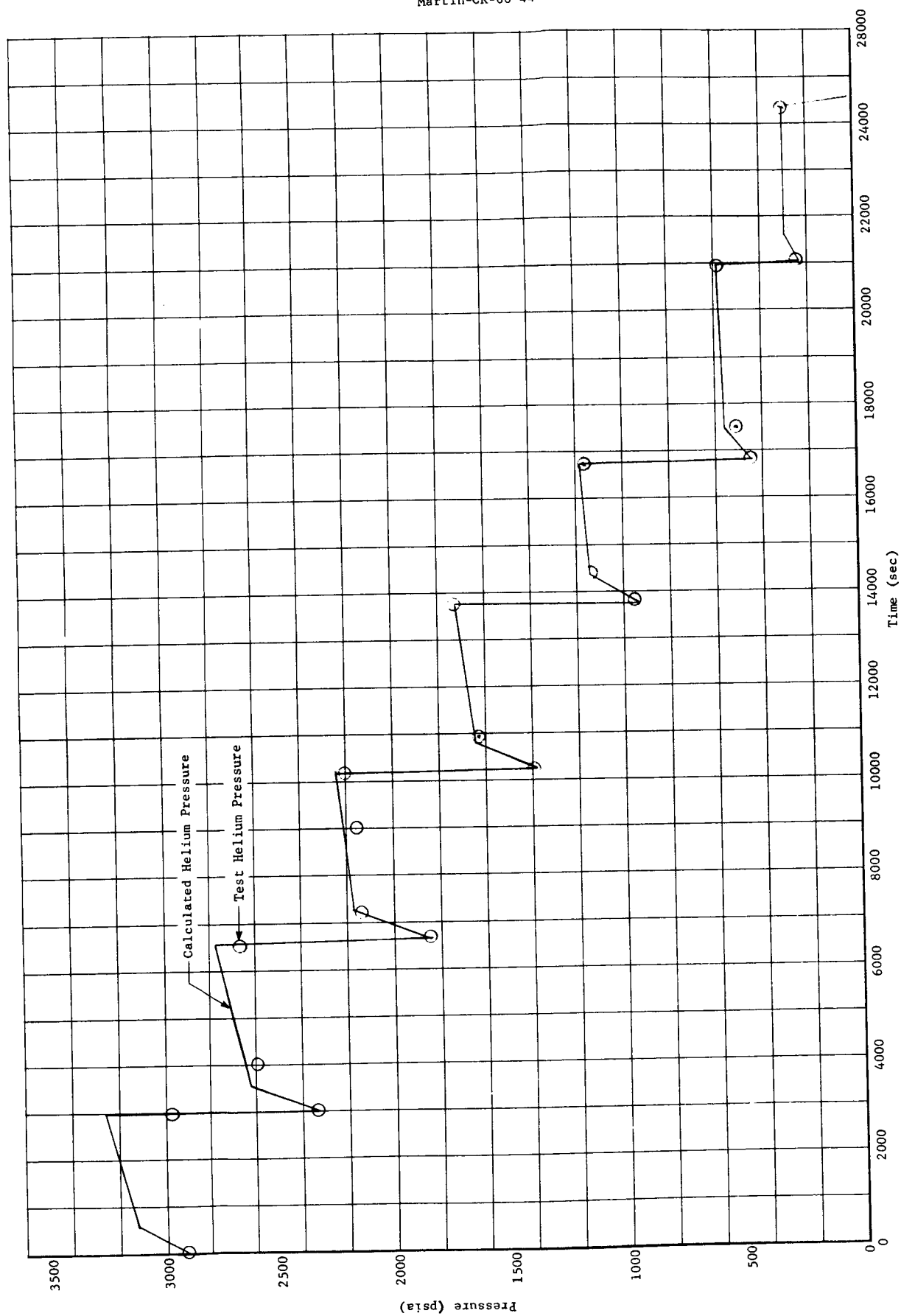
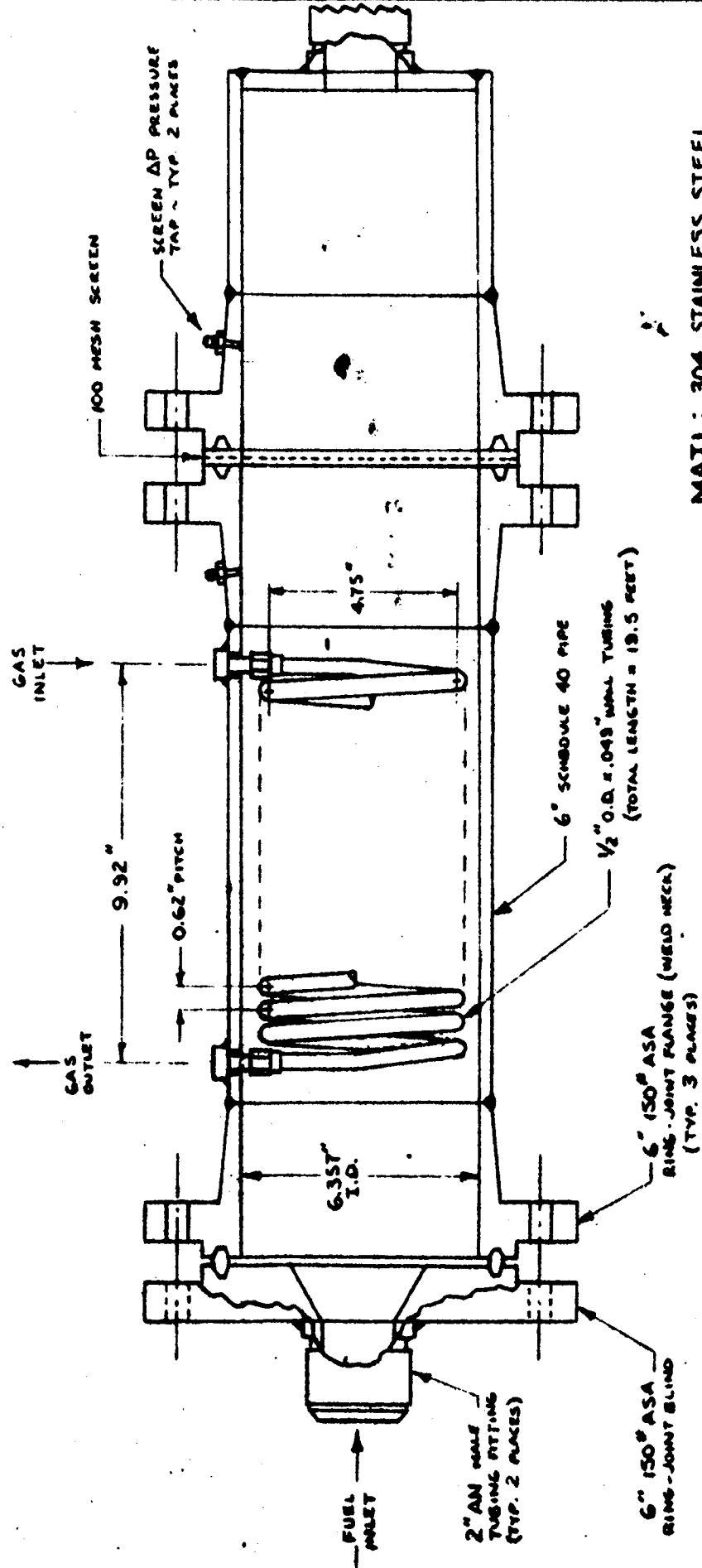
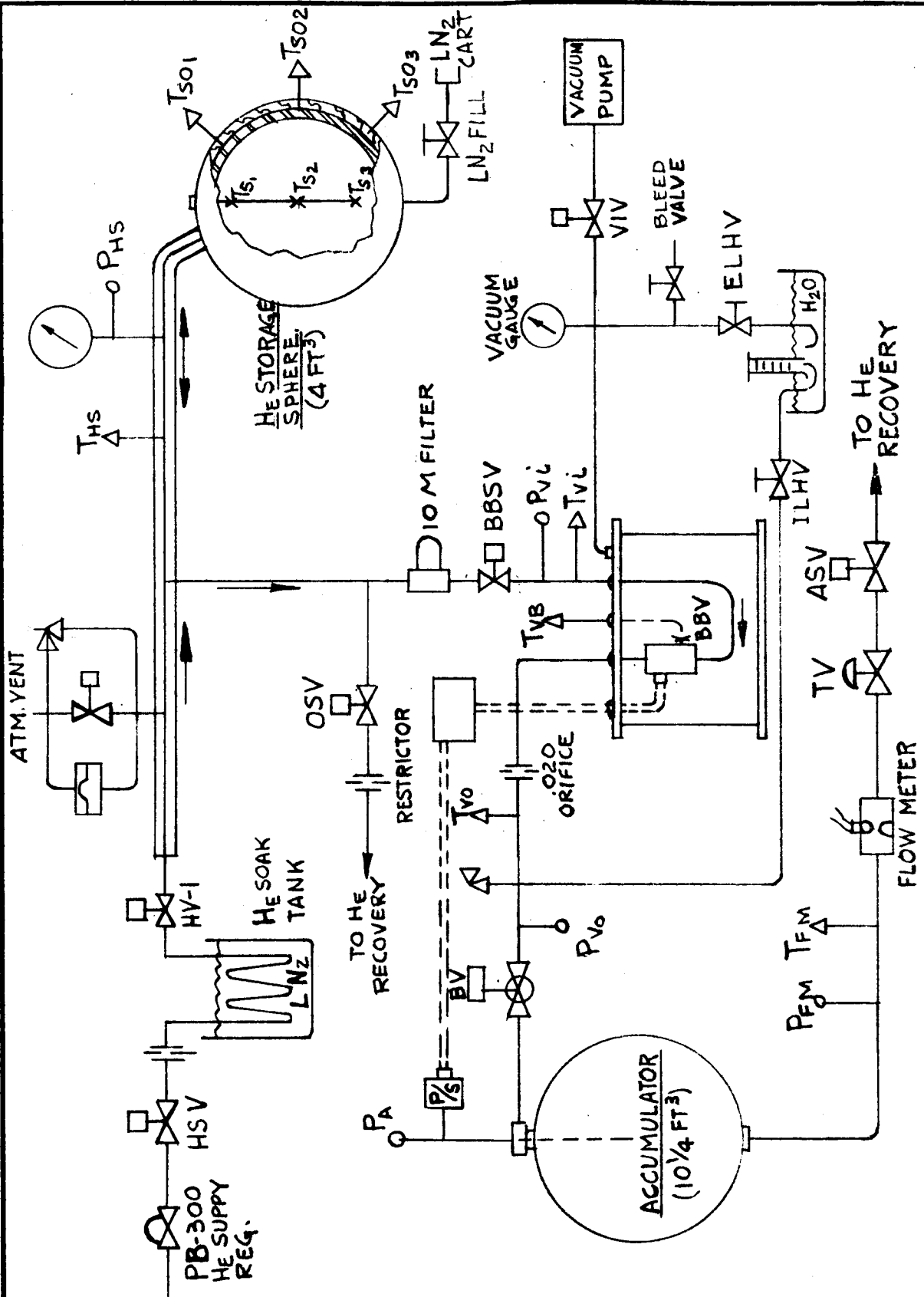


Fig. 28 Test and Calculated Data, Helium Storage Test 6



**FIGURE 29**  
**FEED LINE HEAT EXCHANGER**  
**SCALE: 1/4" = 1"**

# FIGURE 30 SOLENOID VALVE TEST SYTEM





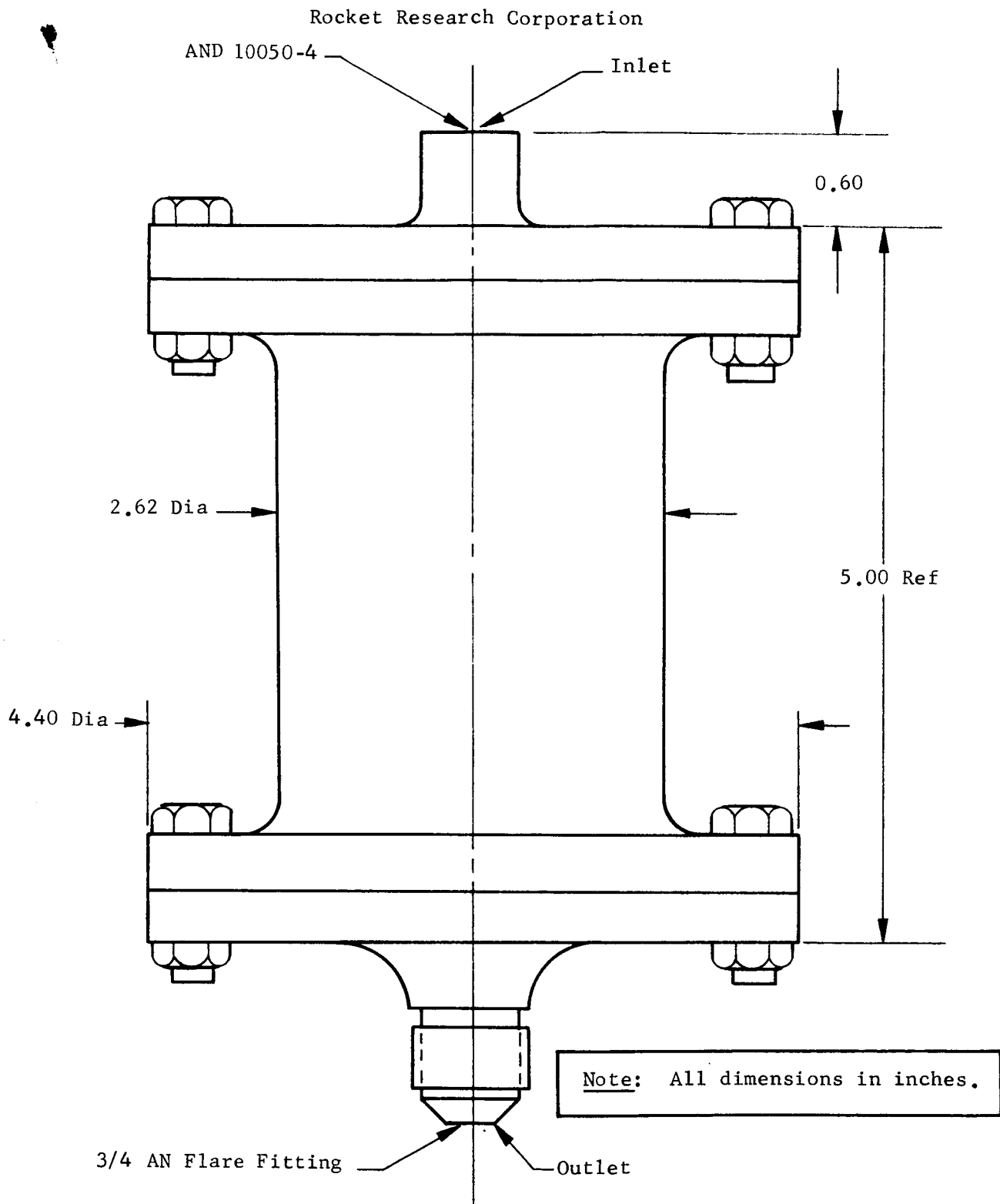
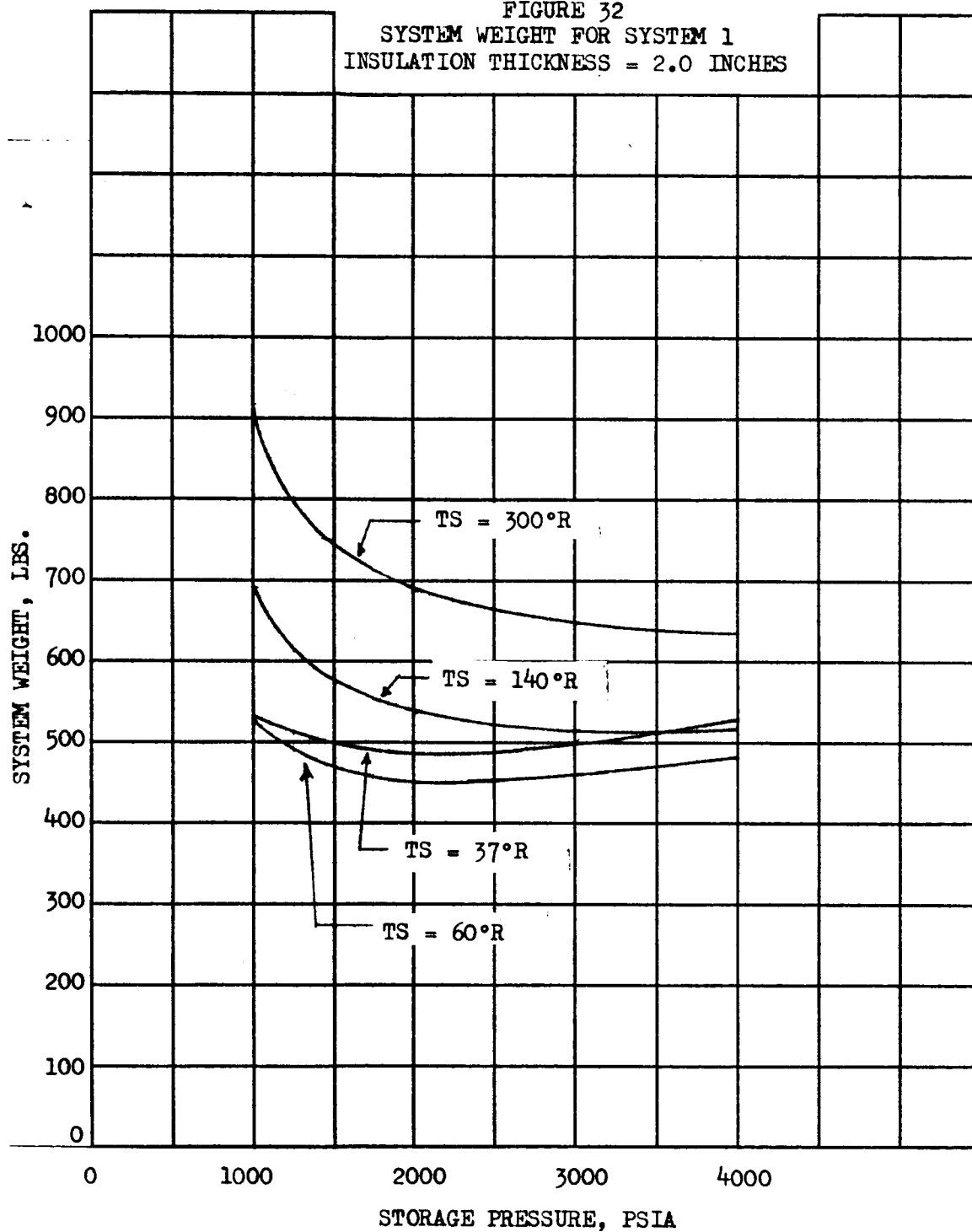
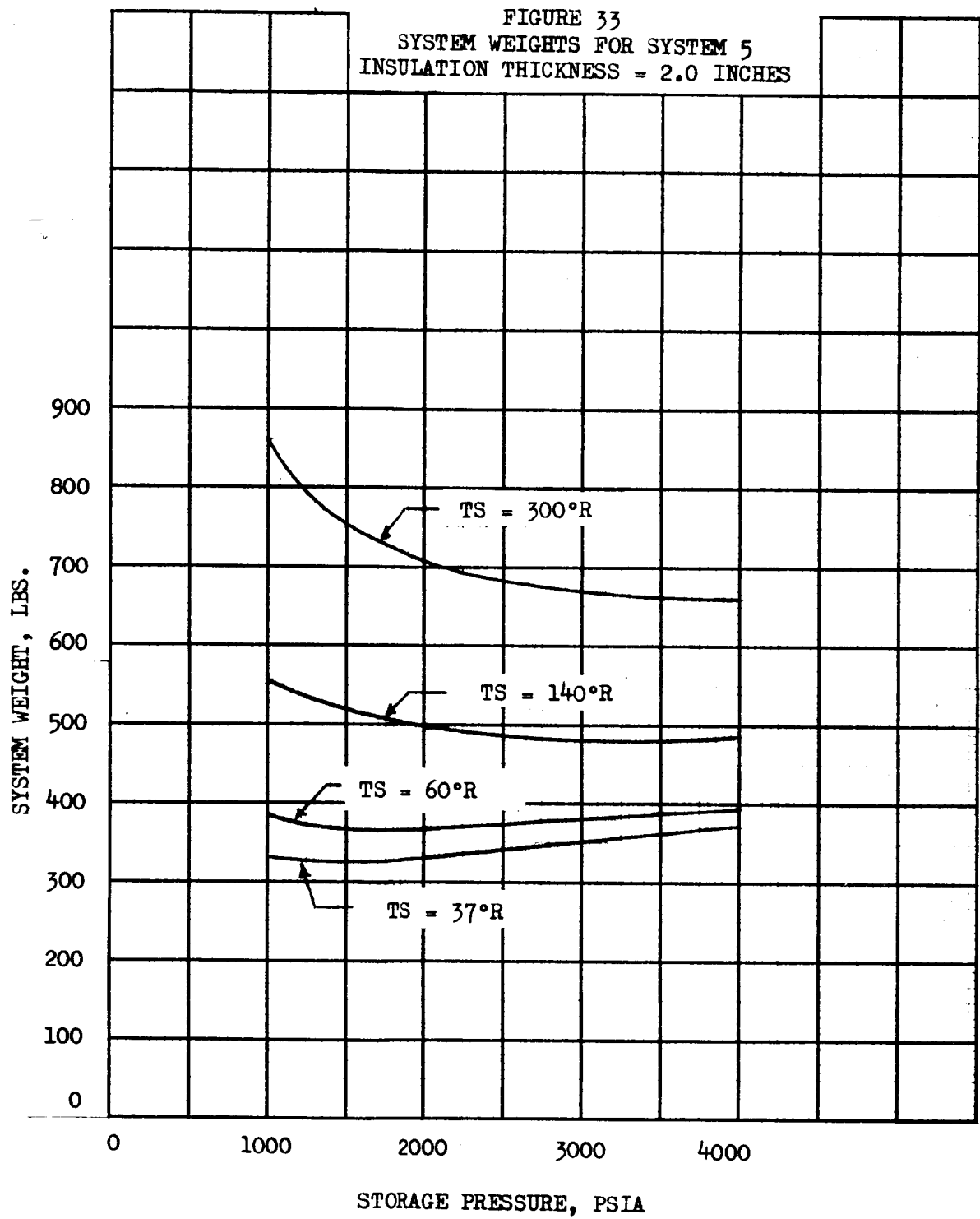


Figure 31a Reactor RB2-100 Envelope

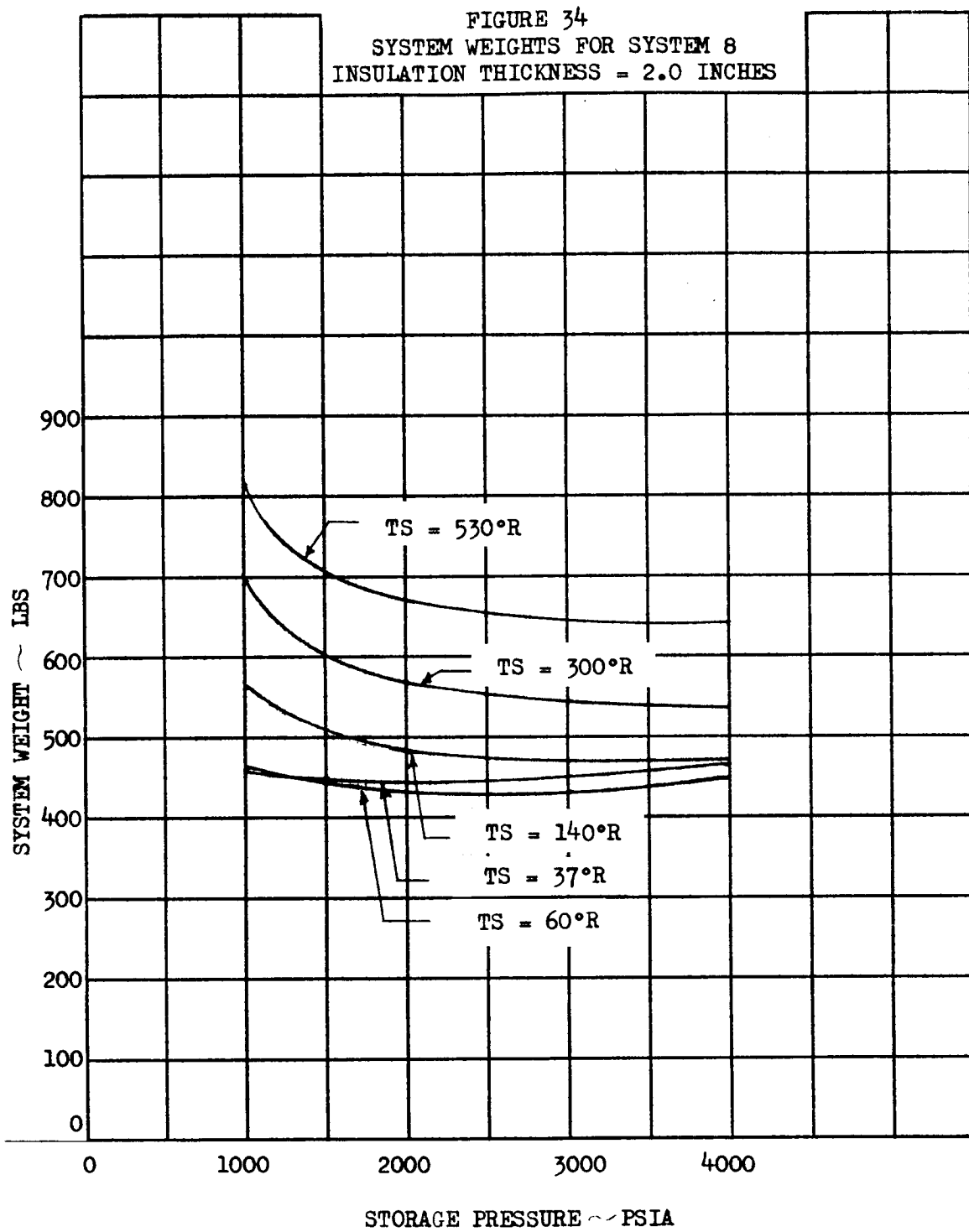
Martin-CR-66-44

FIGURE 32  
SYSTEM WEIGHT FOR SYSTEM 1  
INSULATION THICKNESS = 2.0 INCHES





Martin-CR-66-44



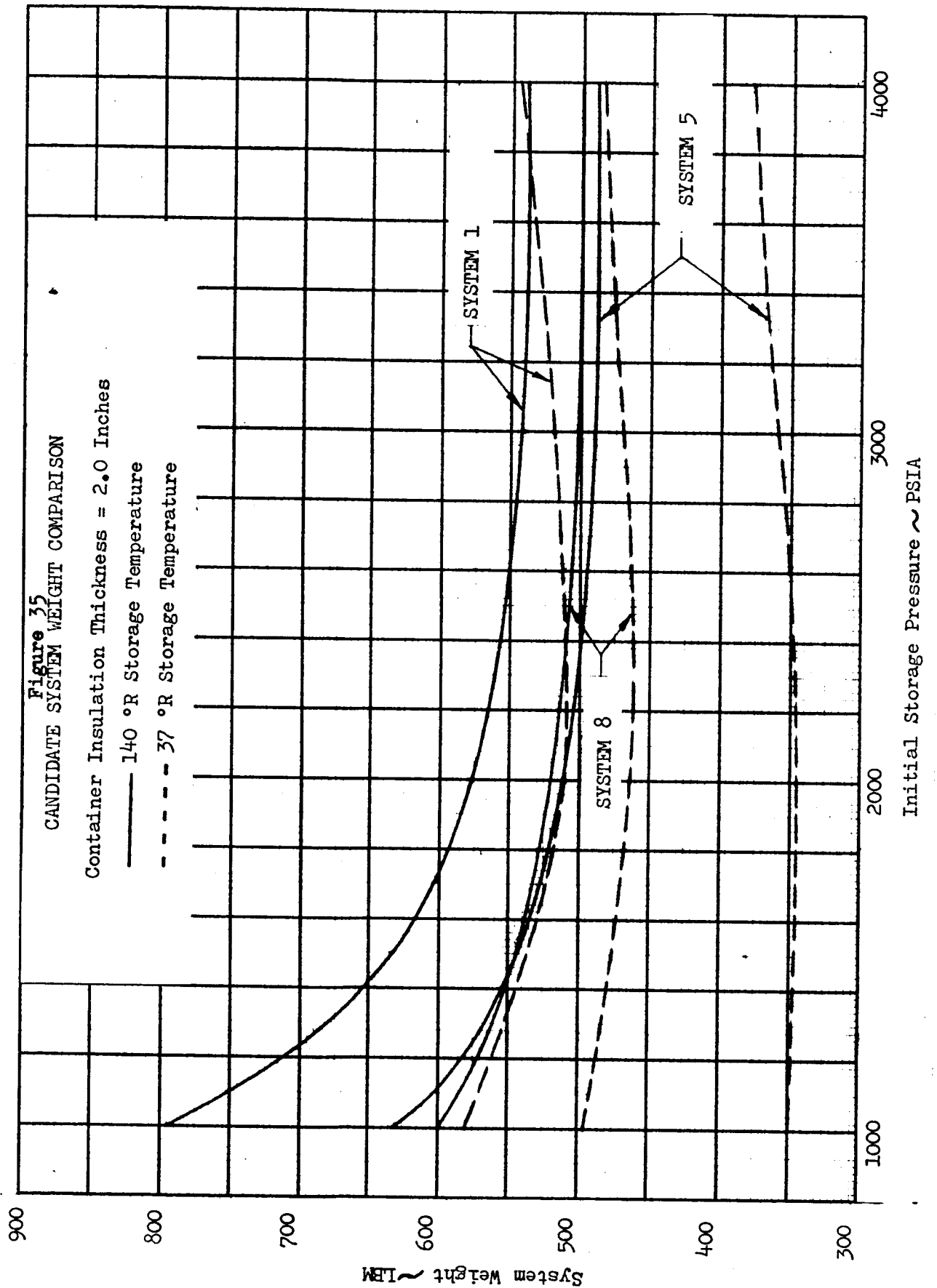
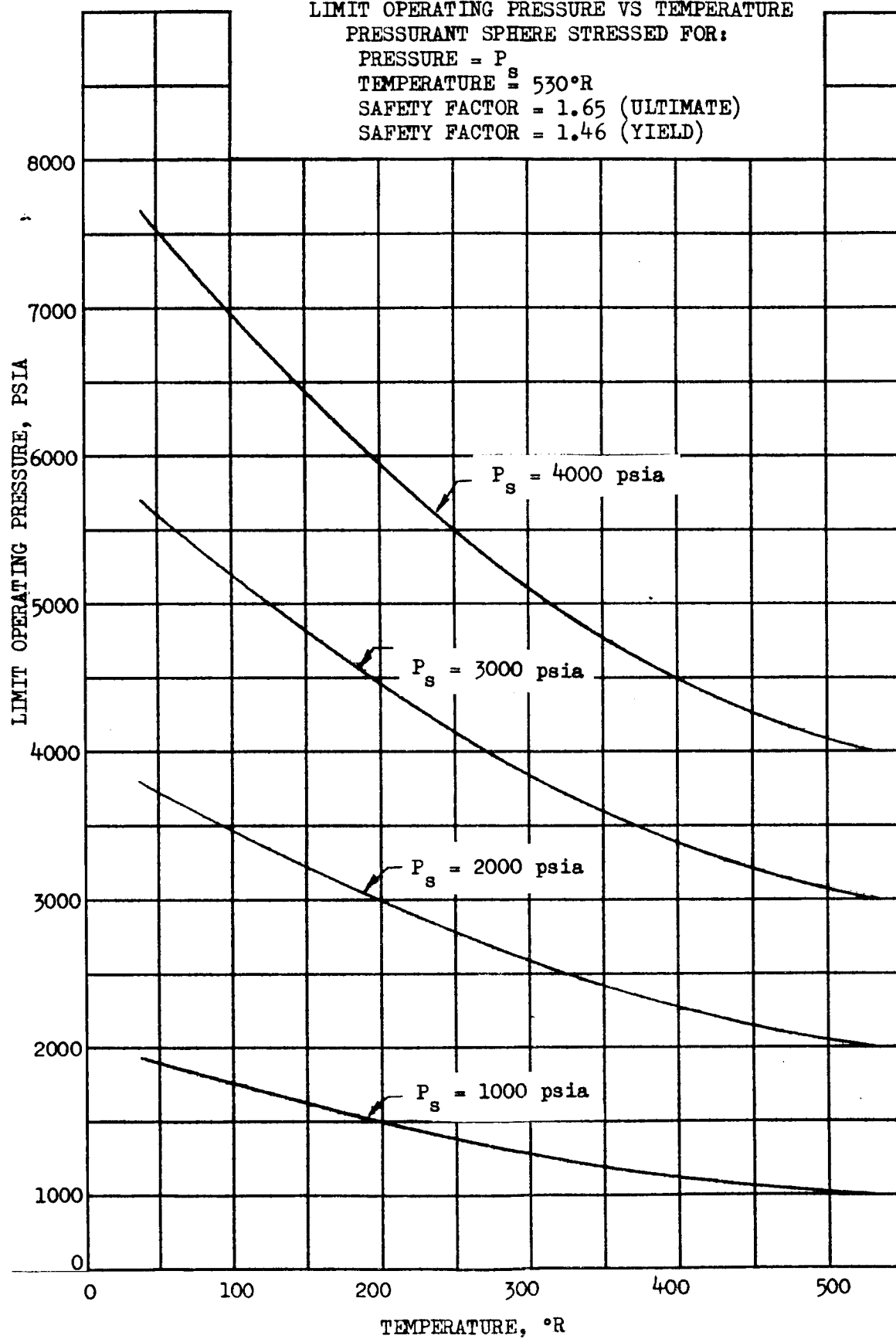


FIGURE 36  
LIMIT OPERATING PRESSURE VS TEMPERATURE  
PRESSURANT SPHERE STRESSED FOR:  
PRESSURE =  $P$   
TEMPERATURE  $\leq 530^{\circ}\text{R}$   
SAFETY FACTOR = 1.65 (ULTIMATE)  
SAFETY FACTOR = 1.46 (YIELD)



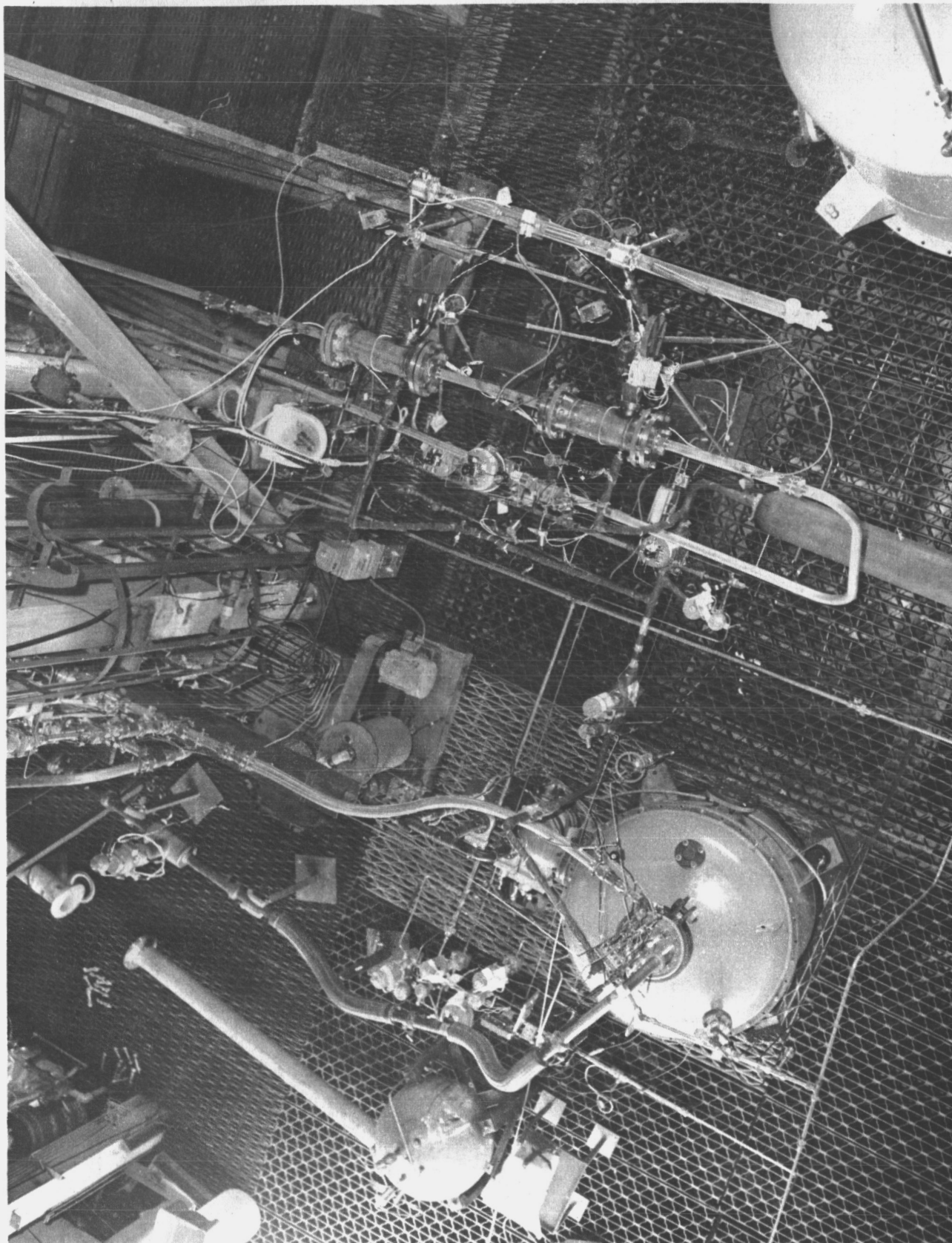


FIGURE 37 CASCADE FEASIBILITY AND HEAT EXCHANGER TEST SETUP

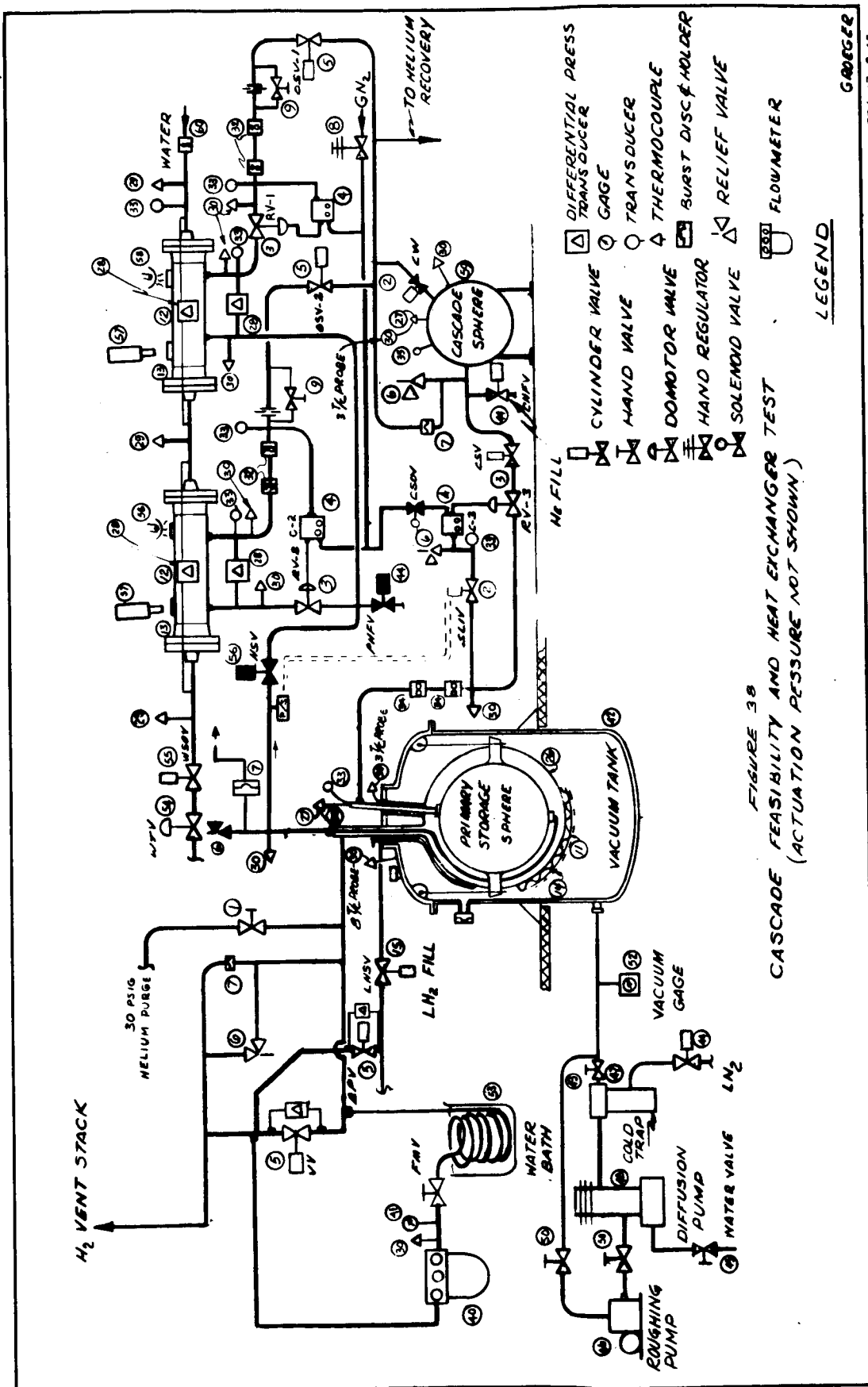


Figure 38 - Sheet 2

<u>Item No.</u>	<u>Description</u>
1	Jamesbury 1-inch Ball Valve
2	Marotta 1/4-inch Solenoid Valve
3	Annin 1-inch Domotor Valve, 1500#, LH <sub>2</sub> Service
4	Mason-Neilan #2715 Controller
5	Jamesbury 1-inch Ball Valve, Remote Operation
6	Republic 3/4-inch Relief Valve
7	Fike 2-inch Burst Disc Holder
8	Apco Regulator Hand Loader
9	Marsh 1-inch Hand Throttling Valve
11	NRC-2 Insulation
12	Stainless Steel Pipe, 6-inch Sch 10
13	Stainless Steel Weld-neck RTJ Flange, 150#
14	Nylon Netting
15	Annin 2-inch Cylinder Valve, 150#, LH <sub>2</sub> Service
25	Hydra-Electric Pressure Switch, 500 p <sub>sia</sub> ± 20 psi
26	Stainless Steel Hemisphere, 38" I.D. x .078" wall
27	Conax Thermister
28	Statham Differential Pressure Transducer
29	Rosemont 179A Precision Temperature Probe
30	Conax Copper-Constantan Thermocouple, sheathed, open-end
30	Conax Copper-Constantan Thermocouple, made from wire
32	Cox Gas Turbine Flowmeter, 6-60 ACFM
33	Statham Pressure Transducer
34	Cox Gas Turbine Flowmeter, 3-30 ACFM
40	Rockwell LPG Gas Test Meter
41	Pressure Gage
42	Vacuum Chamber
44	Annin 1/2-inch Cylinder Valve, 2500#
45	Dragon 1/2-inch Valve
46	Kinney KS-47 Vacuum Pump
47	NRC Cold Trap
48	NRC Diffusion Pump
49	CVC 6-inch Valve
50	CVC 3-inch Valve
52	Phillips Cold-Cathode Ionization Gage
53	Open Tank
54	Annin 2-inch Domotor Valve
55	Annin 2-inch Cylinder Valve
56	Annin 1-inch Cylinder Valve
57	Movie Camera
58	Camera Light
59	Cascade Sphere
60	Cox Turbine Flowmeter, water



FIGURE 39 PRIMARY TANK PRESSURE VESSEL

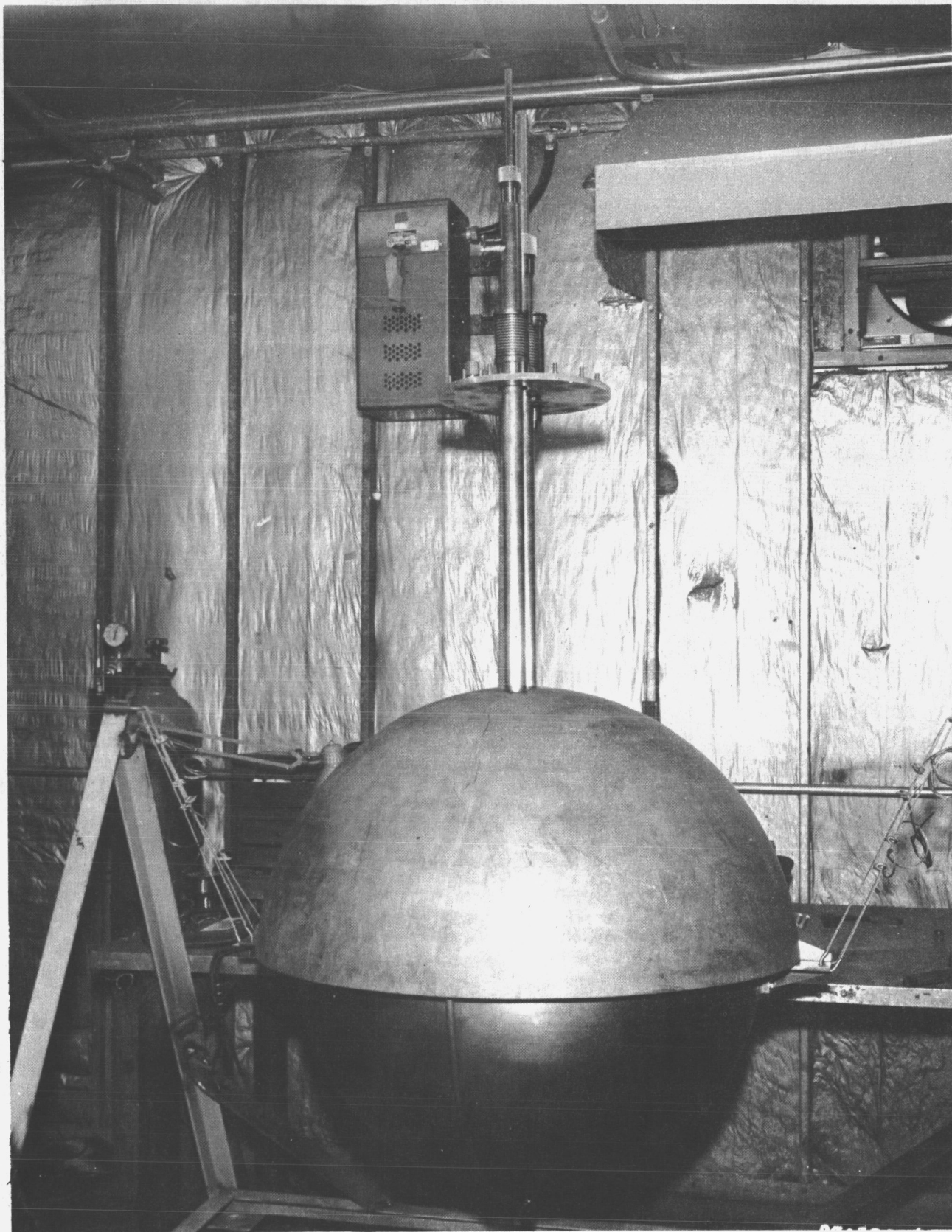


FIGURE 40 PRIMARY TANK PRESSURE VESSEL WITH LH<sub>2</sub> JACKET HEMISPHERE

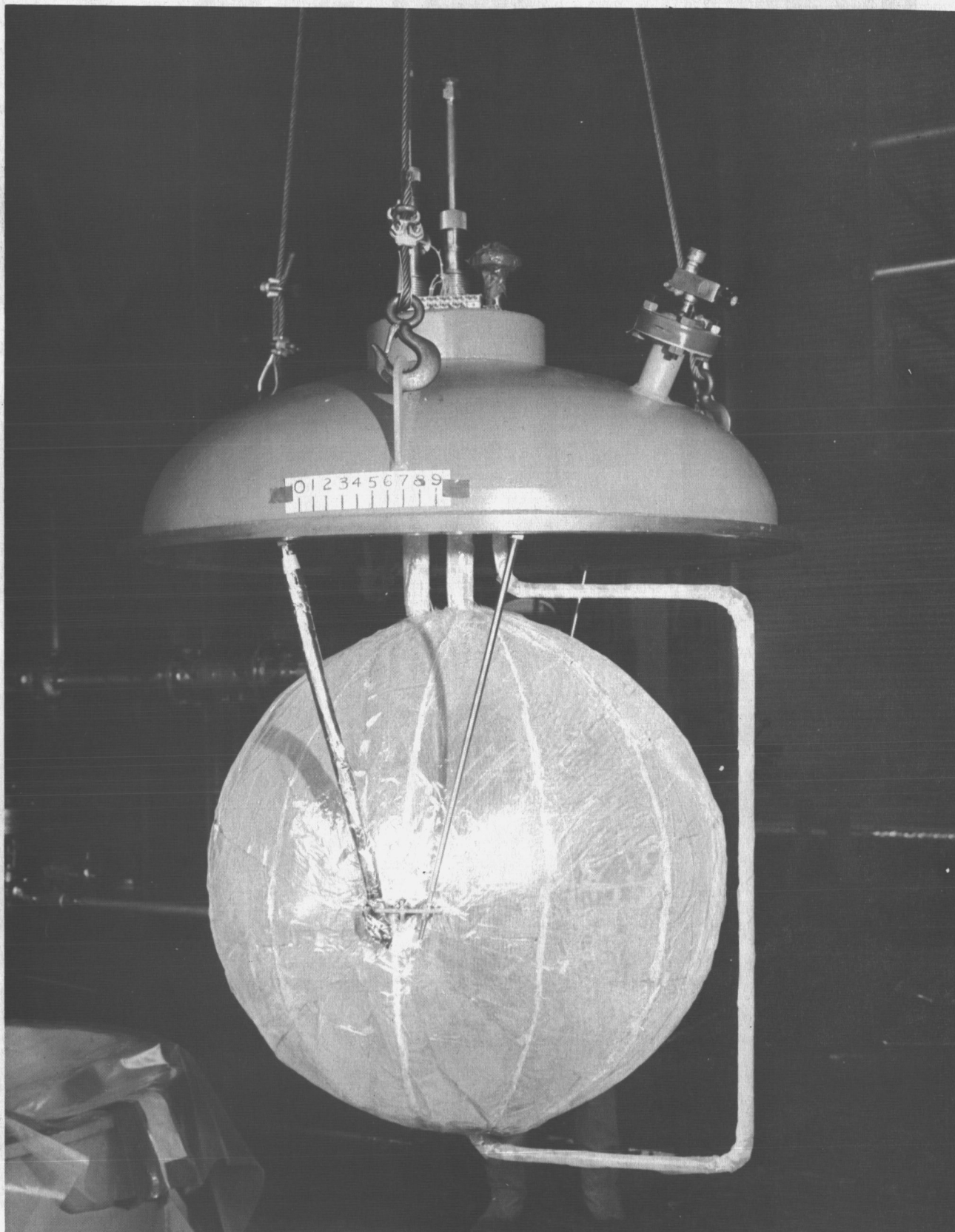
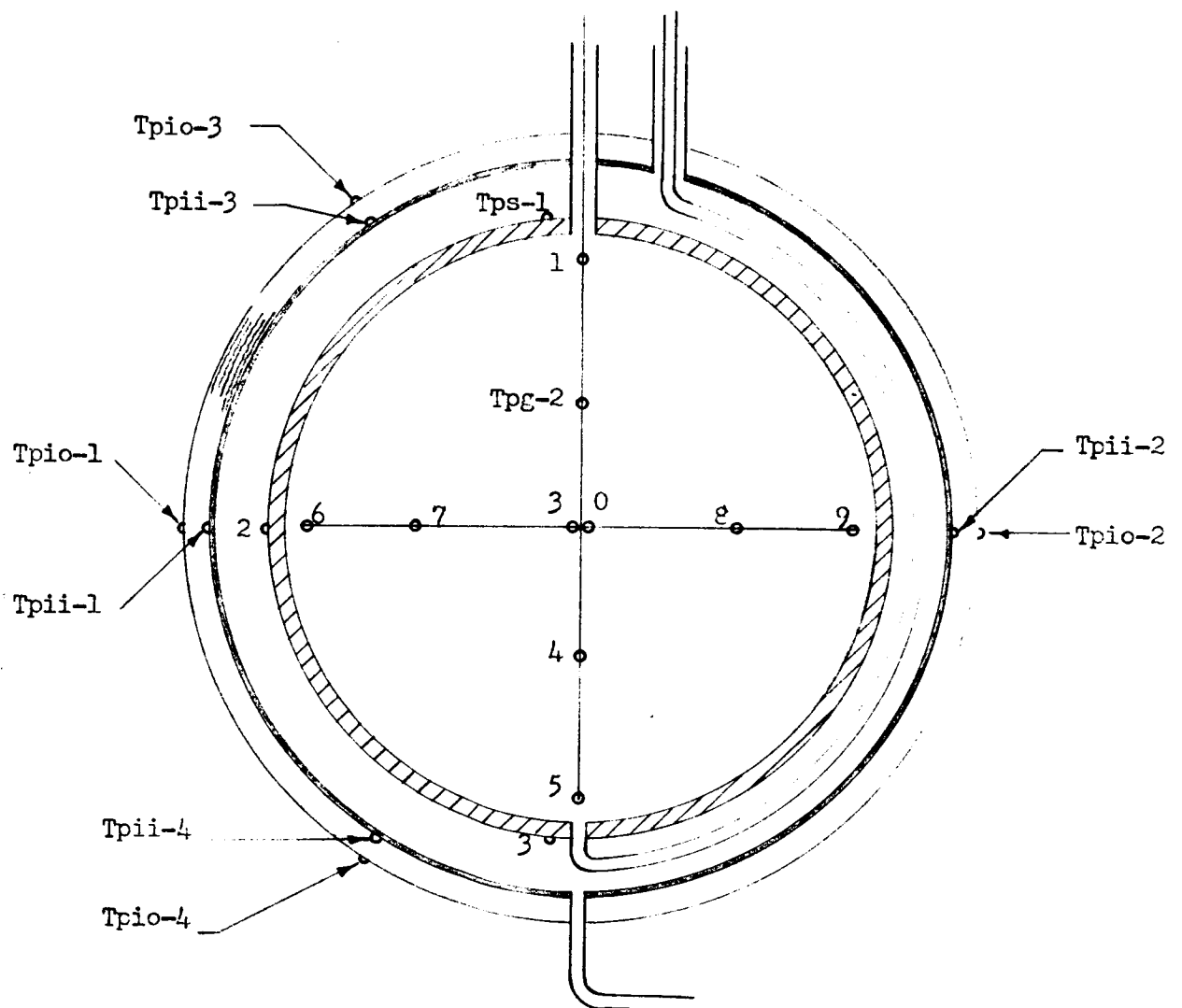


FIGURE 41 COMPLETED PRIMARY TANK ASSEMBLY



PRIMARY STORAGE CONTAINER  
TEMPERATURE INSTRUMENTATION LOCATIONS

Figure 42

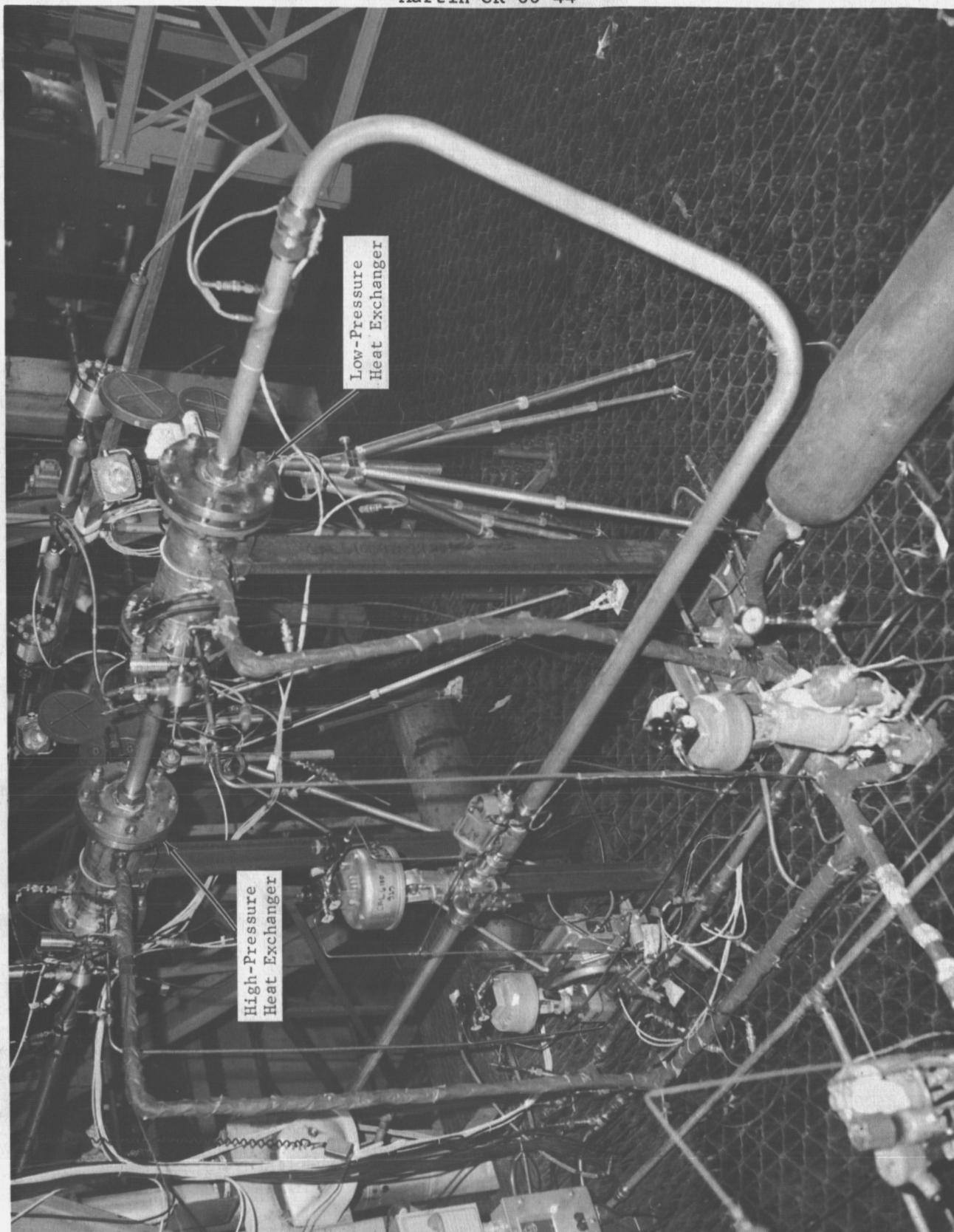


Fig. 43 Water Flow Loop with Propellant Feedline Heat Exchangers

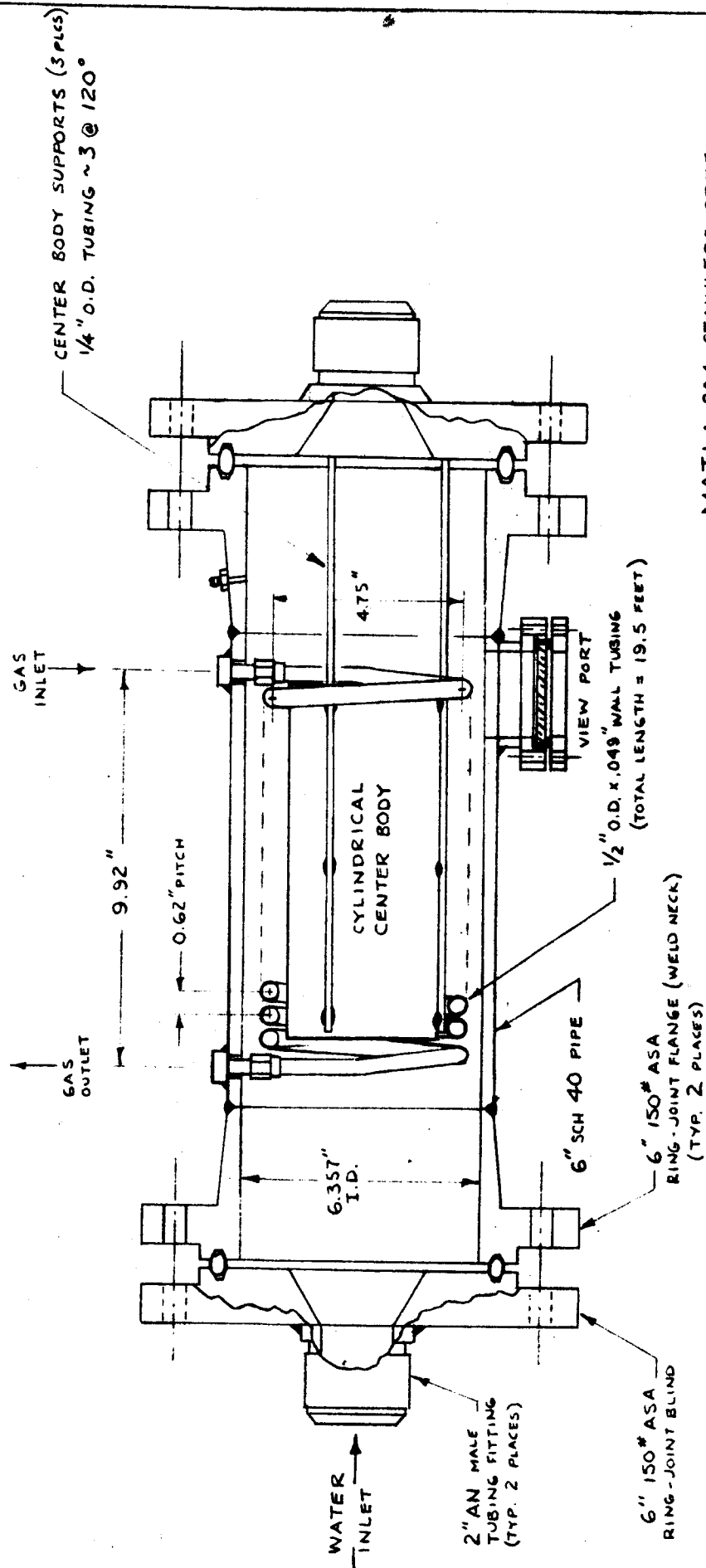


FIGURE 44  
FEED LINE HEAT EXCHANGER  
SCALE:  $\frac{1}{4}" = 1"$

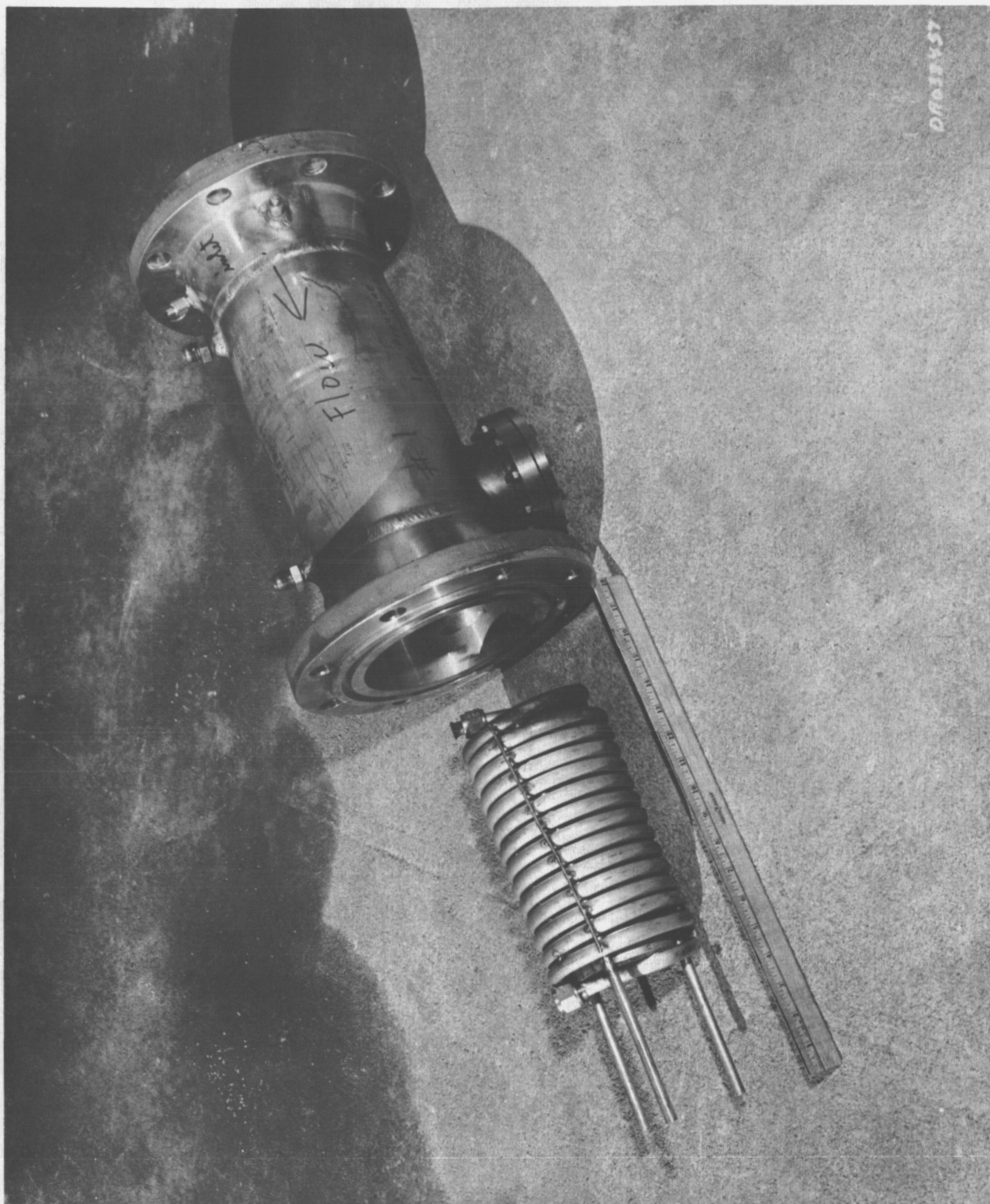


FIGURE 45 FEED LINE HEAT EXCHANGER PHOTOGRAPH

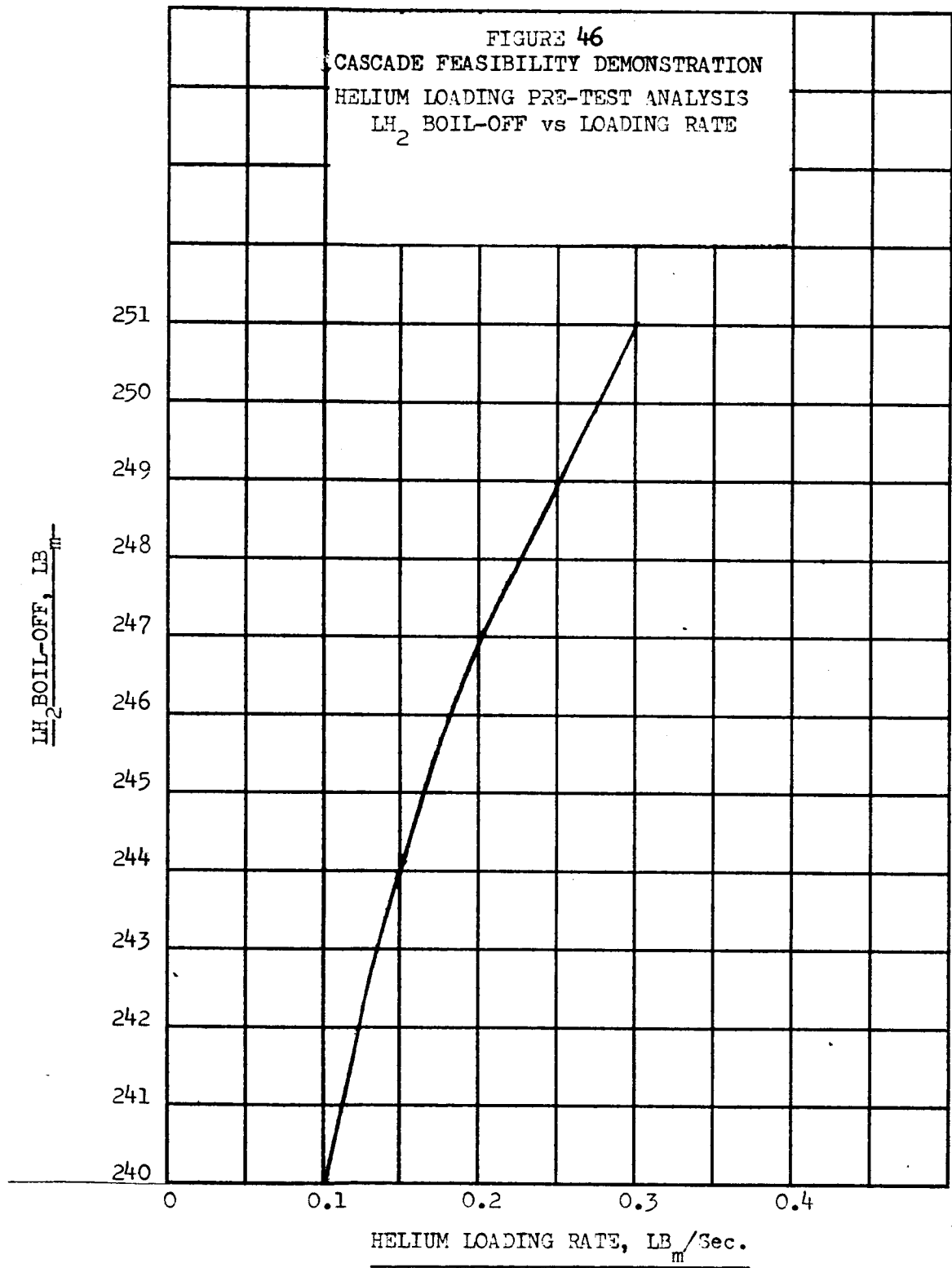


FIGURE 47  
CASCADE FEASIBILITY DEMONSTRATION  
HELIUM LOADING PRE-TEST ANALYSIS  
LOADING TIME VS LOADING RATE

HELIUM LOADING TIME, MINUTES

240  
238  
236  
234  
232  
230  
228  
226  
224  
222  
220  
218  
216  
214  
212  
210

0.05 0.10 0.15 0.20 0.25 0.30

HELIUM LOADING RATE, LB/SEC

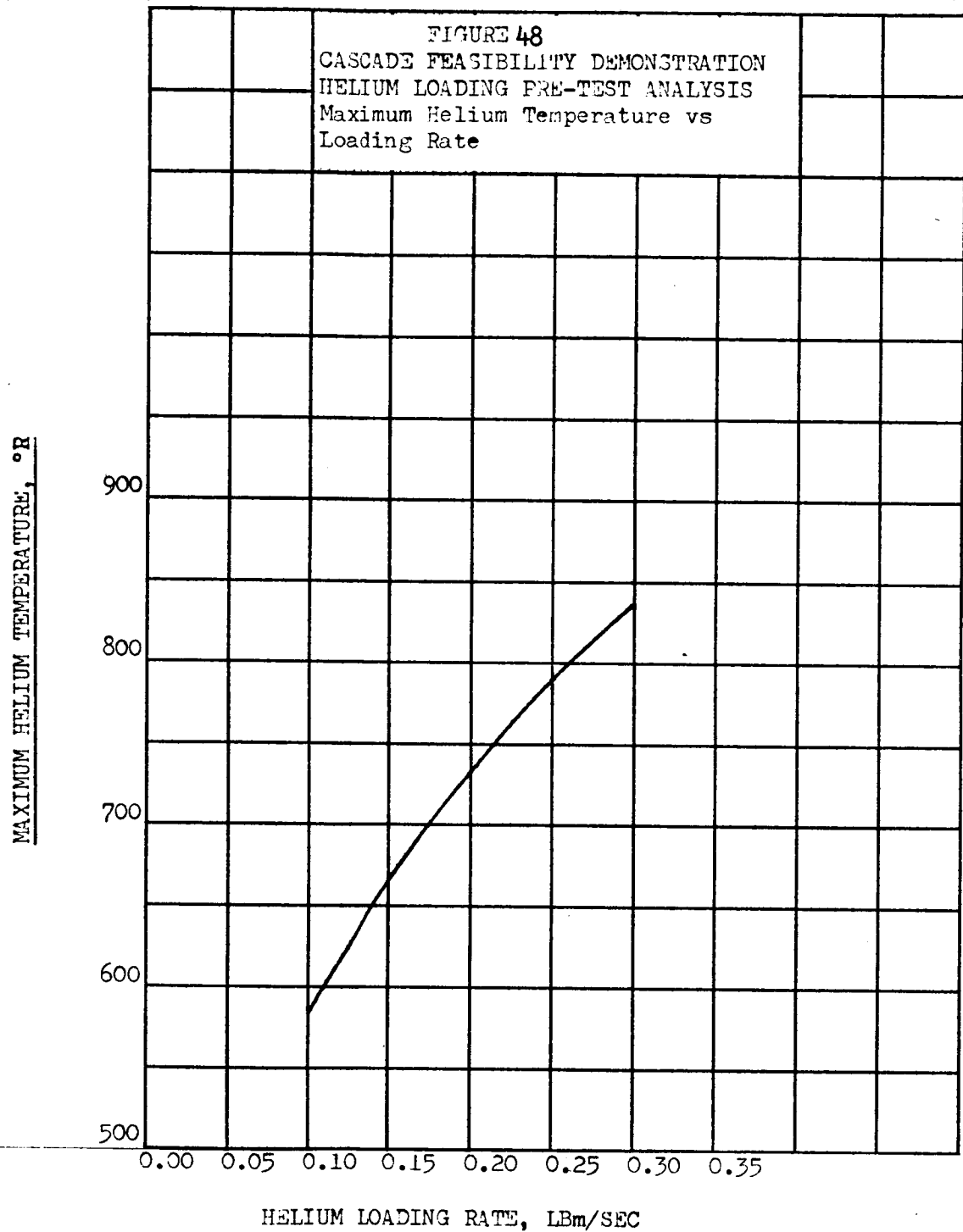
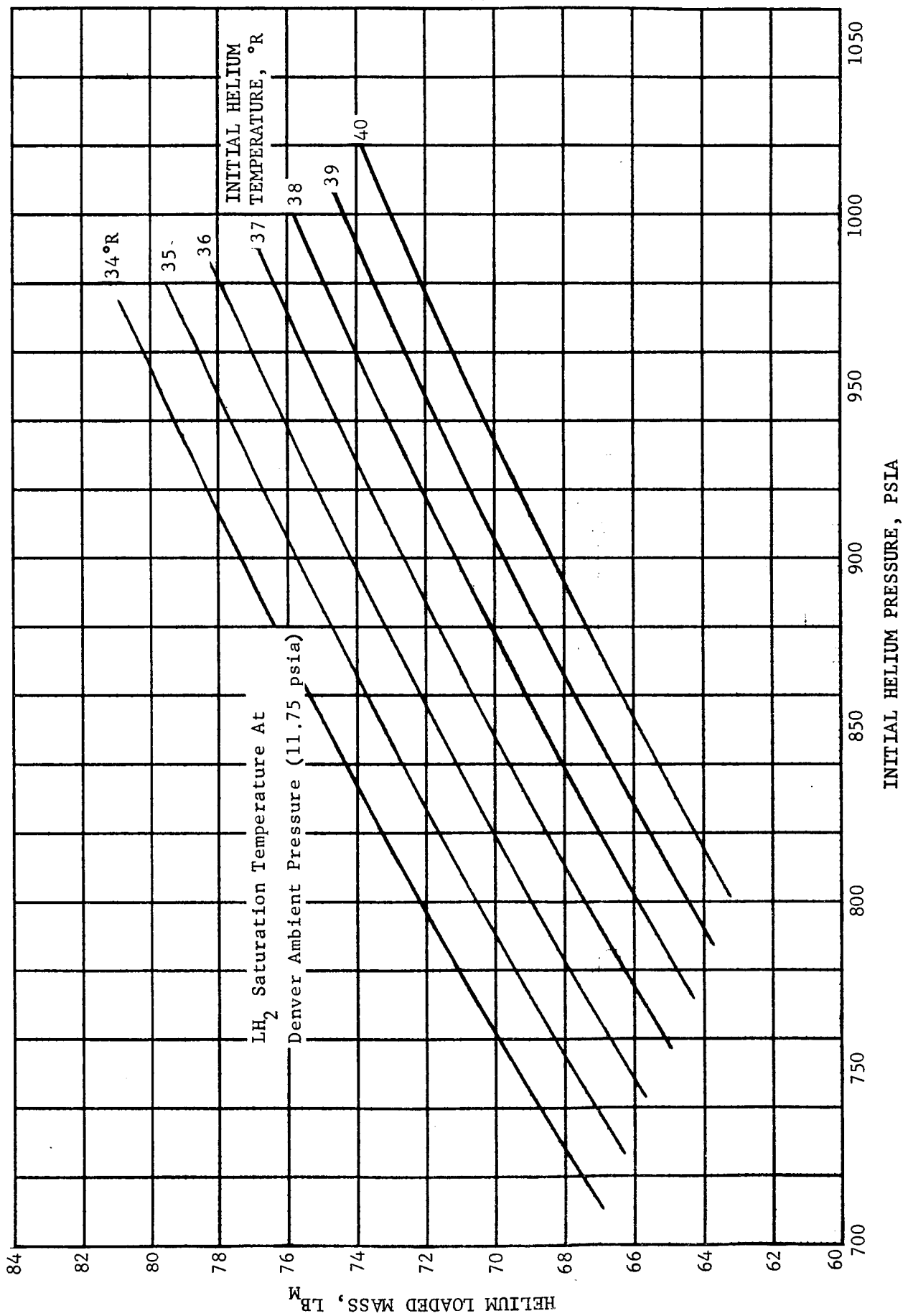
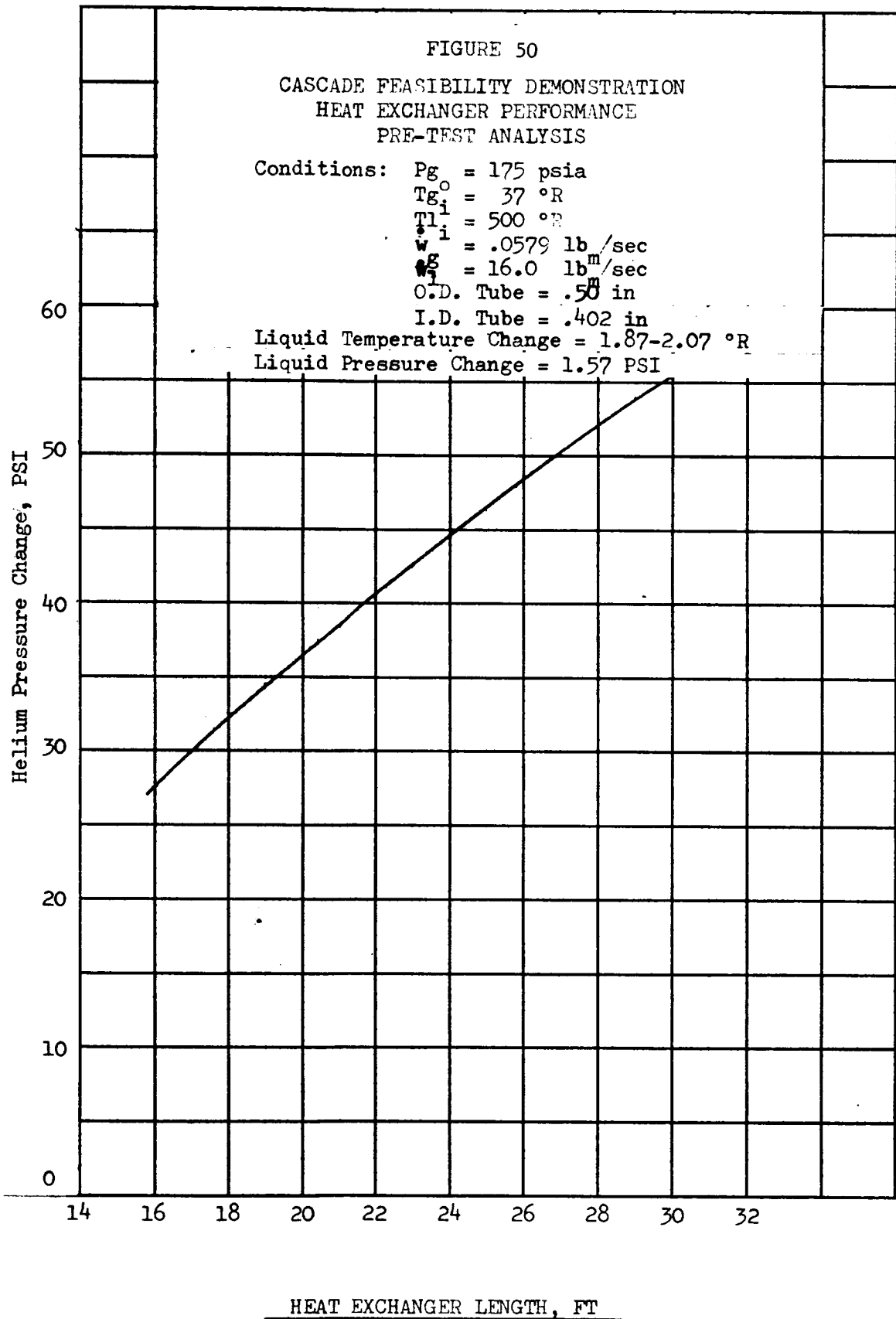
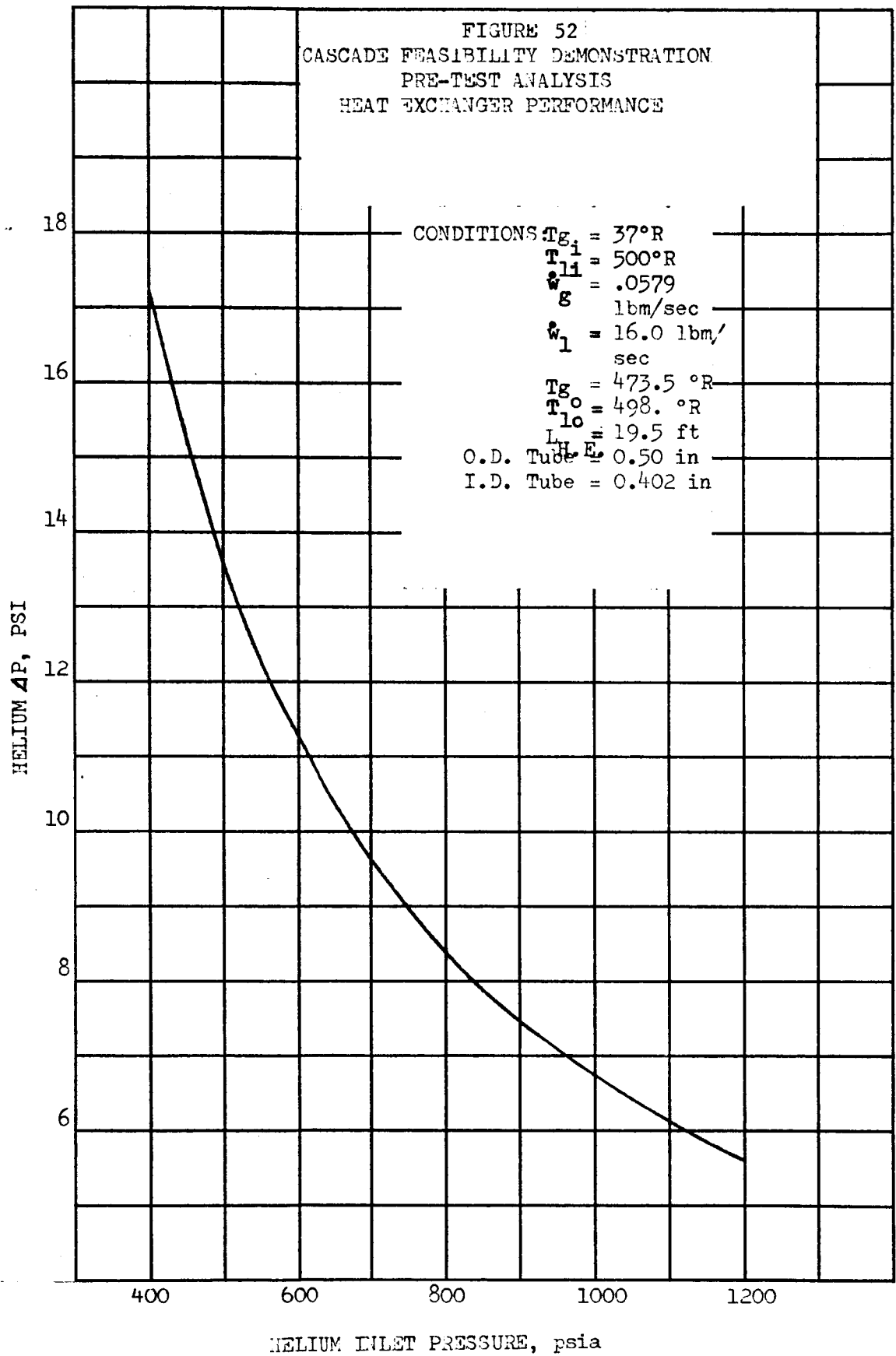


Figure 49  
CASCADE FEASIBILITY DEMONSTRATION  
Initial Operating Conditions for the Primary Sphere







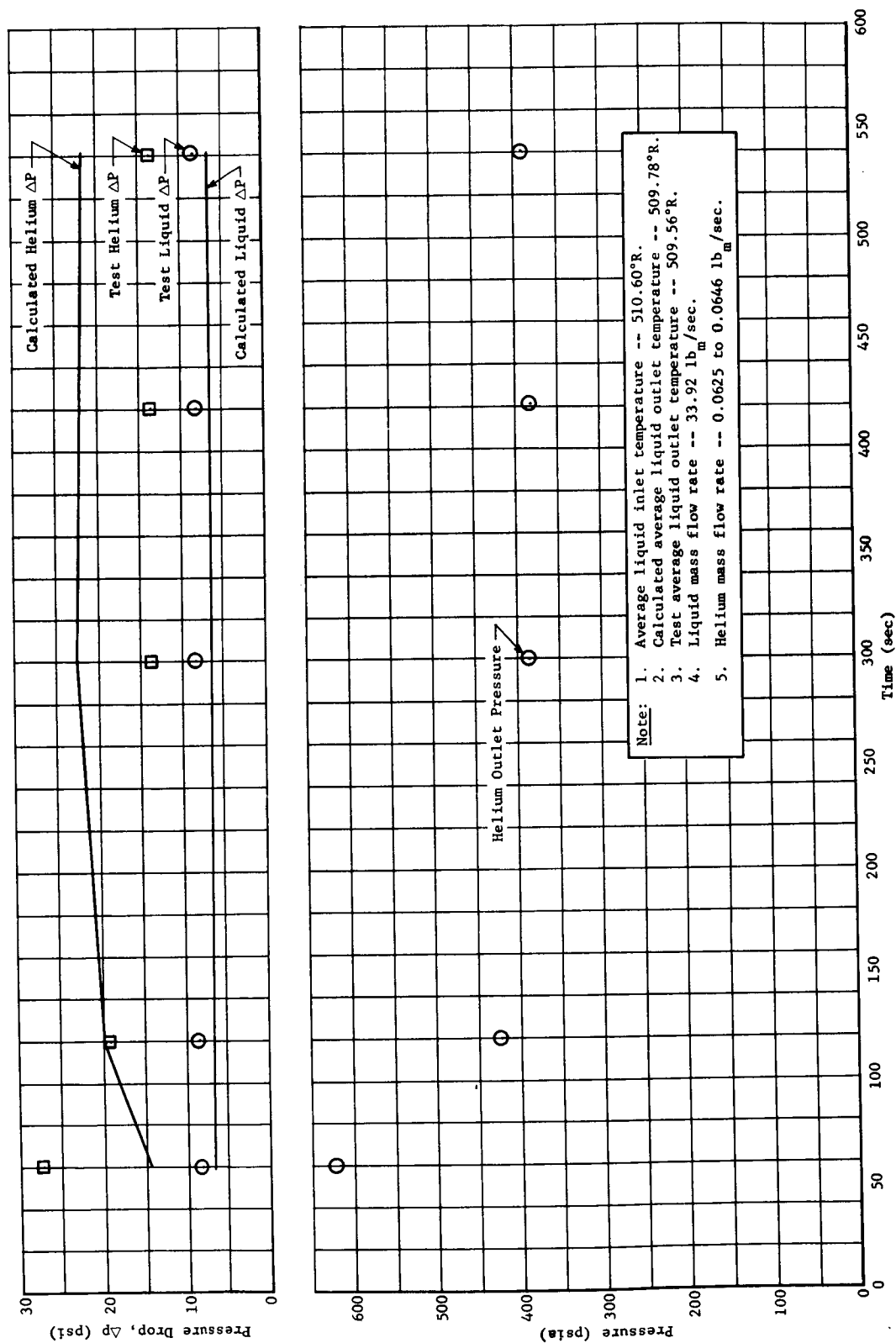


Fig. 53a High-Pressure Heat Exchanger Posttest Analysis, Nine-Day Mission Abort, Run 1

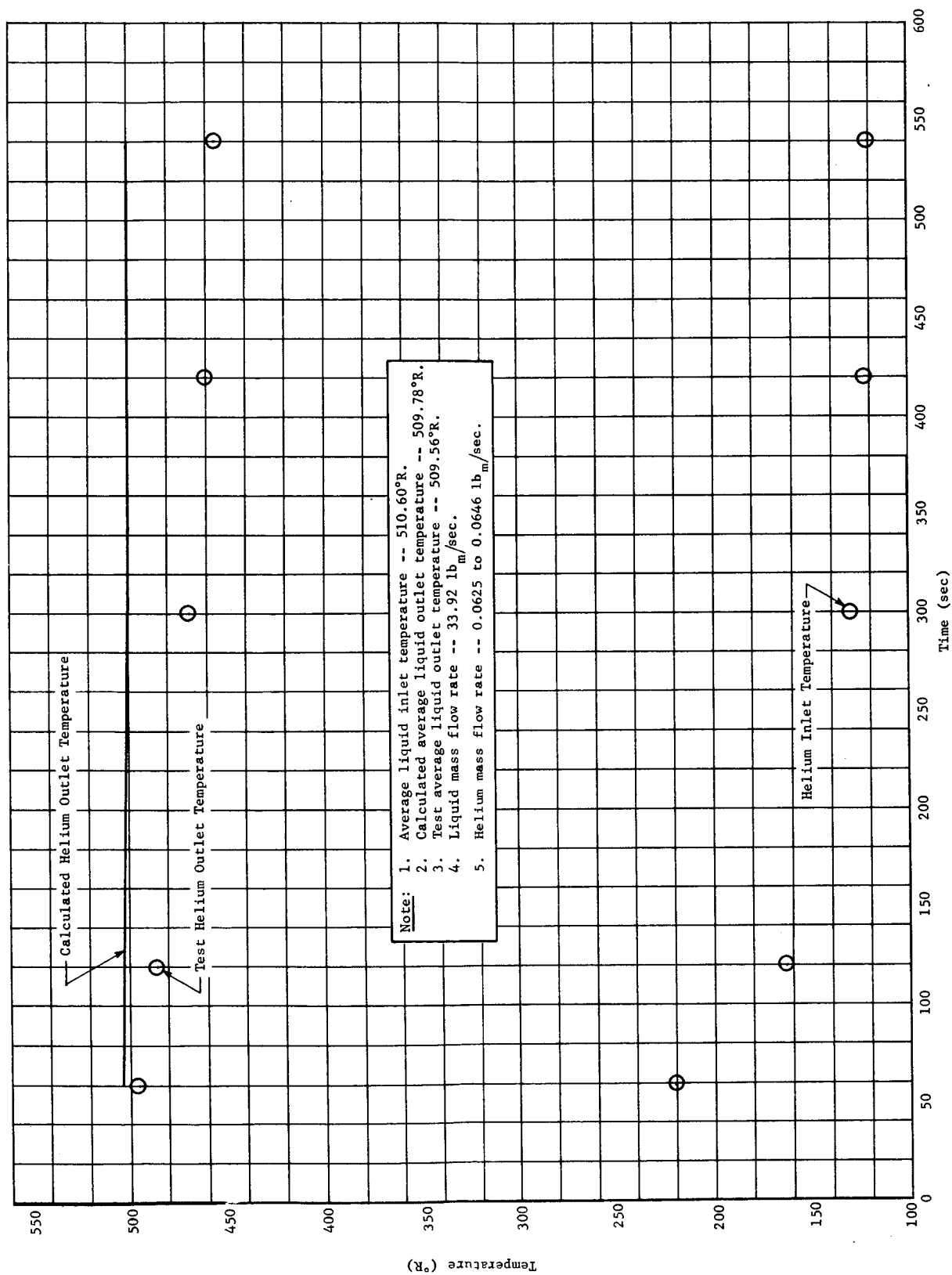


Fig. 53b High-Pressure Heat Exchanger Posttest Analysis, Nine-Day Mission Abort, Run 1

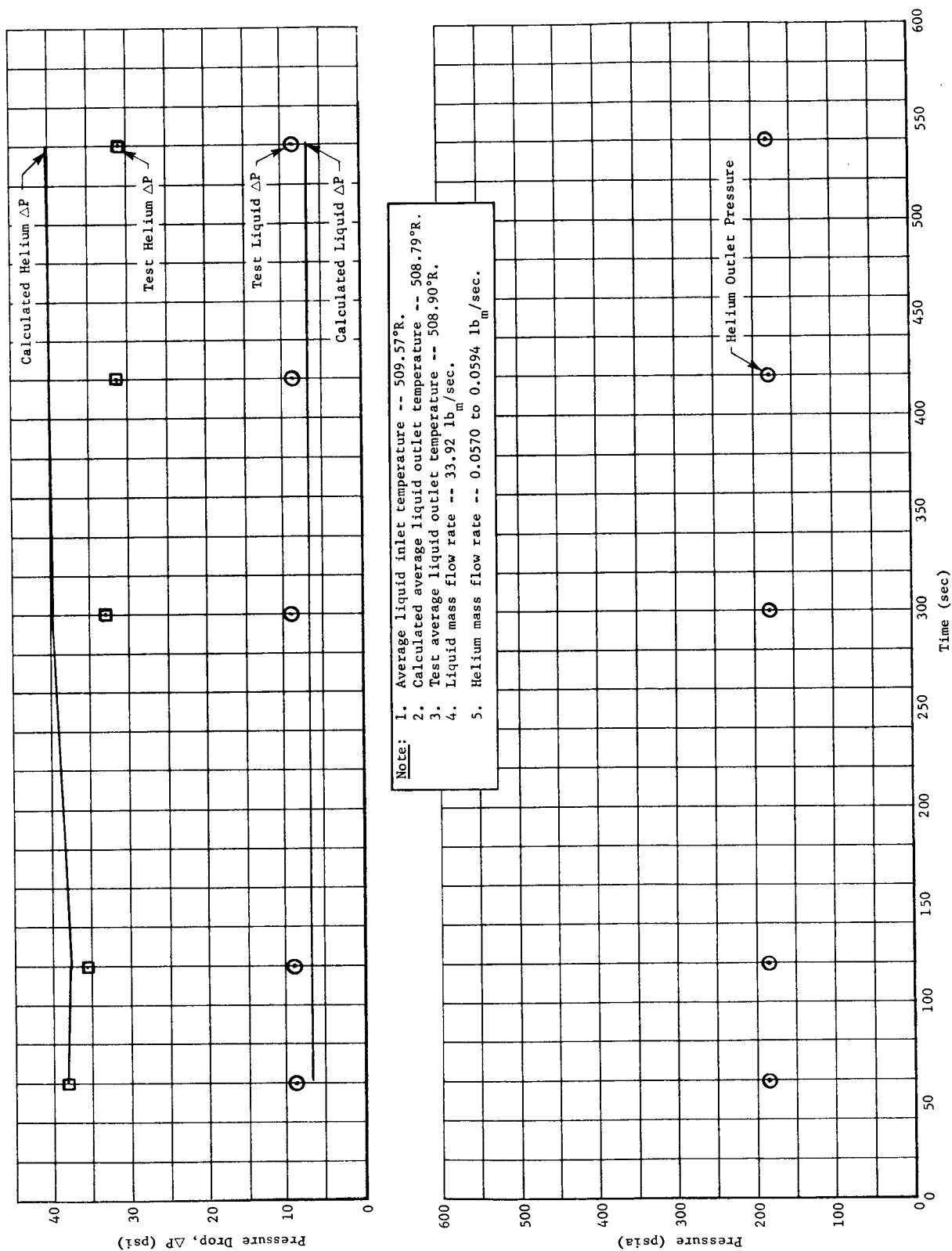


Fig. 54a Low-Pressure Heat Exchanger Posttest Analysis, Nine-Day Mission Abort, Test Run 1

Martin-CR-66-44

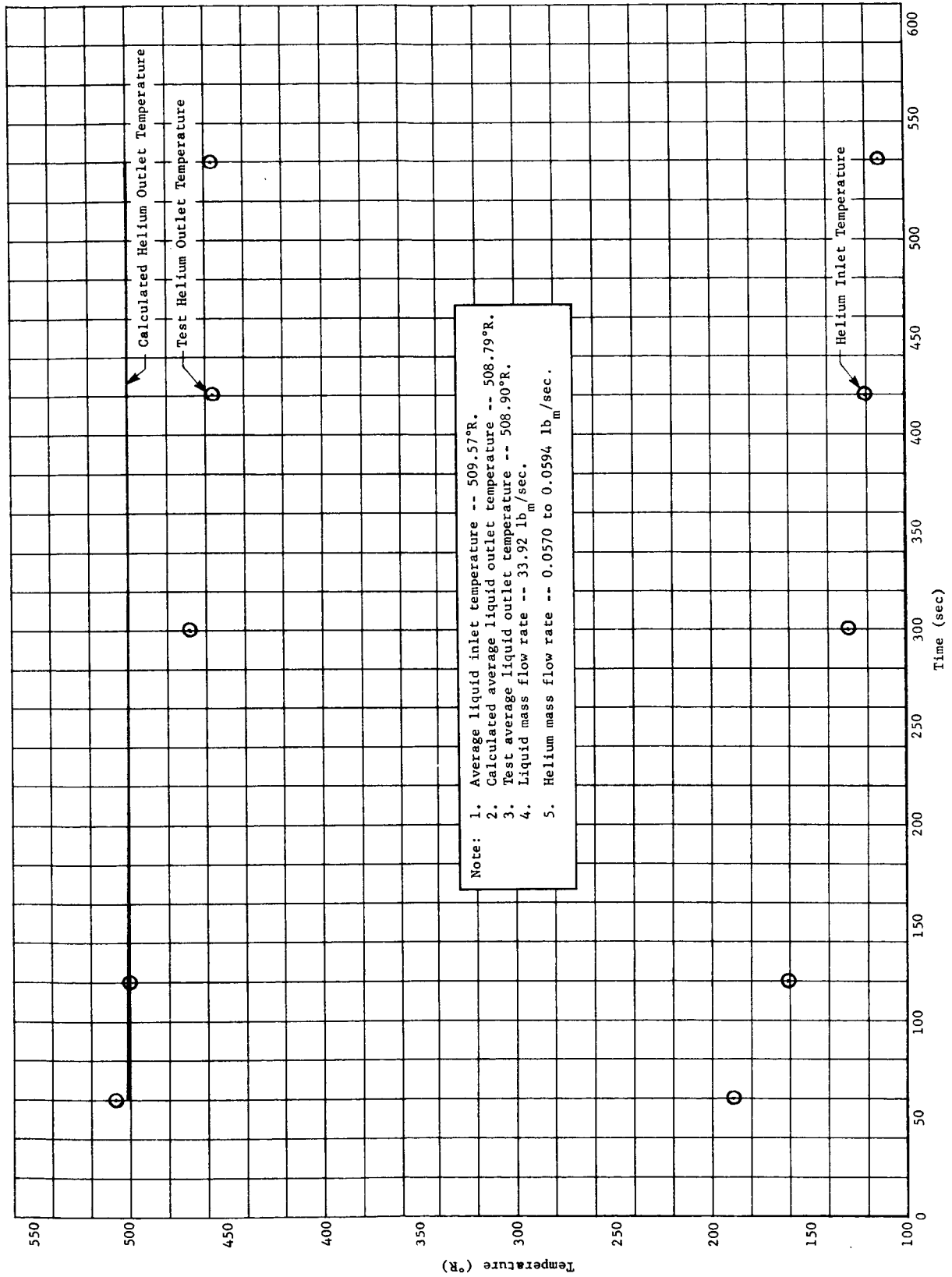


Fig. 54b Low-Pressure Heat Exchanger Posttest Analysis, Nine-Day Mission Abort, Test Run 1

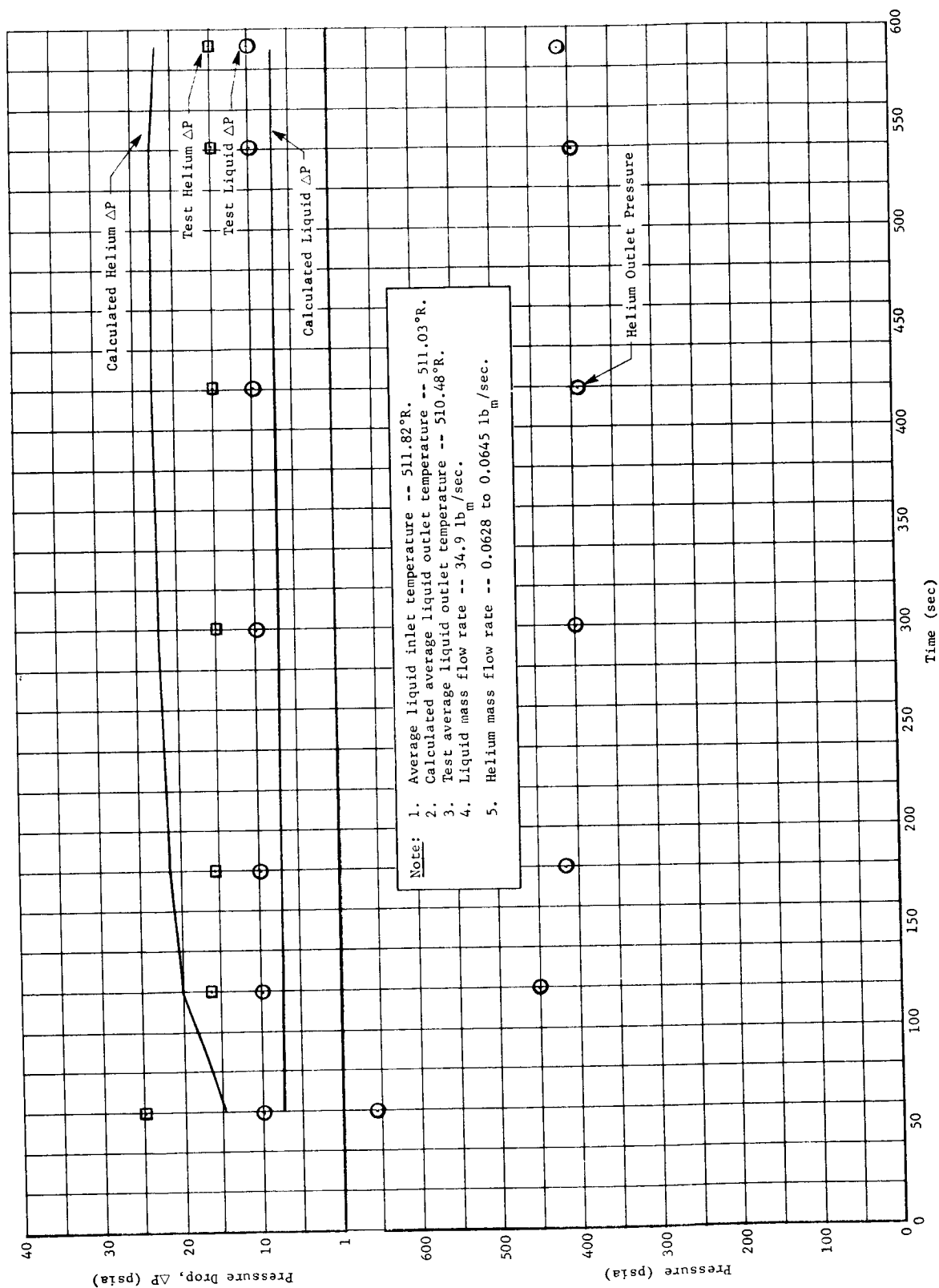


Fig. 55a High-Pressure Heat Exchanger Posttest Analysis, Nine-Day Mission Abort, Test Run 2

Martin-CR-66-44

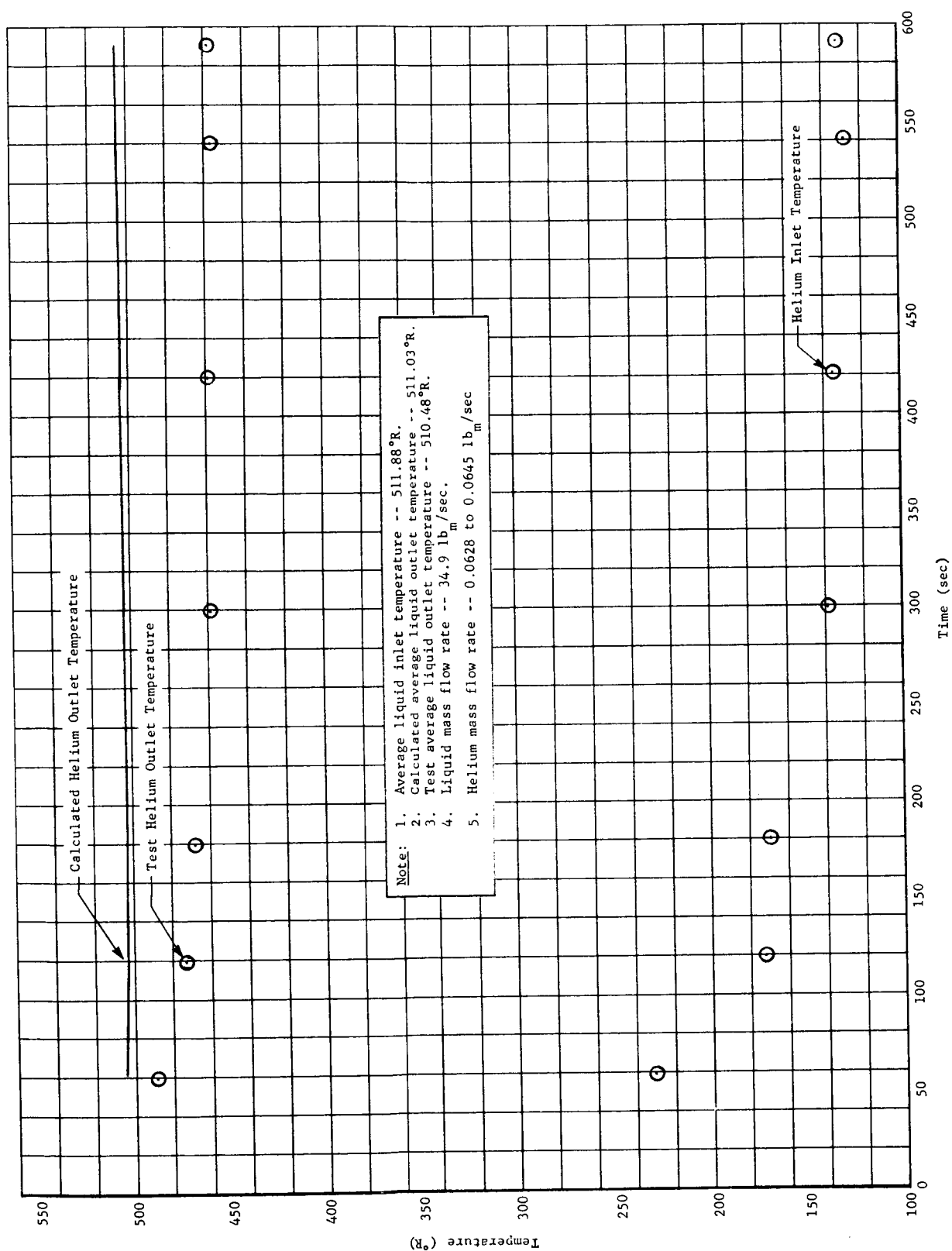


Fig. 55b High-Pressure Heat Exchanger Posttest Analysis, Nine-Day Mission Abort, Test Run 2

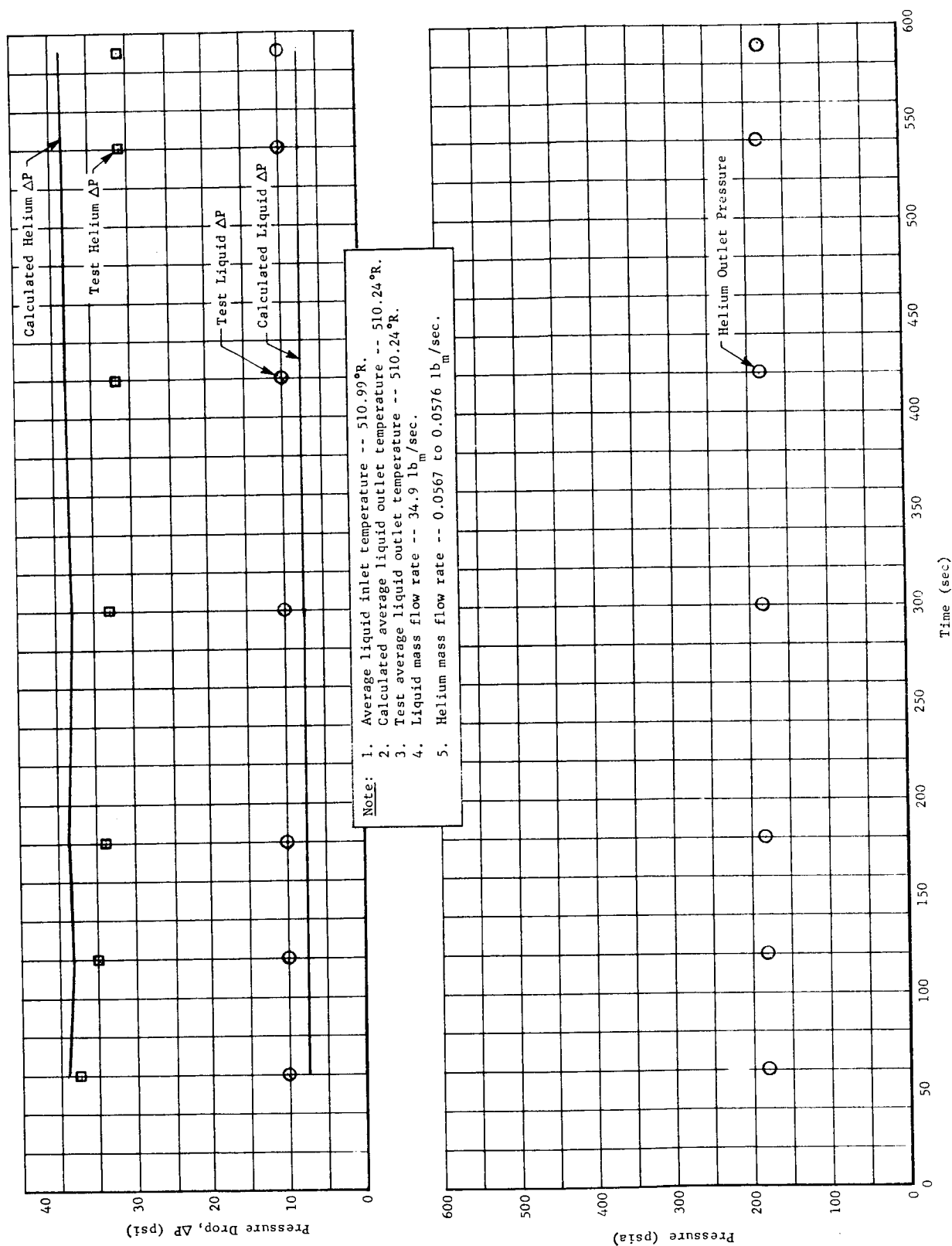


Fig. 56a Low-Pressure Heat Exchanger Posttest Analysis, Nine-Day Mission Abort, Test Run 2

Mertin-CR-66-44

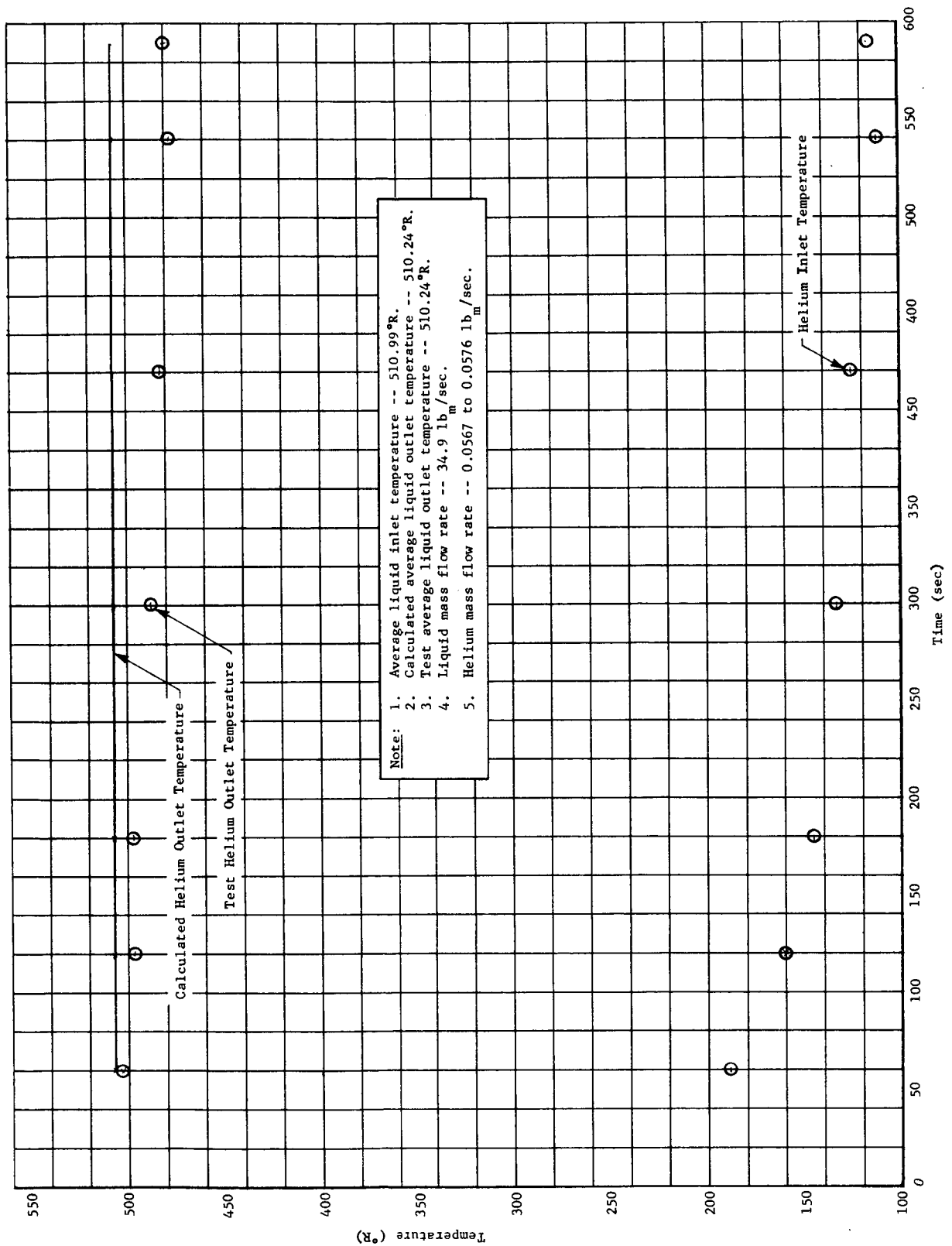


Fig. 56b Low-Pressure Heat Exchanger Posttest Analysis, Nine-Day Mission Abort, Test Run 2

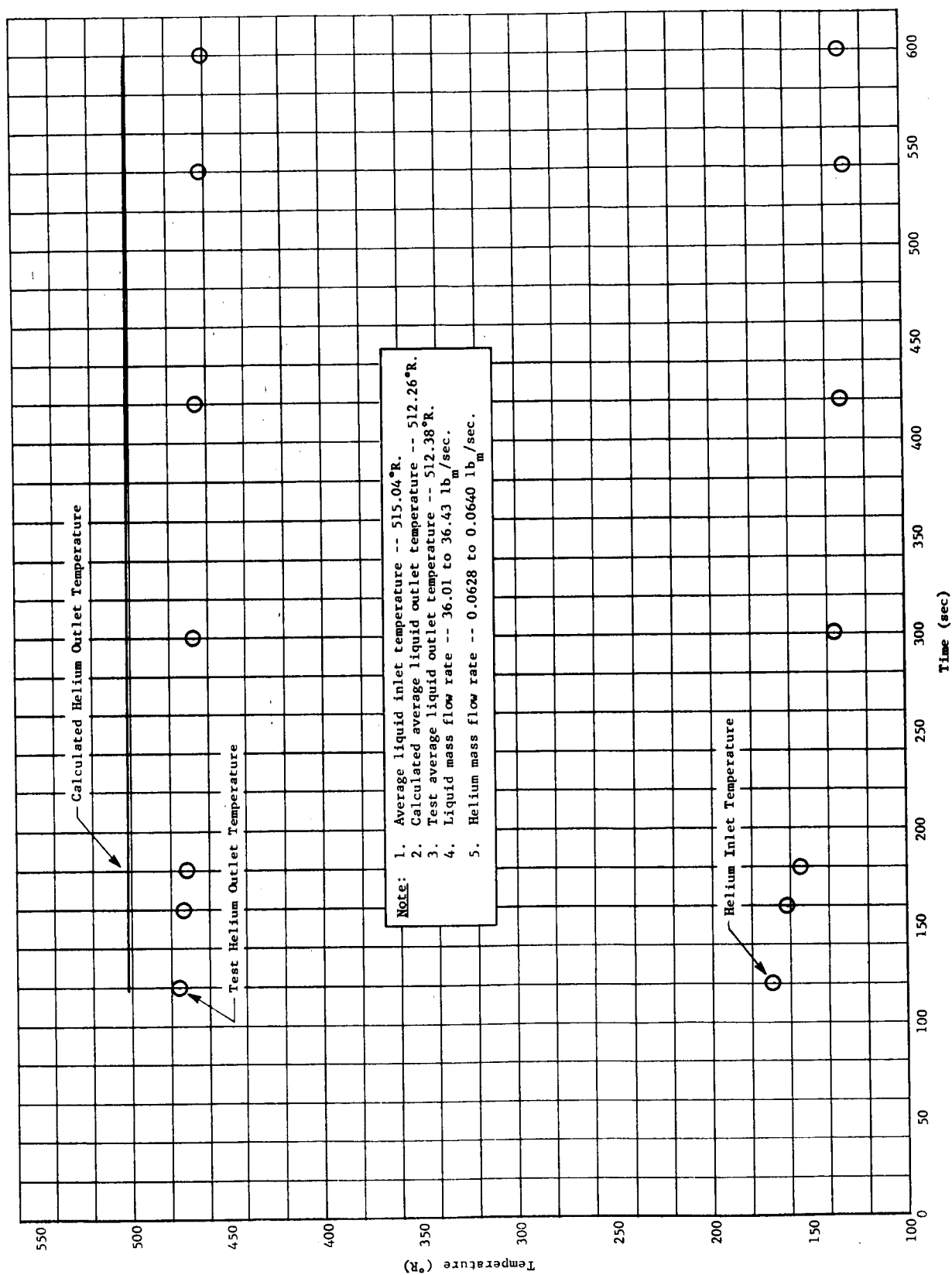


Fig. 57a High-Pressure Heat Exchanger Posttest Analysis, 90-Day Mission Abort, Test Run 2

Martin-CR-66-44

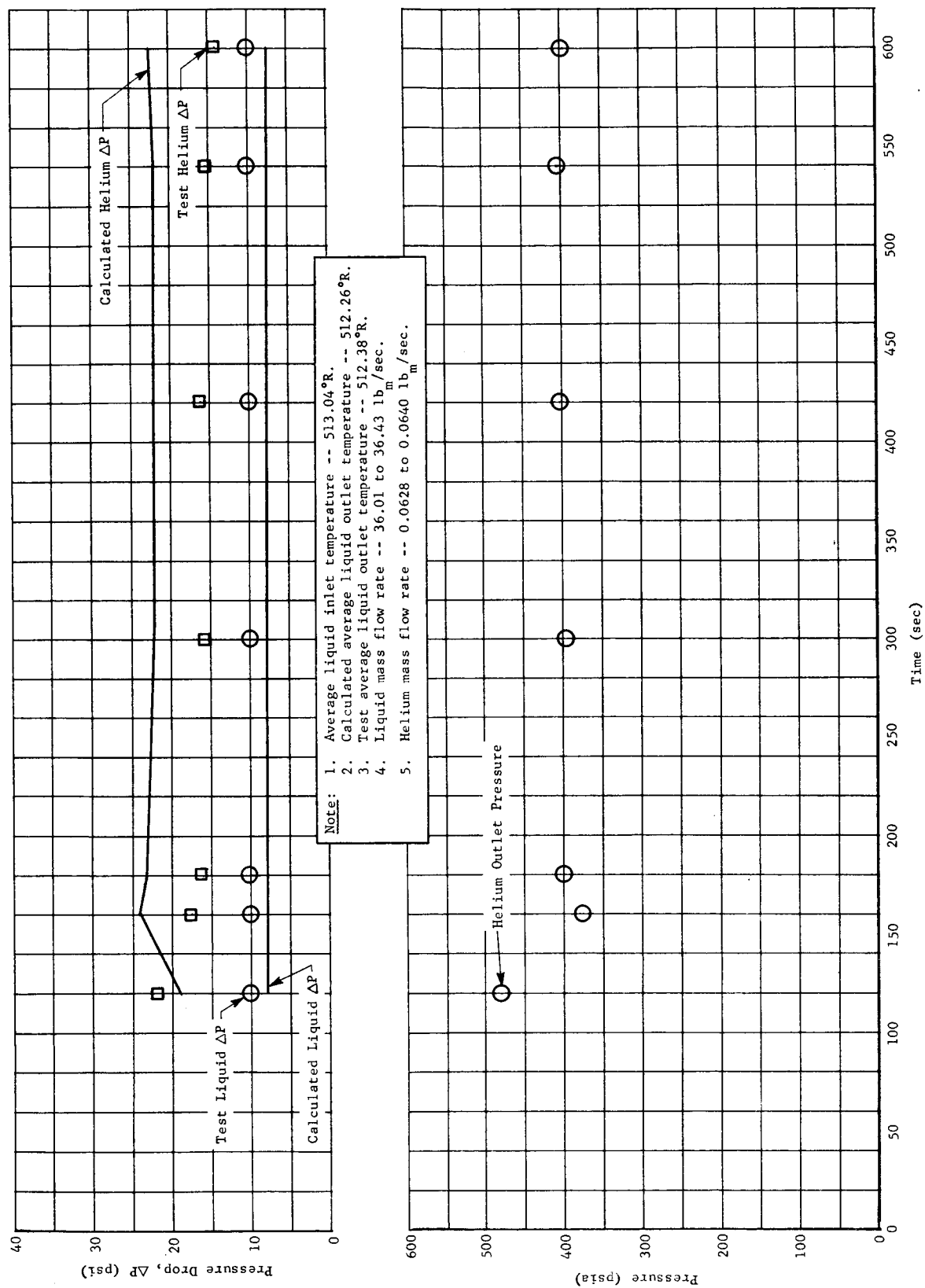


Fig. 57b High-Pressure Heat Exchanger Posttest Analysis, 90-Day Mission Abort, Test Run 2

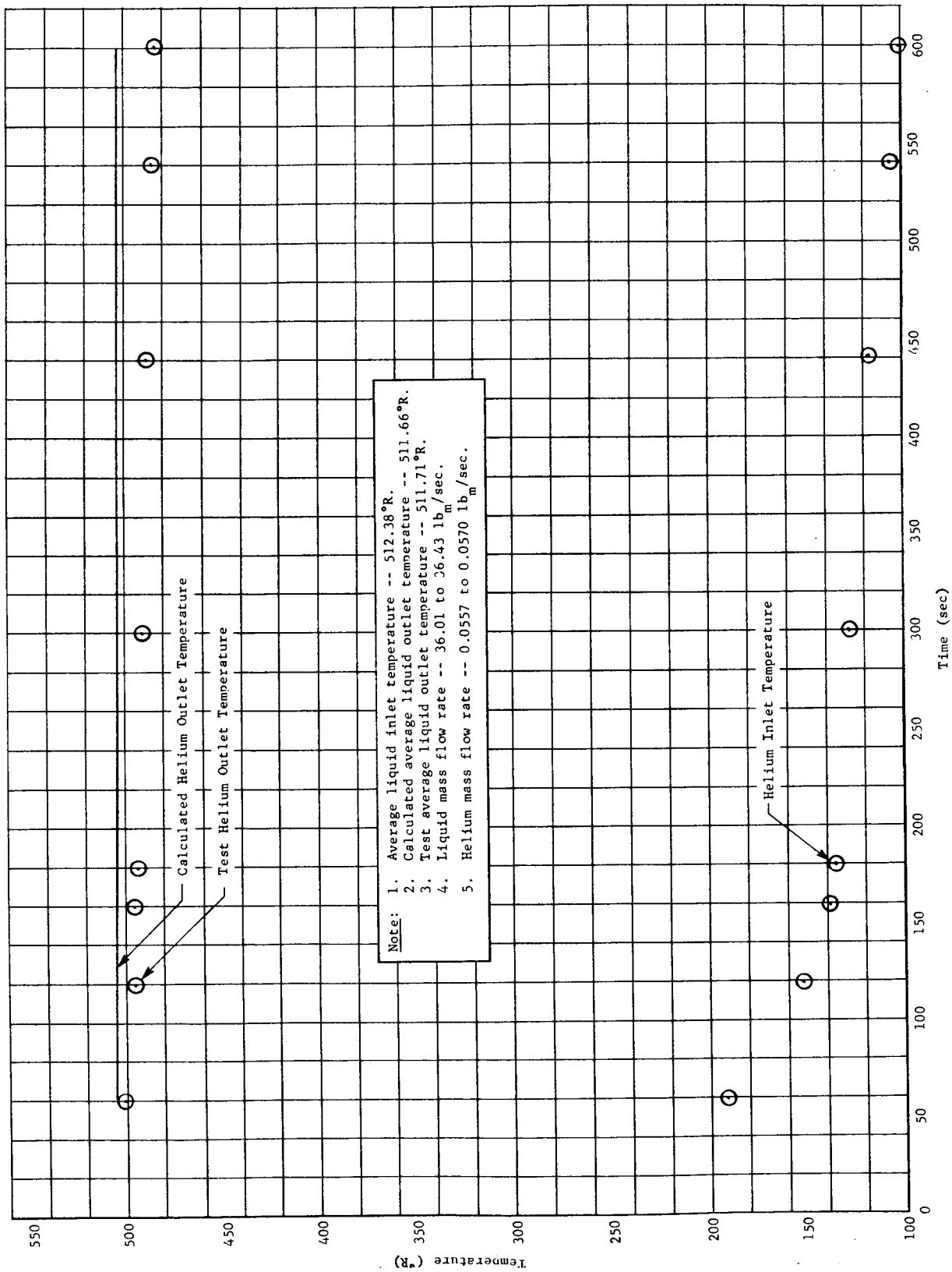


Fig. 58a Low-Pressure Heat Exchanger Posttest Analysis, 90-Day Mission Abort, Test Run 2

Martin-CR-66-44

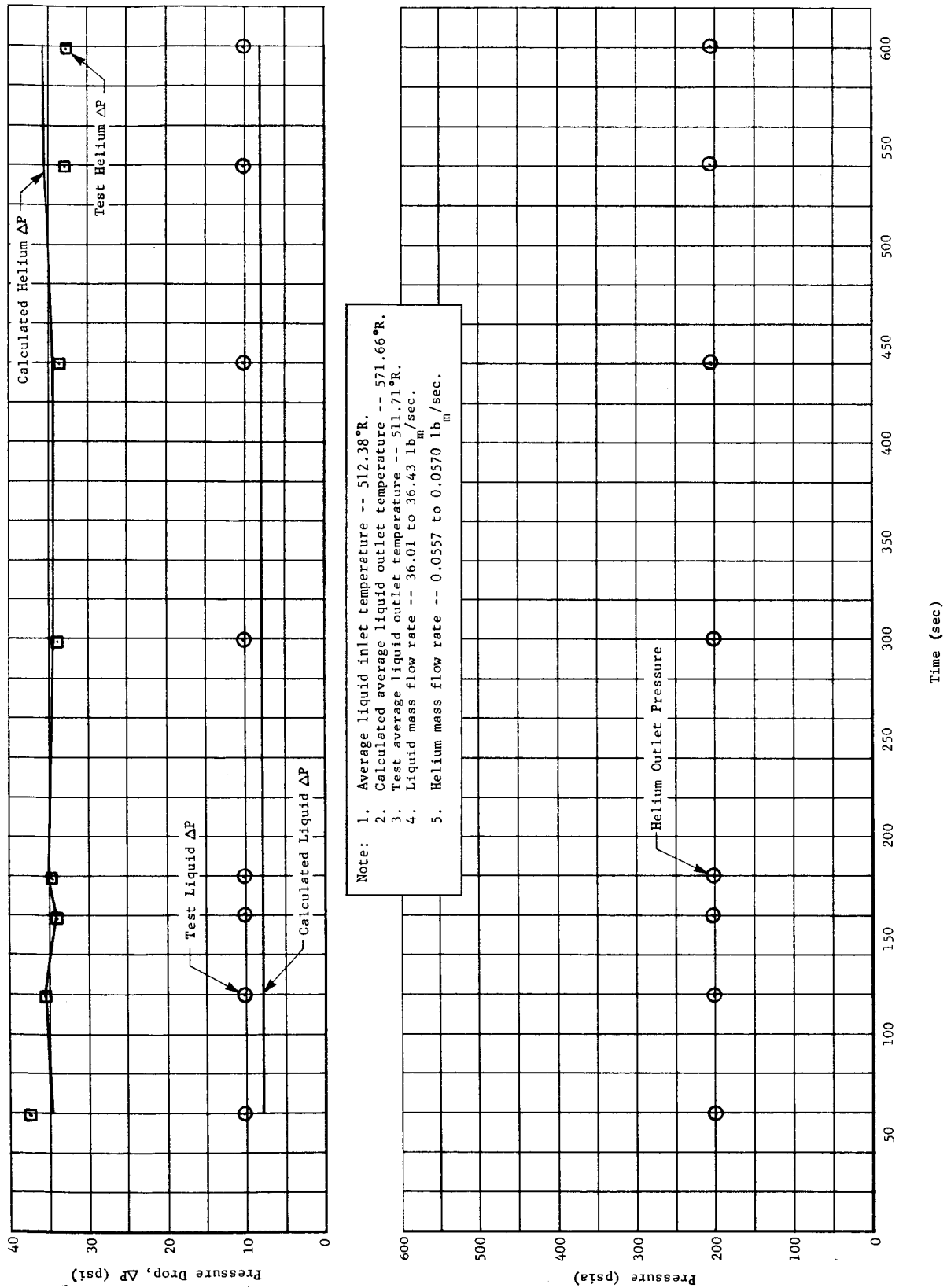
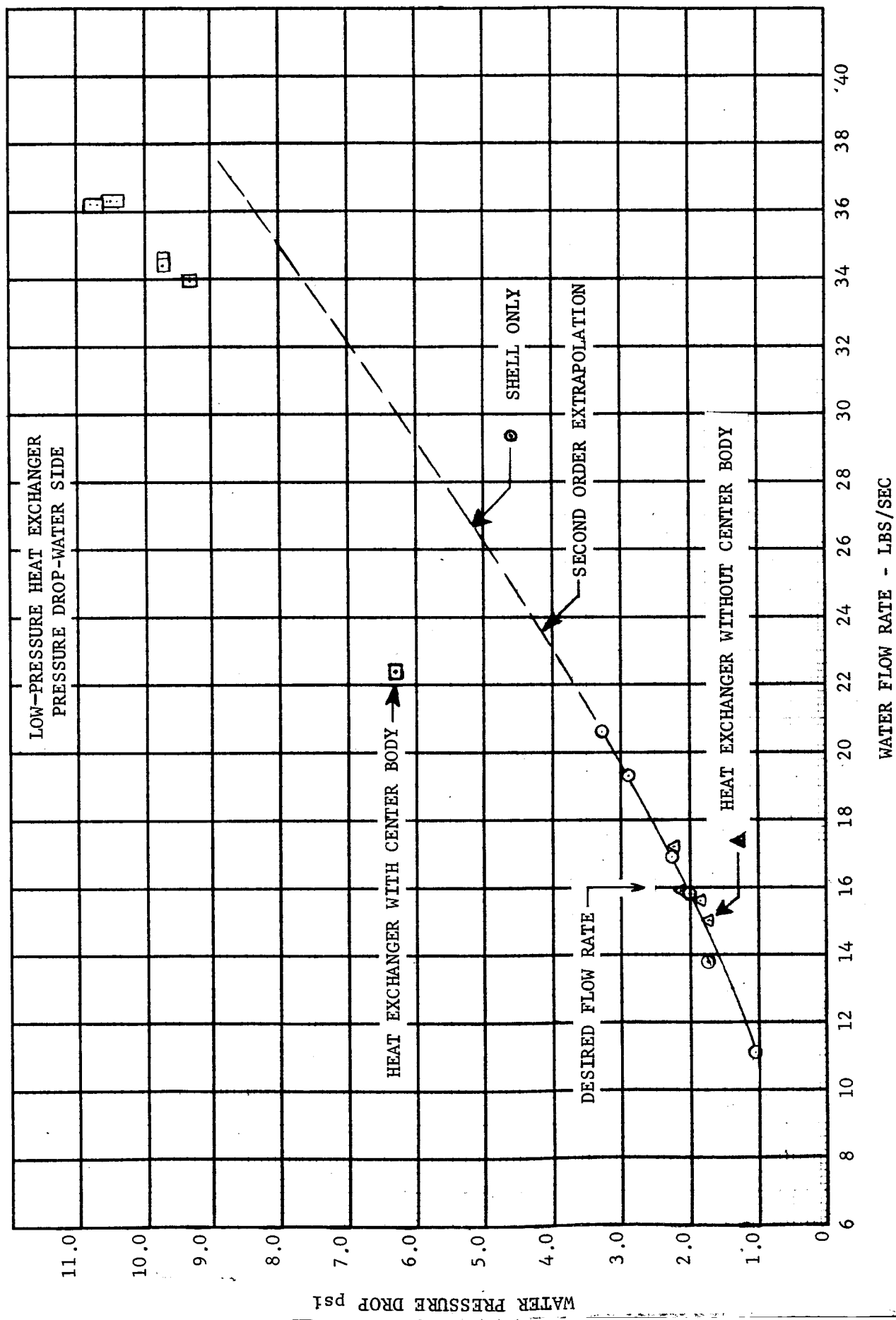


Fig. 58b Low-Pressure Heat Exchanger Posttest Analysis, 90-Day Mission Abort, Test Run 2

FIGURE 59



Martin-CR-66-44

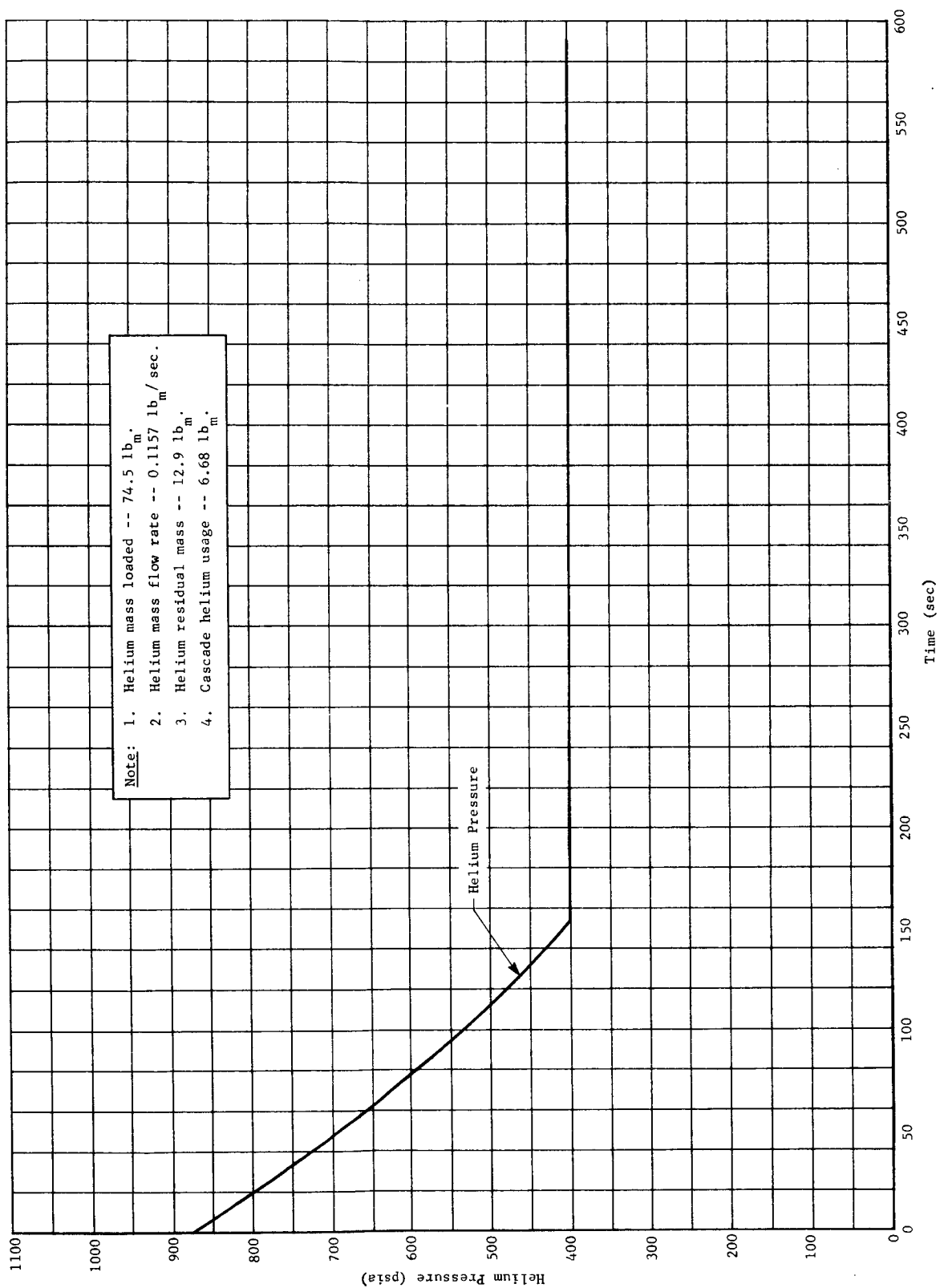


Fig. 60a Primary Storage Container Pretest Analysis, Nine-Day Mission Abort

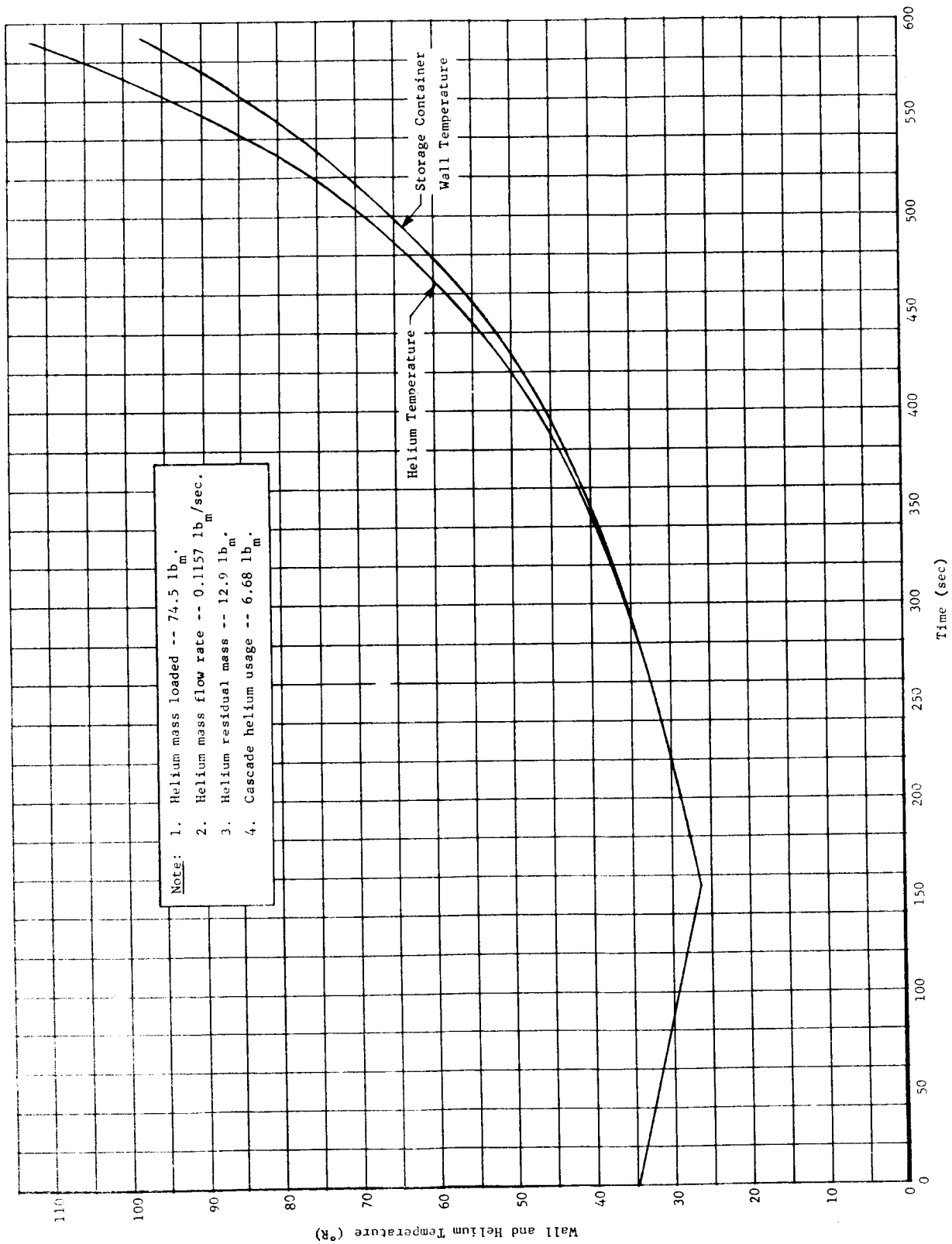


Fig. 60b Primary Storage Container Pretest Analysis, Nine-Day Mission Abort

Martin-CR-66-44

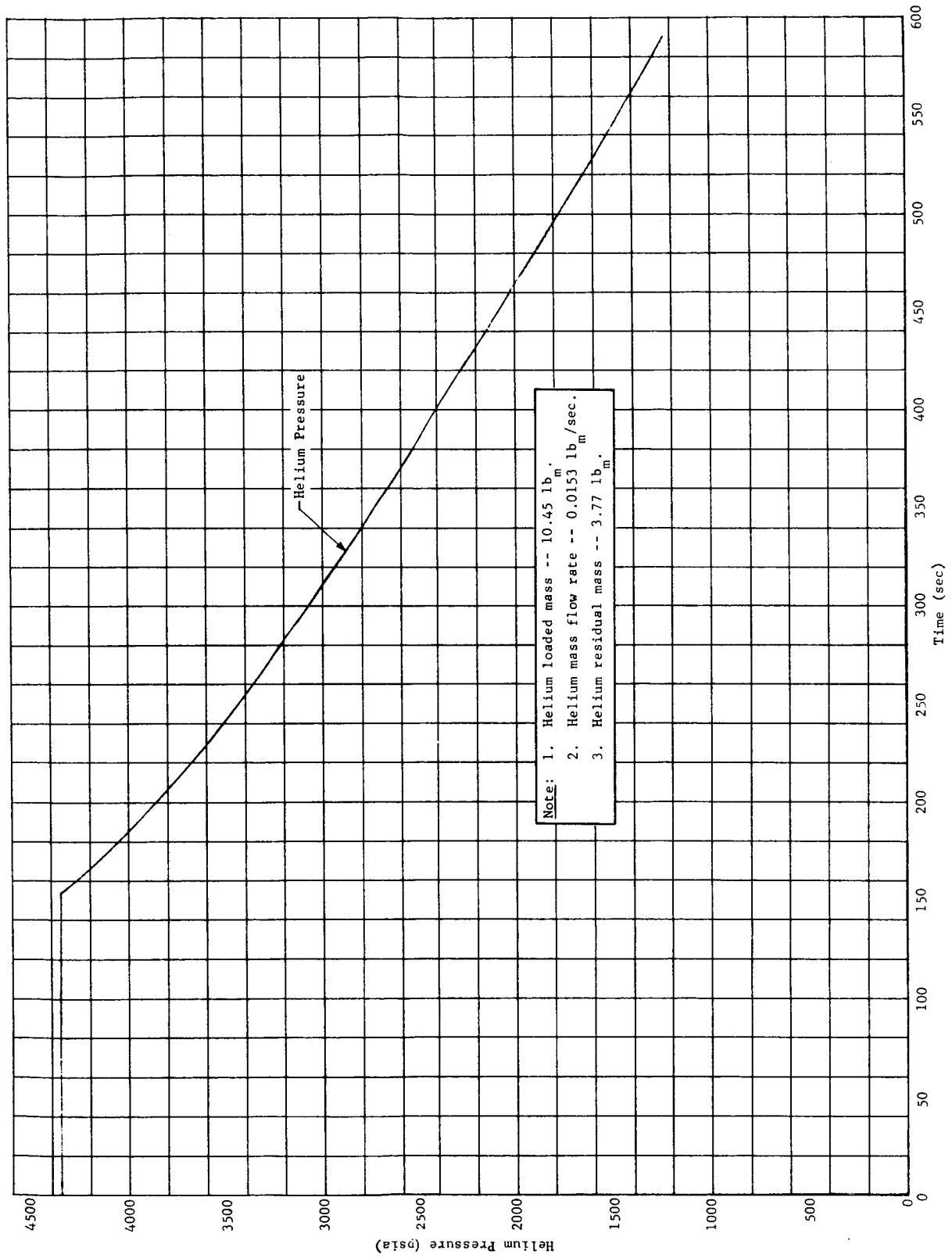


Fig. 61a Cascade Storage Container Pretest Analysis, Nine-Day Mission Abort

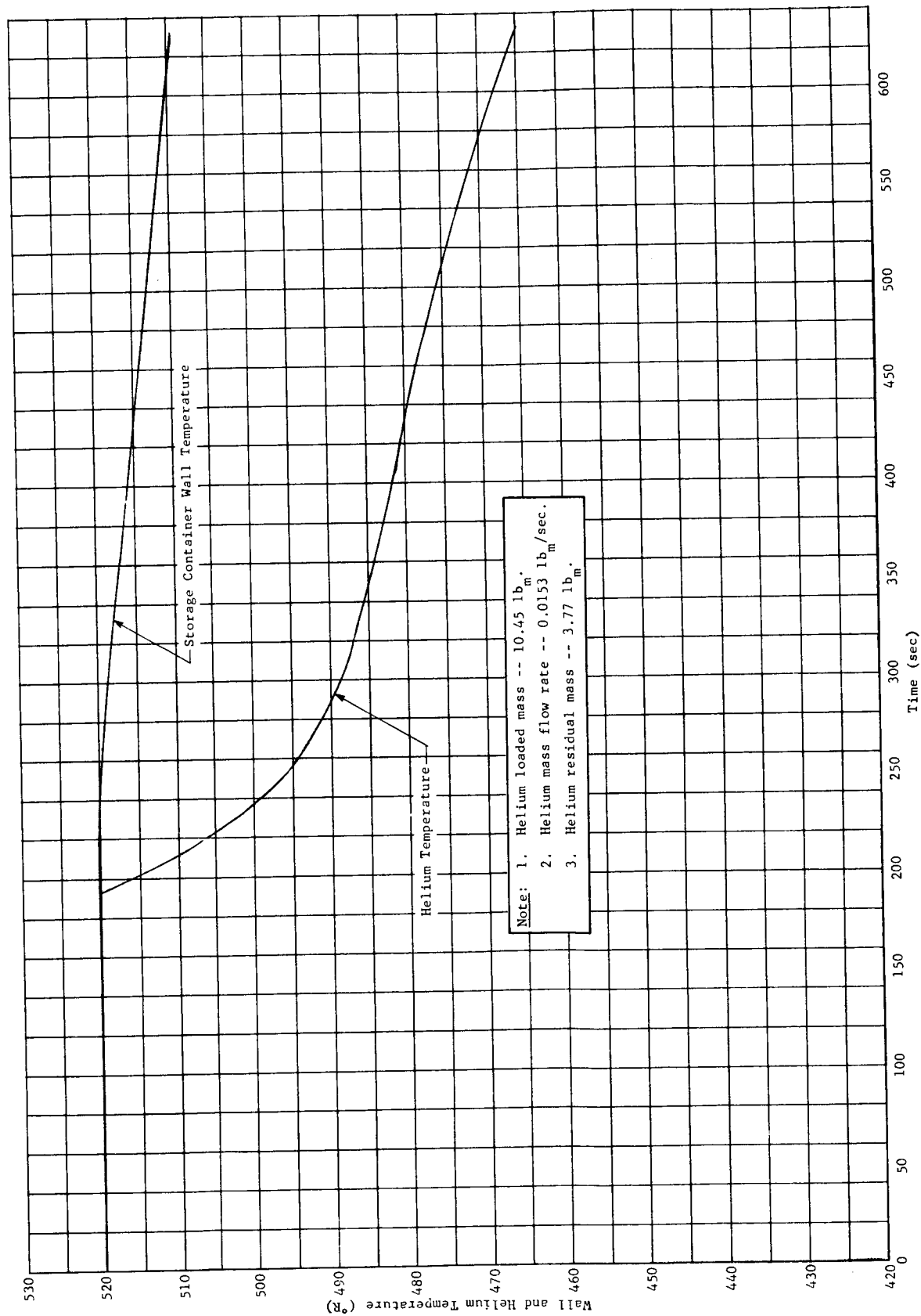


Fig. 6lb Cascade Storage Container Pretest Analysis, Nine-Day Mission Abort

Martin-CR-66-44

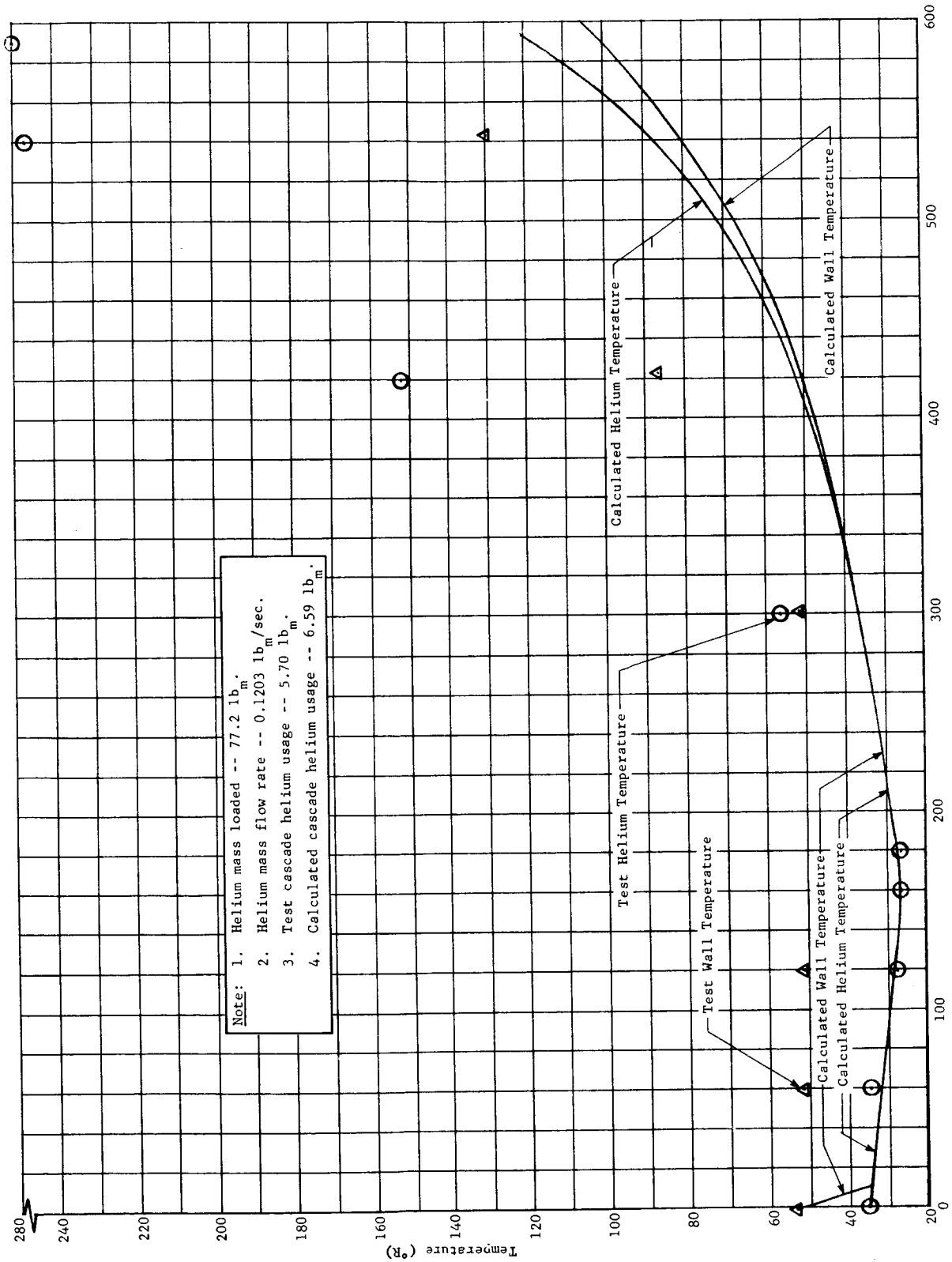


Fig. 62a Primary Storage Container Posttest Analysis, Nine-Day Mission Abort, Test Run 1

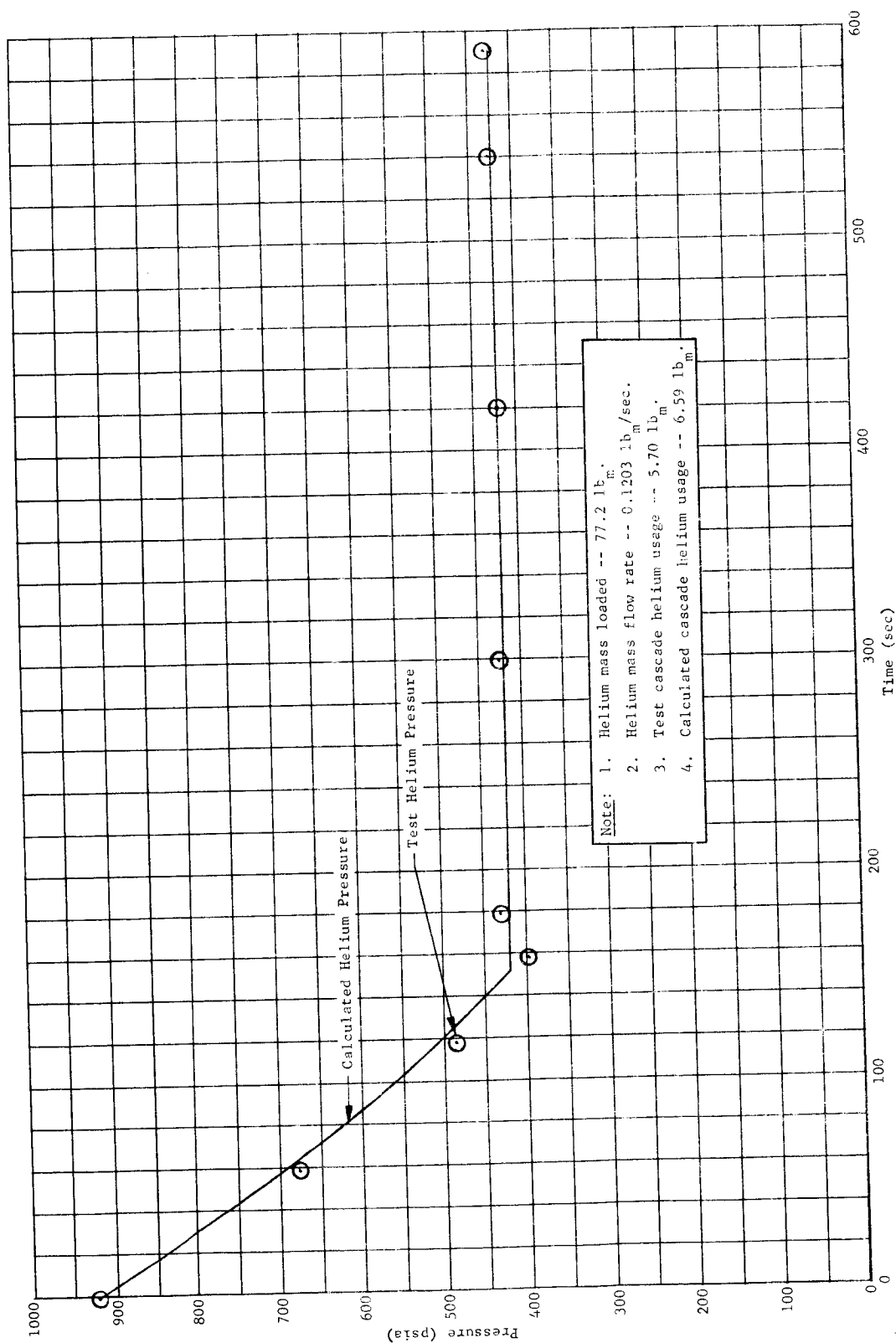


Fig. 62b Primary Storage Container Posttest Analysis, Nine-Day Mission Abort, Test Run 1

Martin-CR-66-44

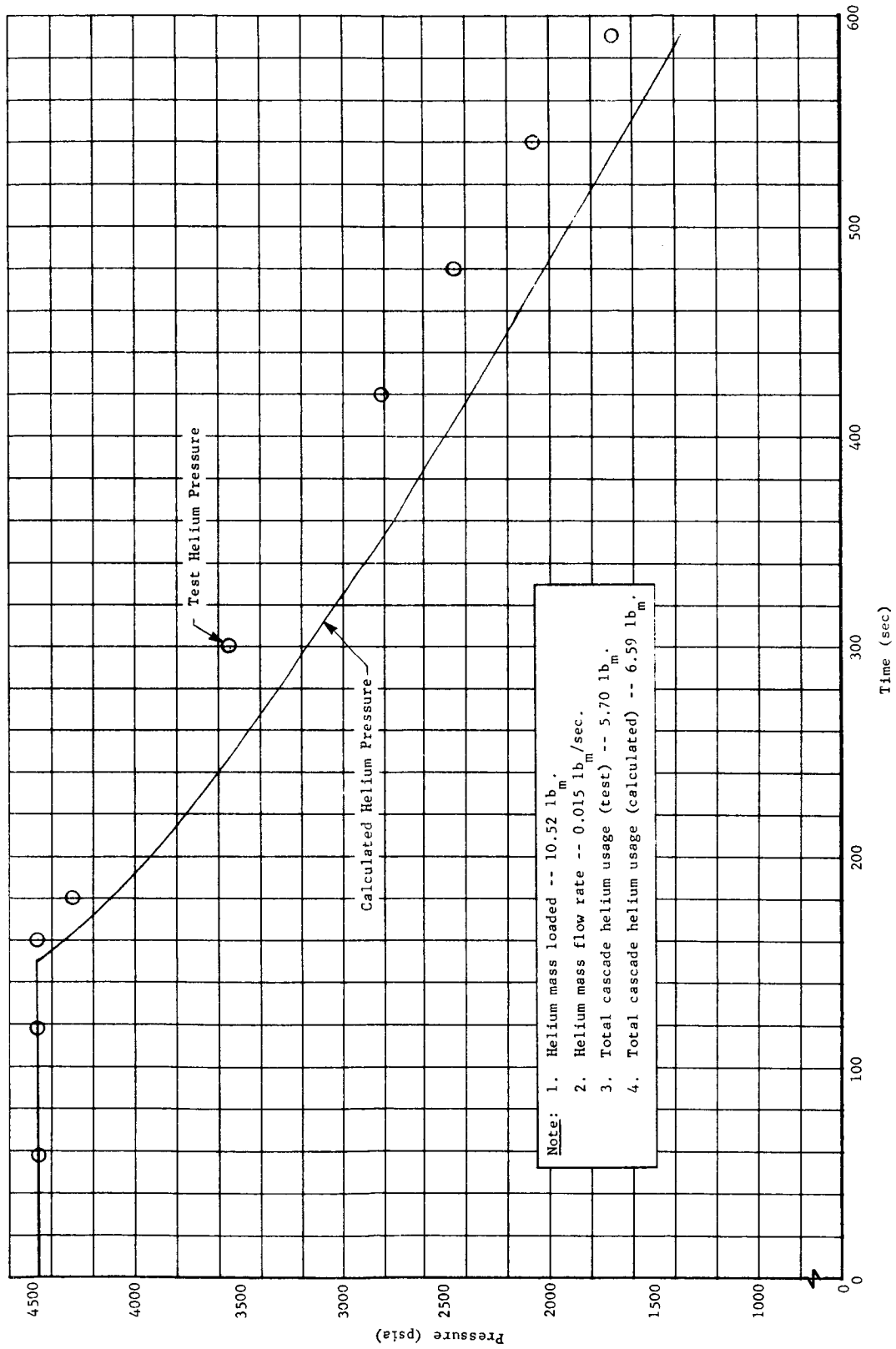


Fig. 63a Cascade Storage Container Posttest Analysis, Nine-Day Mission Abort, Test Run 1

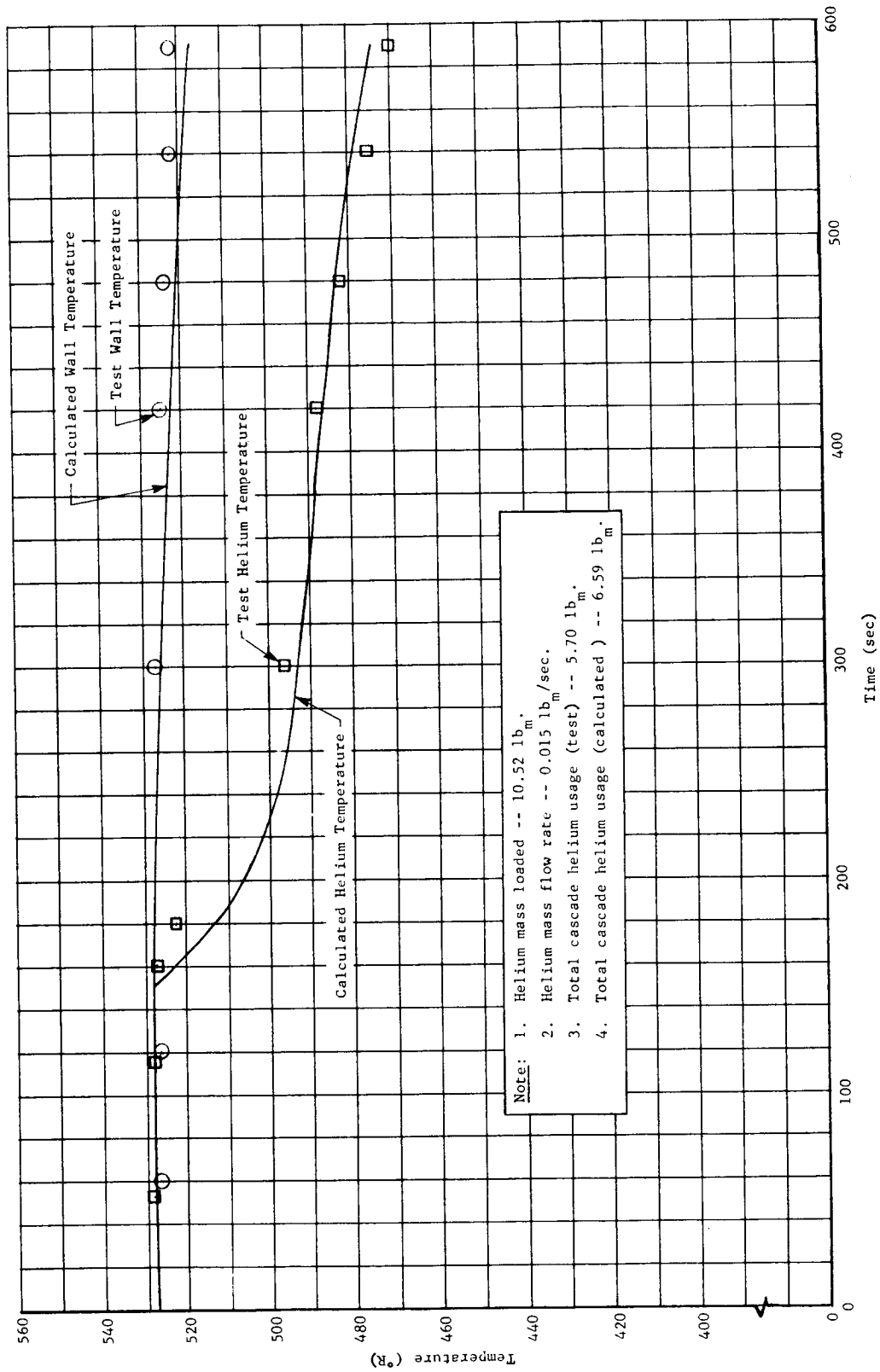


Fig. 63b Cascade Storage Container Posttest Analysis, Nine-Day Mission Abort, Test Run 1

Martin-CR-66-44

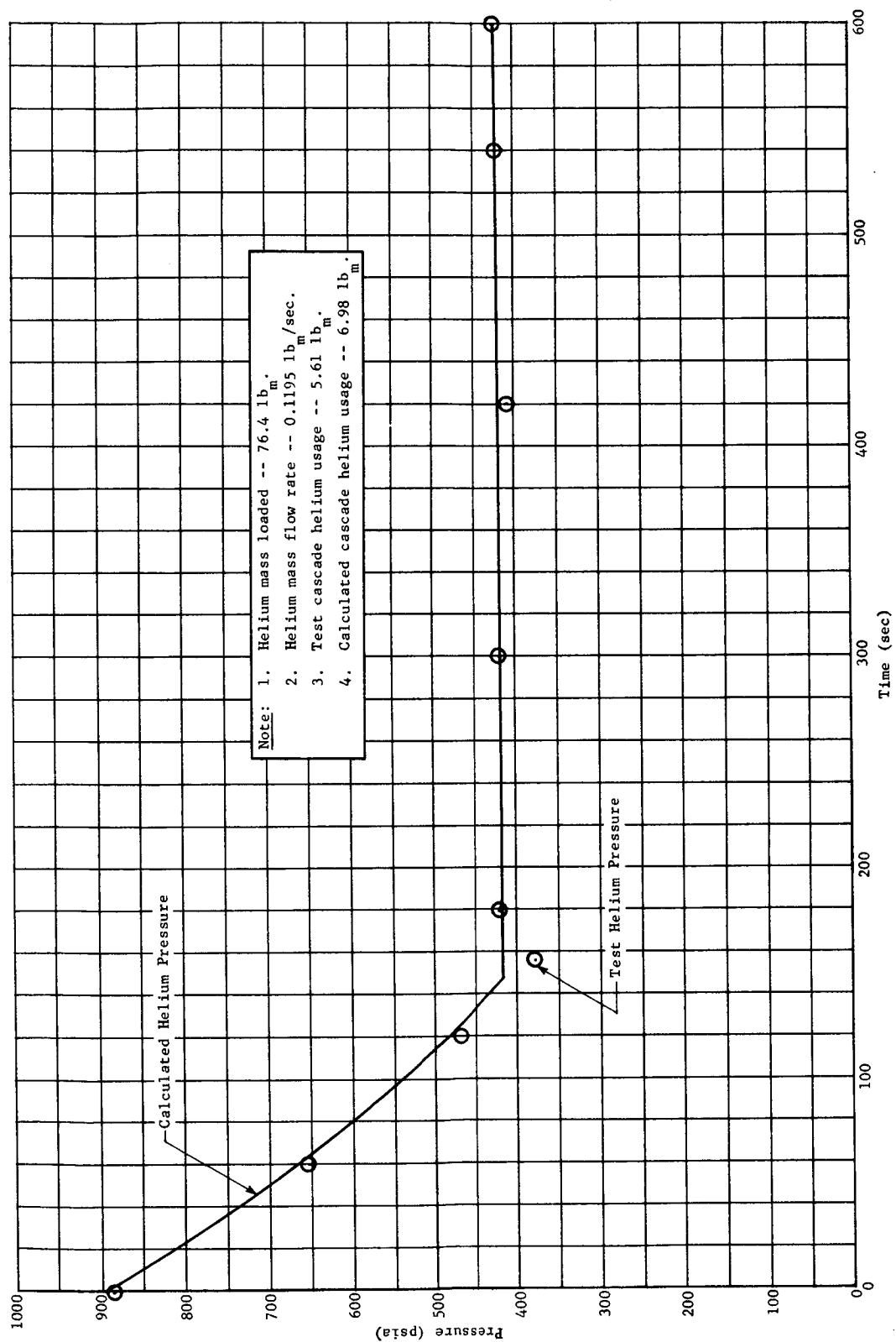


Fig. 64a Primary Storage Container Posttest Analysis, Nine-Day Mission

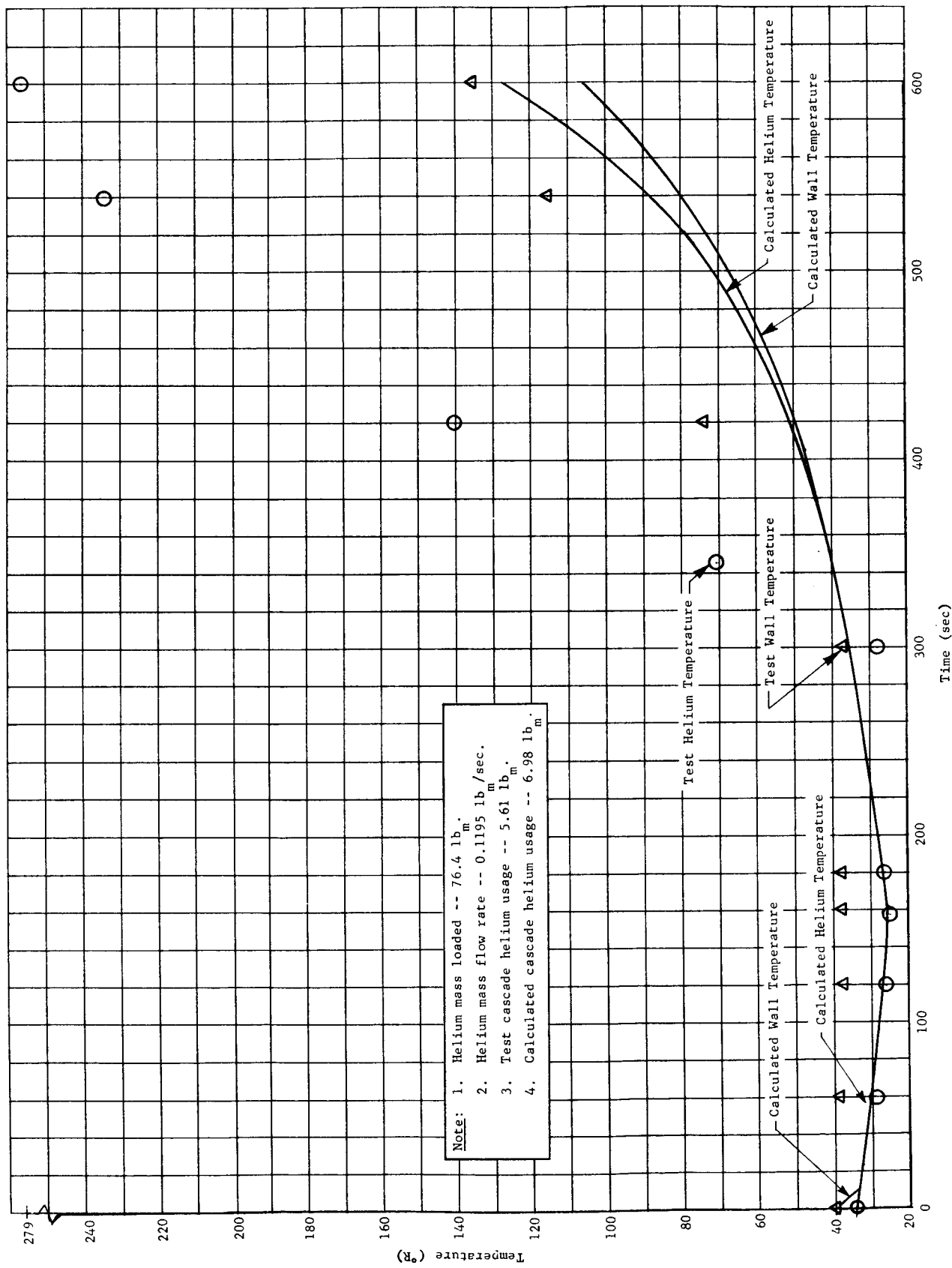


Fig. 64b Primary Storage Container Posttest Analysis, Nine-Day Mission Abort, Test Run 2

Martin-CR-66-44

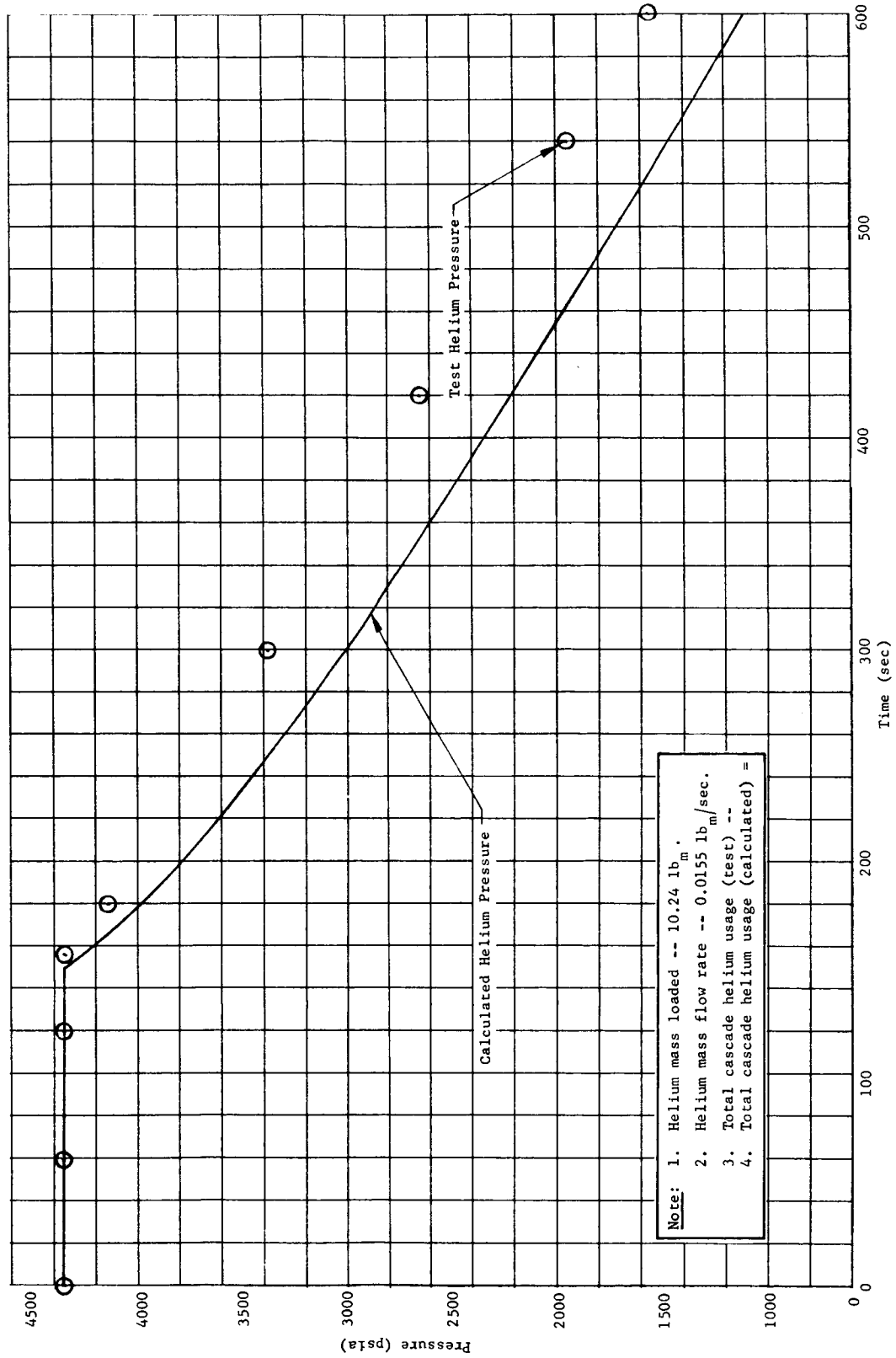


Fig. 65a Cascade Storage Container Posttest Analysis, Nine-Day Mission Abort, Test Run 2

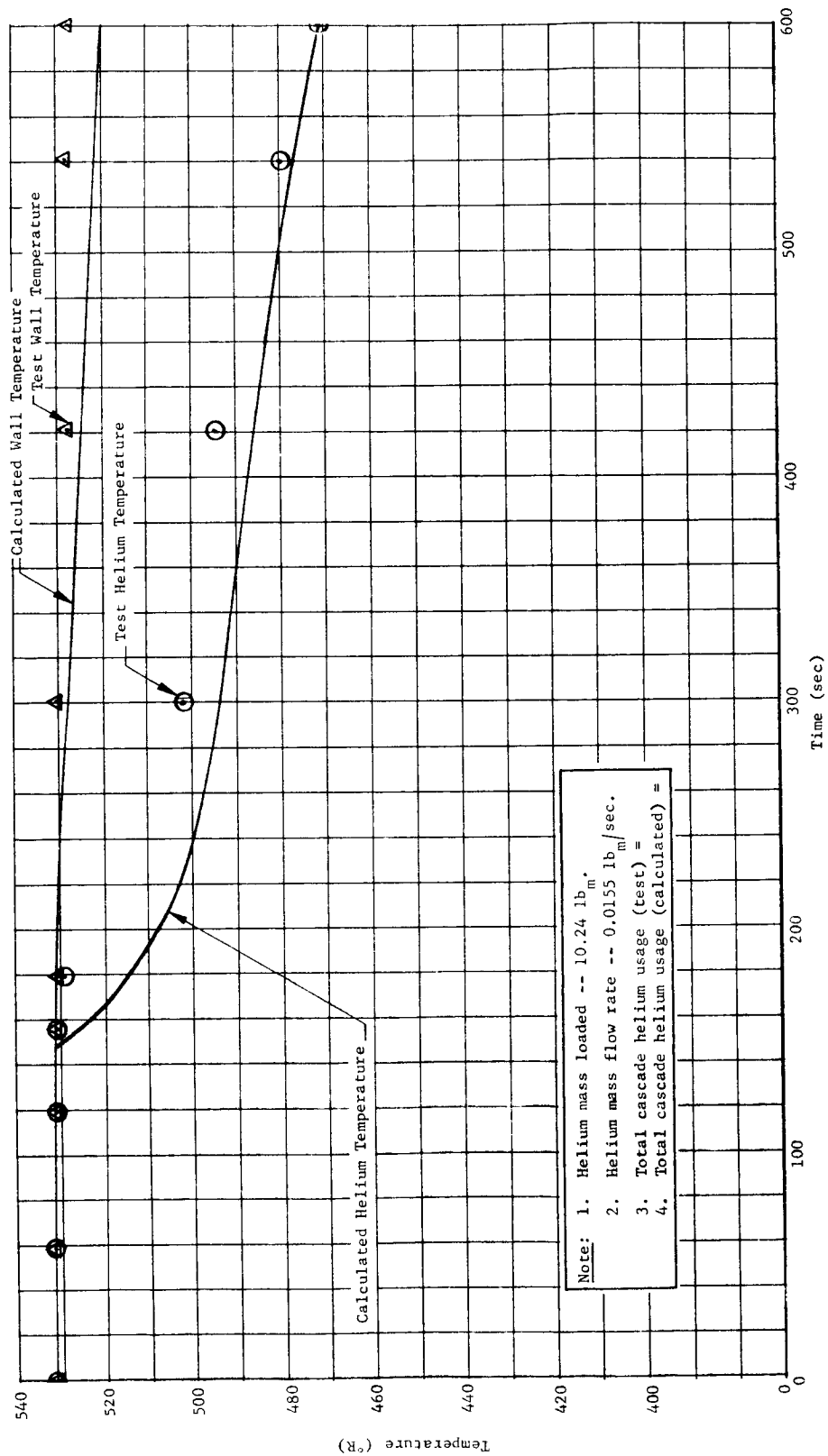


Fig. 65b Cascade Storage Container Posttest Analysis, Nine-Day Mission Abort, Test Run 2

Martin-CR-66-44

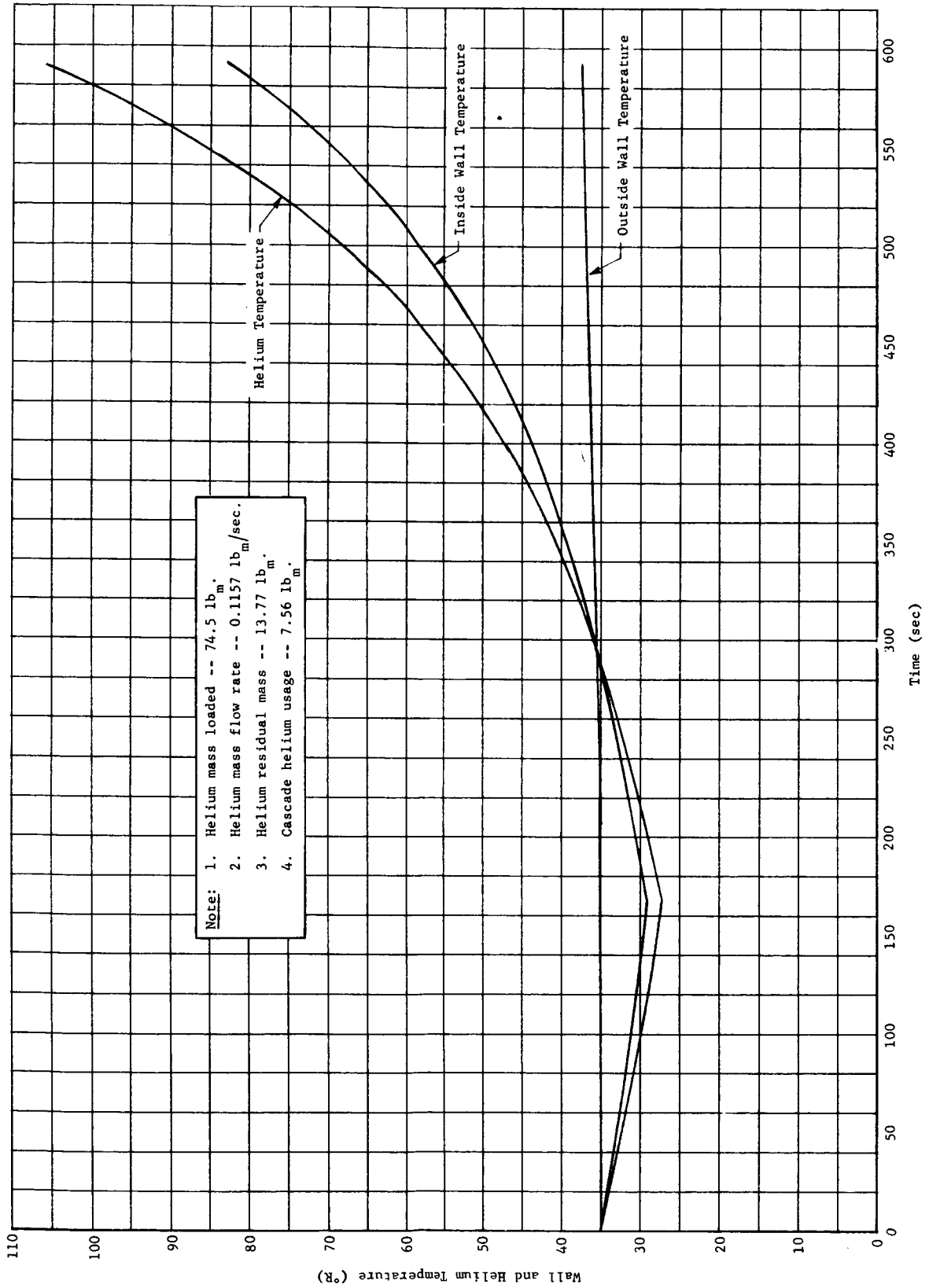


Fig. 66a Primary Storage Container Pretest Analysis, 90-Day Mission Abort

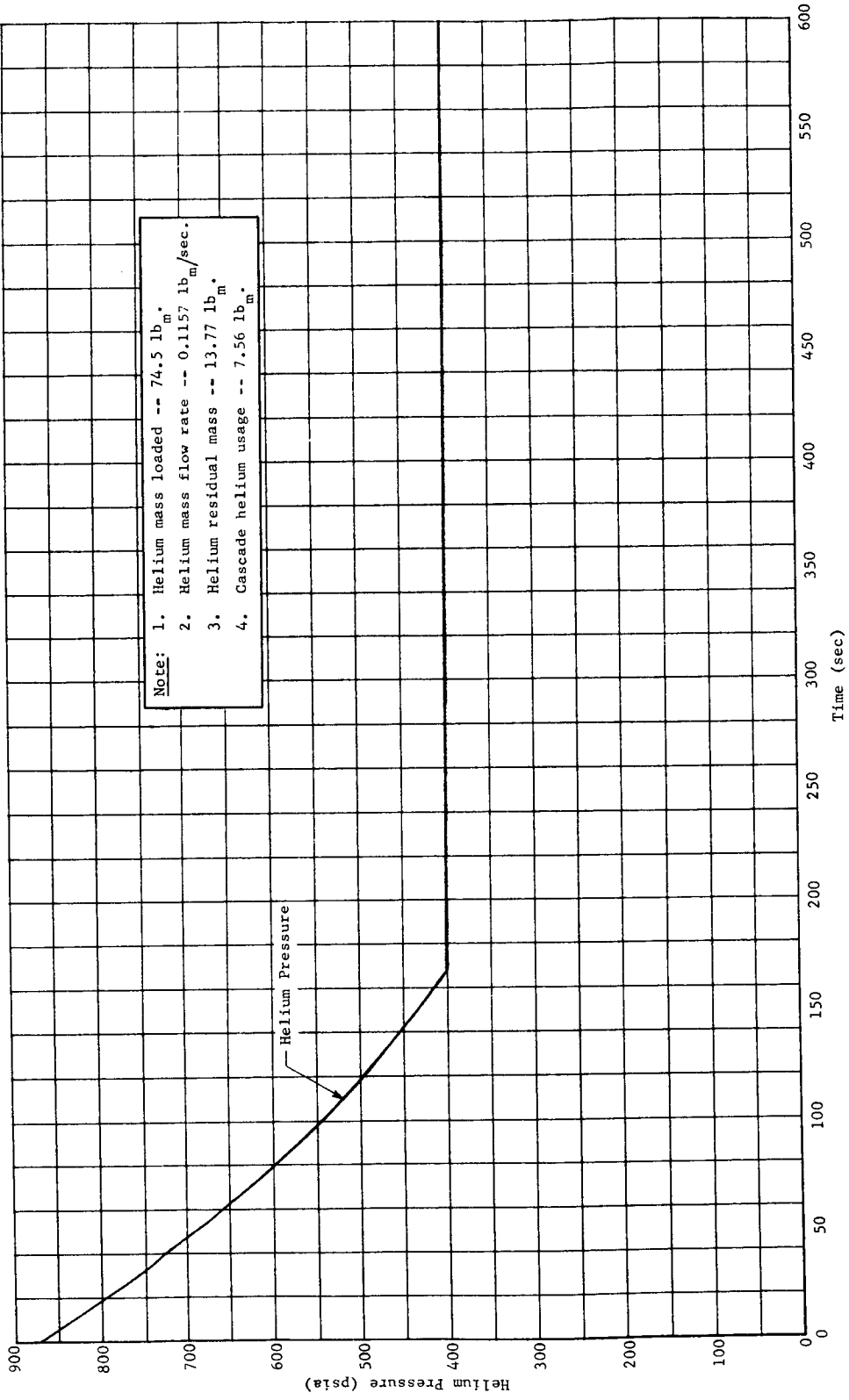


Fig. 66b Primary Storage Container Pretest Analysis, 90-Day Mission Abort

Martin-CR-66-44

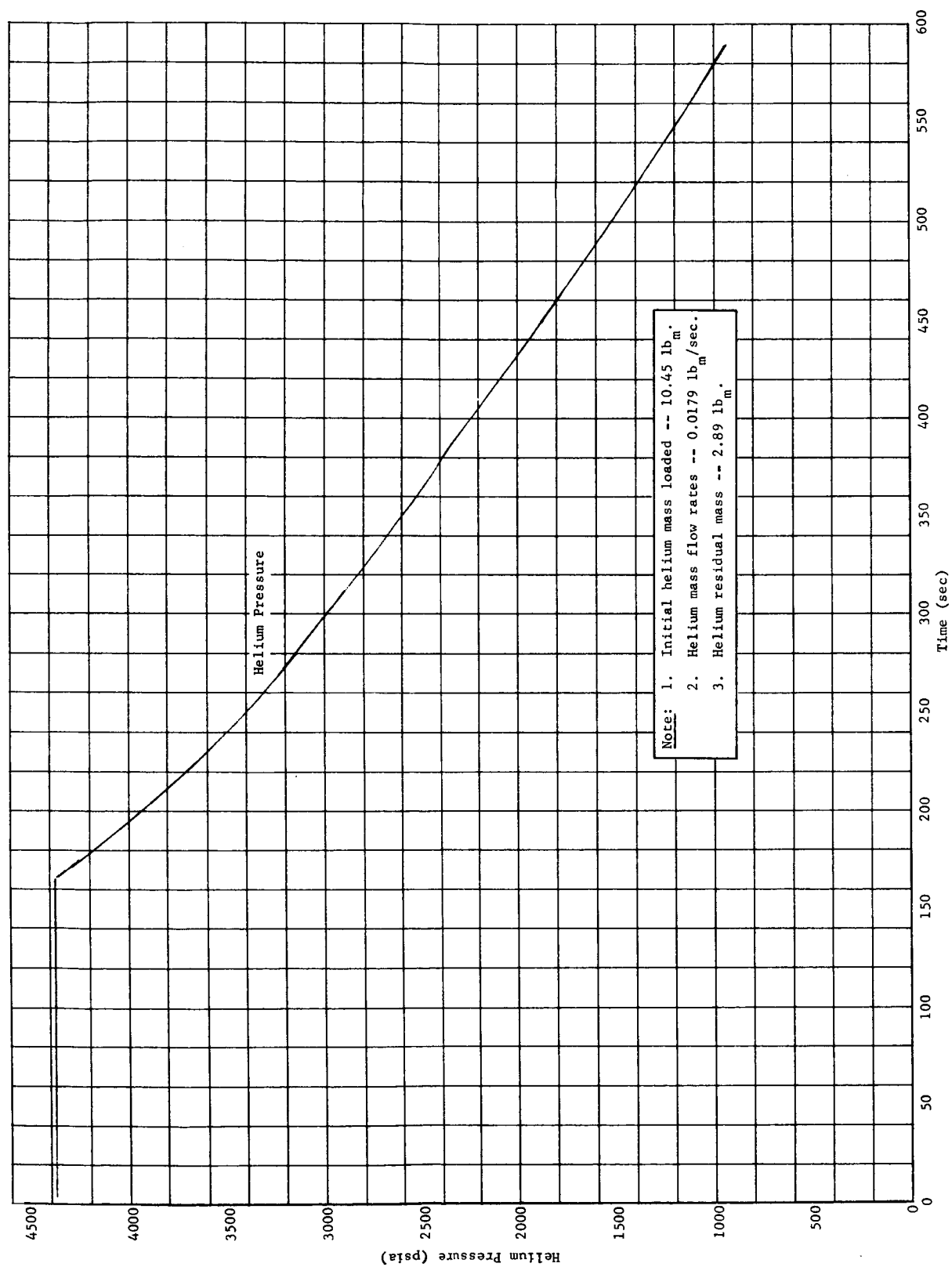


Fig. 67a Cascade Storage Container Pretest Analysis, 90-Day Mission Abort

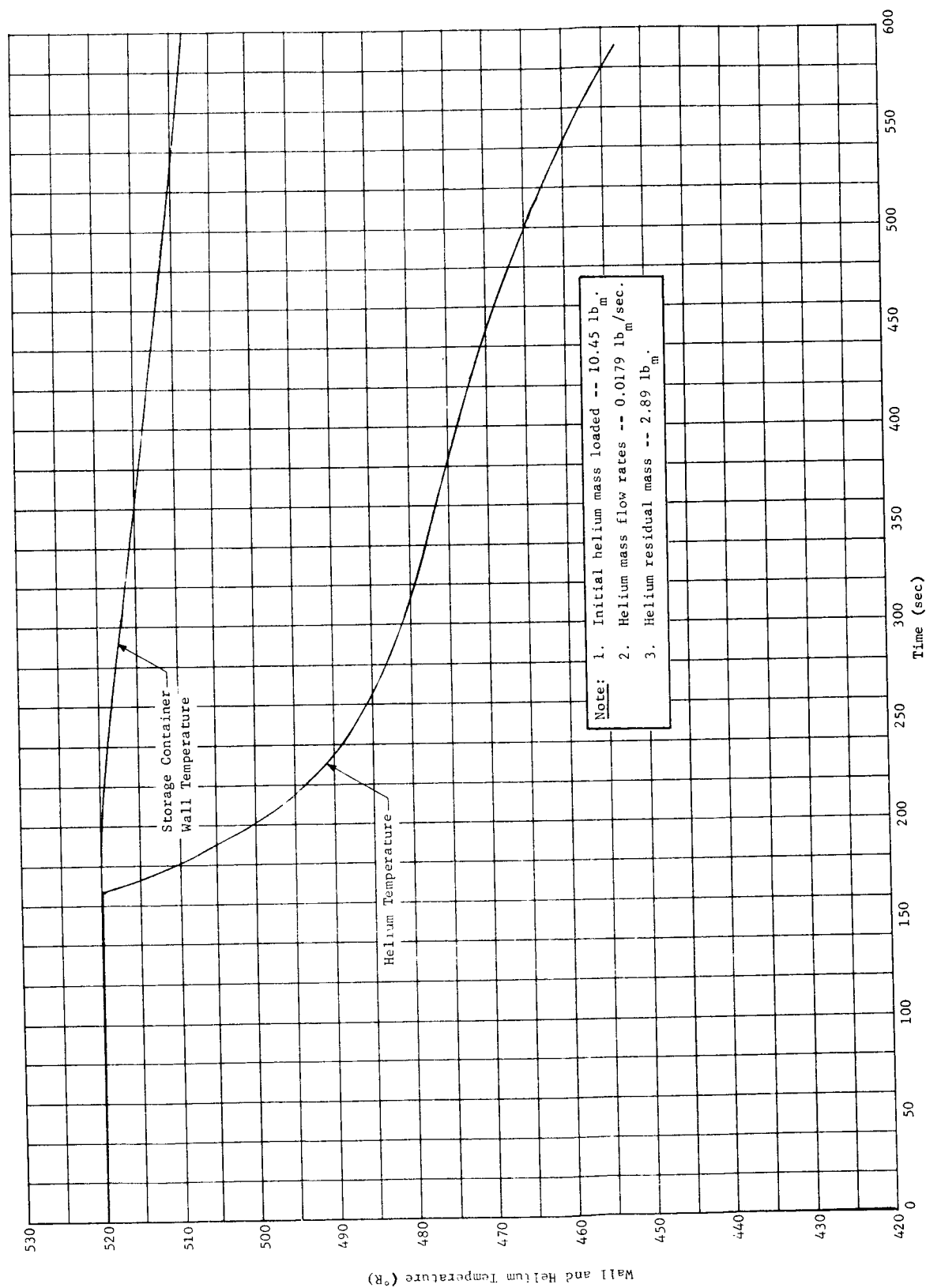


Fig. 67b Cascade Storage Container Pretest Analysis, 90-Day Mission Abort

Martin-CR-66-44

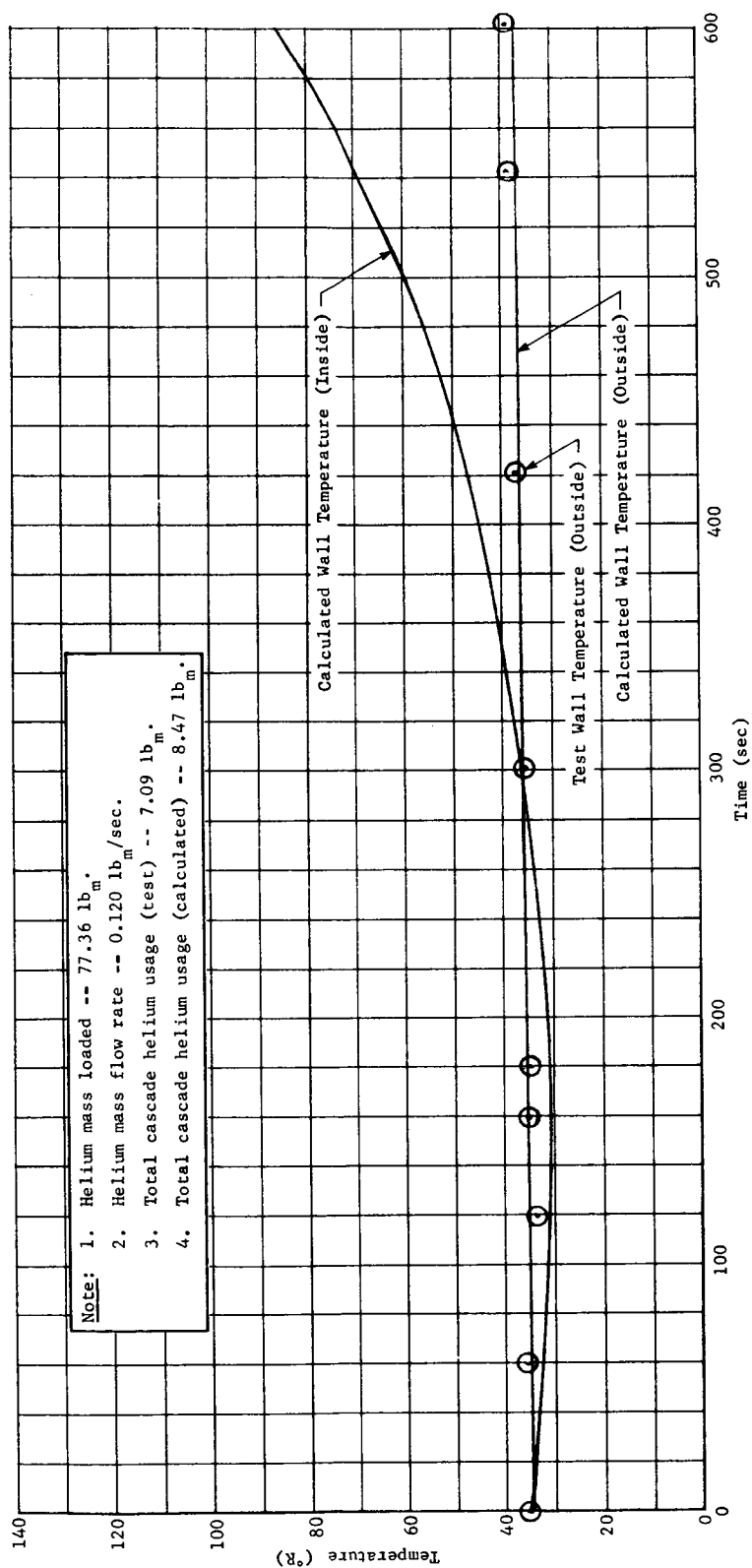


Fig. 68a Primary Storage Container Posttest Analysis, 90-Day Mission Abort, Test Run 1

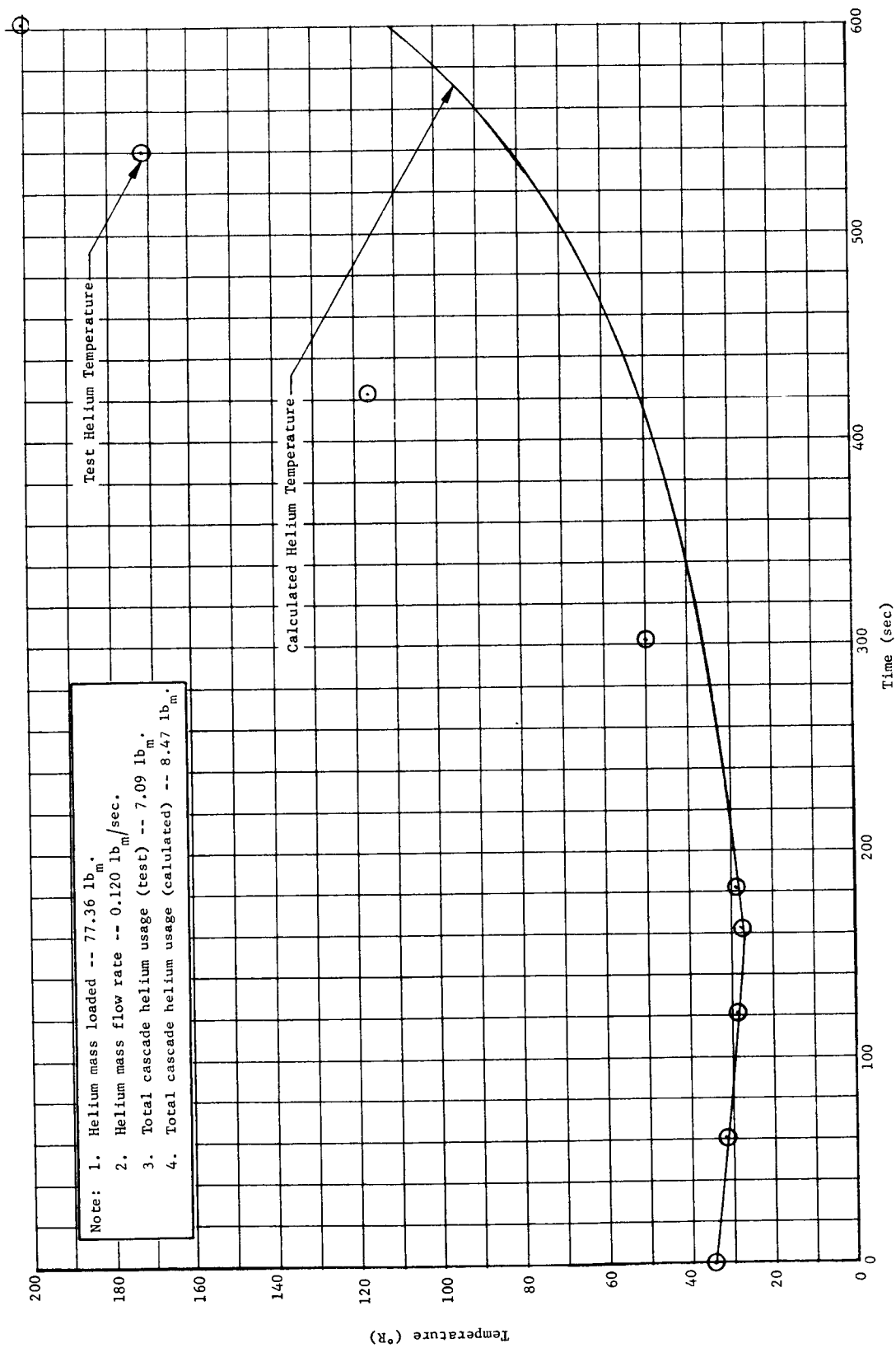


Fig. 68b Primary Storage Container Posttest Analysis, 90-Day Mission Abort, Test Run 1

Martin-CR-66-44

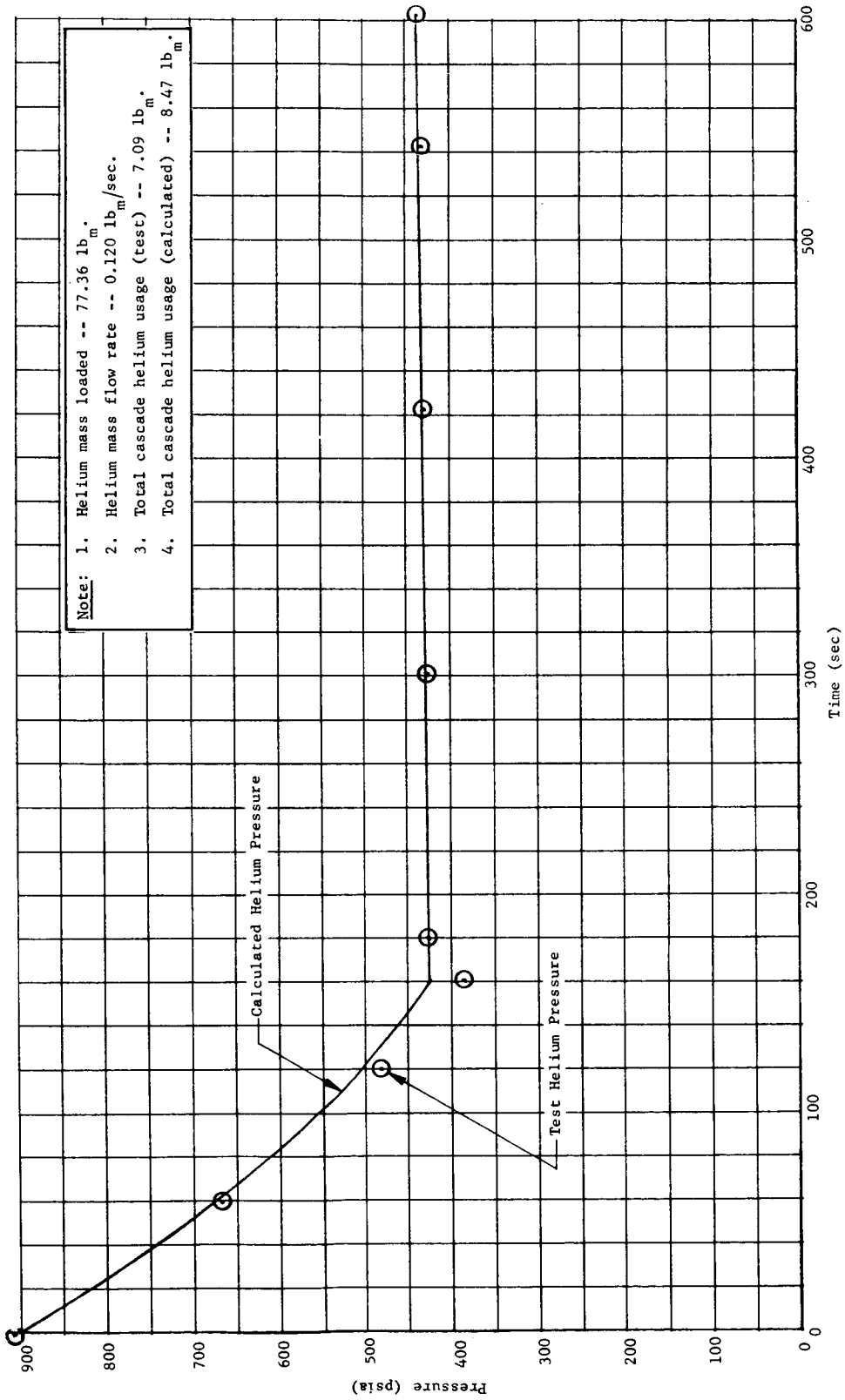


Fig. 68c Primary Storage Container Posttest Analysis, 90-Day Mission Abort, Test Run 1

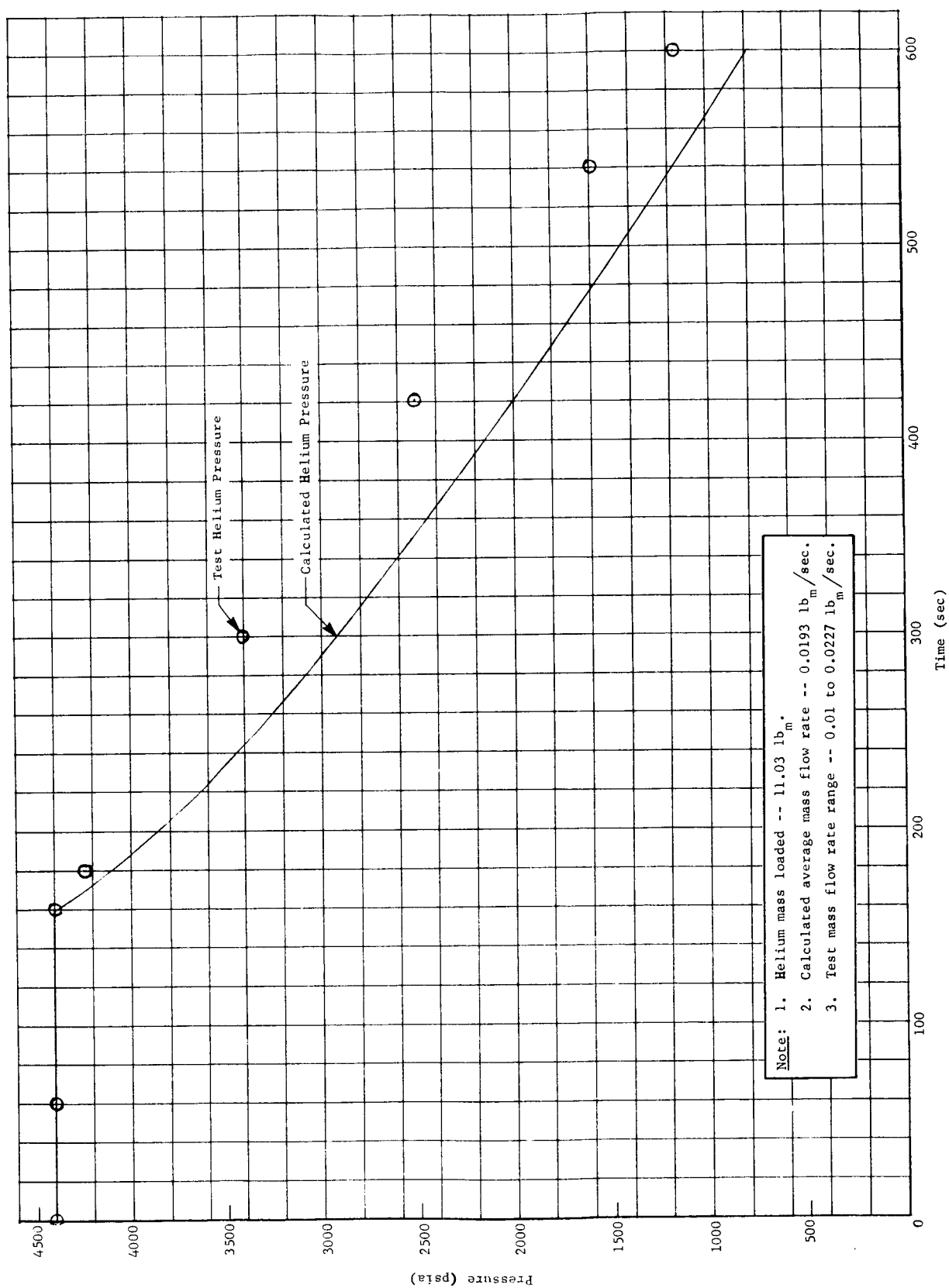


Fig. 69a Cascade Storage Container Posttest Analysis, 90-Day Mission Abort, Test Run 1

Martin-CR-66-44

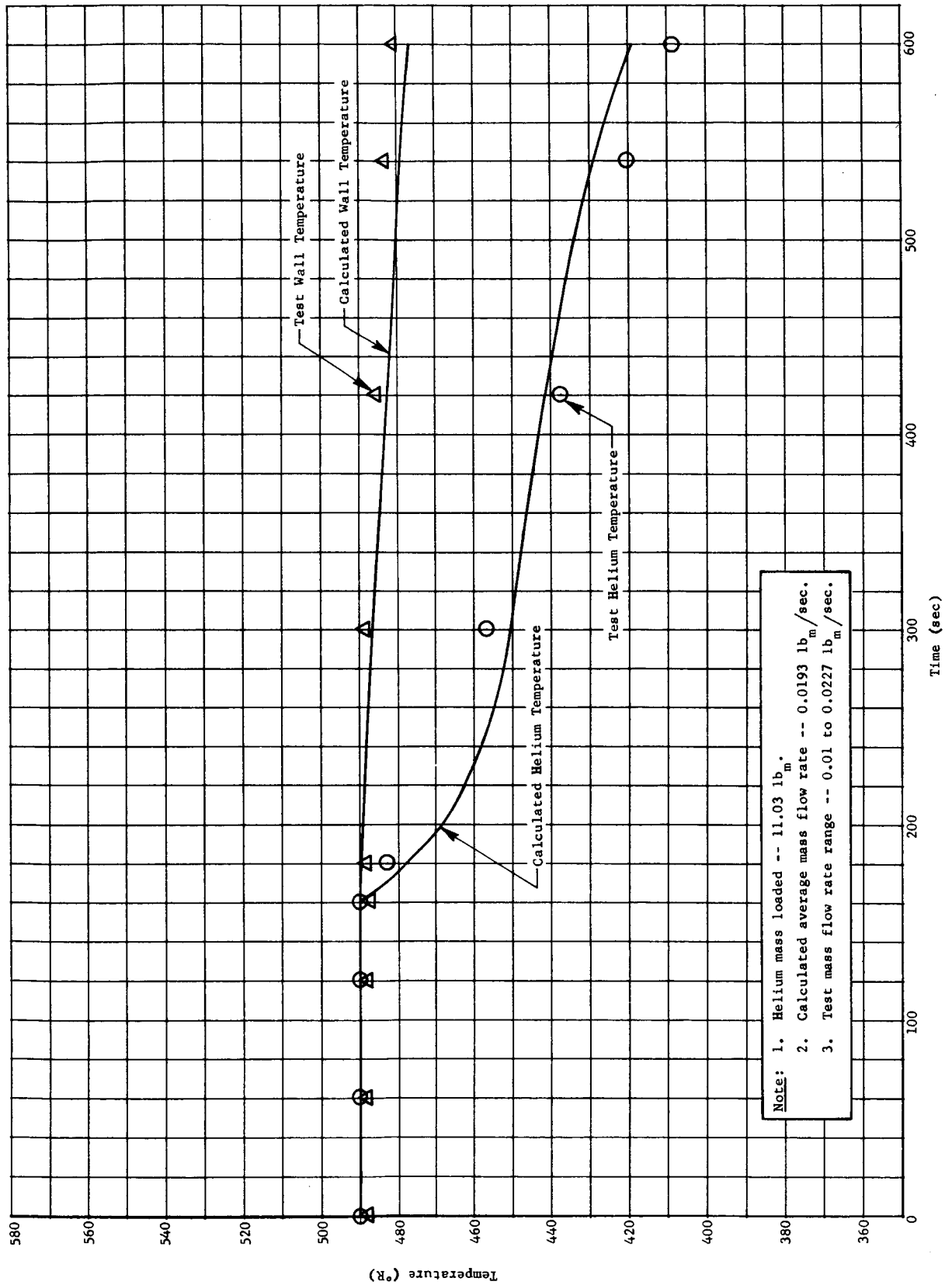


Fig. 69b Cascade Storage Container Posttest Analysis, 90-Day Mission Abort, Test Run 1

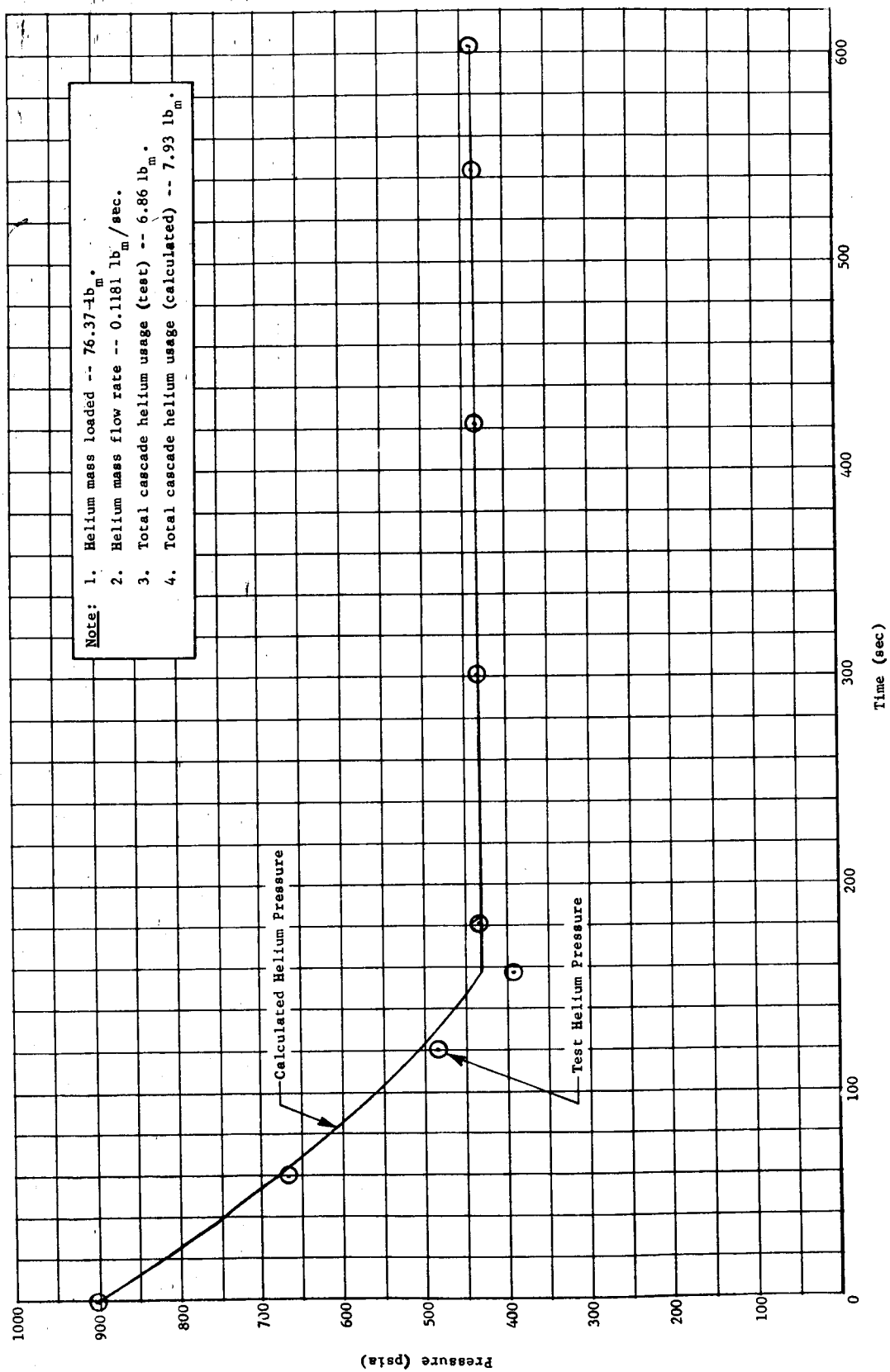


Fig. 70a Primary Storage Container Posttest Analysis, 90-Day Mission Abort, Test Run 2

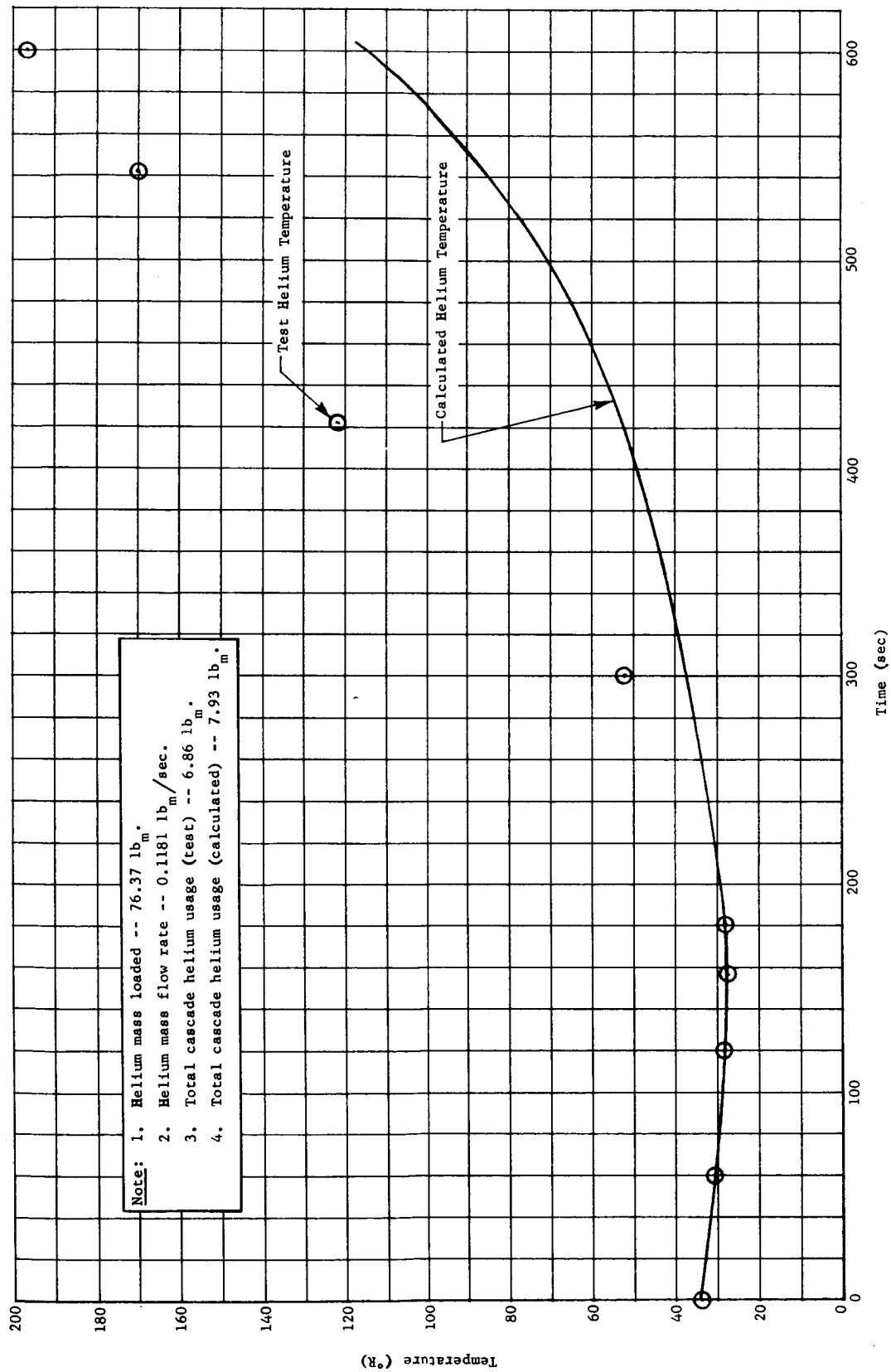


Fig. 70b Primary Storage Container Posttest Analysis, 90-Day Mission Abort, Test Run 2

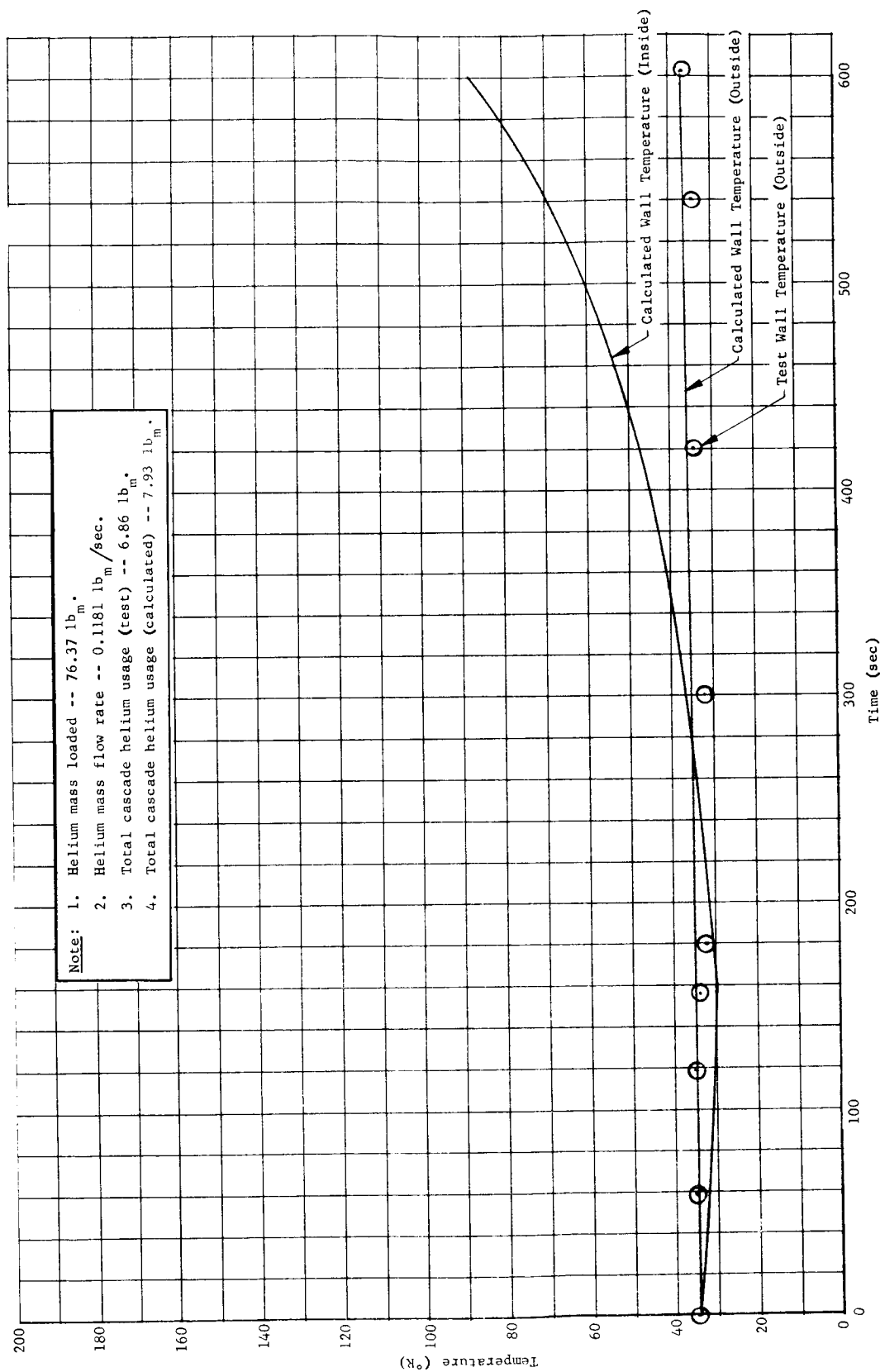


Fig. 70c Primary Storage Container Posttest Analysis, 90-Day Mission Abort, Test Run 2

Martin-CR-66-44

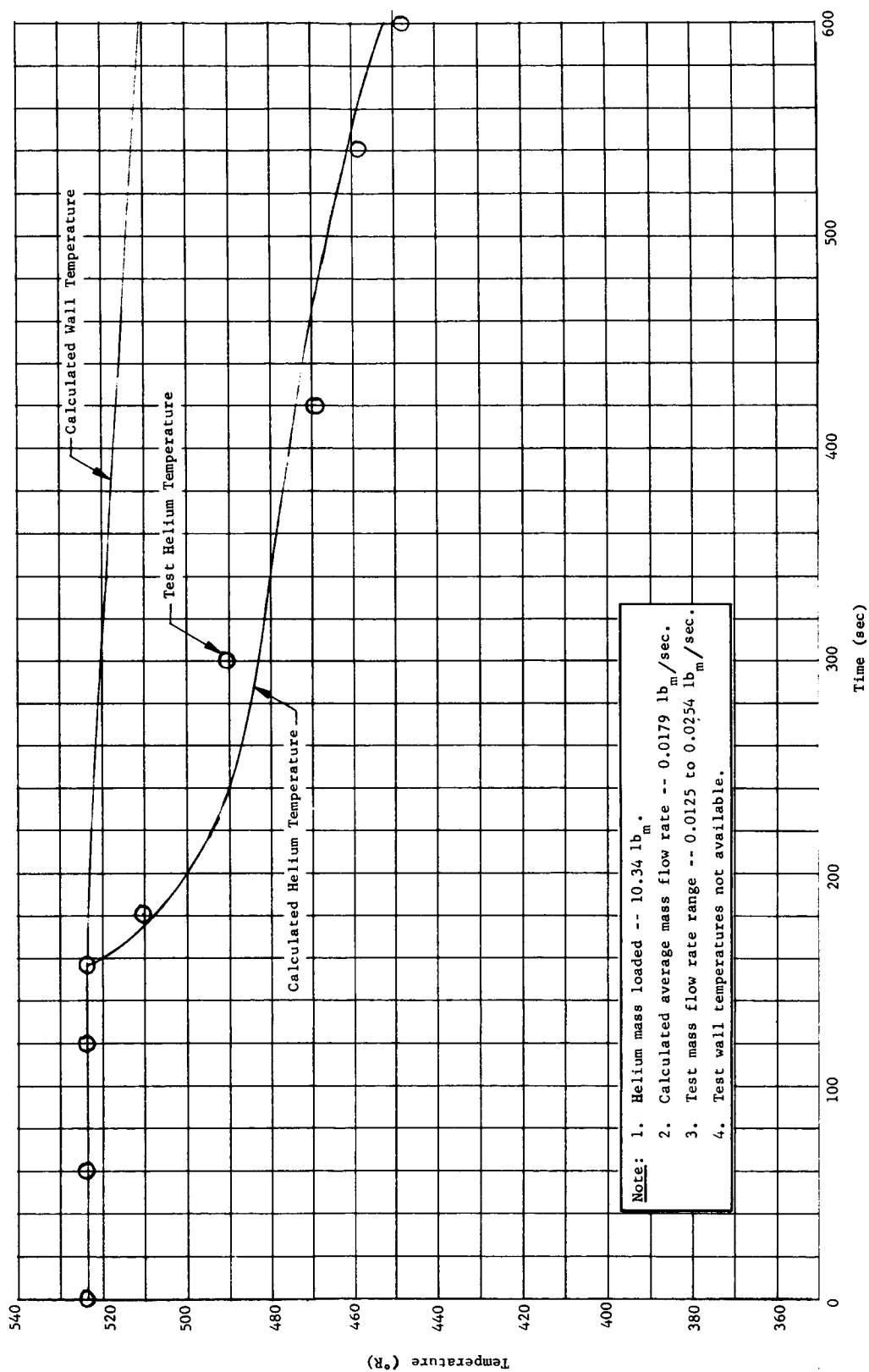


Fig. 71a Cascade Storage Container Posttest Analysis, 90-Day Mission Abort, Test Run 2

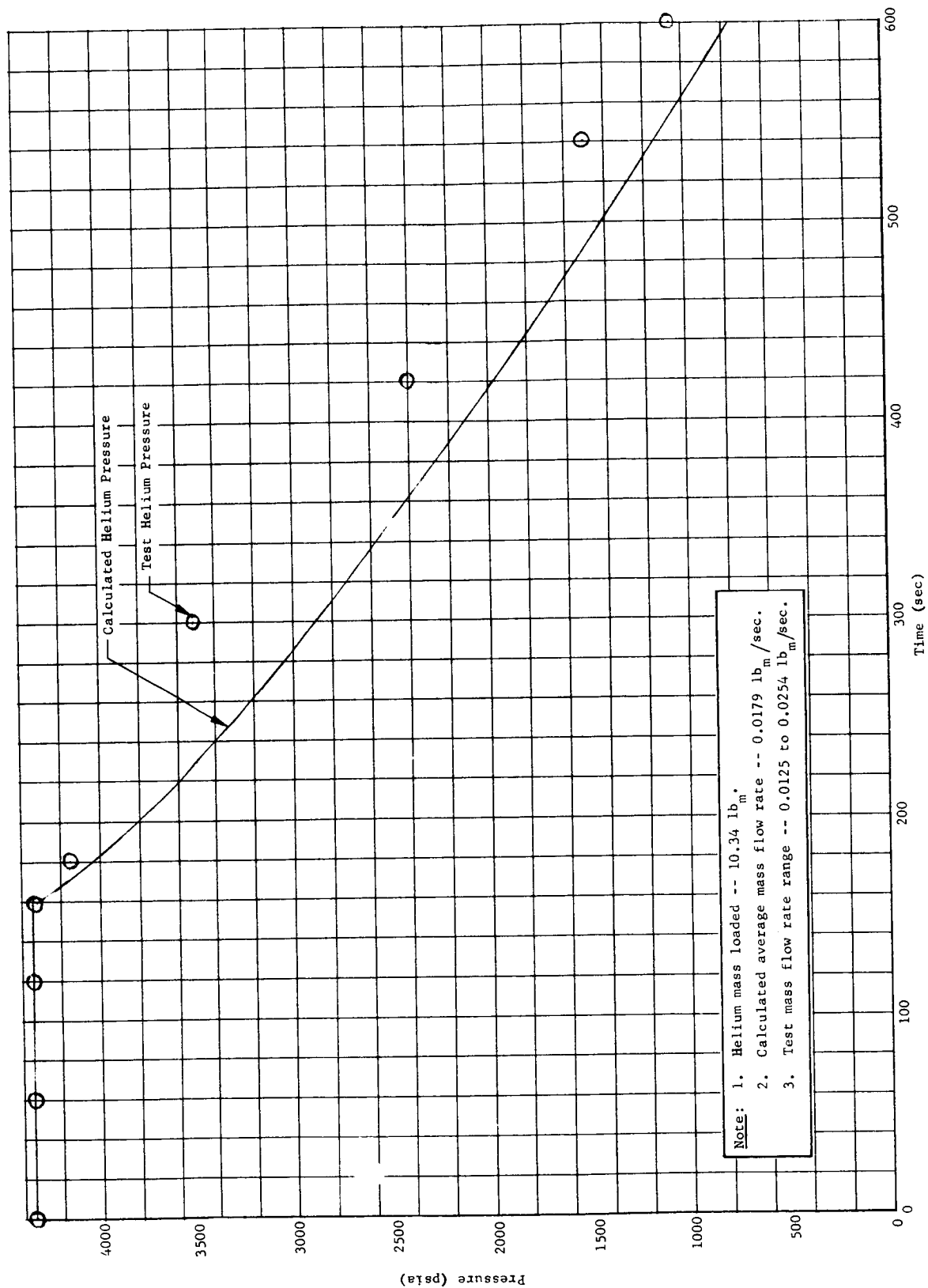


Fig. 71b Cascade Storage Container Posttest Analysis, 90-Day Mission Abort, Test Run 2

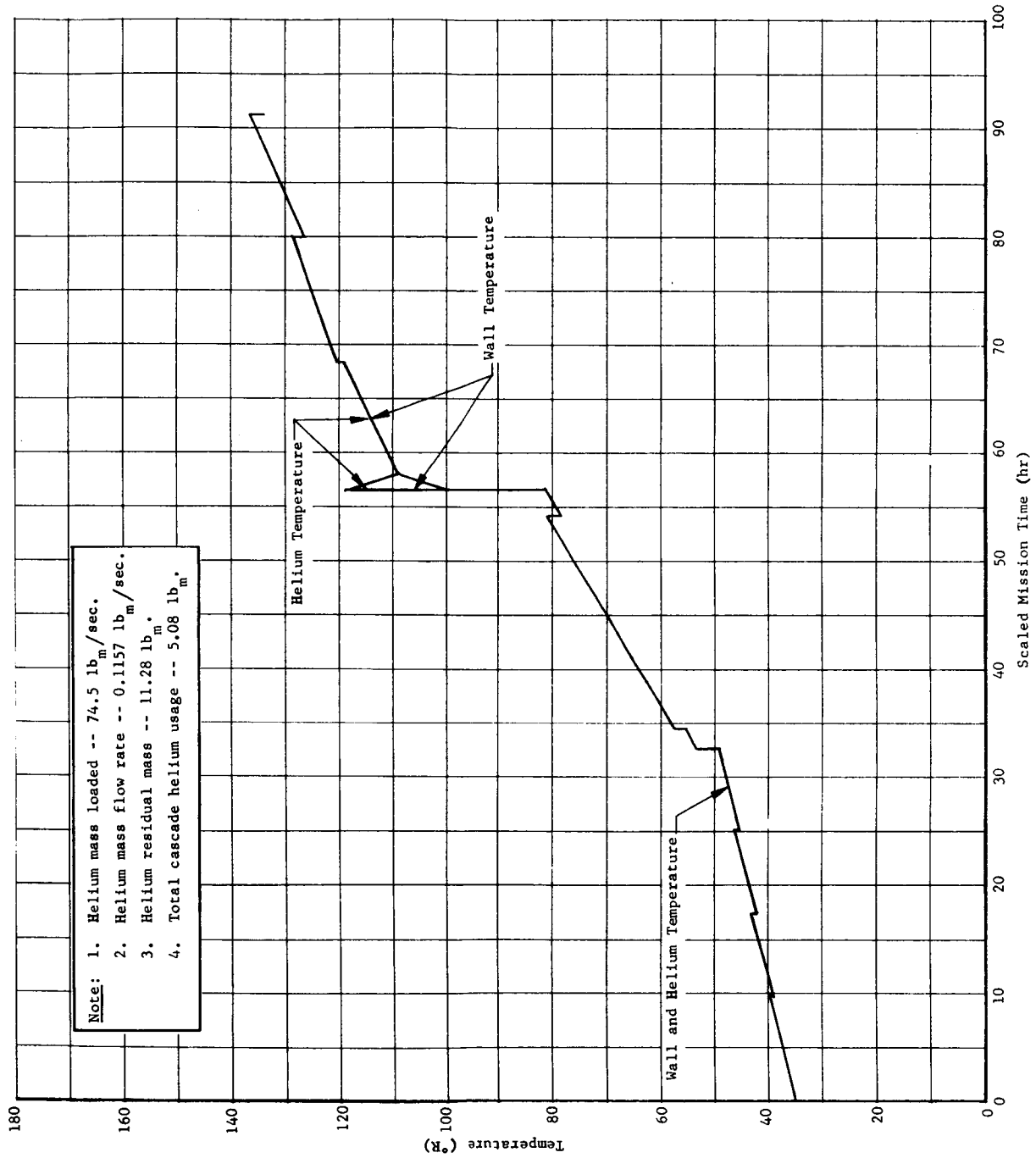


Fig. 72a Primary Storage Container Pretest Analysis, Nine-Day Mission

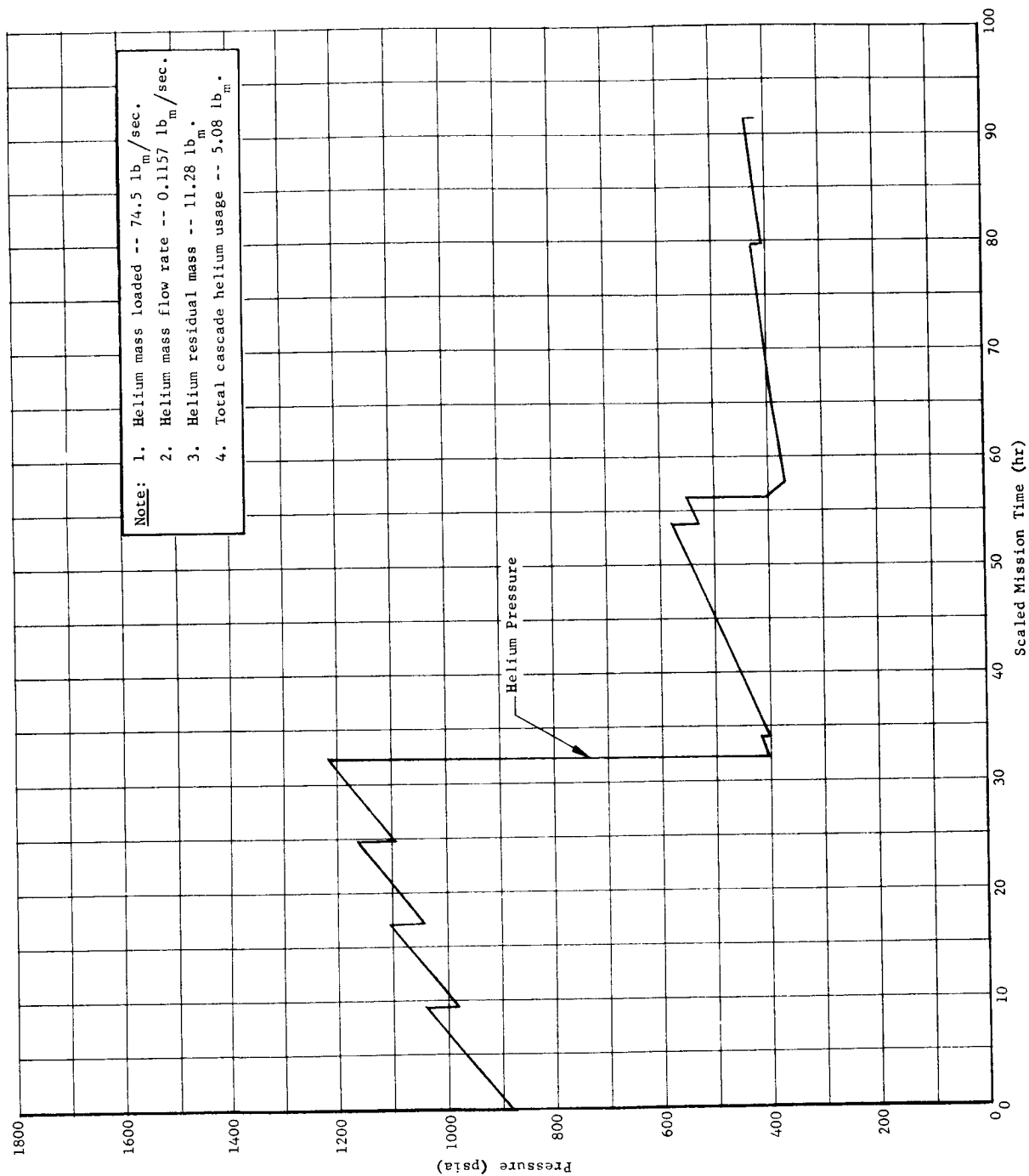


Fig. 72b Primary Storage Container Pretest Analysis, Nine-Day Mission

Martin-CR-66-44

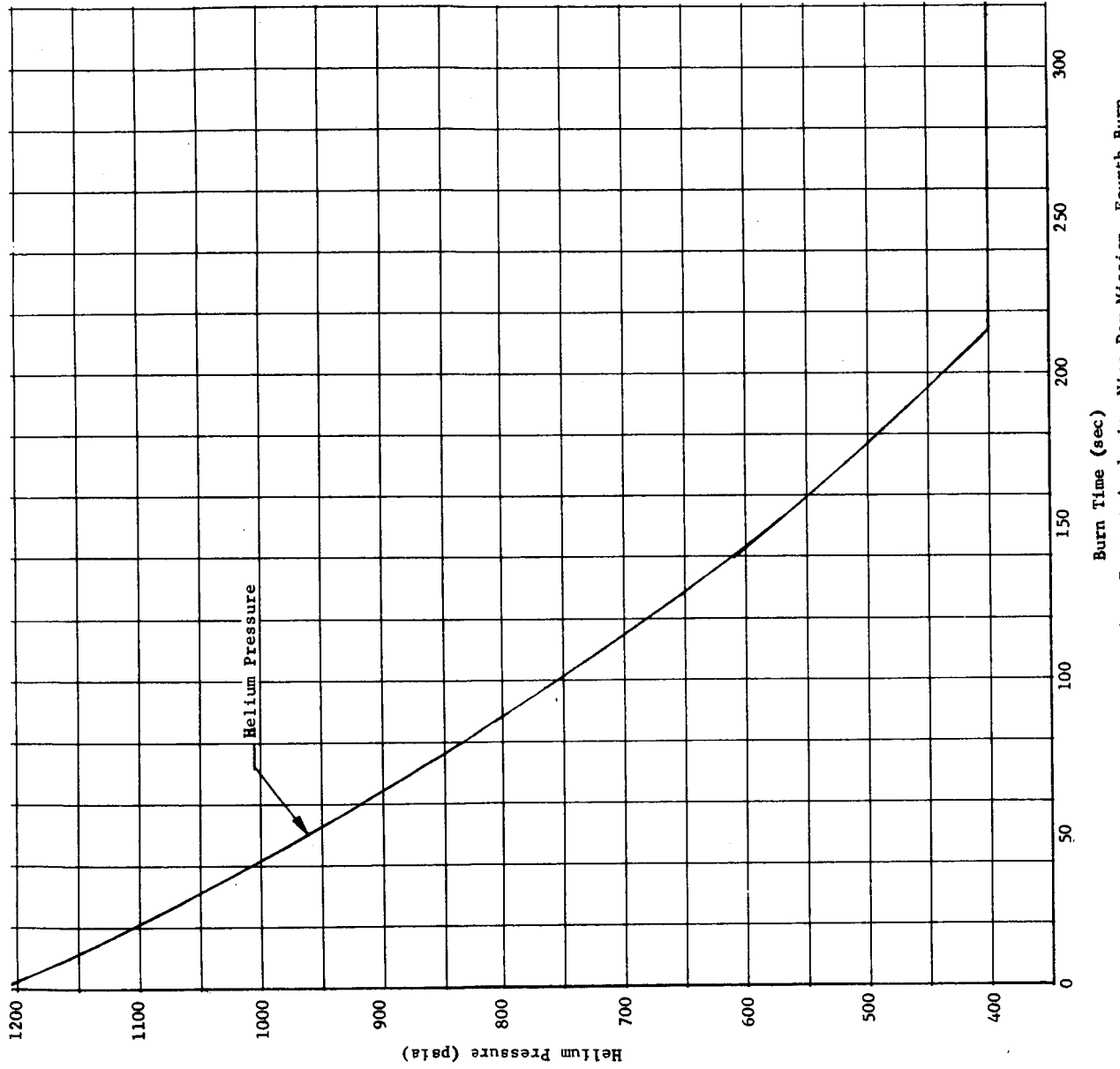


Fig. 73a Primary Storage Container Pretest Analysis, Nine-Day Mission, Fourth Burn

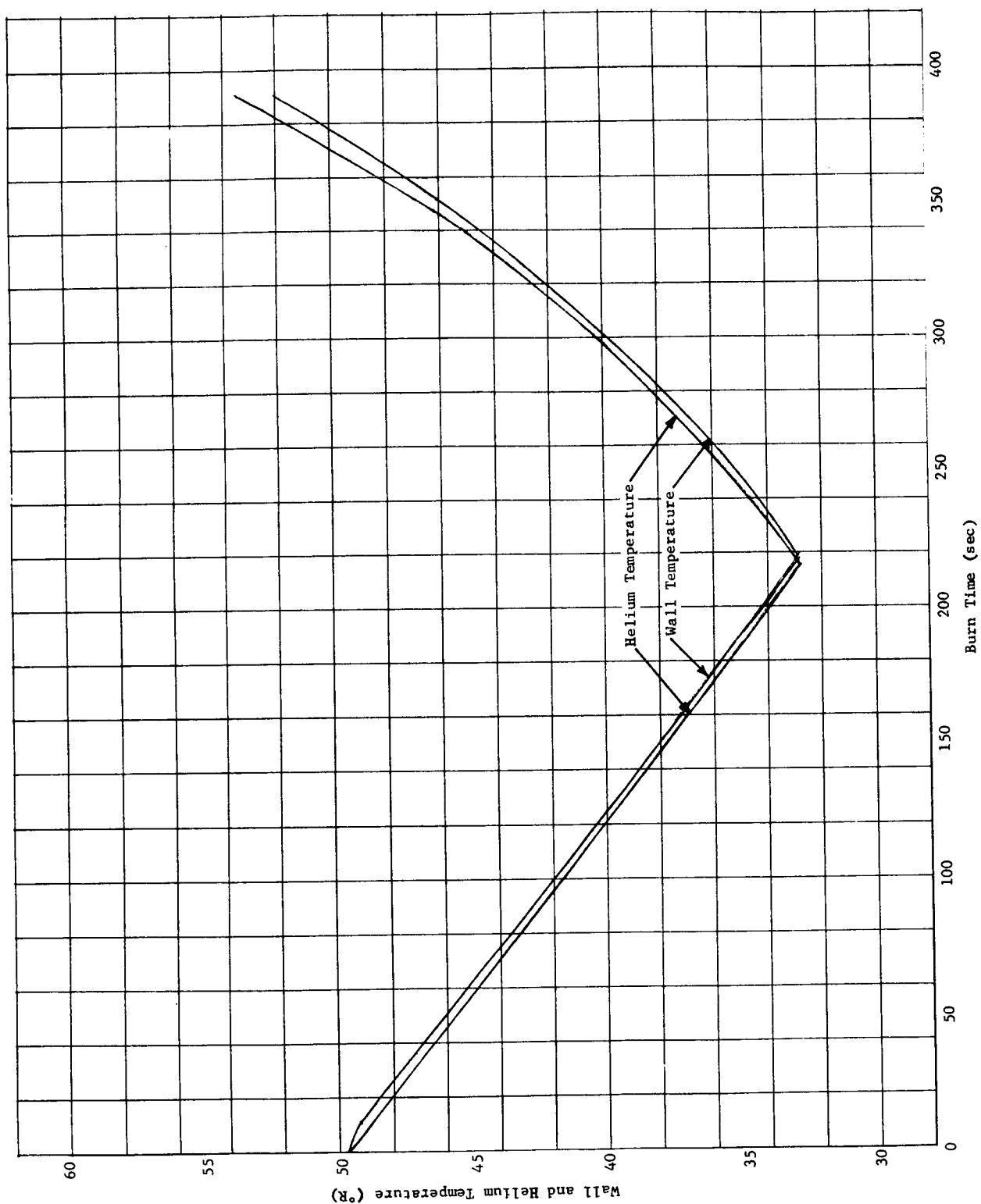


Fig. 73b Primary Storage Container Pretest Analysis, Nine-Day Mission, Fourth Burn

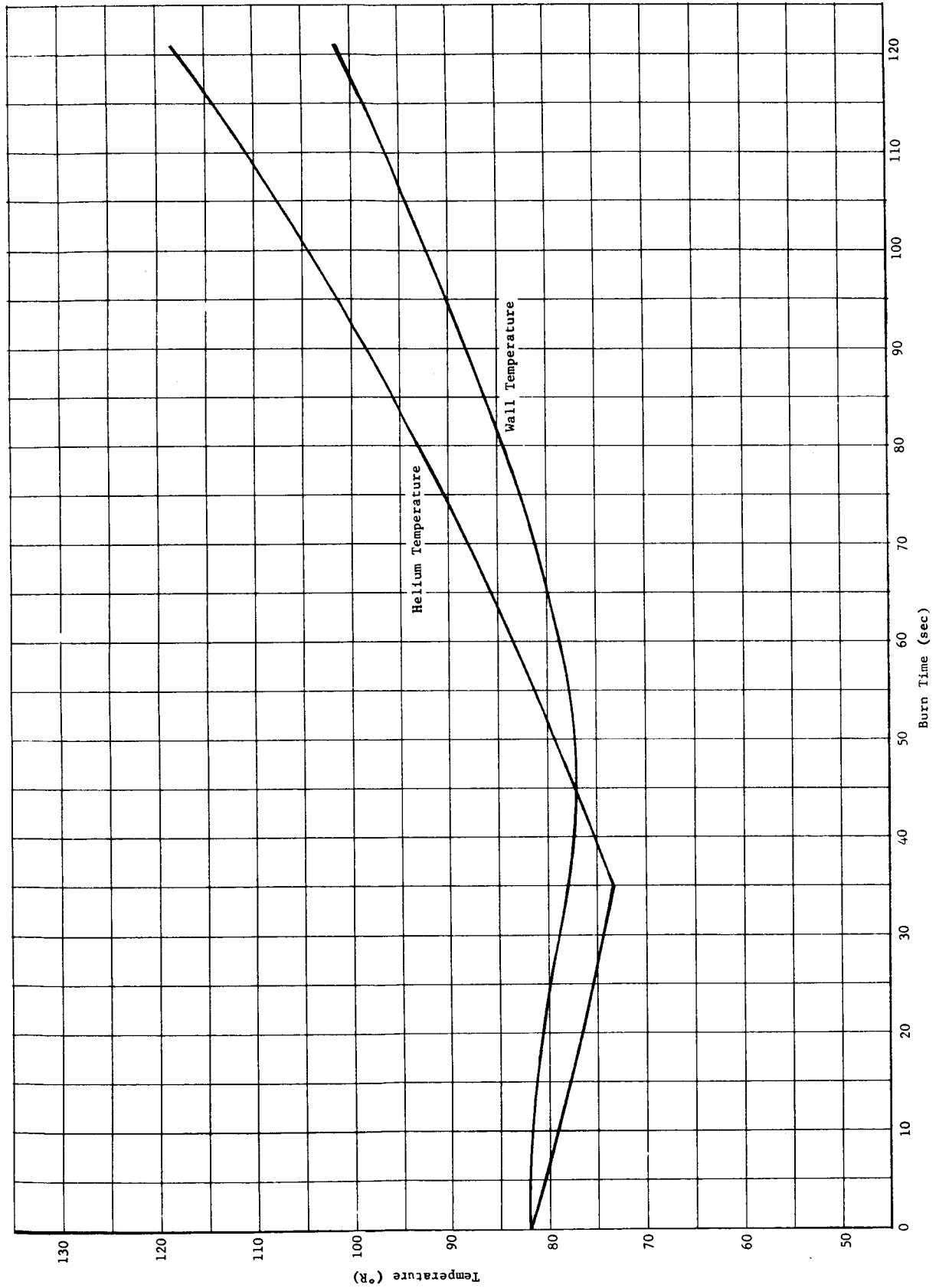


Fig. 74a Primary Storage Container Pretest Analysis, Nine-Day Mission, Seventh Burn

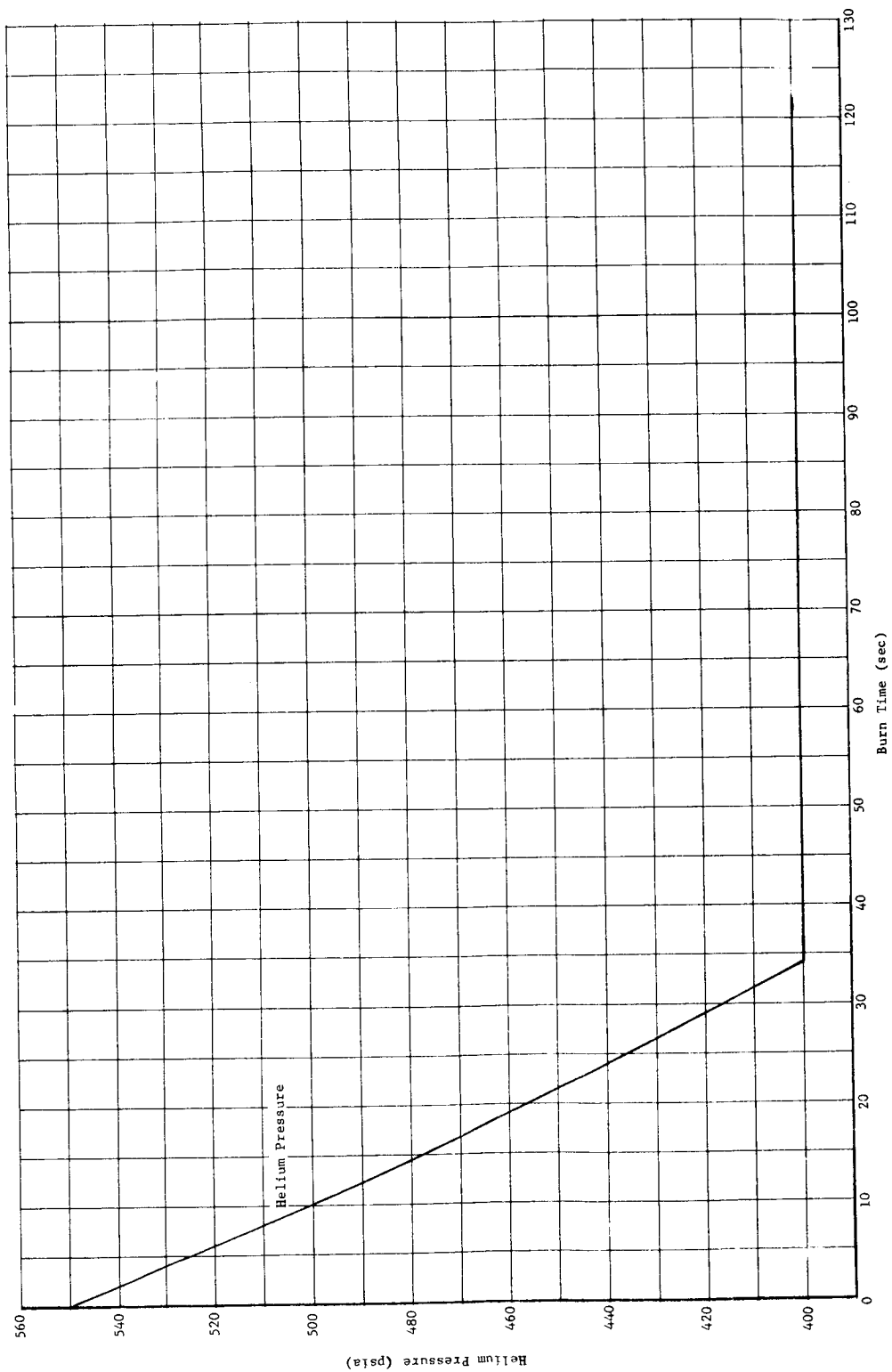


Fig. 74b Primary Storage Container Pretest Analysis, Nine-Day Mission, Seventh Burn

Martin-CR-66-44

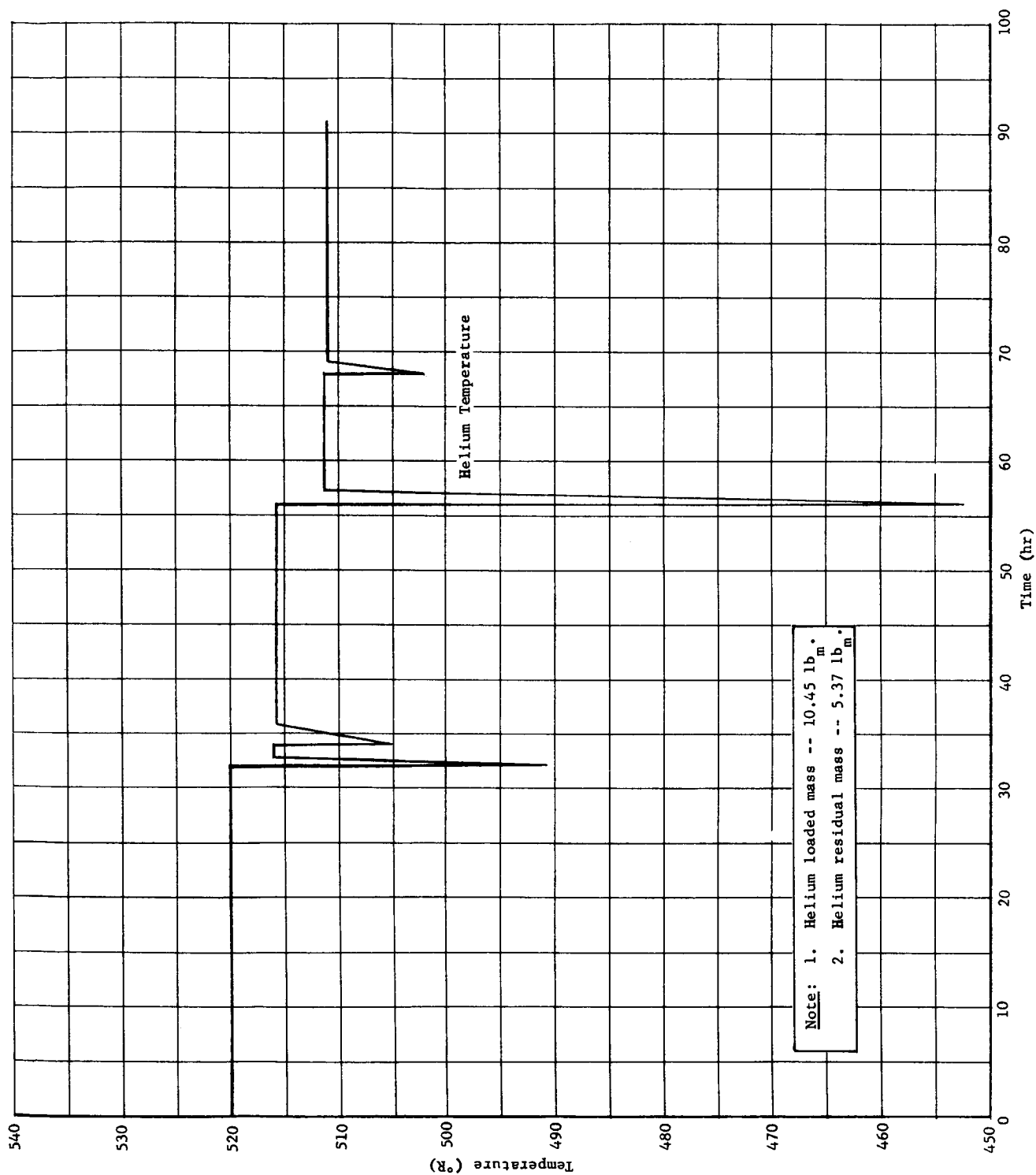


Fig. 75a Cascade Storage Container Pretest Analysis, Nine-Day Mission

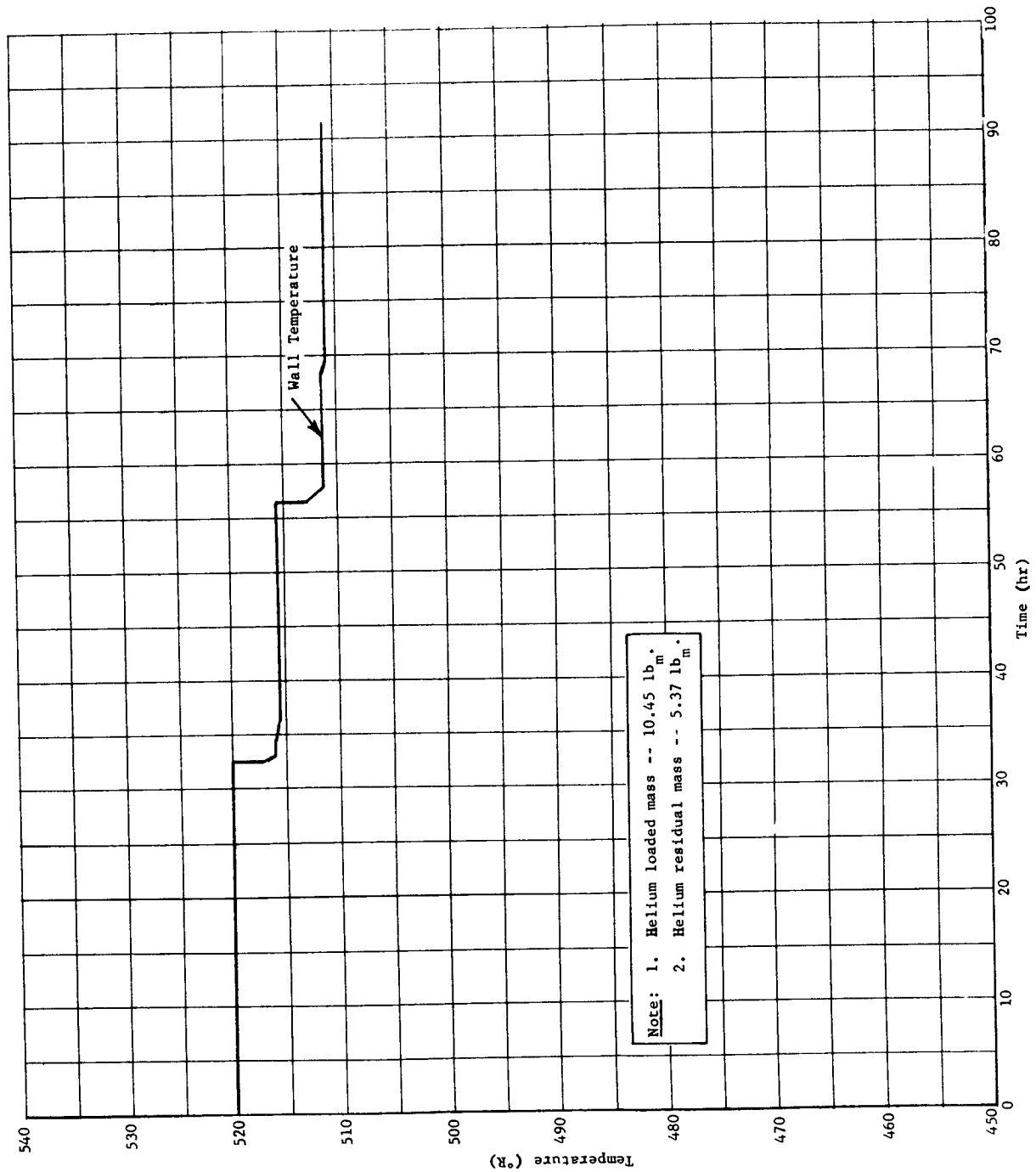


Fig. 75b Cascade Storage Container Pretest Analysis, Nine-Day Mission

Martin-CR-66-44

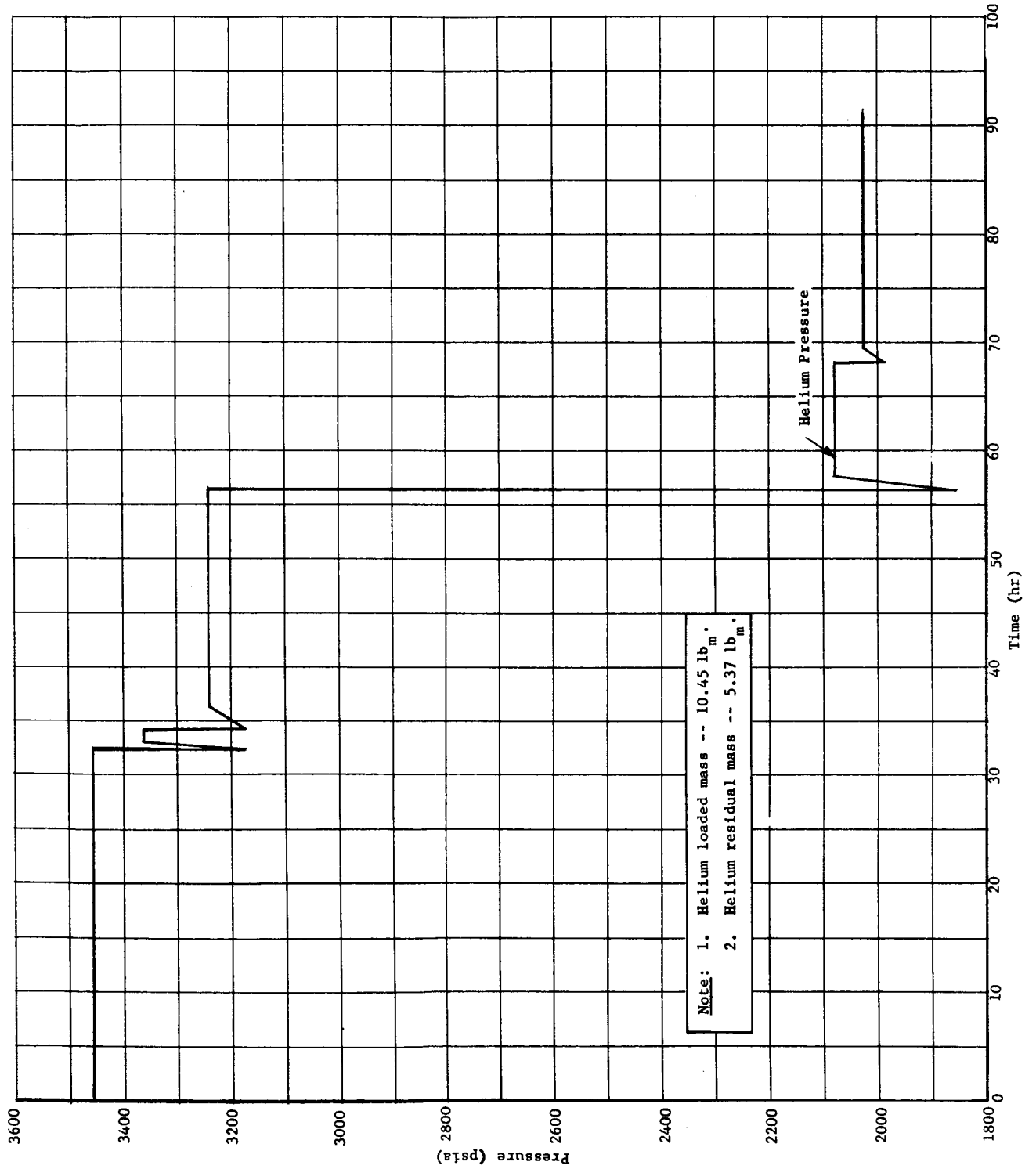


Fig. 75c Cascade Storage Container Pretest Analysis, Nine-Day Mission

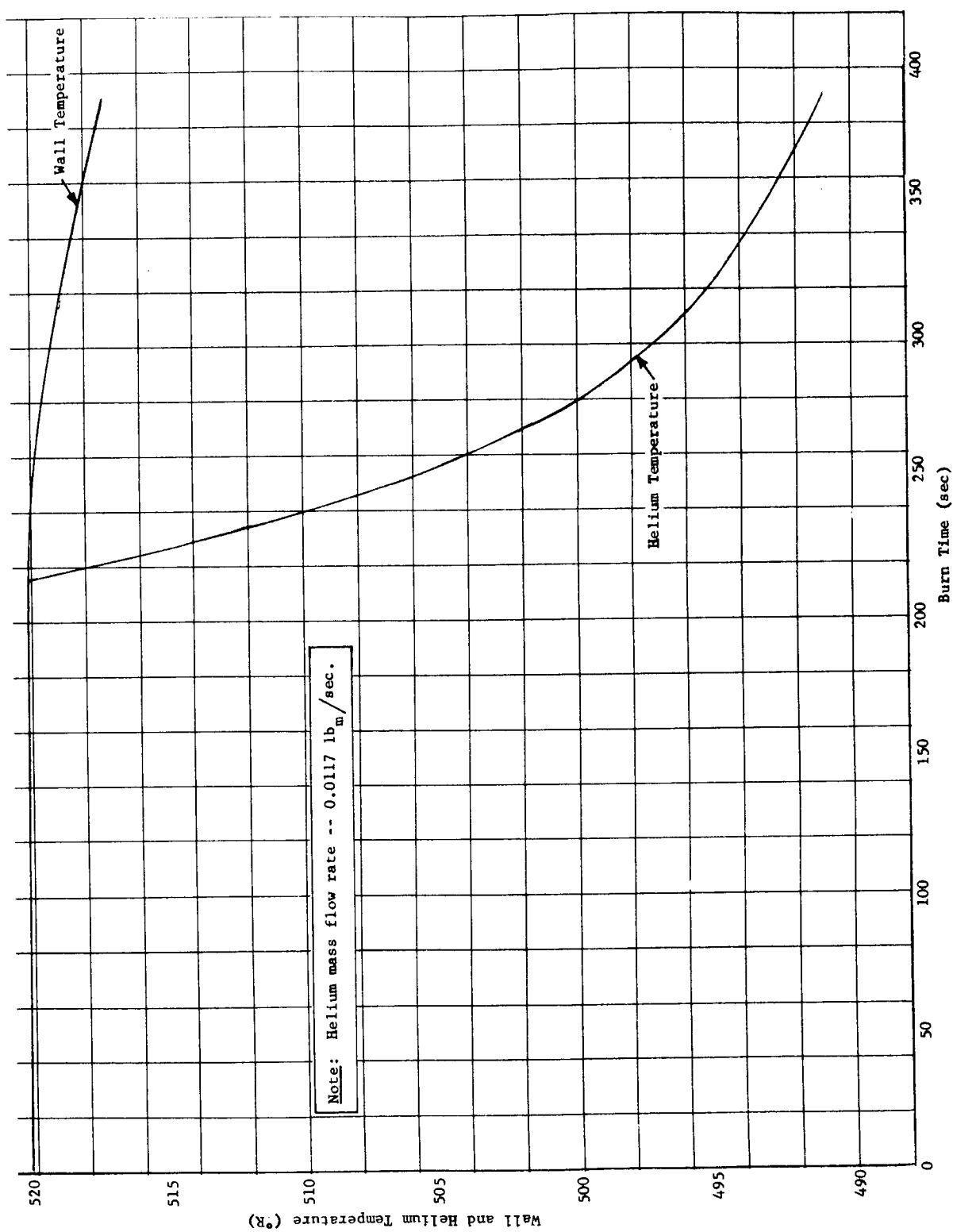


Fig. 76a Cascade Storage Container Pretest Analysis, Nine-Day Mission, Fourth Burn

Martin-CR-66-44

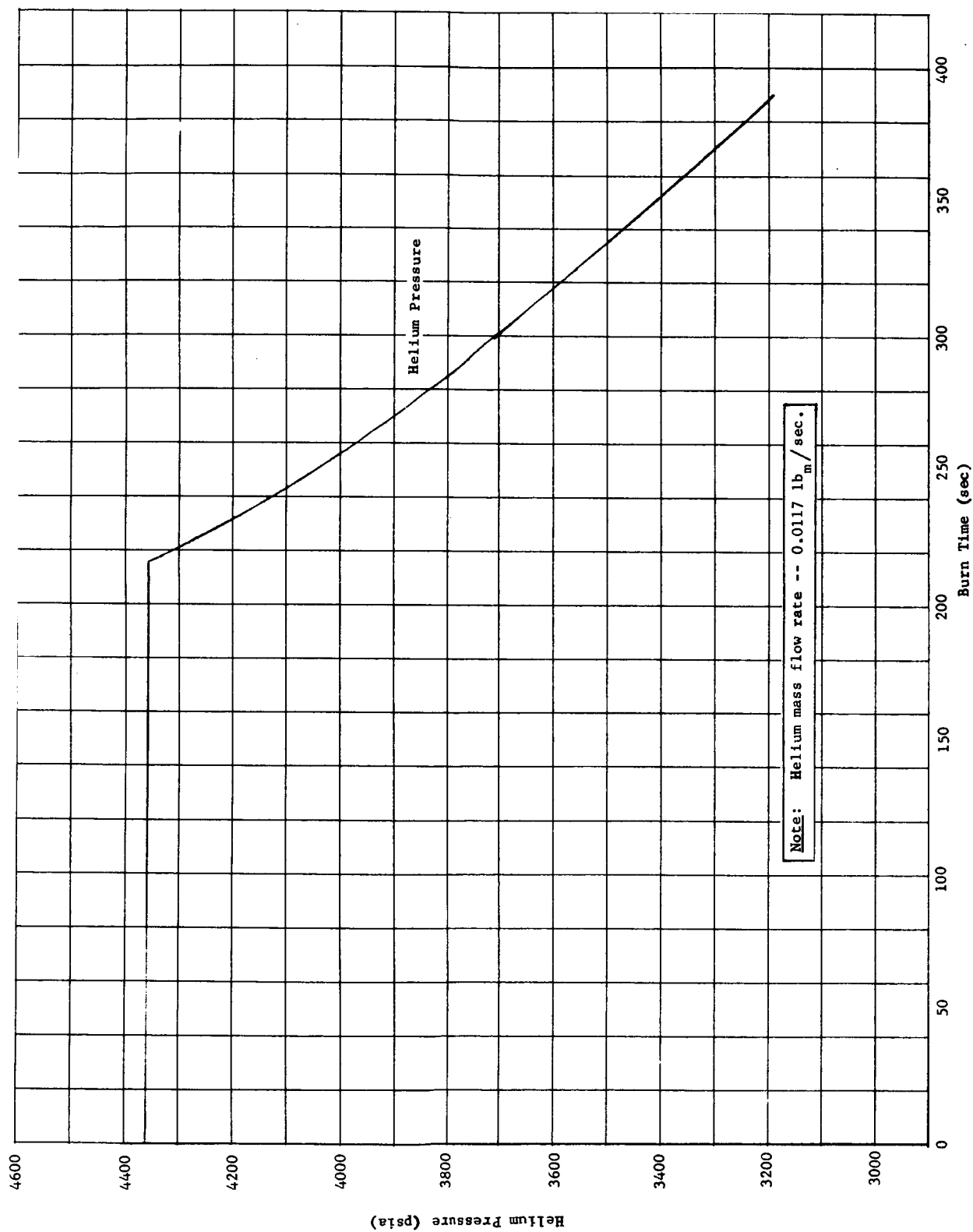


Fig. 76b Cascade Storage Container Pretest Analysis, Nine-Day Mission, Fourth Burn

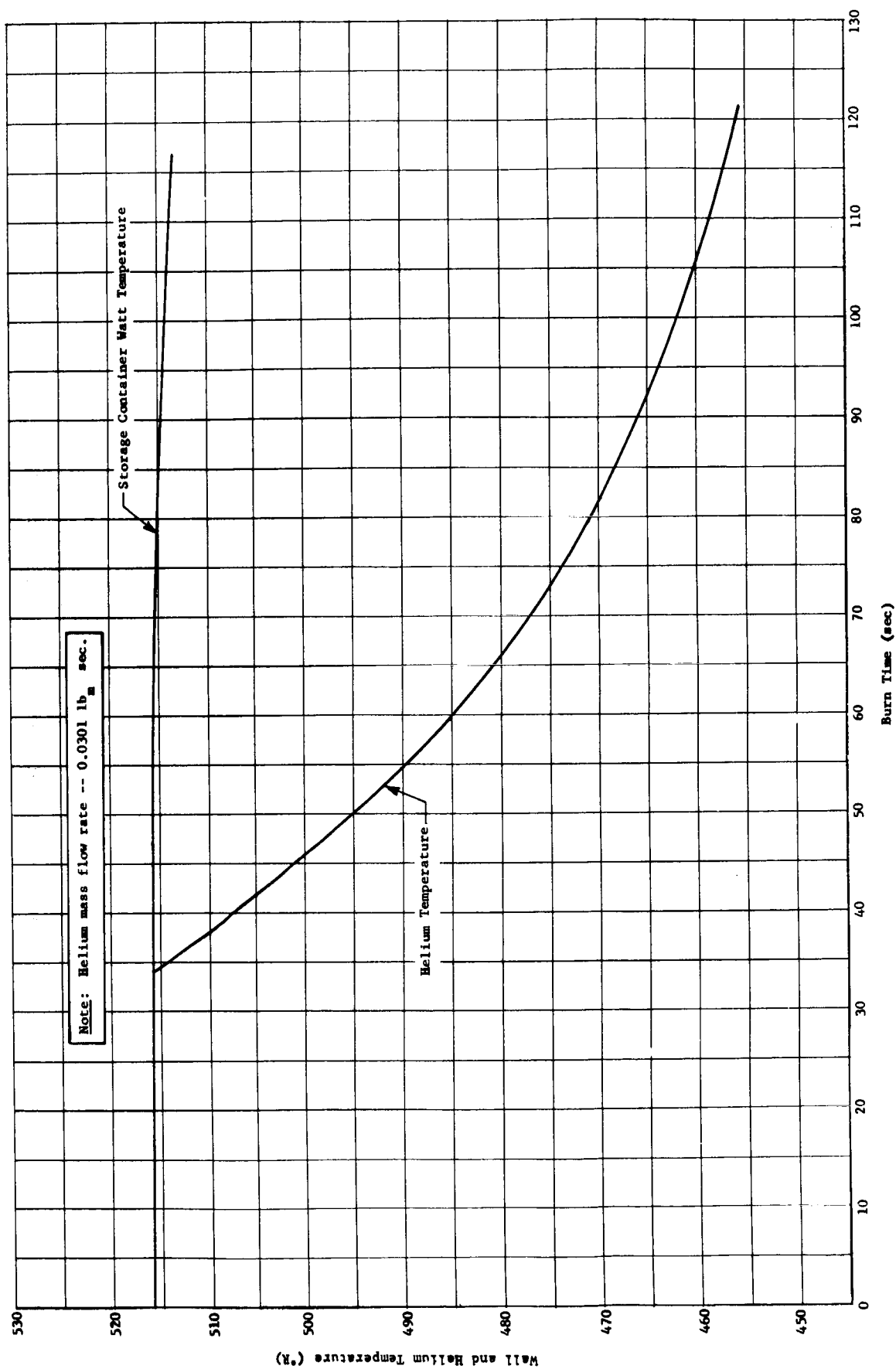


Fig. 77a Cascade Storage Container Pretest Analysis, Nine-Day Mission, Seventh Burn

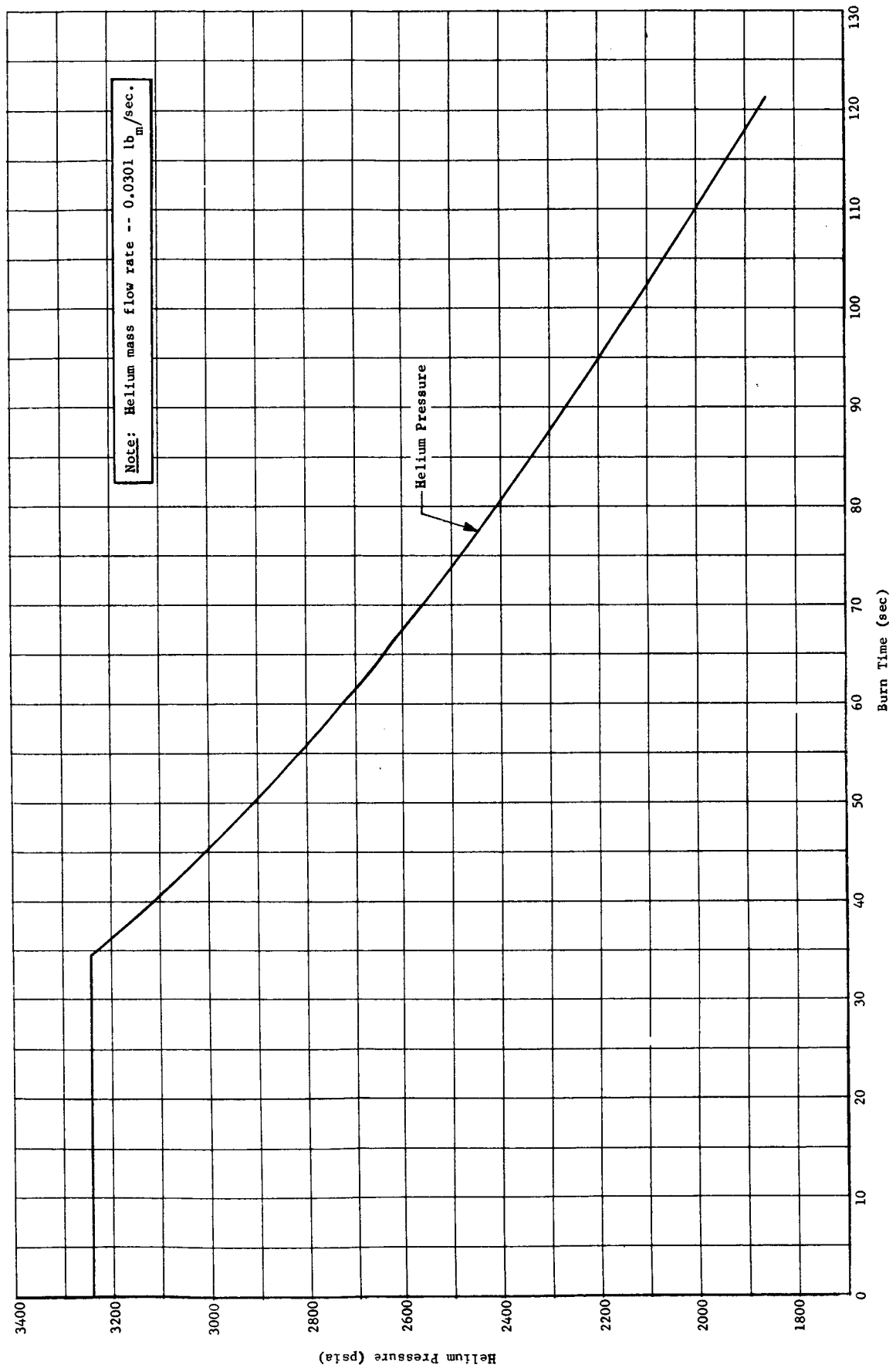


Fig. 77b Cascade Storage Container Pretest Analysis, Nine-Day Mission, Seventh Burn

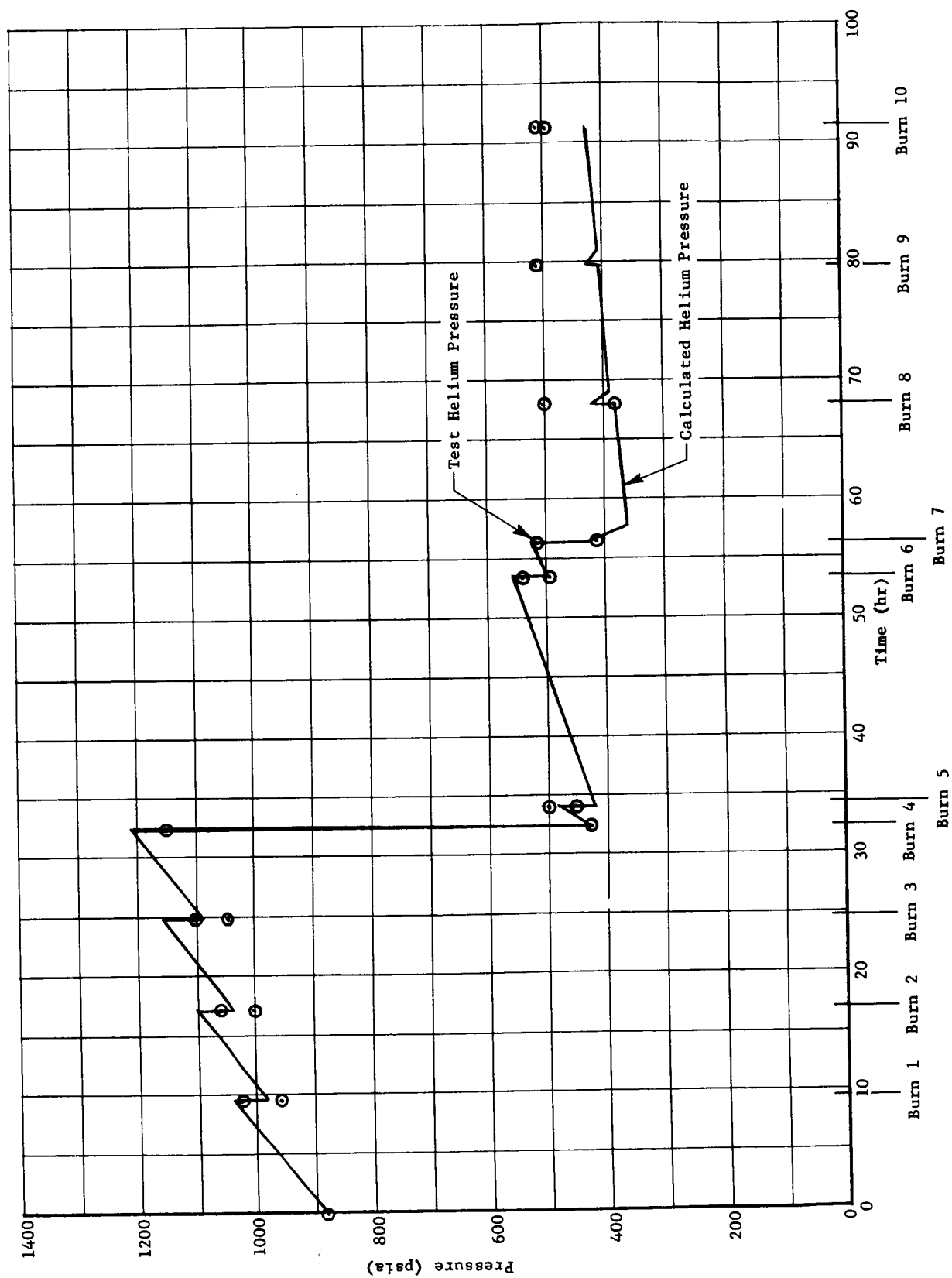


Fig. 78a Primary Container Posttest Analysis, Nine-Day Mission, Test Run 1 (Test Mission Profile)

Martin-CR-66-44

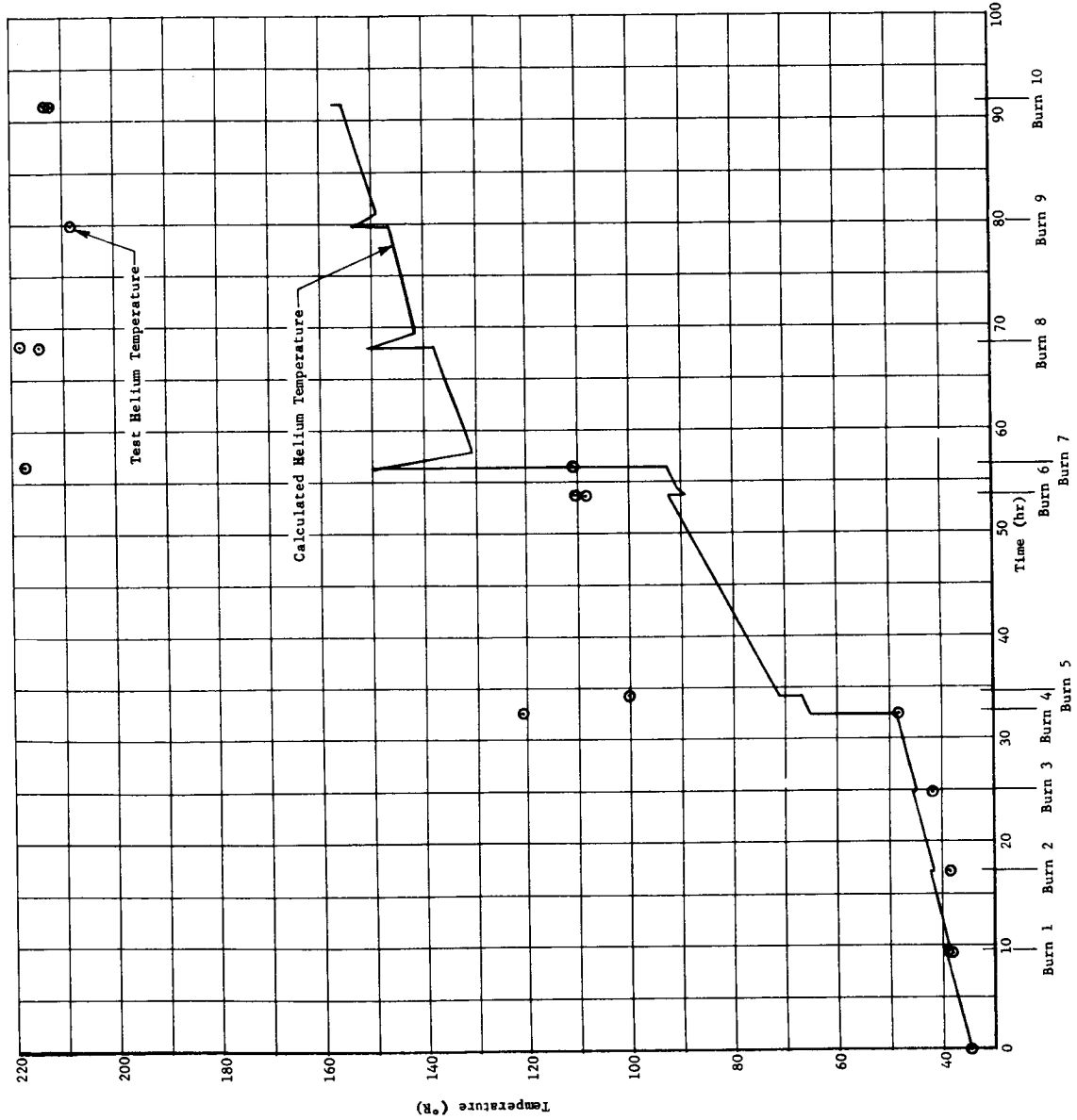


Fig. 78b Primary Container Posttest Analysis, Nine-Day Mission, Test Run 1 (Test Mission Profile)

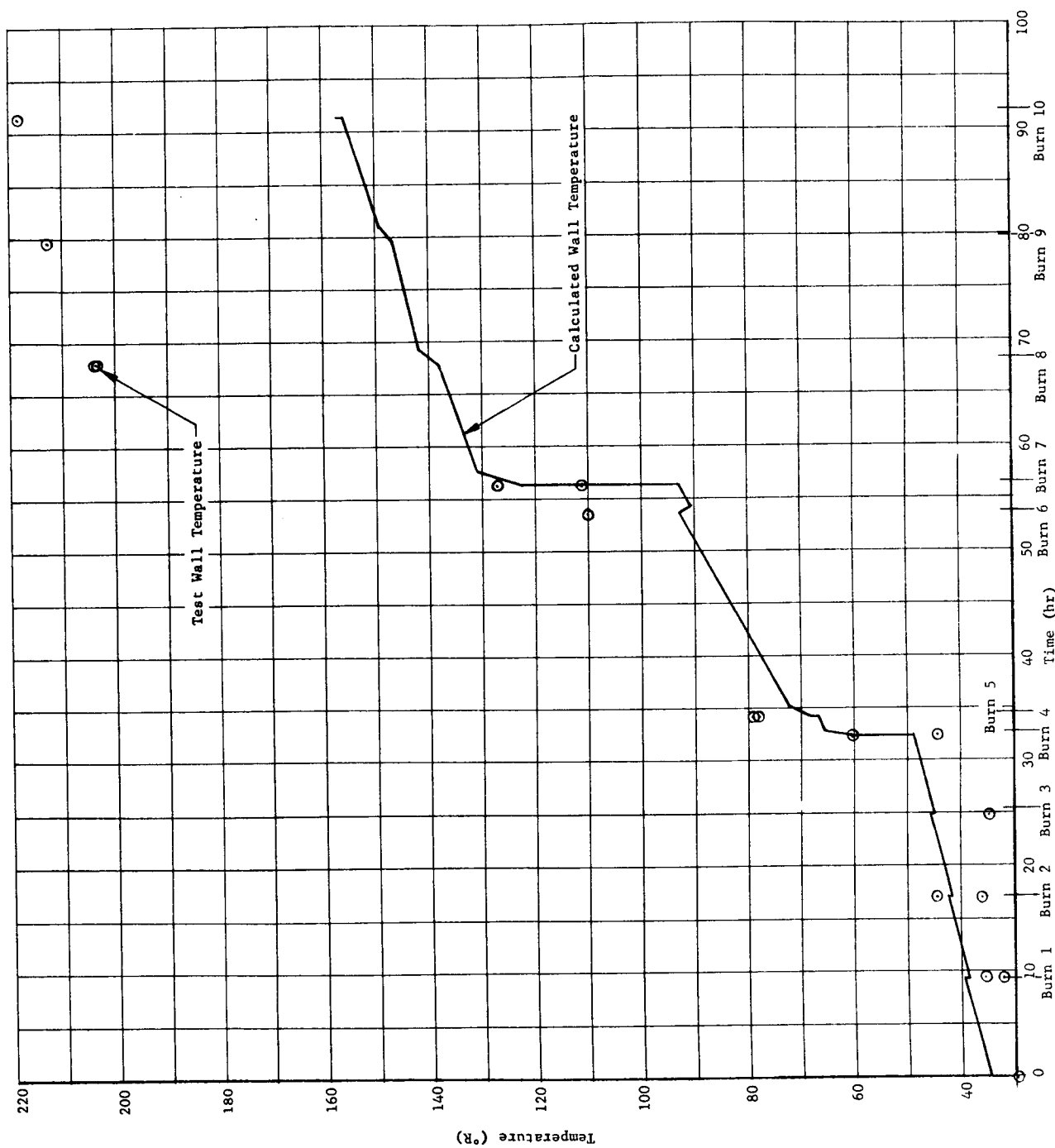


Fig. 78c Primary Container Posttest Analysis, Nine-Day Mission, Test Run 1 (Test Mission Profile)

Martin-CR-66-44

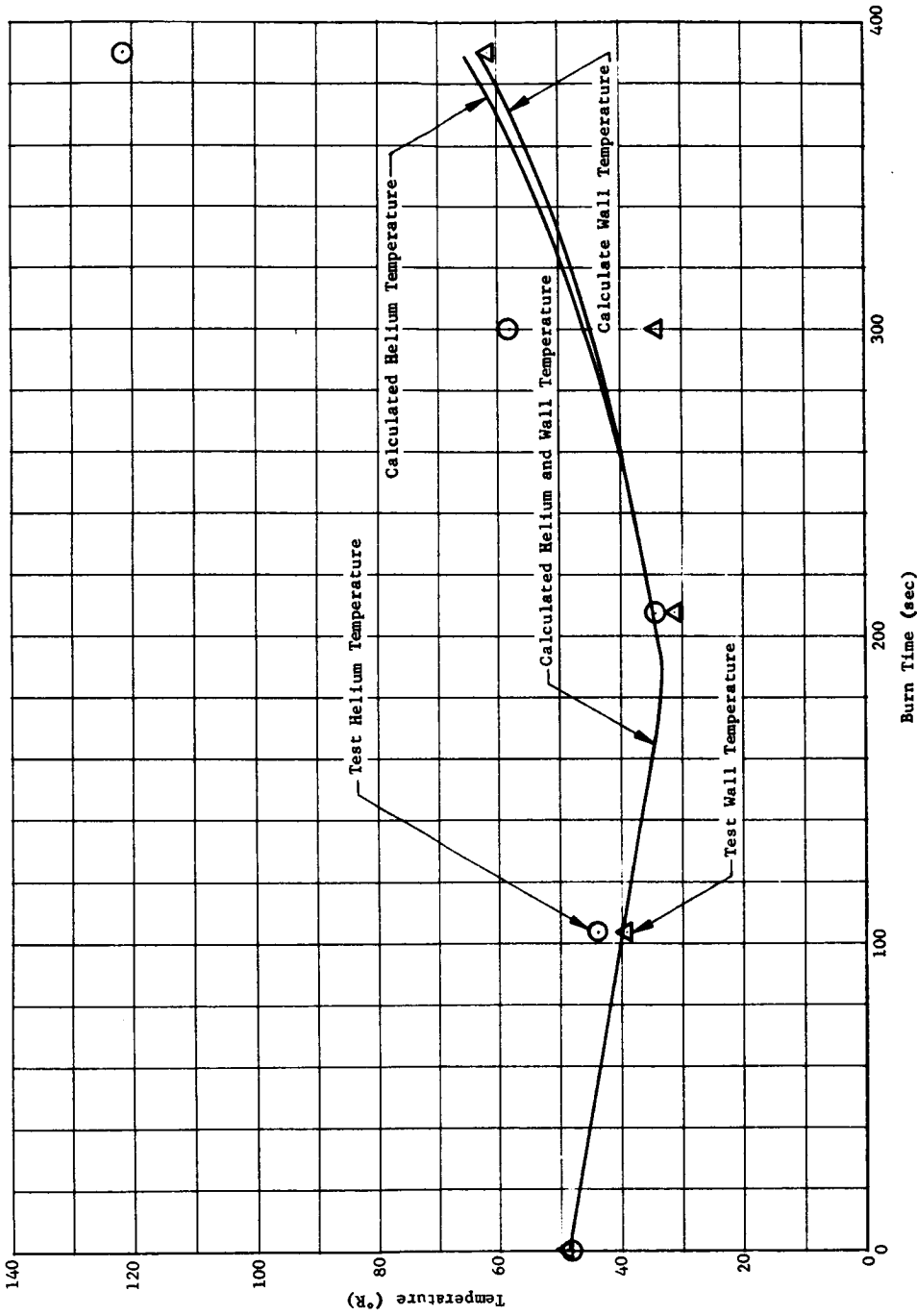


Fig. 79a Primary Container Posttest Analysis, Nine-Day Mission, Test Run 1, Burn 4

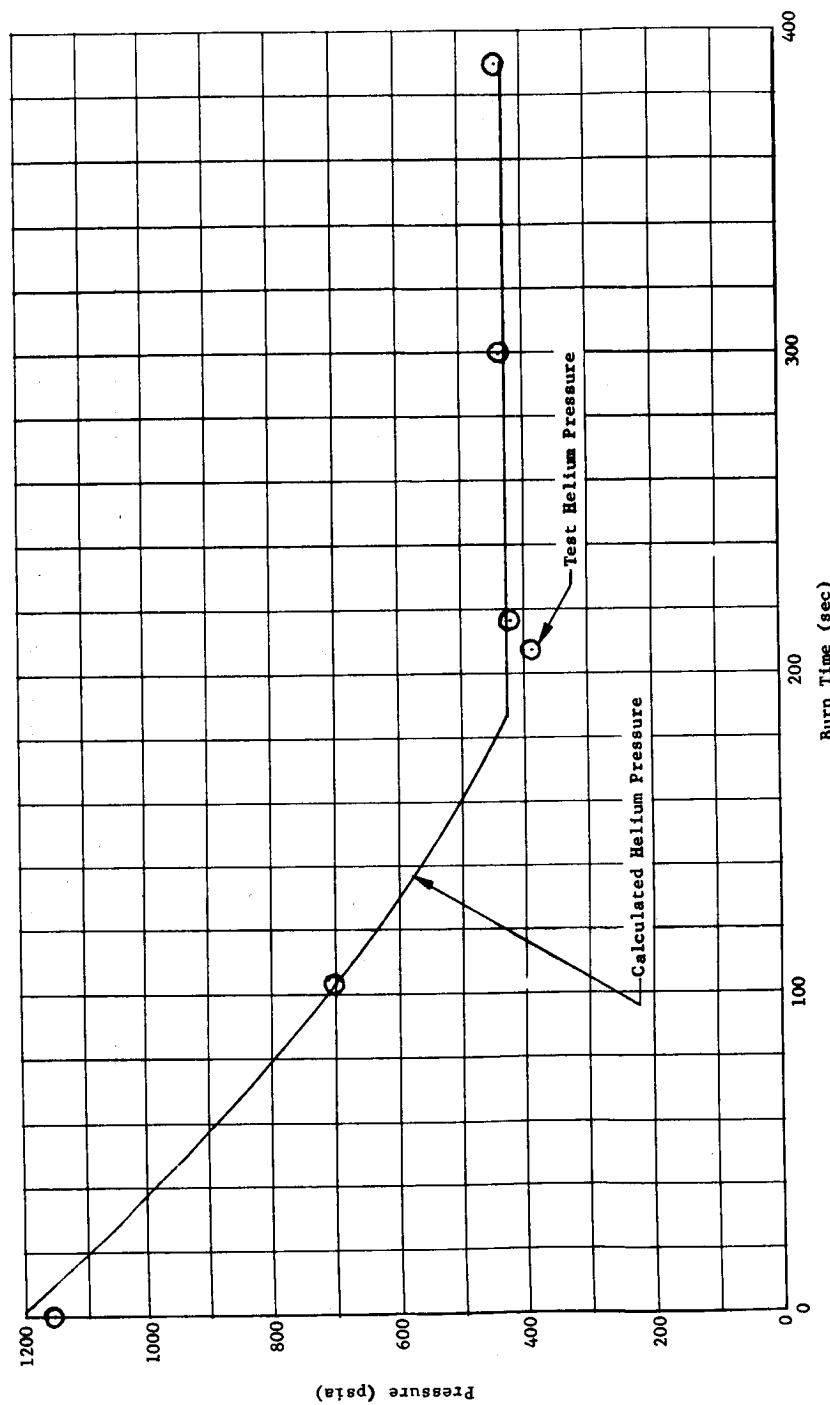


Fig. 79b Primary Container Posttest Analysis, Nine-Day Mission, Test Run 1, Burn 4

Martin-CR-66-44

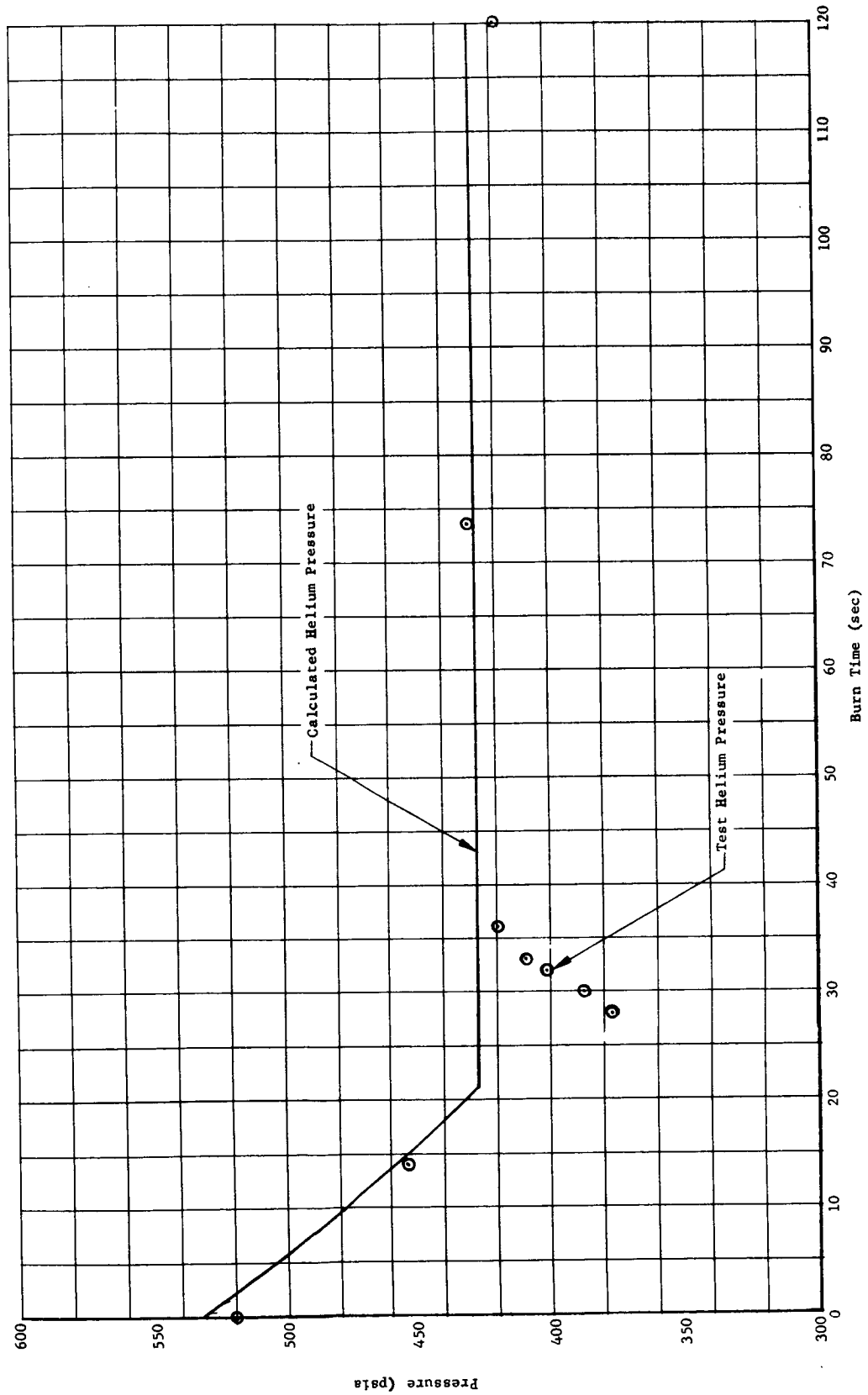


Fig. 80a Primary Container Posttest Analysis, Nine-Day Mission, Test Run 1, Burn 7

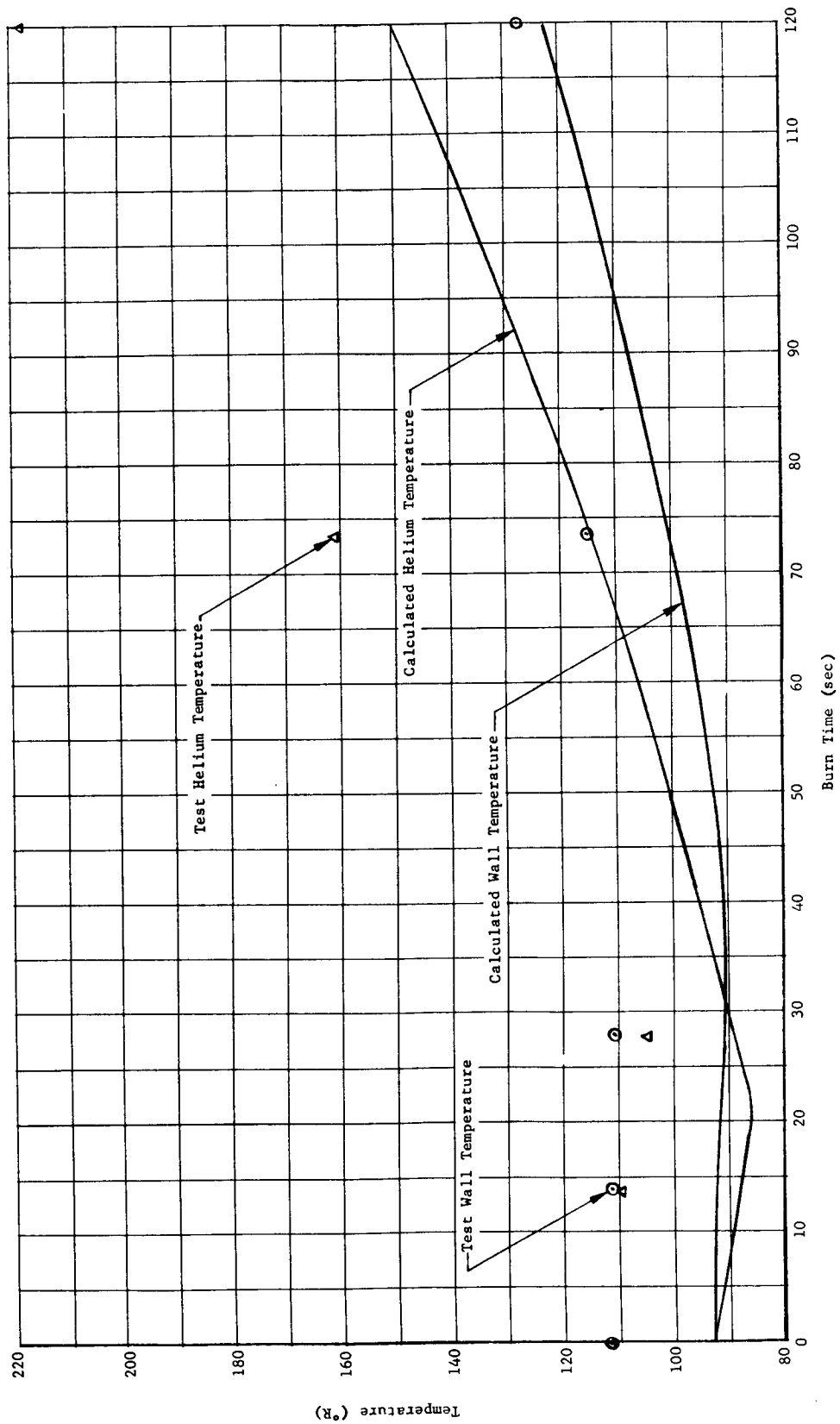


Fig. 80b Primary Container Posttest Analysis, Nine-Day Mission, Test Run 1, Burn 7

Martin-CR-66-44

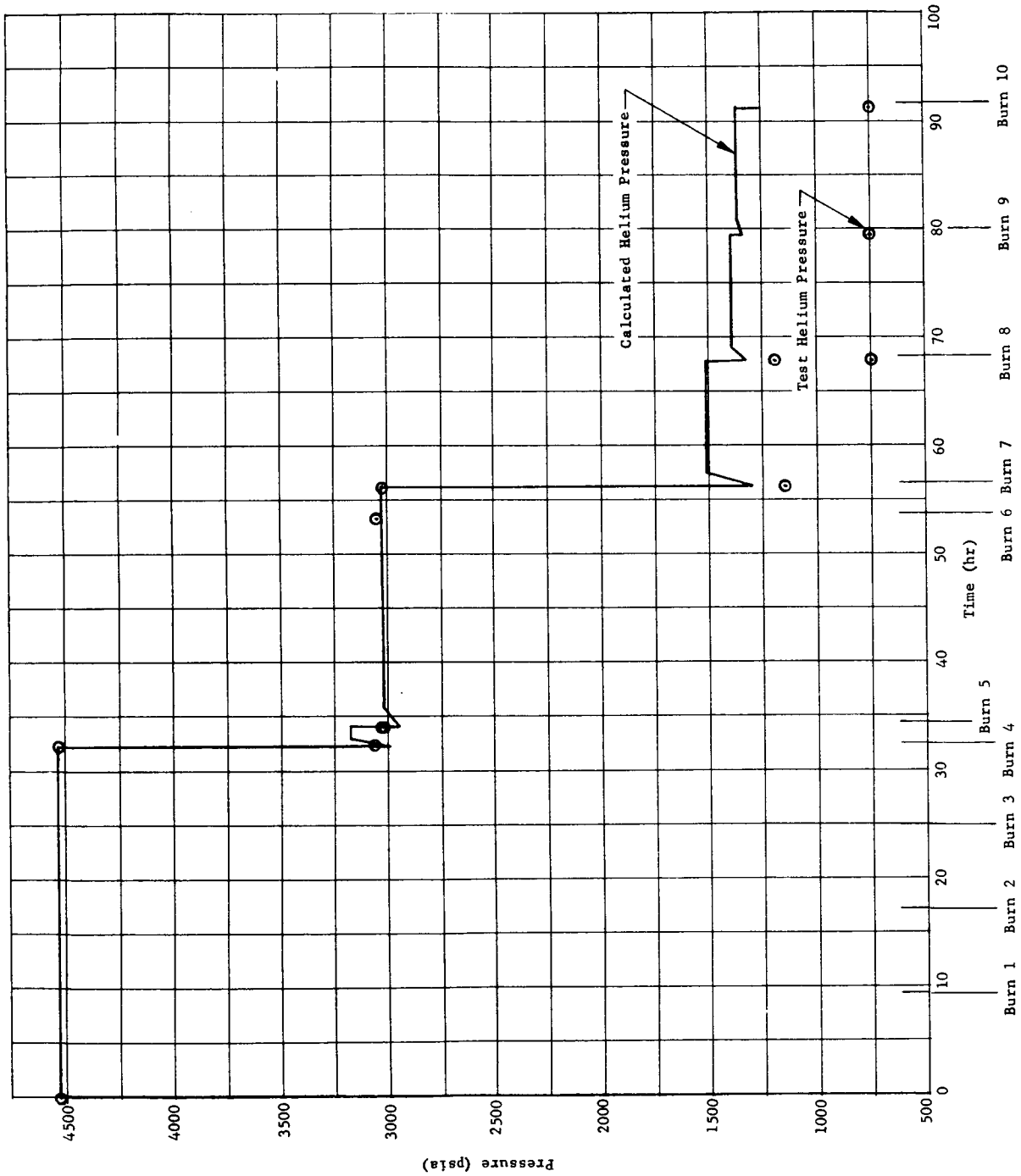


Fig. 81a Cascade Container Posttest Analysis, Nine-Day Mission, Test Run 1 (Test Mission Profile)

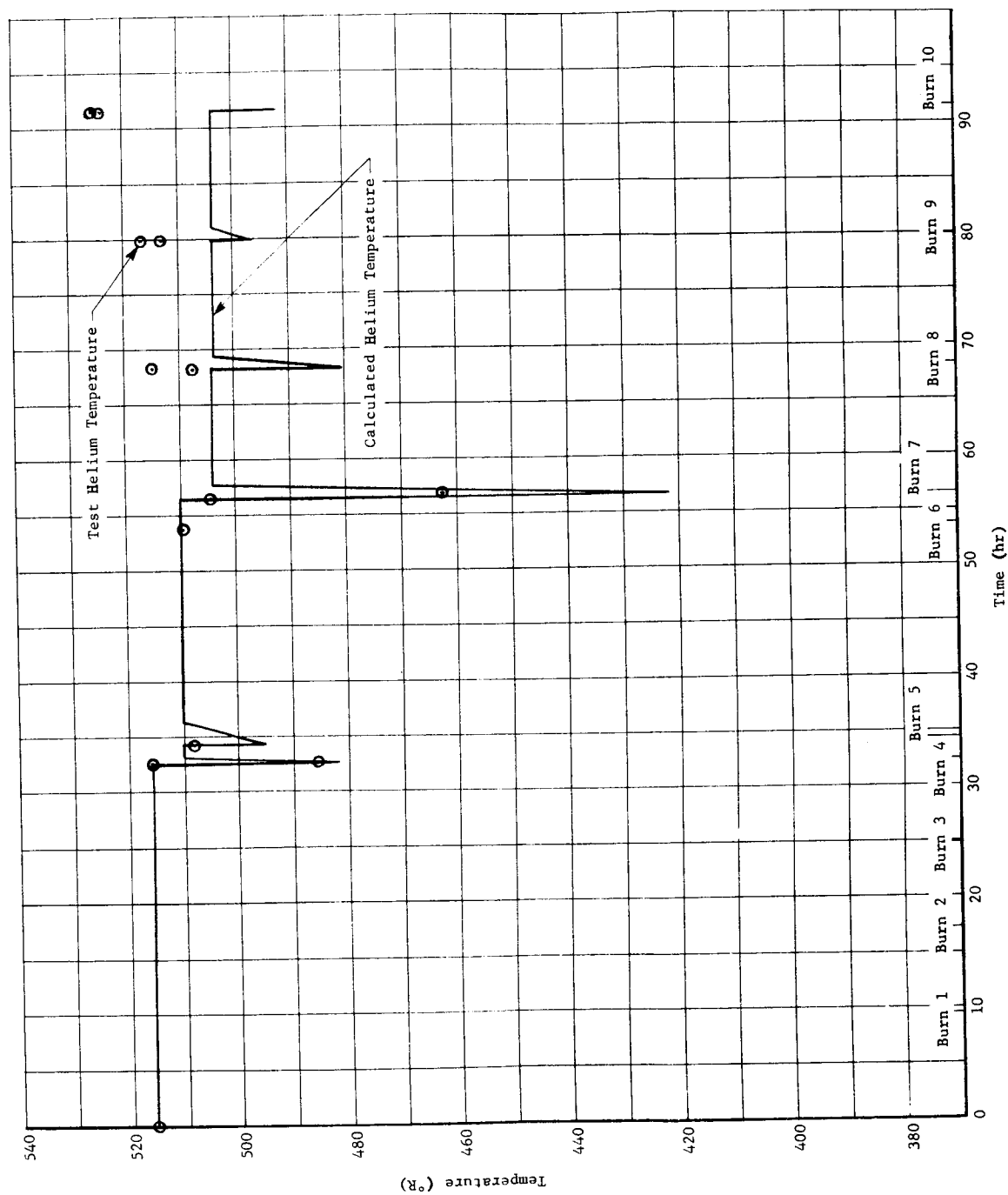


Fig. 8lb Cascade Container Posttest Analysis, Nine-Day Mission, Test Run 1 (Test Mission Profile)

Martin-CR-66-44

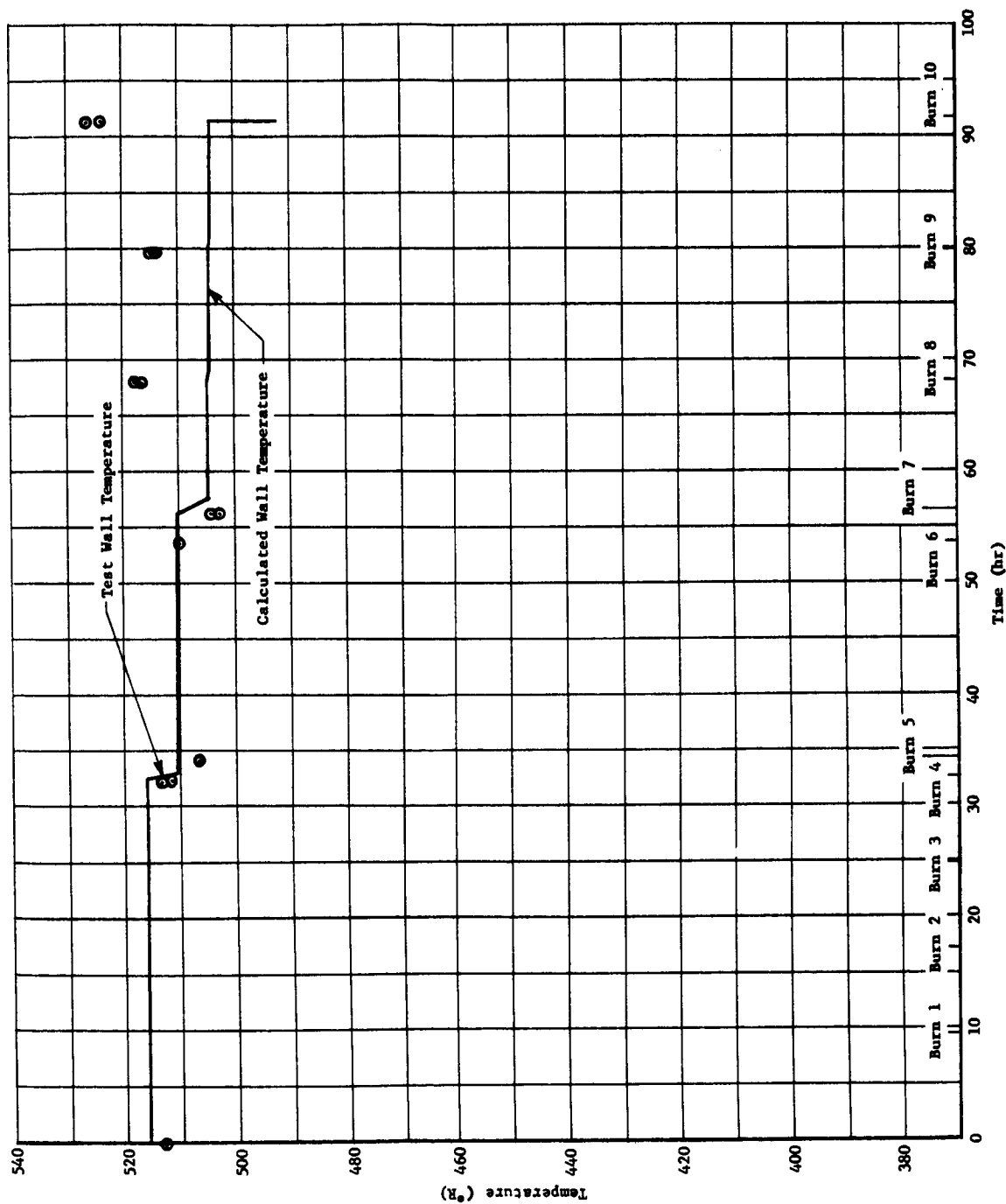


Fig. 81c Cascade Container Posttest Analysis, Nine-Day Mission, Test Run 1 (Test Mission Profile)

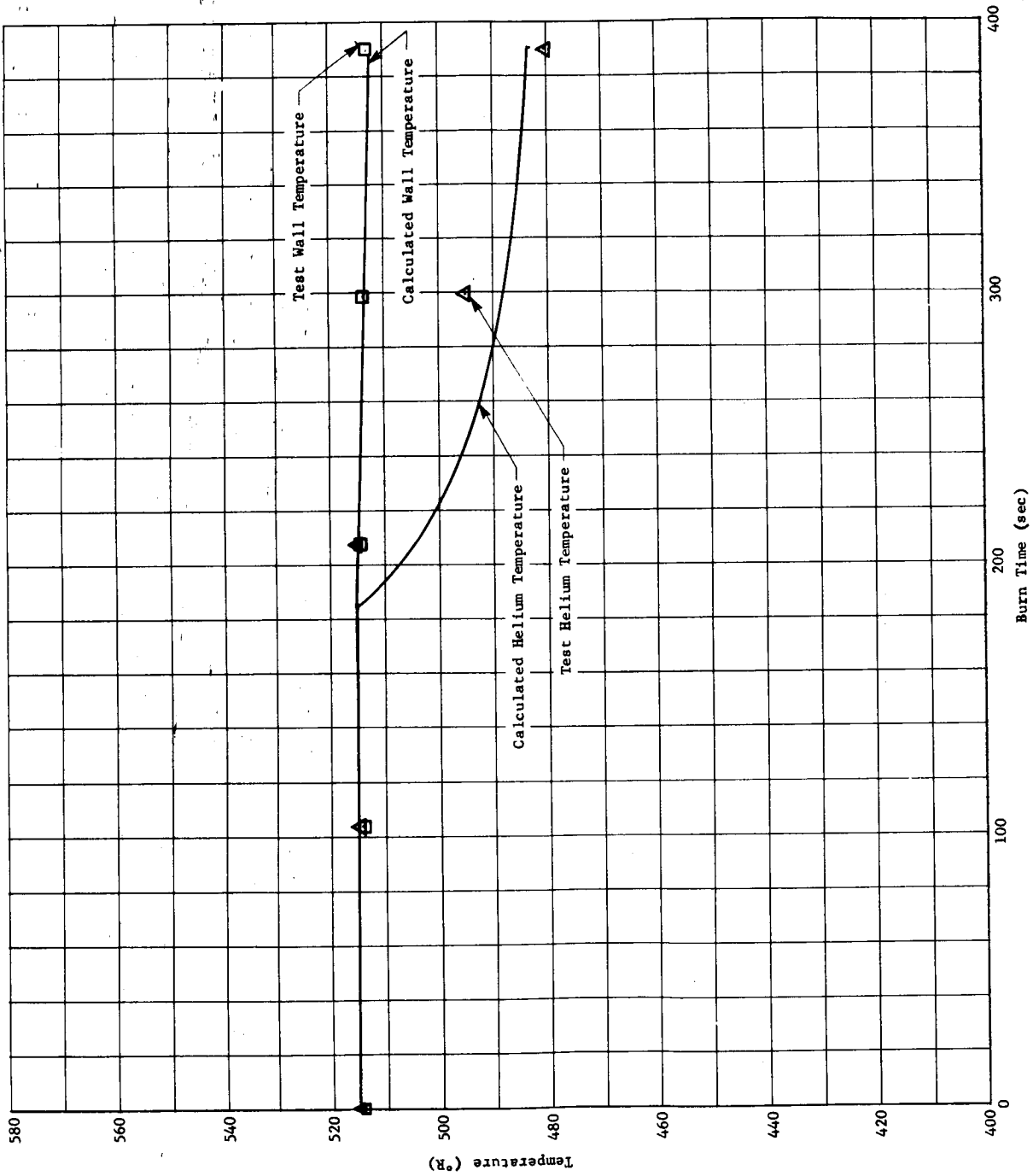


Fig. 82a Cascade Container Posttest Analysis, Nine-Day Mission, Test Run 1, Burn 4

Martin-CR-66-44

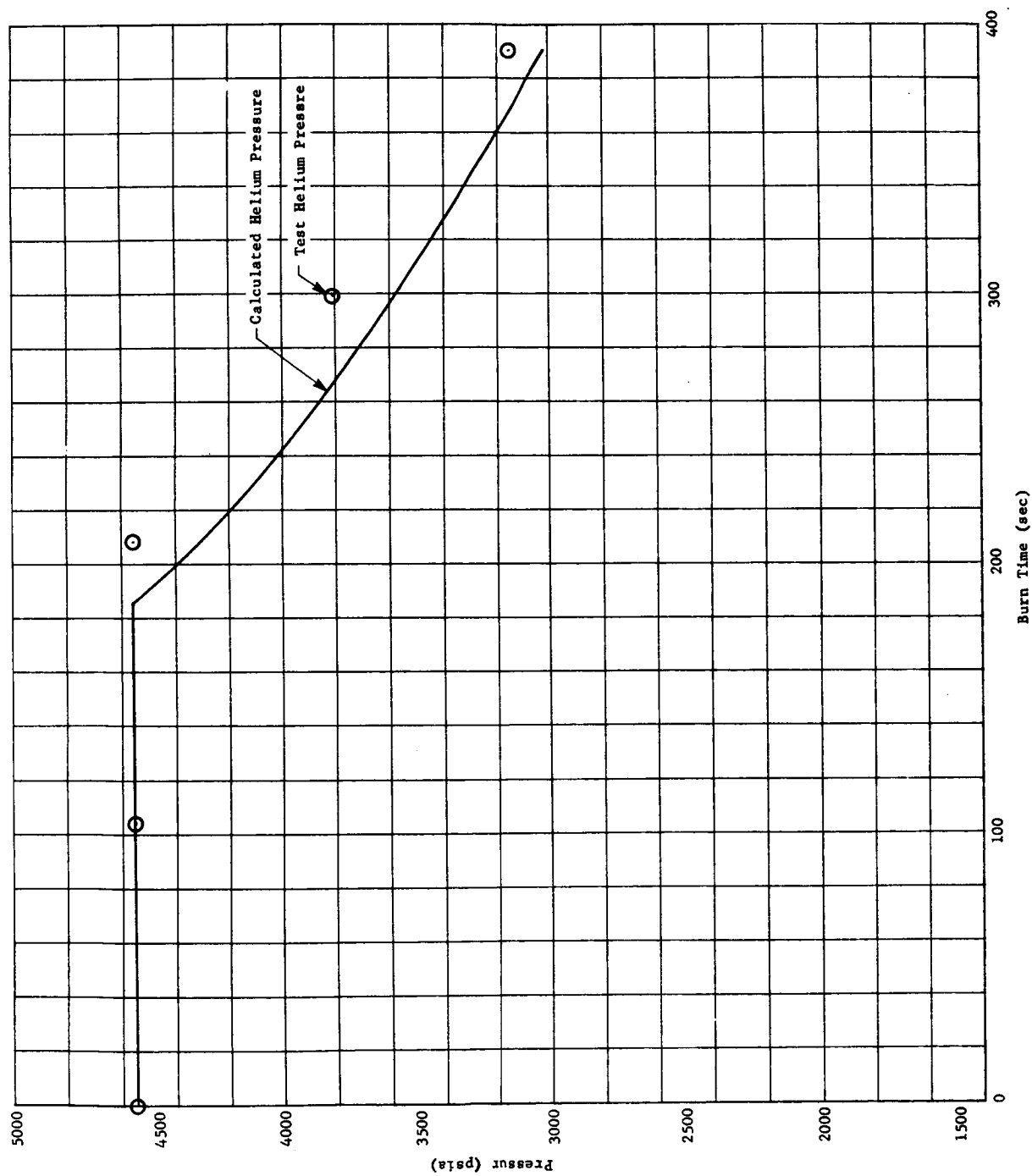


Fig. 82b Cascade Container Posttest Analysis, Nine-Day Mission, Test Run 1, Burn 4

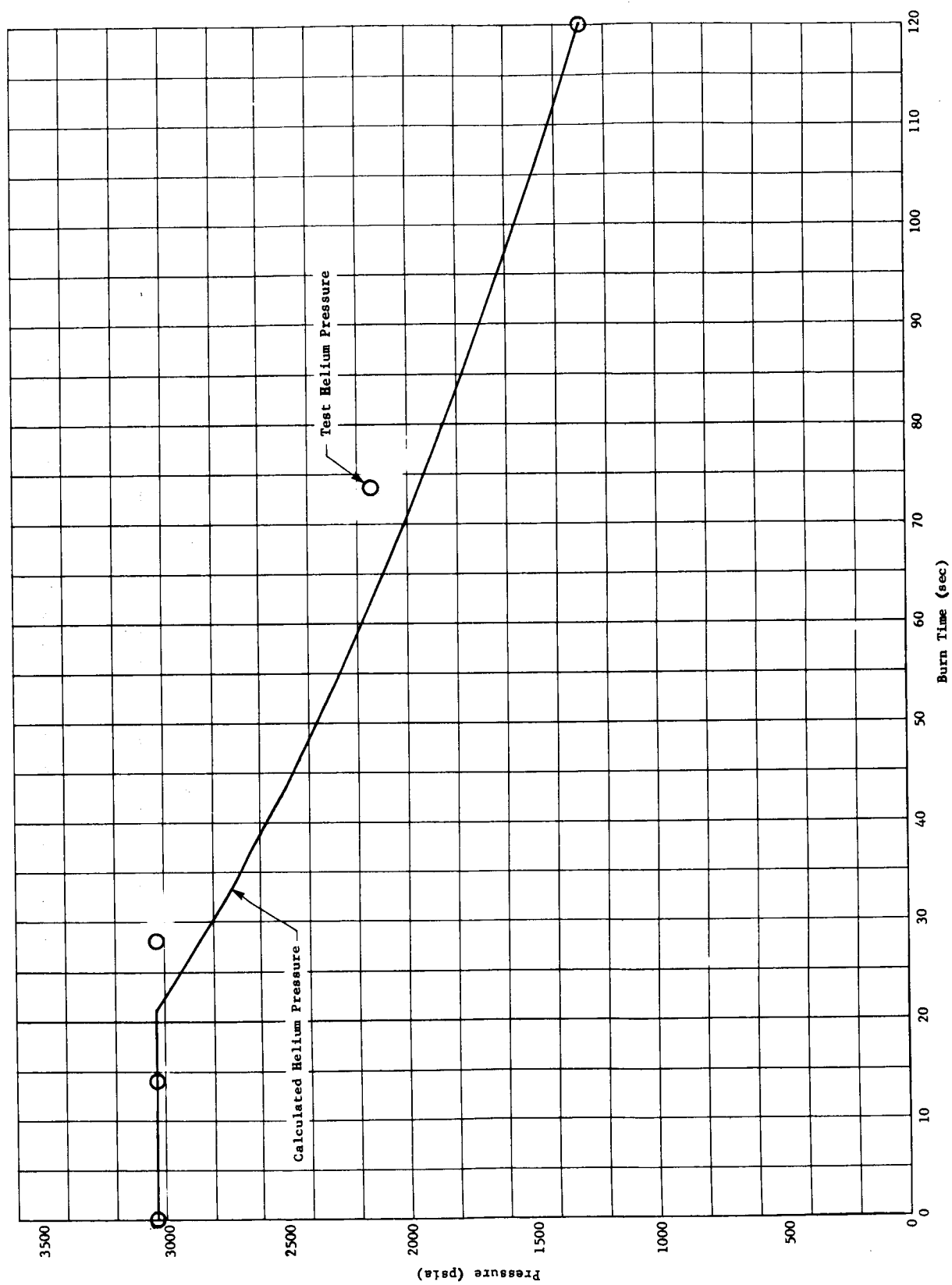


Fig. 83a Cascade Container Posttest Analysis, Nine-Day Mission, Test Run 1, Burn 7

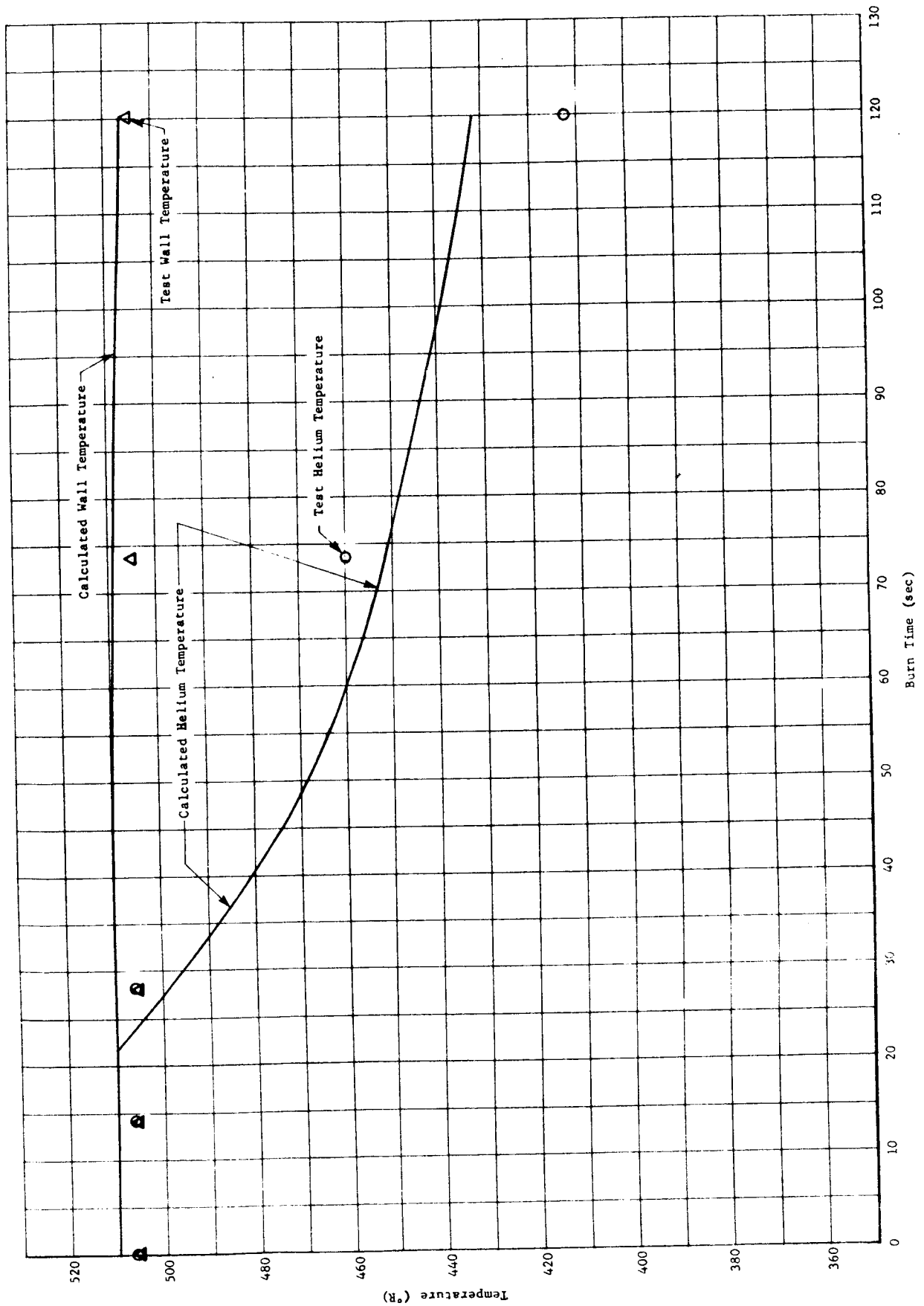


Fig. 83h Cascade Container Posttest Analysis, Nine-Day Mission, Test Run 1, Burn 7

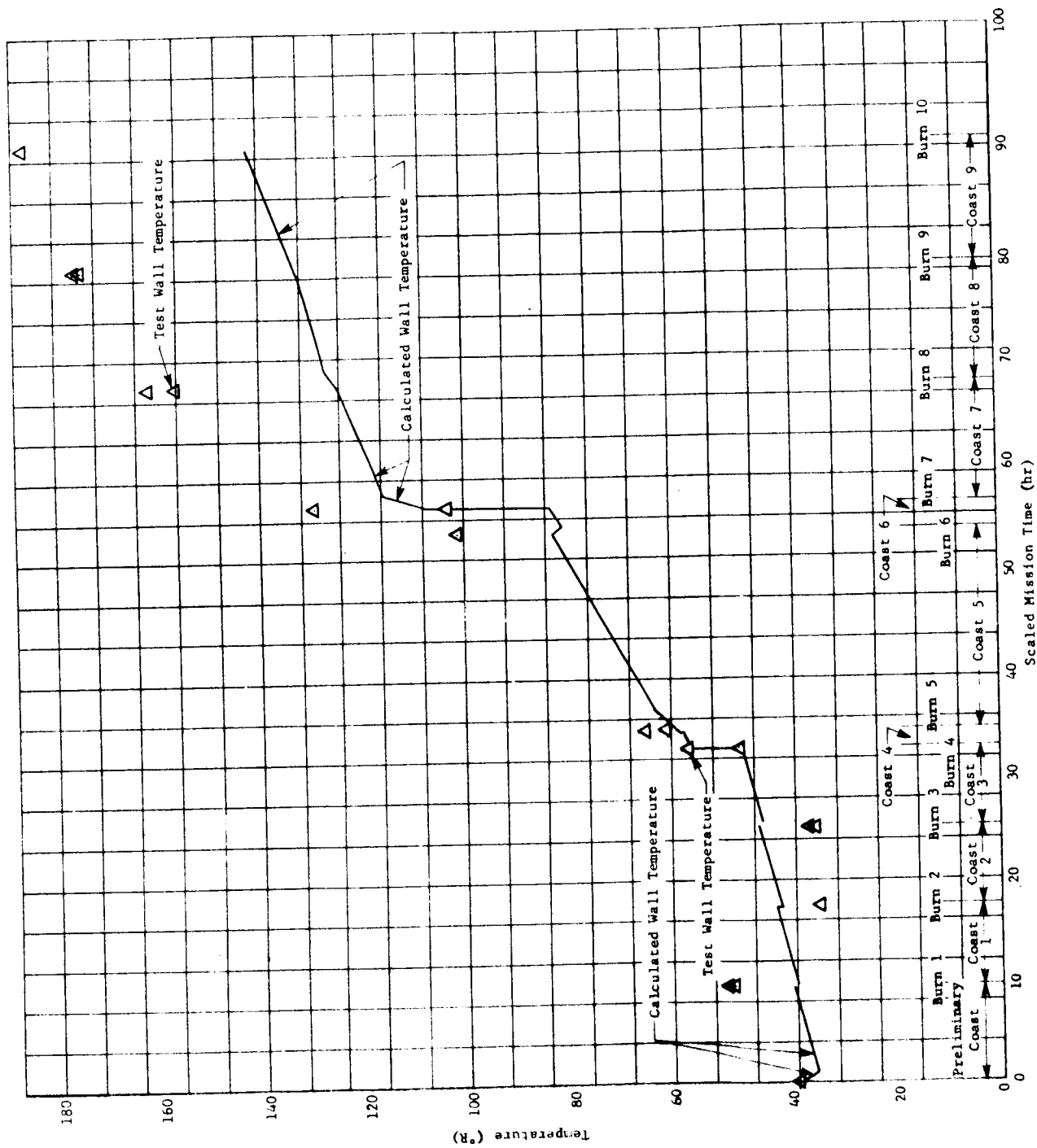


Fig. 84a Primary Container Posttest Analysis, Nine-Day Mission, Test Run 2 (Test Mission Profile)

Martin-CR-66-44

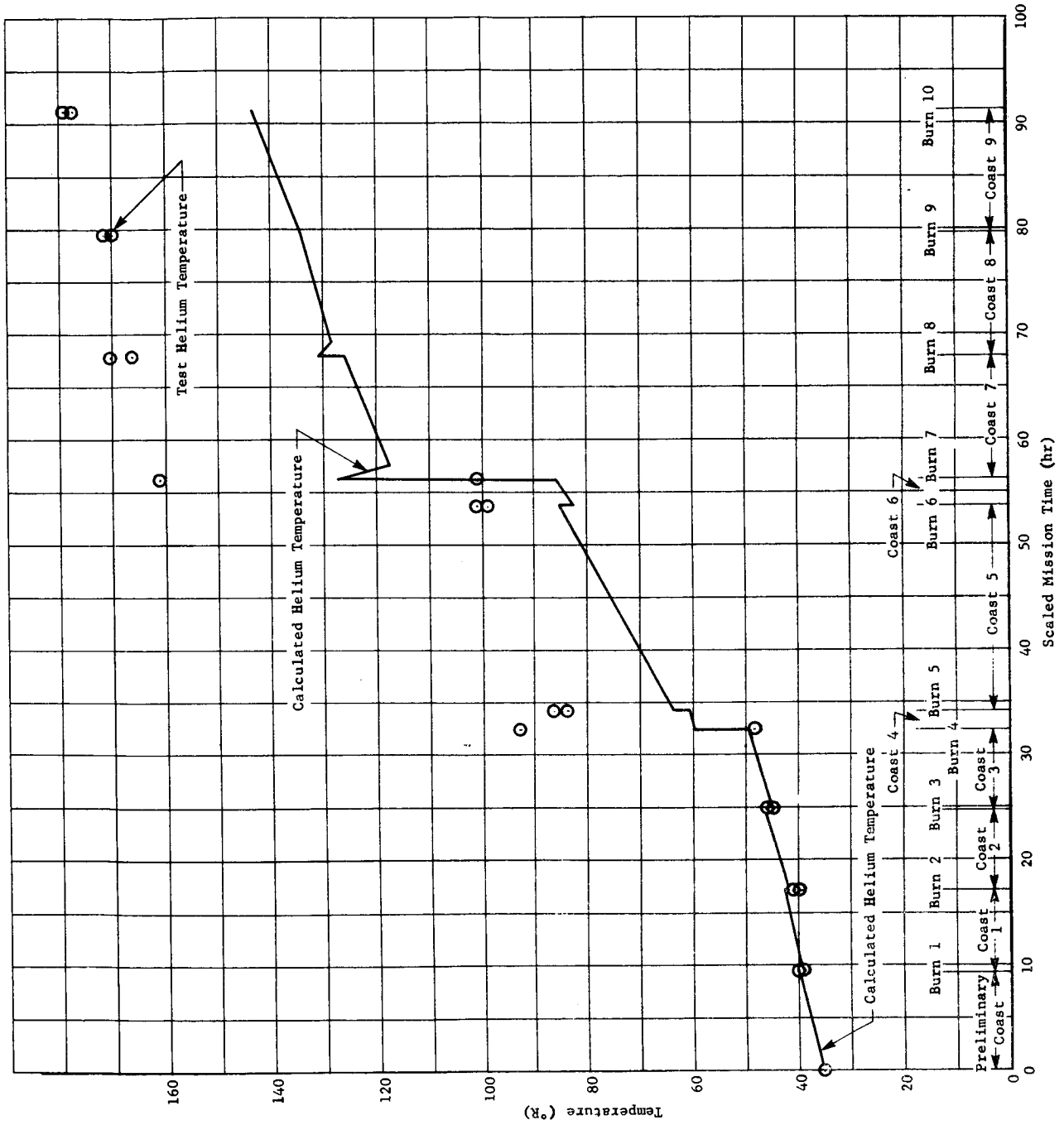


Fig. 84b Primary Container Posttest Analysis, Nine-Day Mission, Test Run 2 (Test Mission Profile)

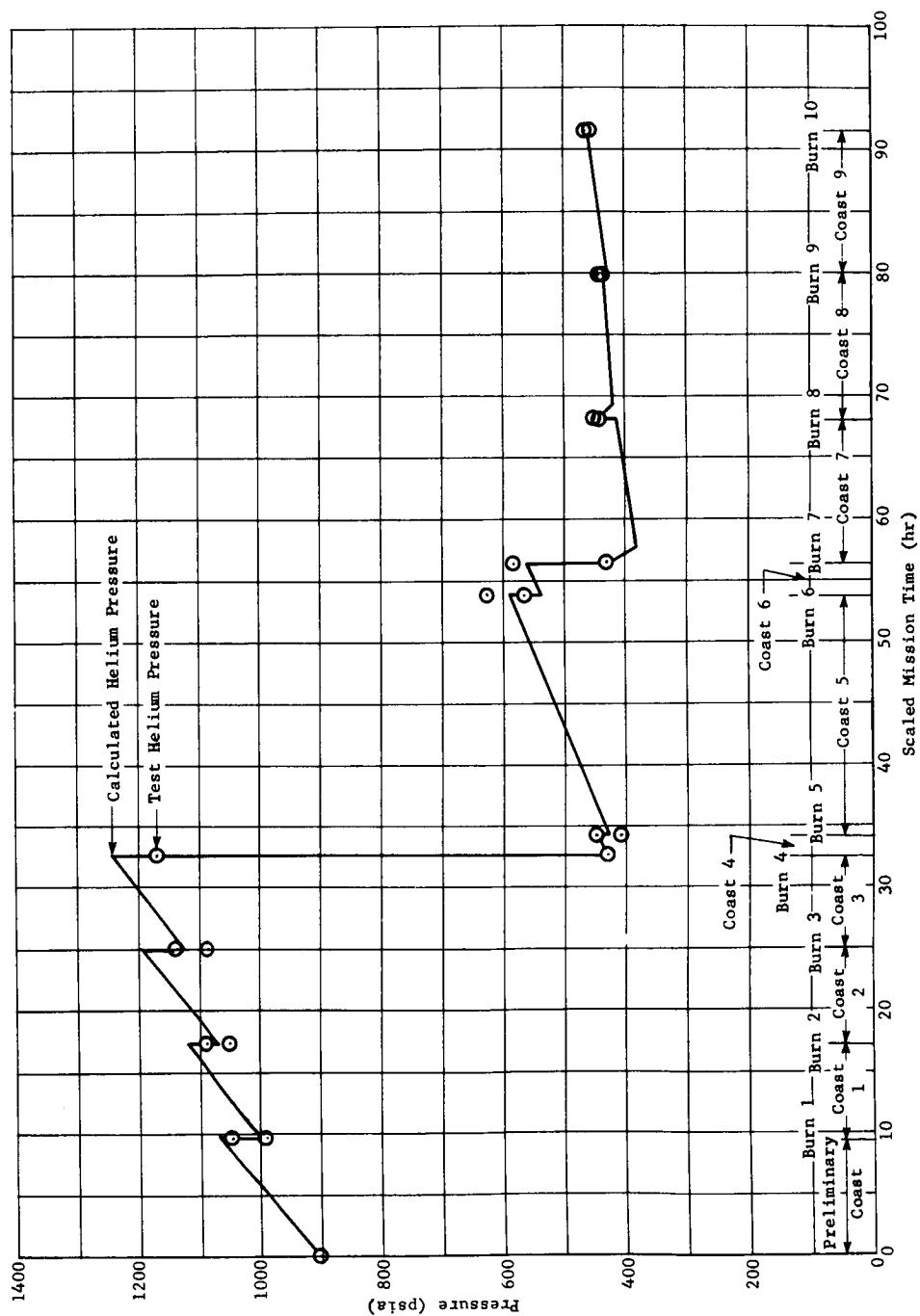


Fig. 84c Primary Container Posttest Analysis, Nine-Day Mission, Test Run 2 (Test Mission Profile)

Martin-CR-66-44

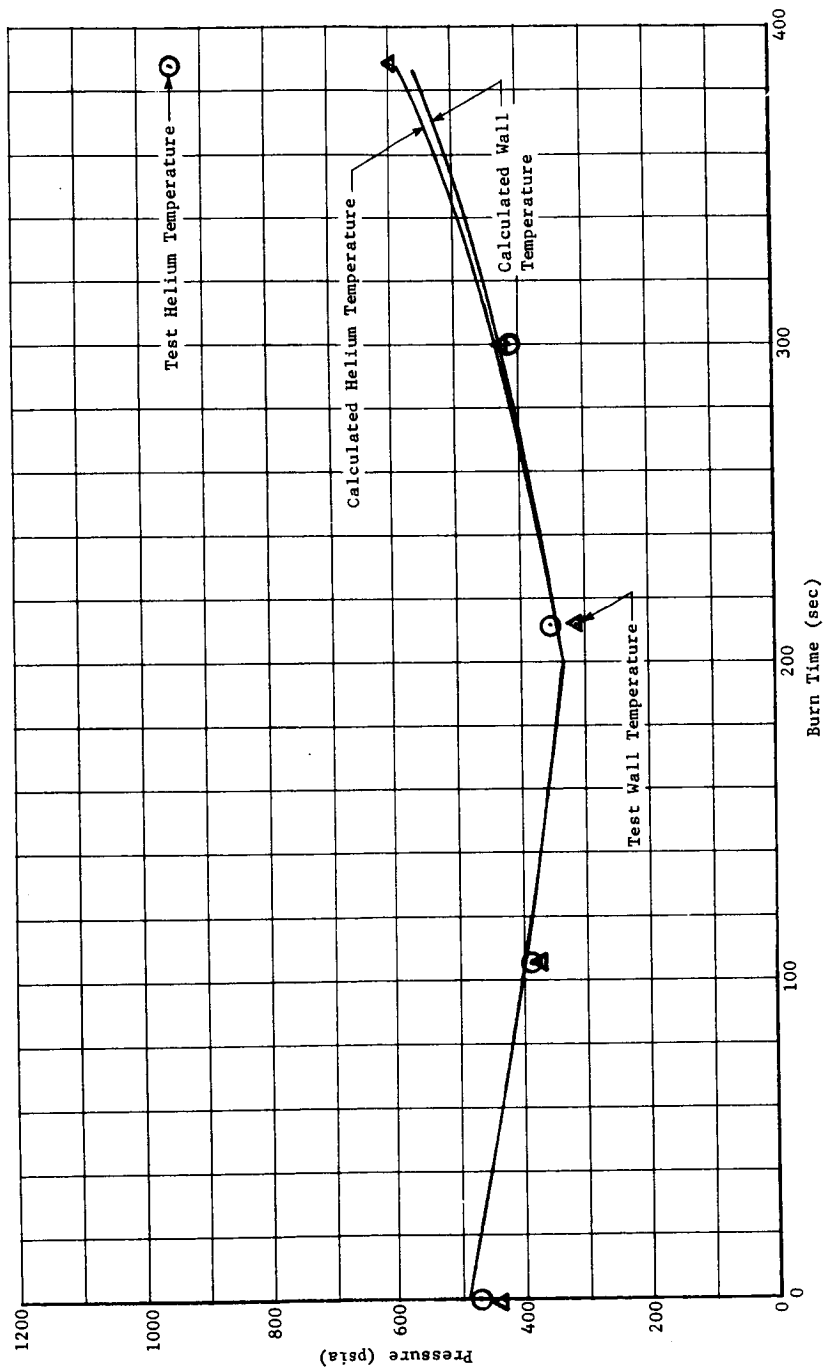


Fig. 85a Primary Container Posttest Analysis, Nine-Day Mission, Test Run 2, Burn 4

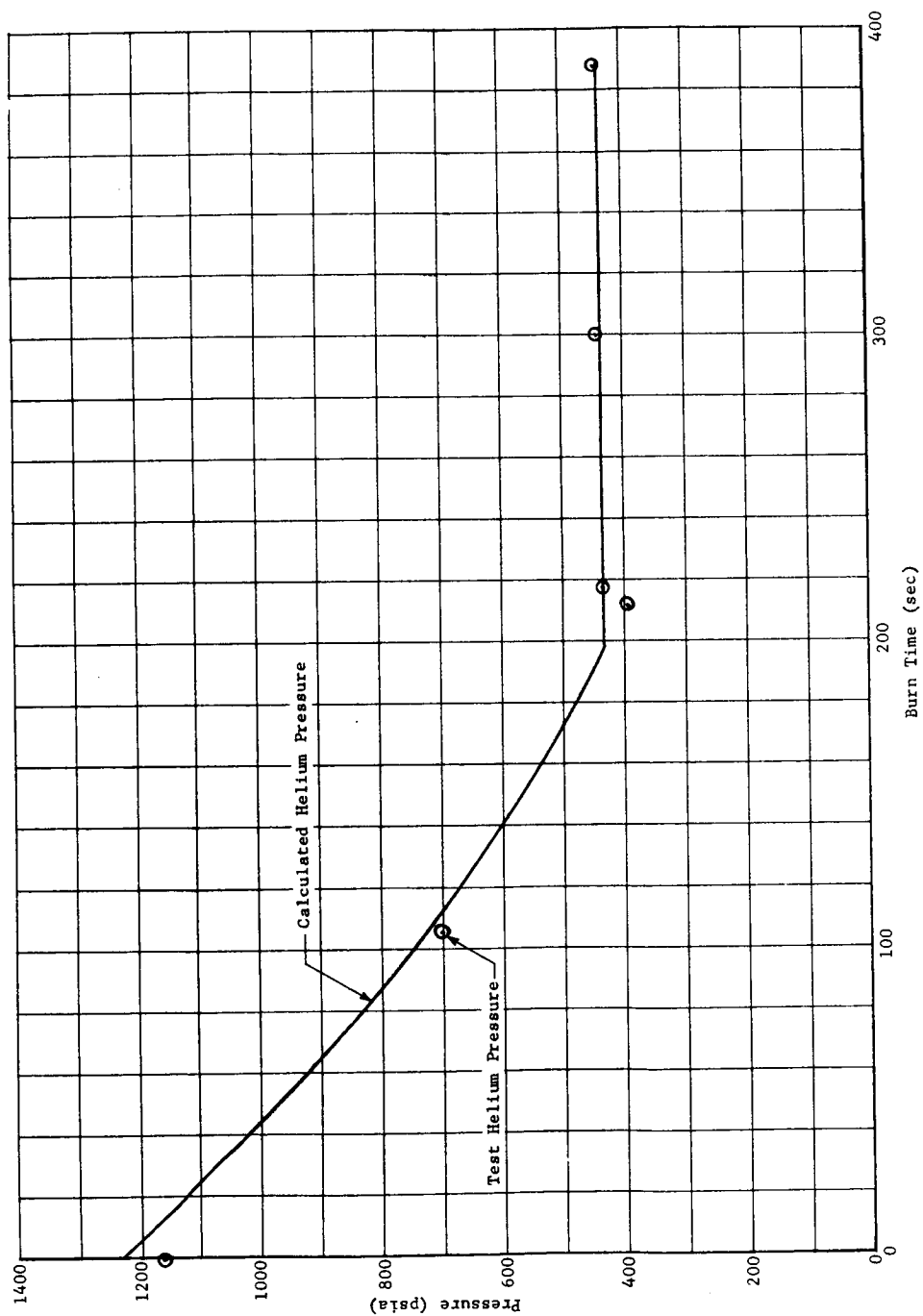


Fig. 85b Primary Container Posttest Analysis, Nine-Day Mission, Test Run 2, Burn 4

Martin-CR-66-44

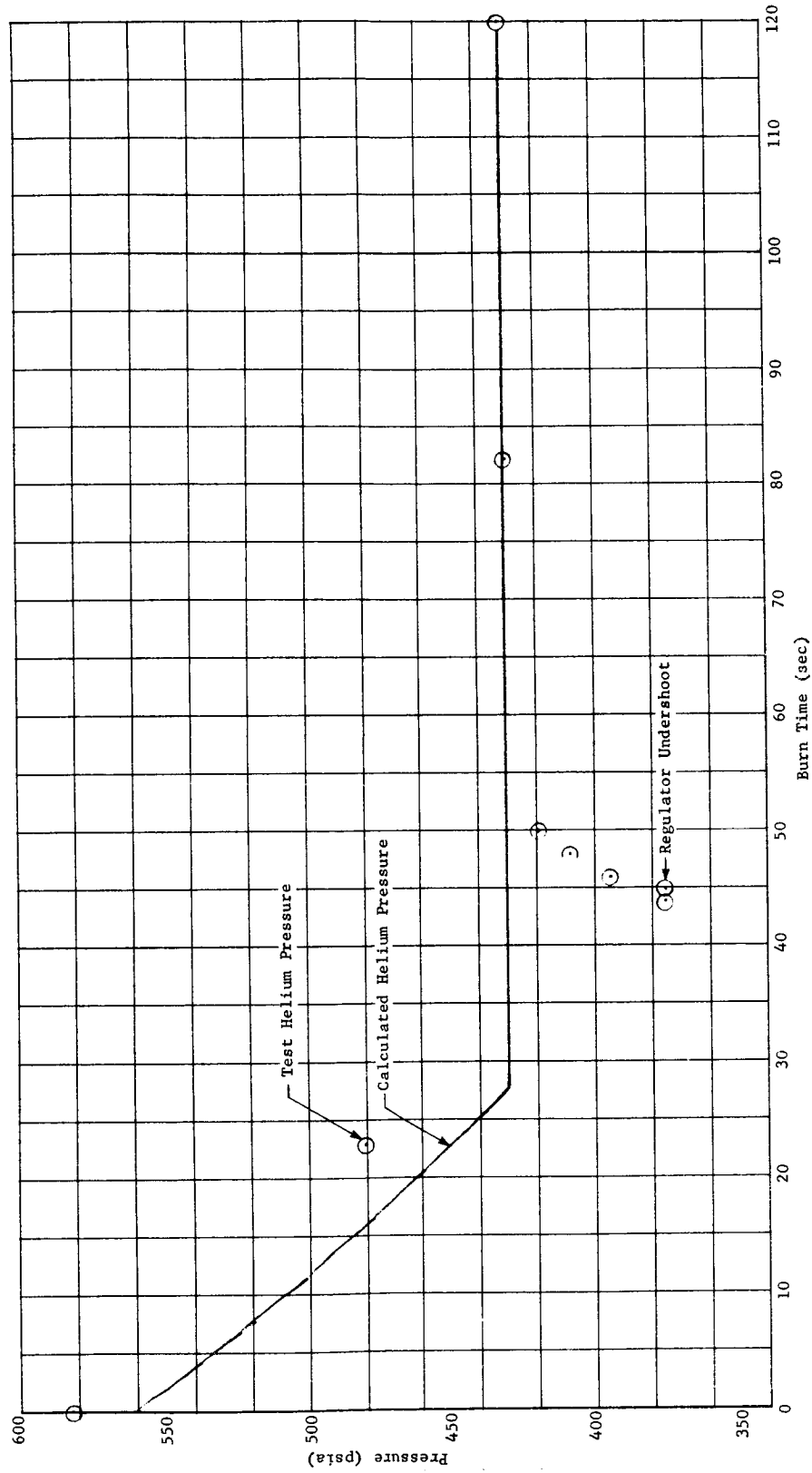


Fig. 86a Primary Container Posttest Analysis, Nine-Day Mission, Test Run 2, Burn 7

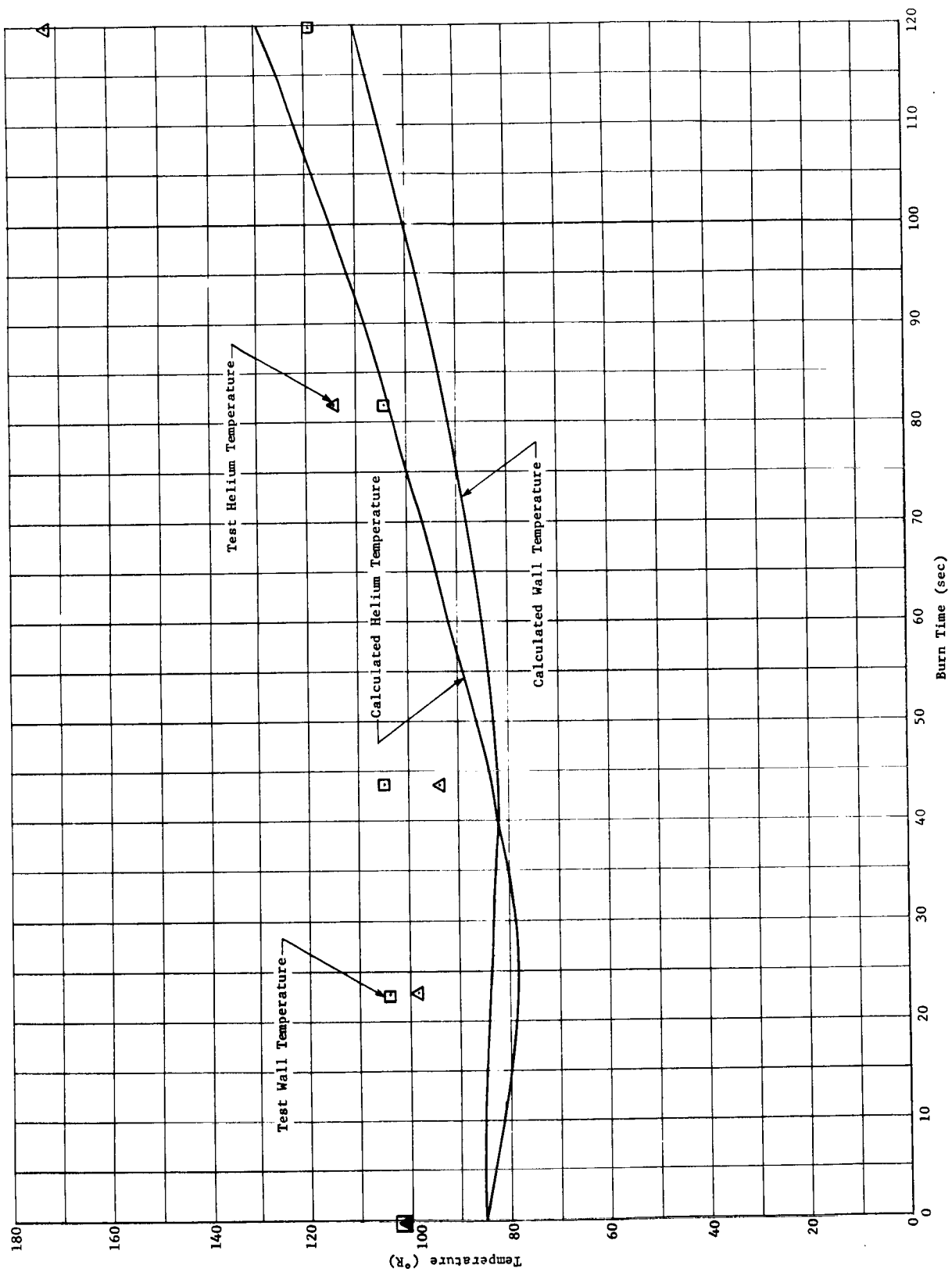


Fig. 86b Primary Container Posttest Analysis, Nine-Day Mission, Test Run 2, Burn 7

Martin-CR-66-44

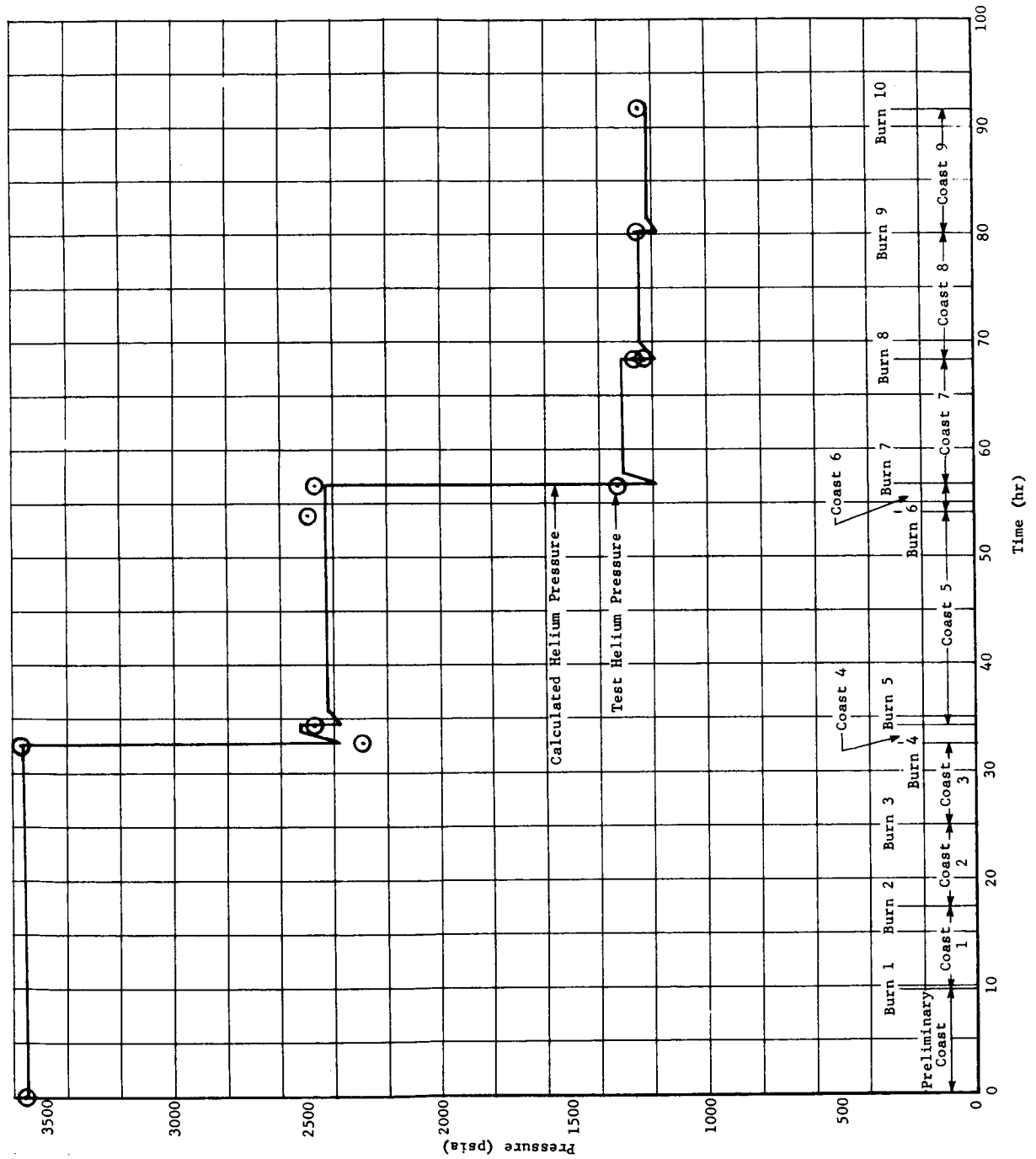


Fig. 87a Cascade Container Posttest Analysis, Nine-Day Mission, Test Run 2 (Test Mission Profile)

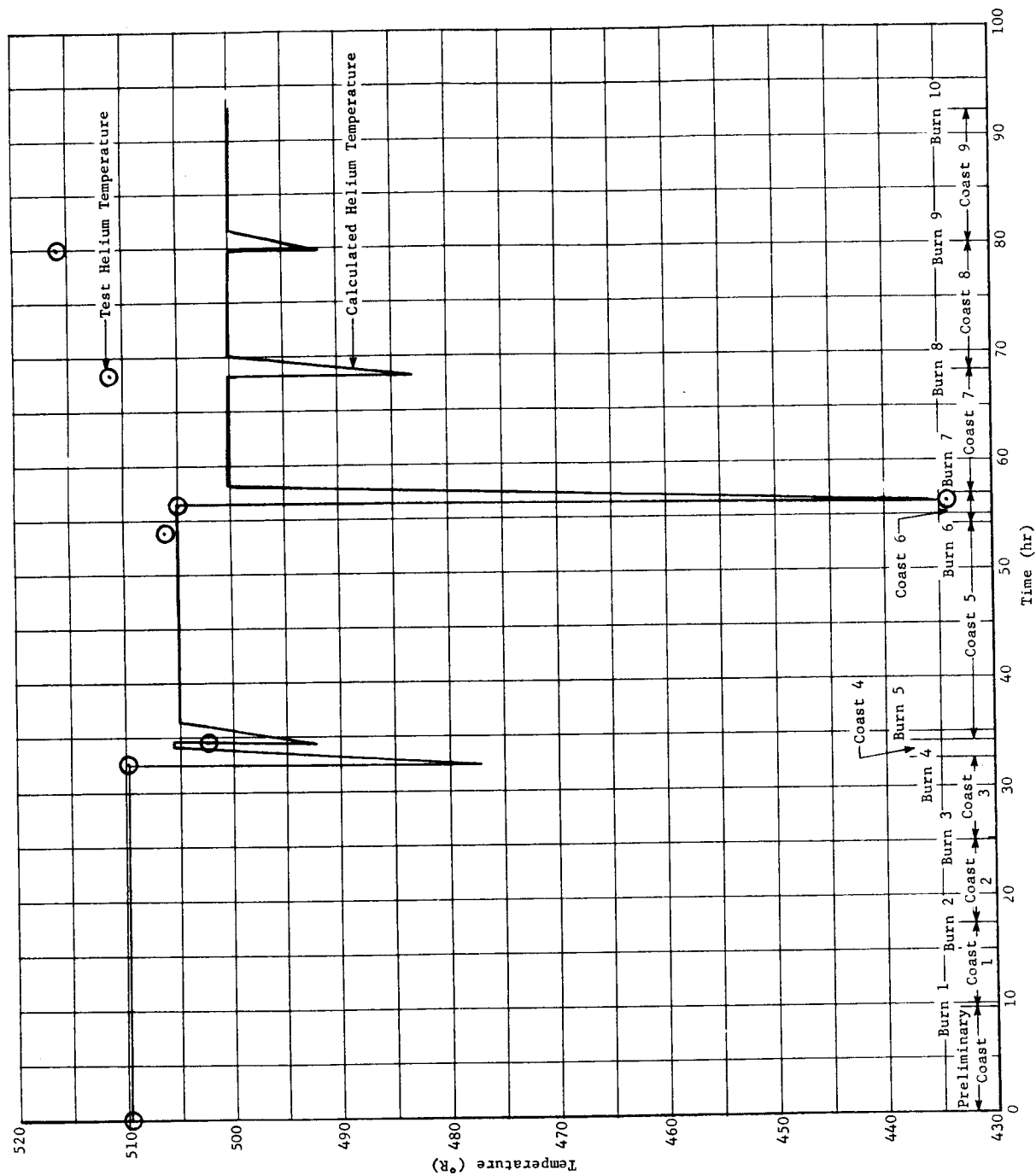


Fig. 87b Cascade Container Posttest Analysis, Nine-Day Mission, Test Run 2 (Test Mission Profile)

Martin-CR-66-44

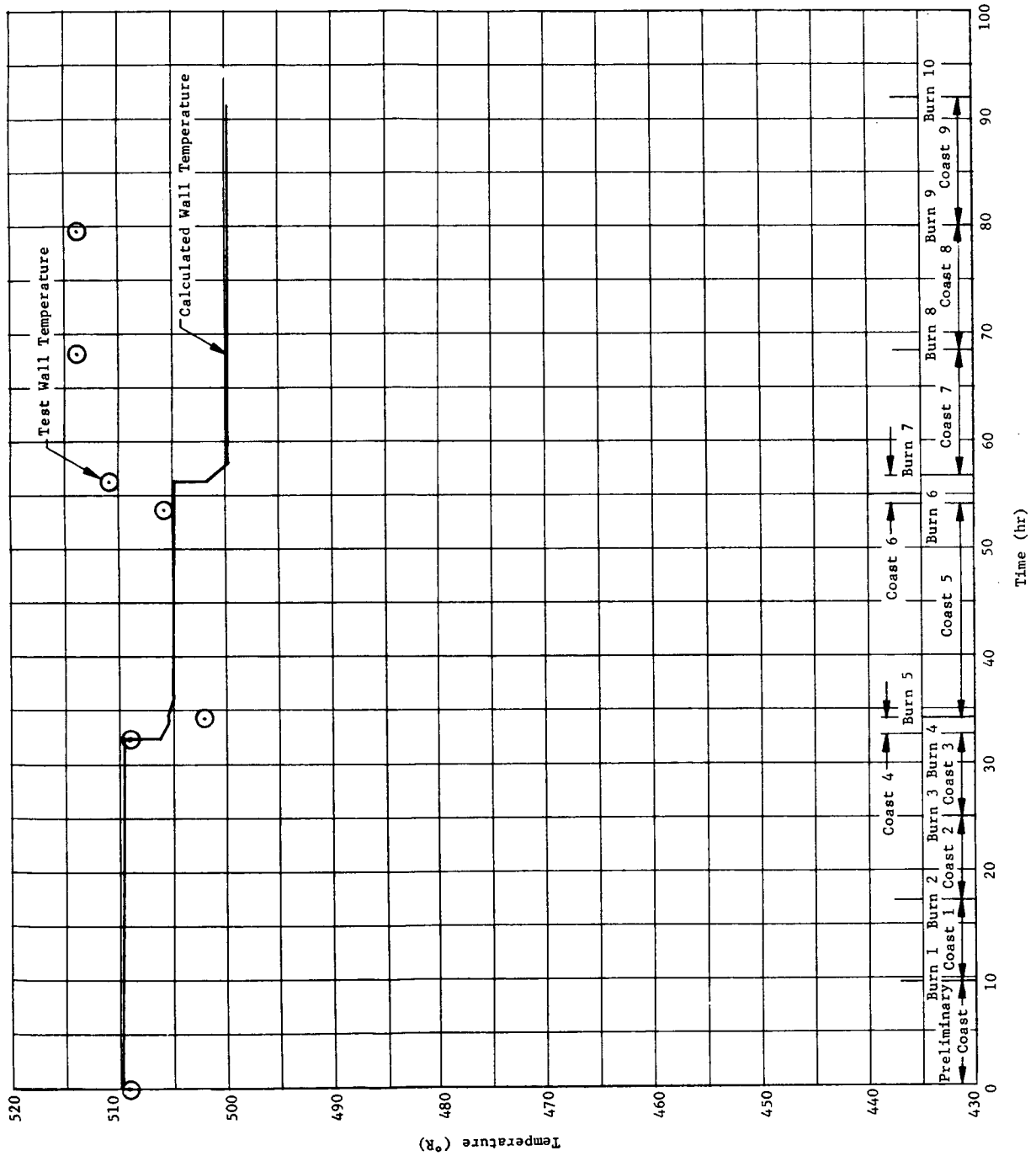


Fig. 87c Cascade Container Posttest Analysis, Nine-Day Mission, Test Run 2  
(Test Mission Profile)

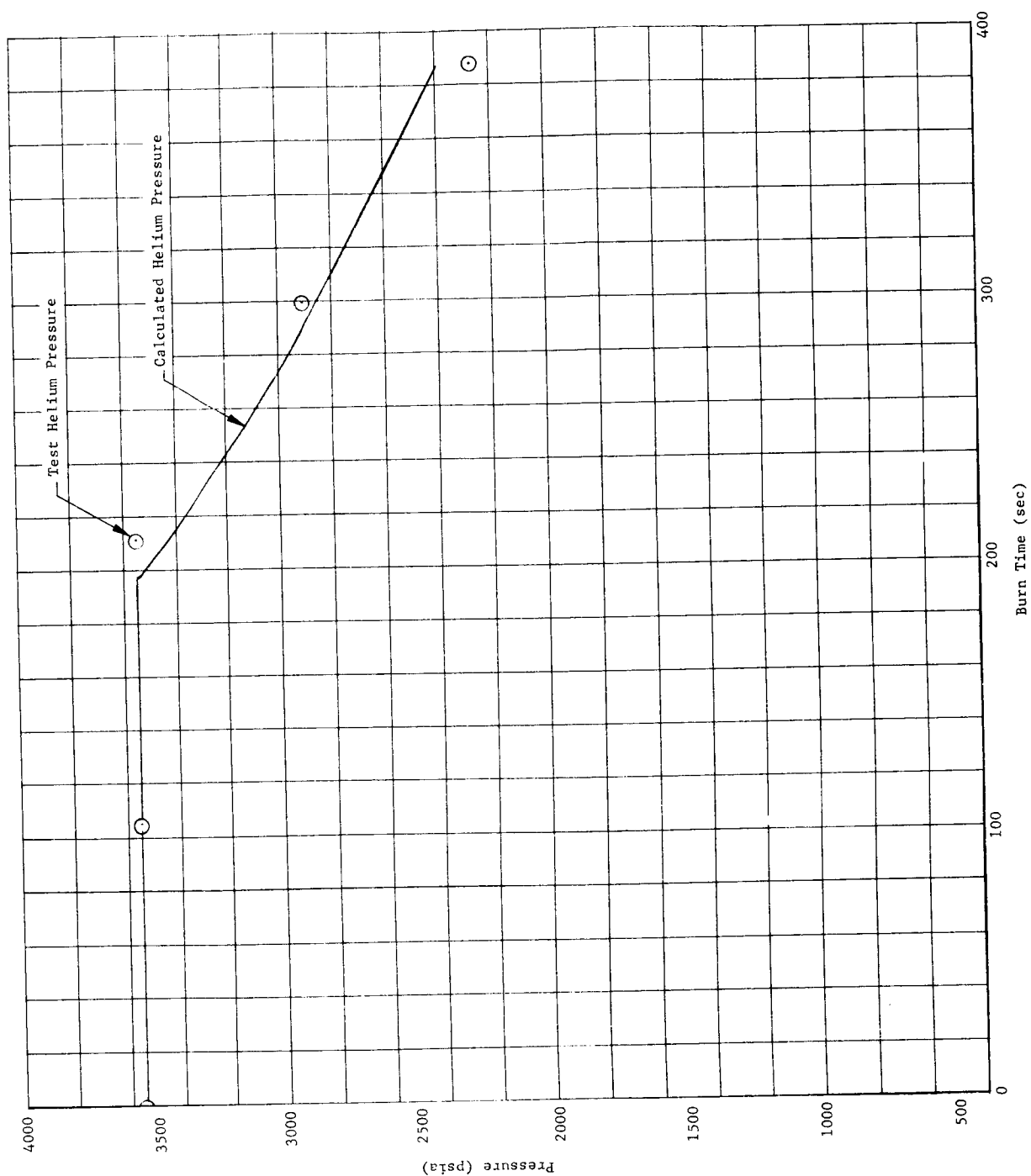


Fig. 88a Cascade Container Posttest Analysis, Nine-Day Mission, Test Run 2, Burn 4

Martin-CR-66-44

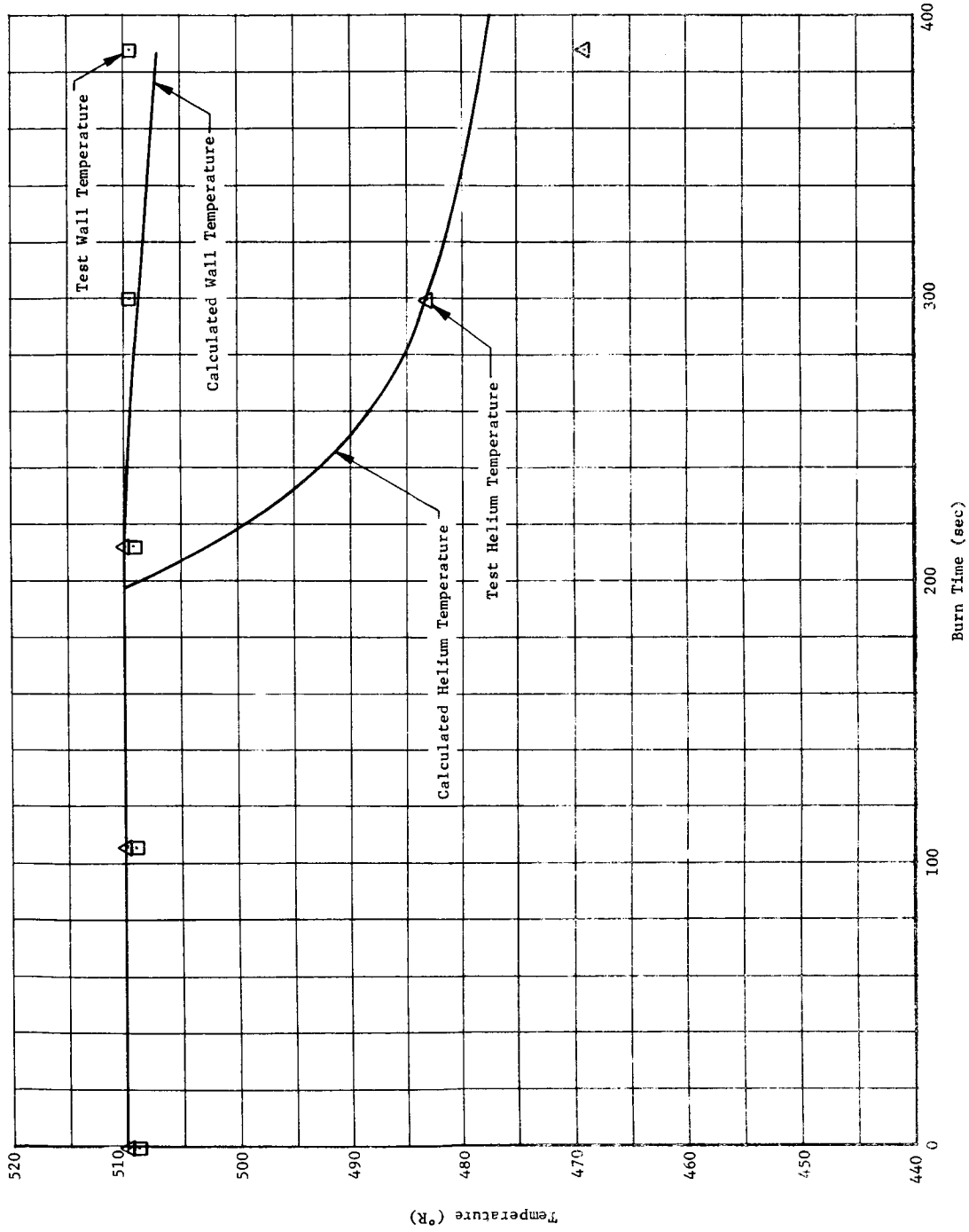


Fig. 88b Cascade Container Posttest Analysis, Nine-Day Mission, Test Run 2, Burn 4

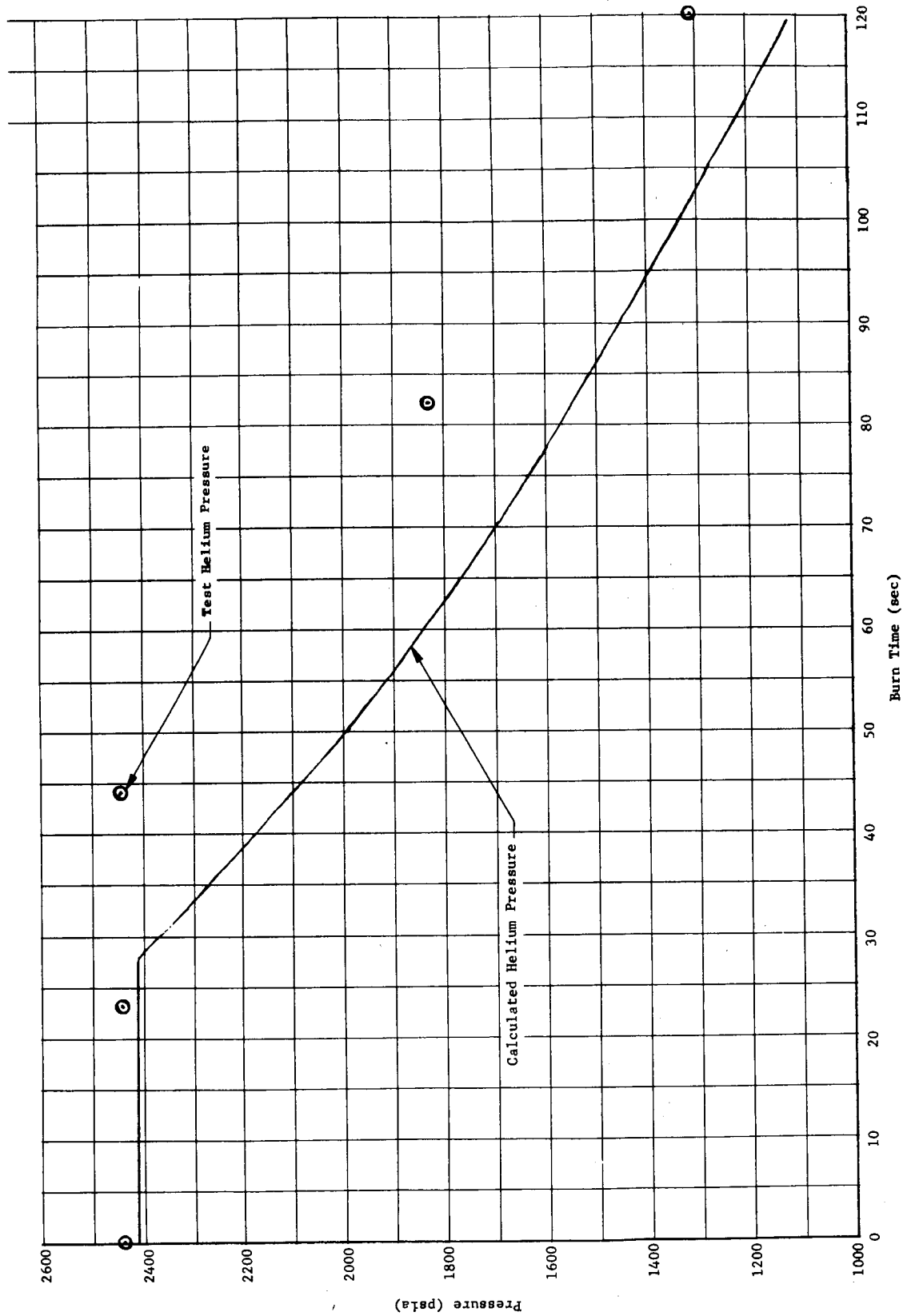


Fig. 89a Cascade Container Posttest Analysis, Nine-Day Mission, Test Run 2, Burn 7

Martin-CR-66-44

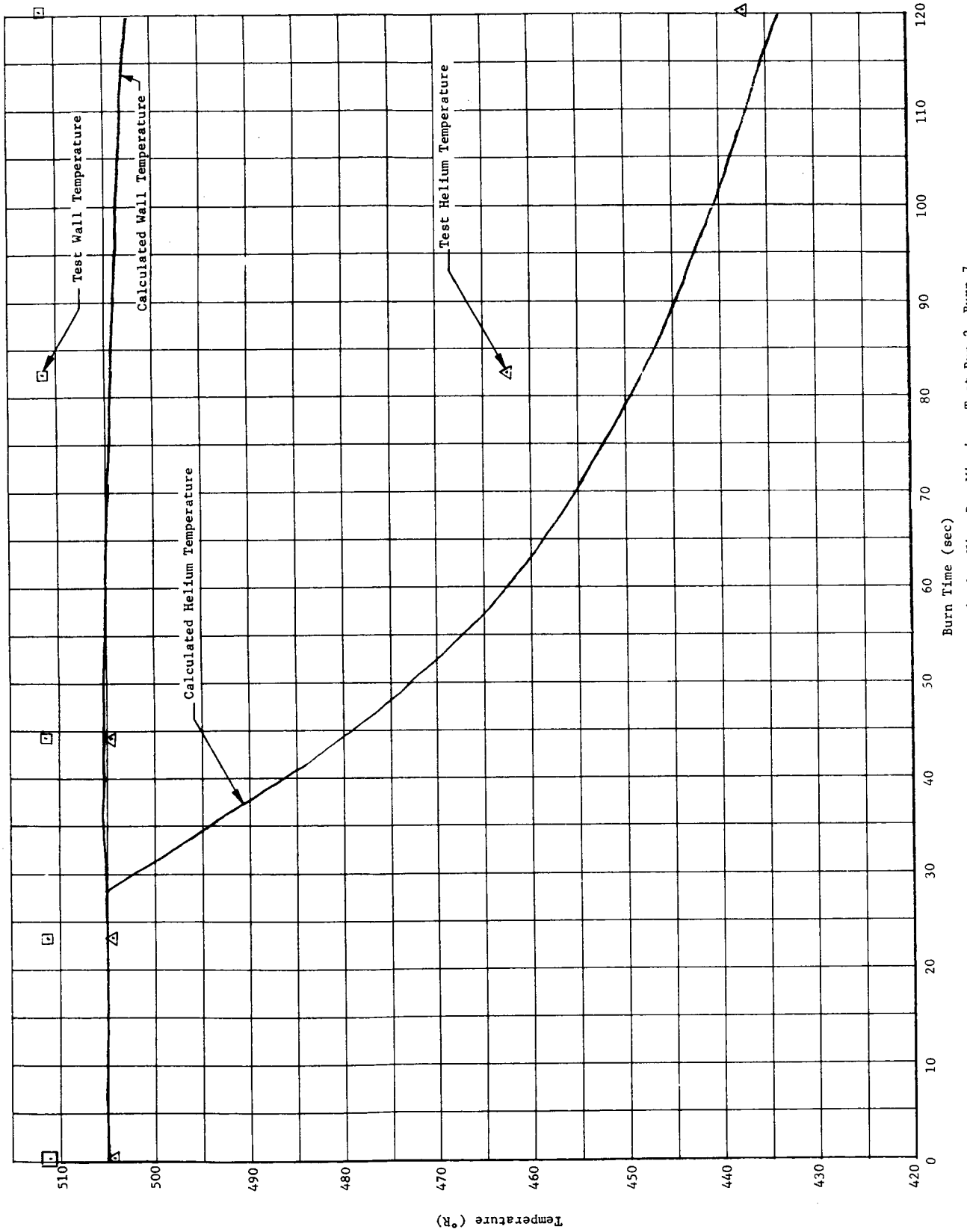
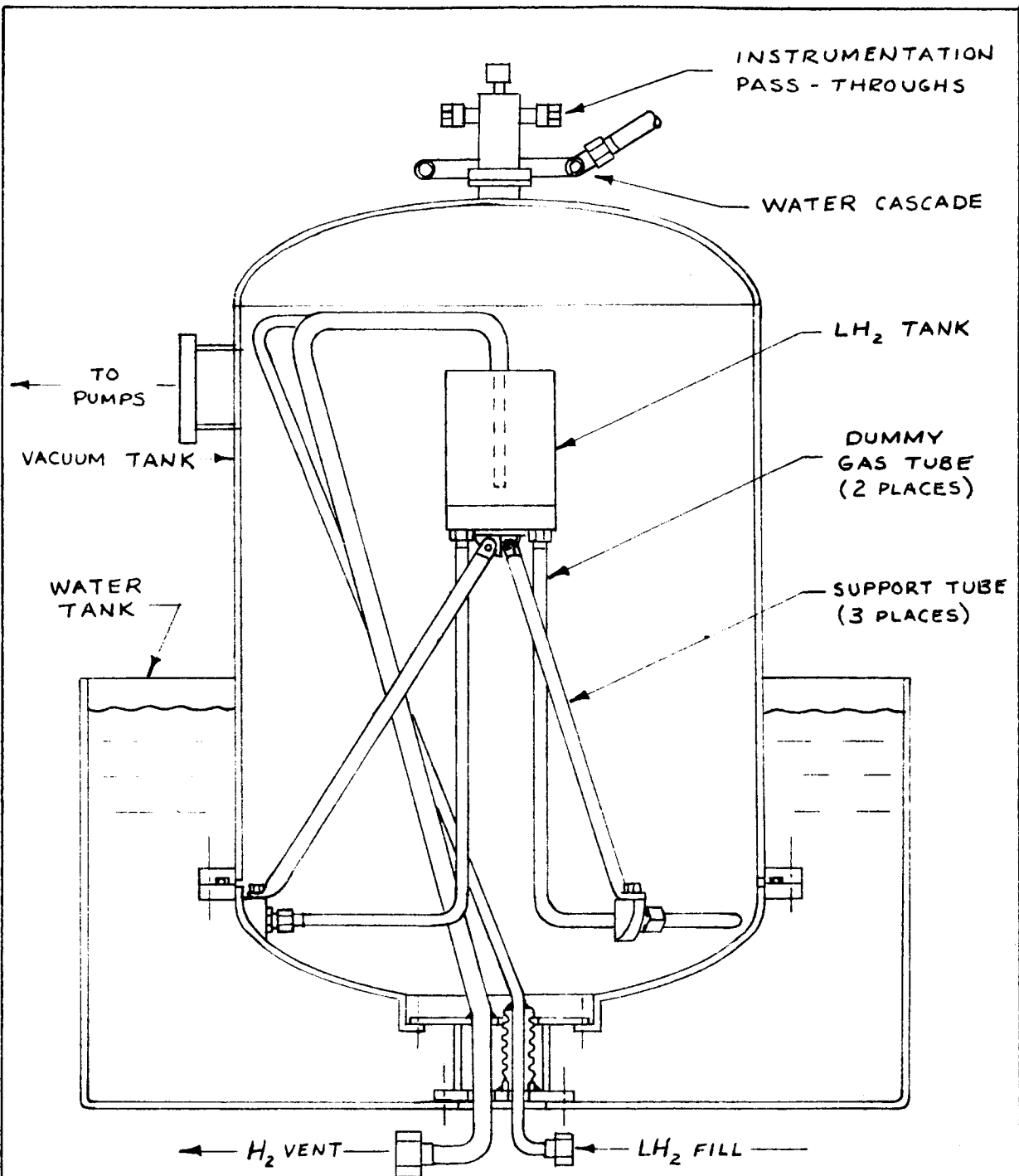


Fig. 89b Cascade Container Posttest Analysis, Nine-Day Mission, Test Run 2, Burn 7



NOTE: NRC-2 INSULATION NOT SHOWN

SUPPORT HEAT LEAK TEST ITEM

FIGURE 90

J.B. KFOUGH

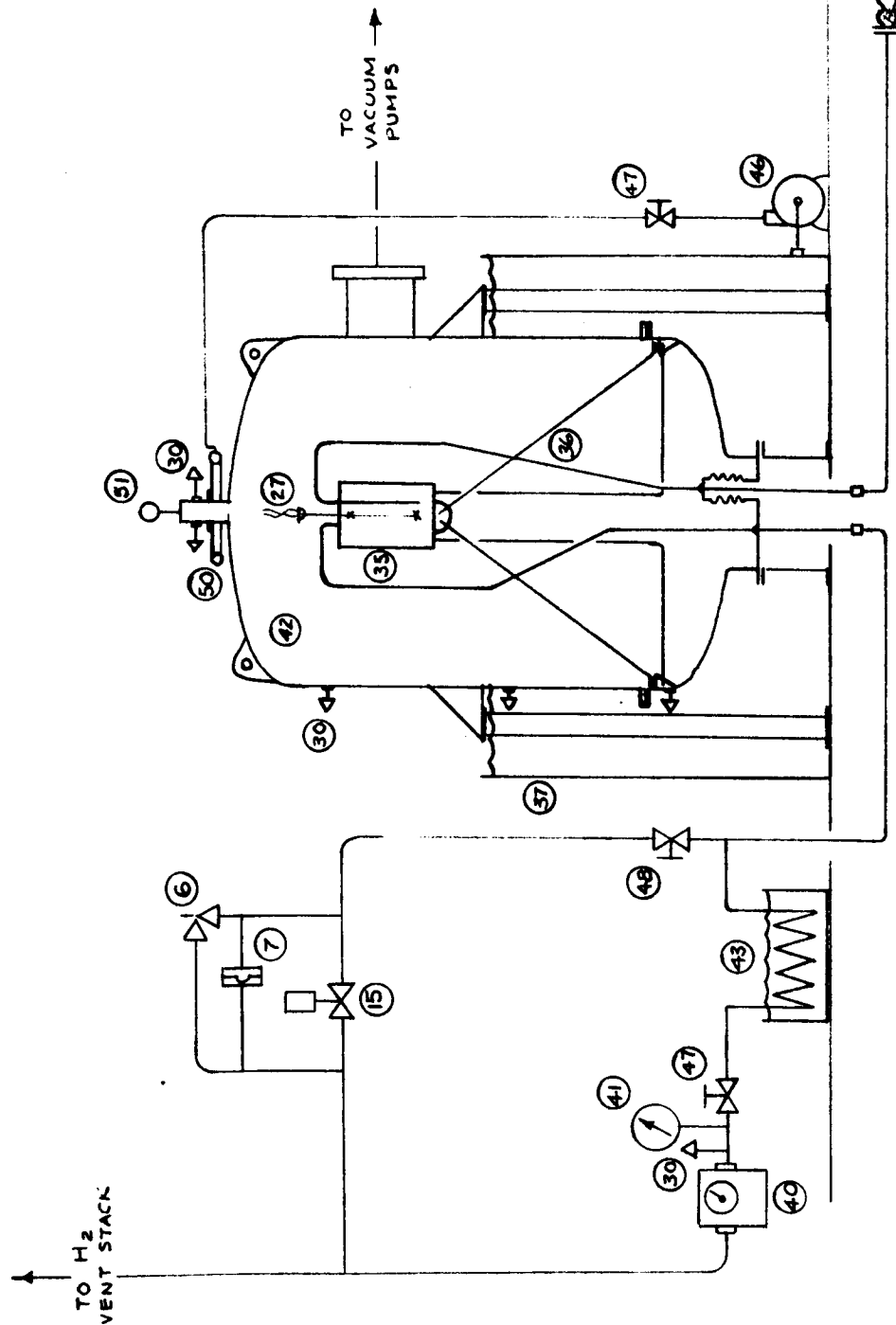


FIGURE 91  
PRIMARY TANK SUPPORT STRUCTURE  
HEAT LEAK TEST FIXTURE

Figure 91      Sheet 2

<u>Item No.</u>	<u>Description</u>
6	Republic 3/4-inch Relief Valve
7	Fike 2-inch Burst Disc Holder
15	Annin 2-inch Cylinder Valve 150# LH <sub>2</sub> Service
27	Conax Thermistors (2), Probe-Mounted
30	Conax Copper-Constantan Thermocouple
35	Liquid Hydrogen Container
36	Tubular Supports, Lines
37	Water Bath Tank
40	Rockwell LPG Gas Test Meter
41	Pressure Gage 0 - 30 Psig, 0.5 Psig graduations
42	Vacuum Chamber
43	Water Bath H <sub>2</sub> Gas Heater
45	Dragon 1/2-inch Hand Valve
46	Water Circulating Pump, 30 GPM Capacity
47	Jamesbury 1/2-inch Ball Valve Manual Operator
48	Annin 1/2-inch Hand Valve, 150#
49	Mobile LH <sub>2</sub> Dewar, 1000 Liter Capacity
50	Water Cascade Distribution Ring
51	Cold Cathode Ionization Vacuum Gage

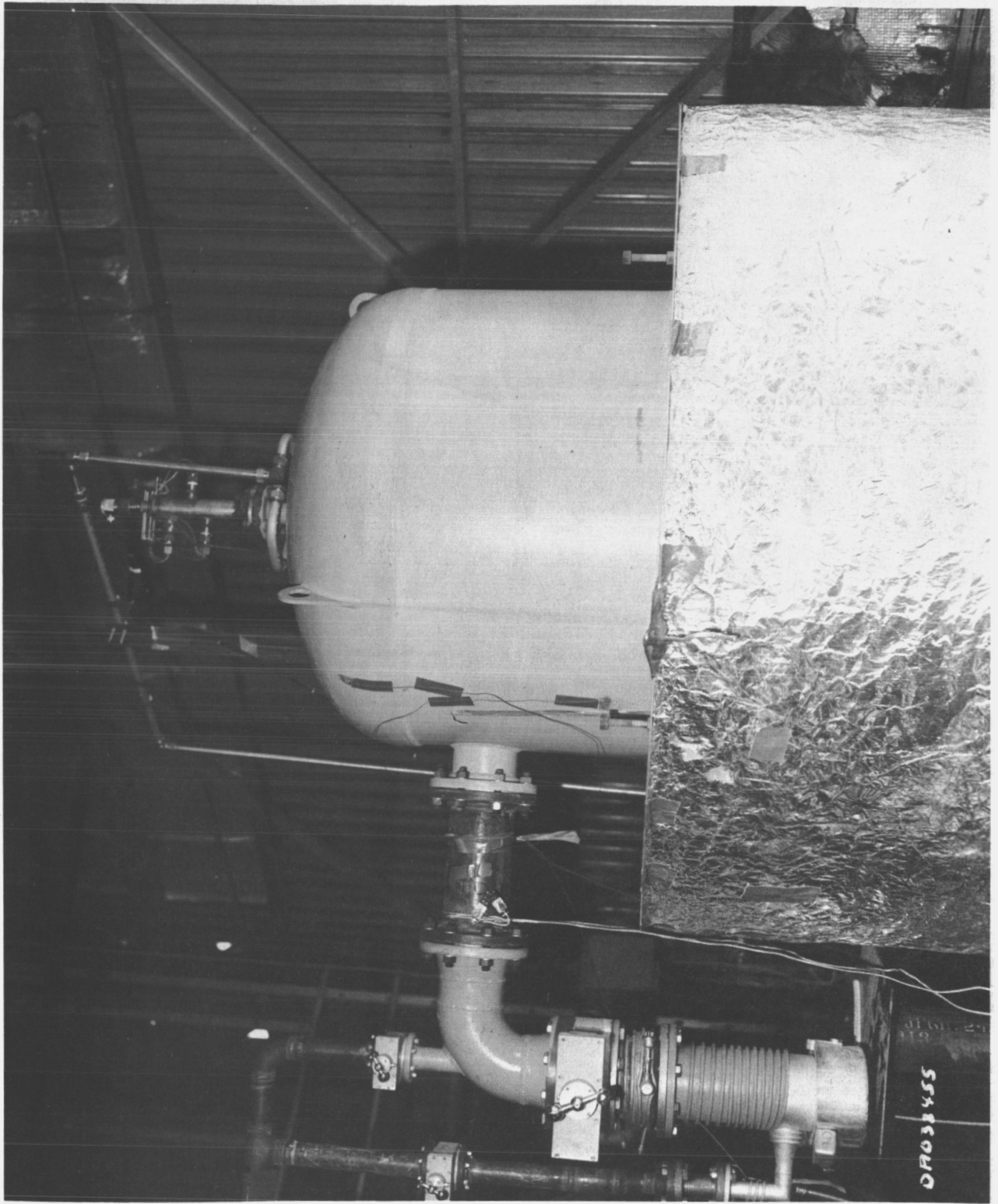


FIGURE 92 PRIMARY TANK SUPPORT STRUCTURE HEAT LEAK TEST SETUP

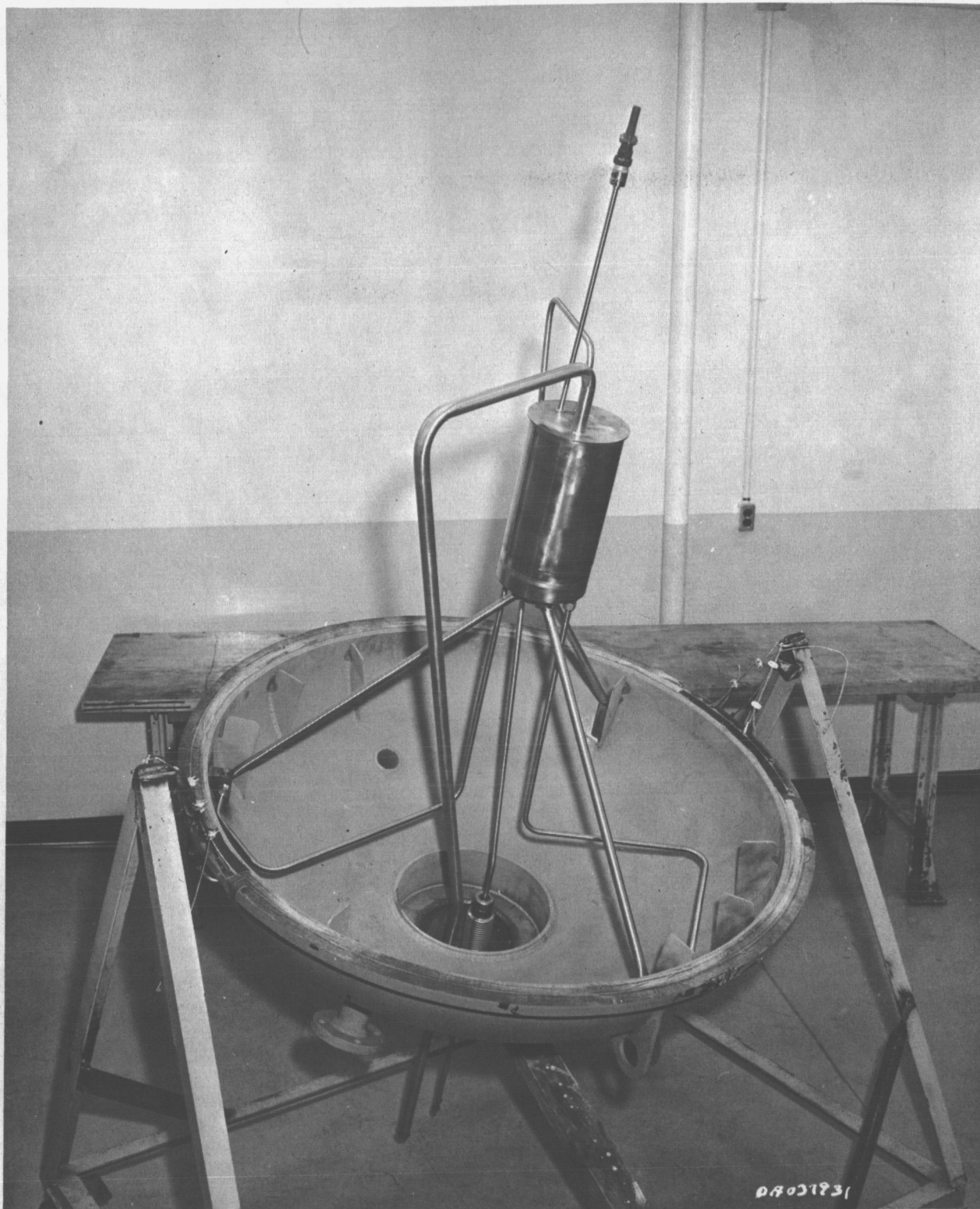


FIGURE 93 SUPPORT STRUCTURE TEST MODEL

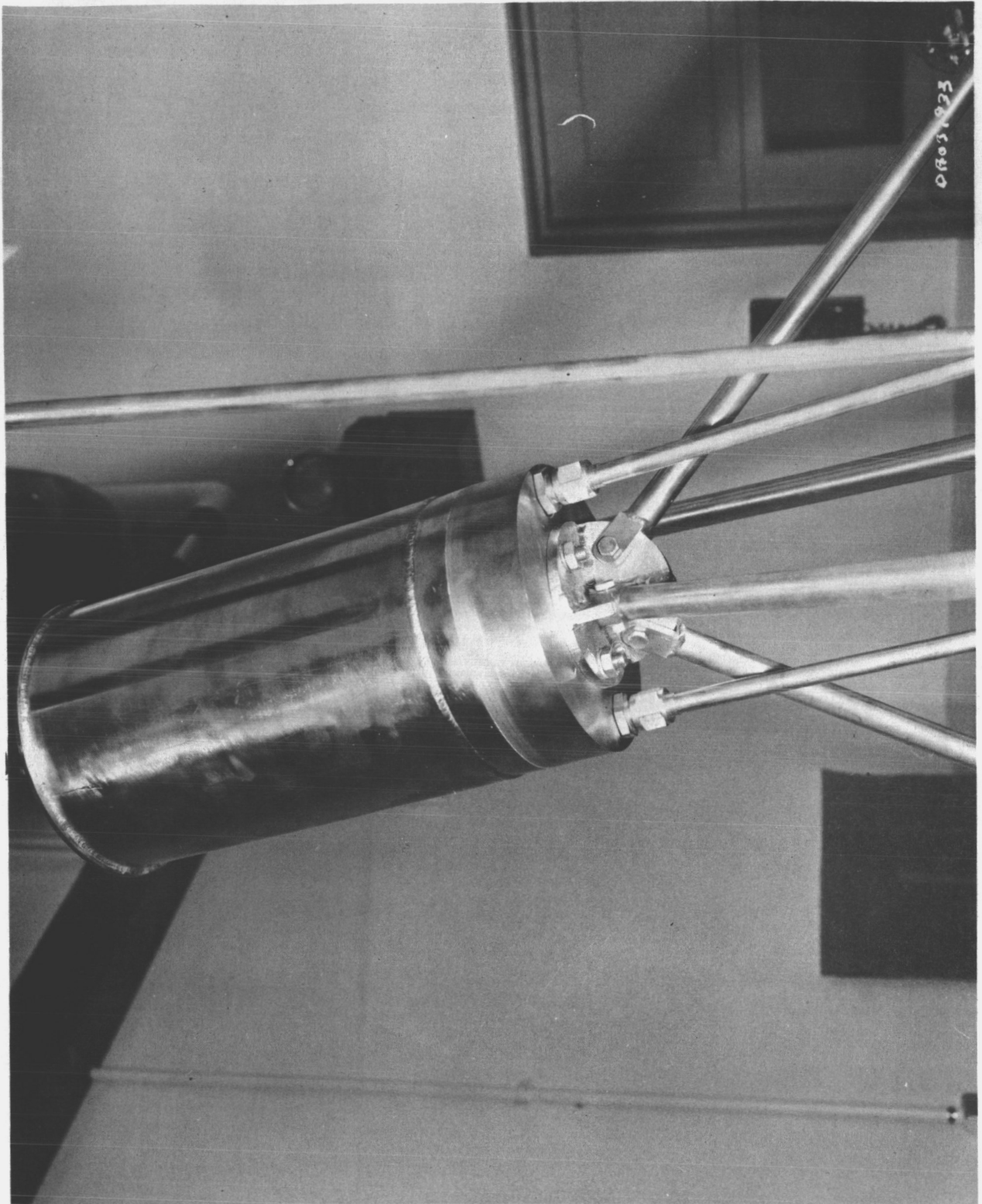


FIGURE 94 SUPPORT STRUCTURE ATTACHMENT BOSS

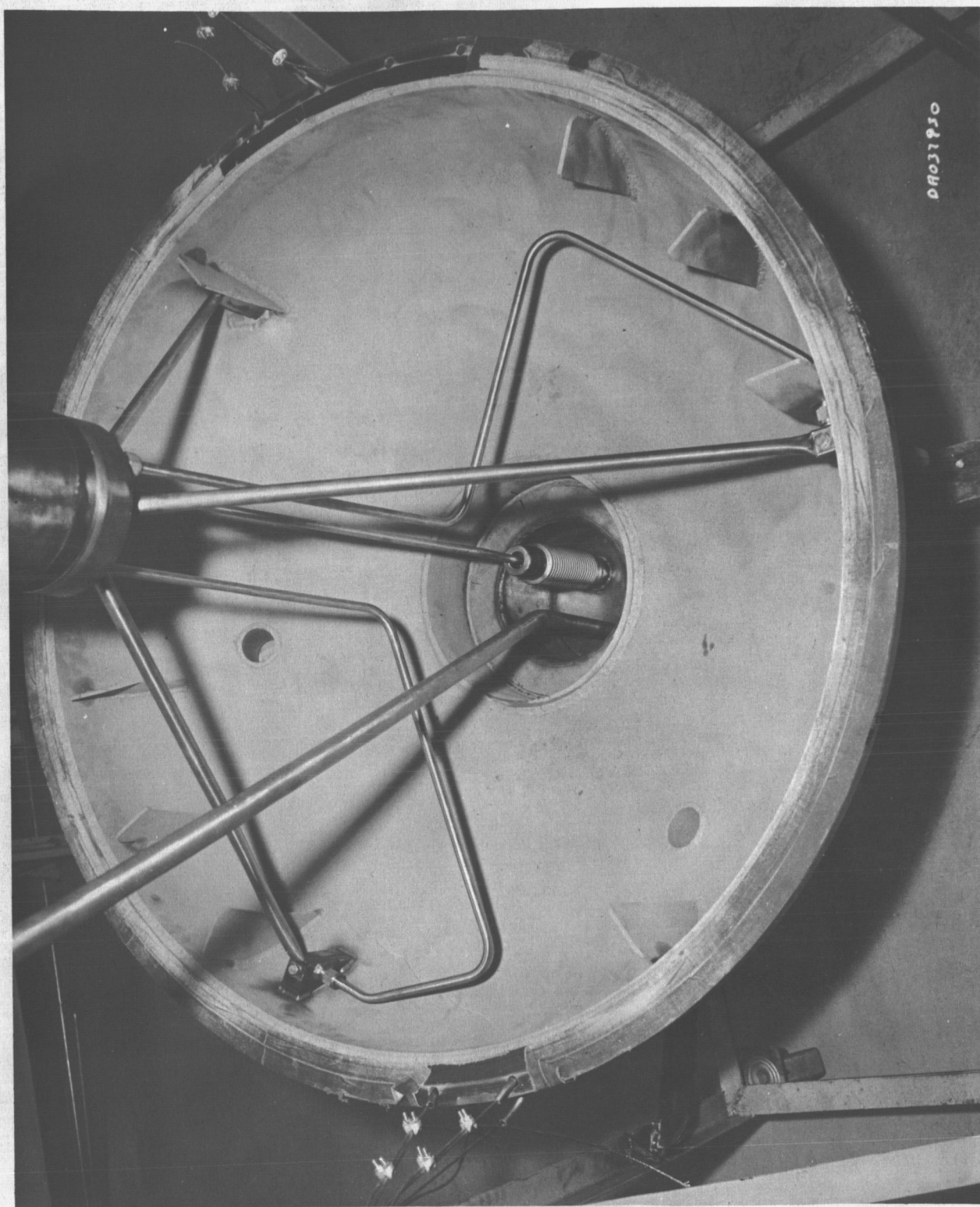


FIGURE 95 SUPPORT STRUCTURE ANCHOR POINTS

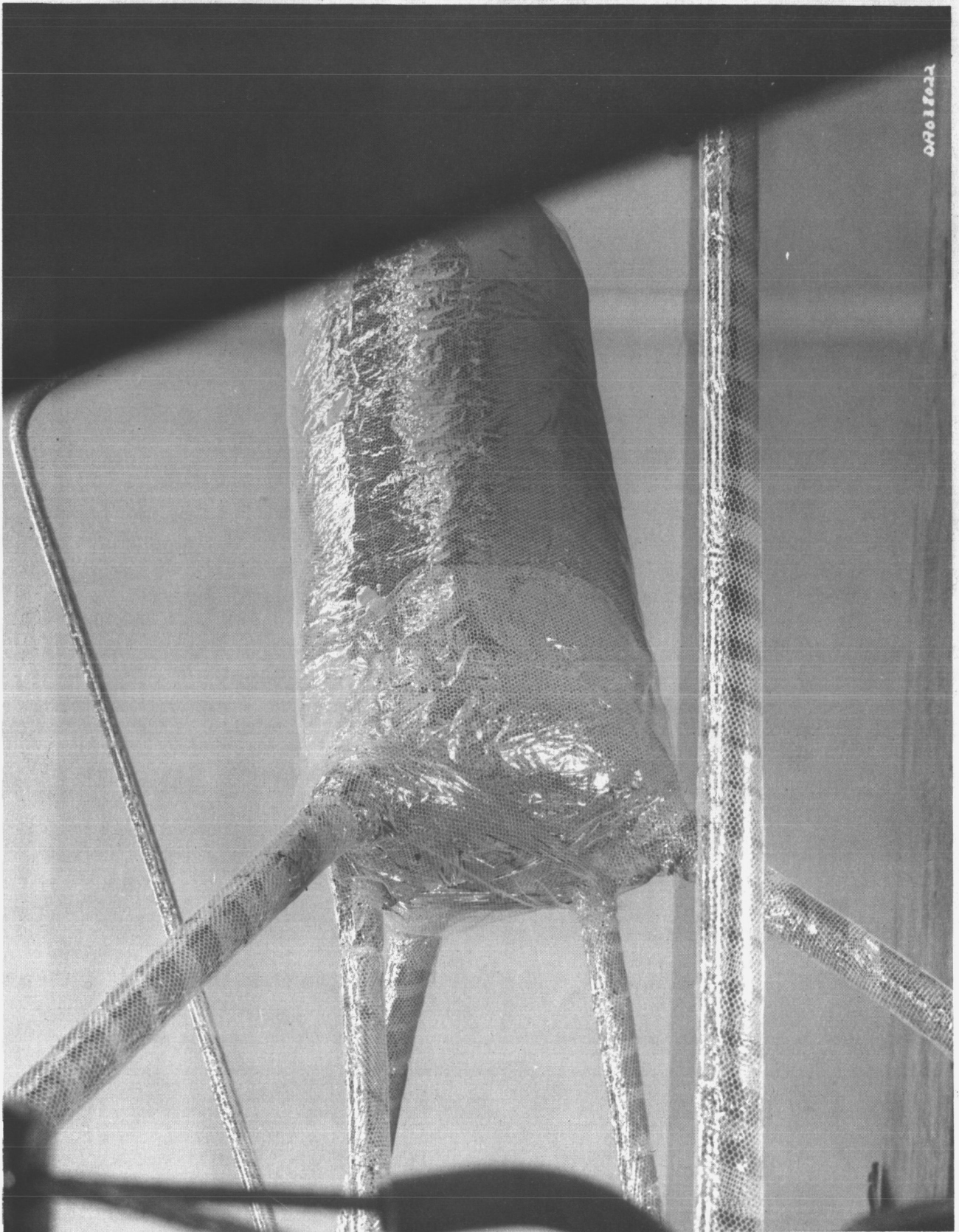


FIGURE 96 SUPPORT STRUCTURE INSULATION

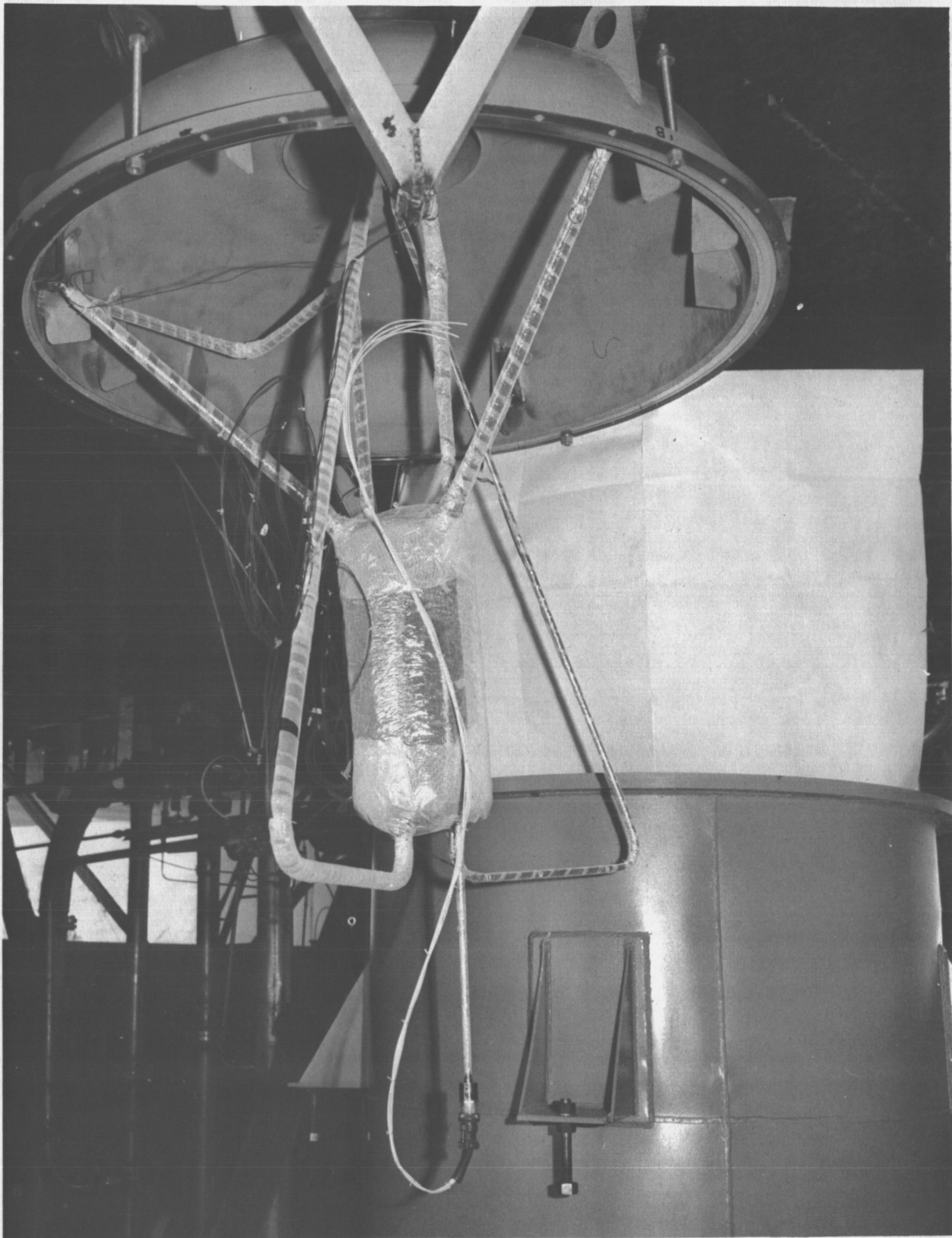


FIGURE 97 SUPPORT STRUCTURE MODEL READY FOR INSTALLATION

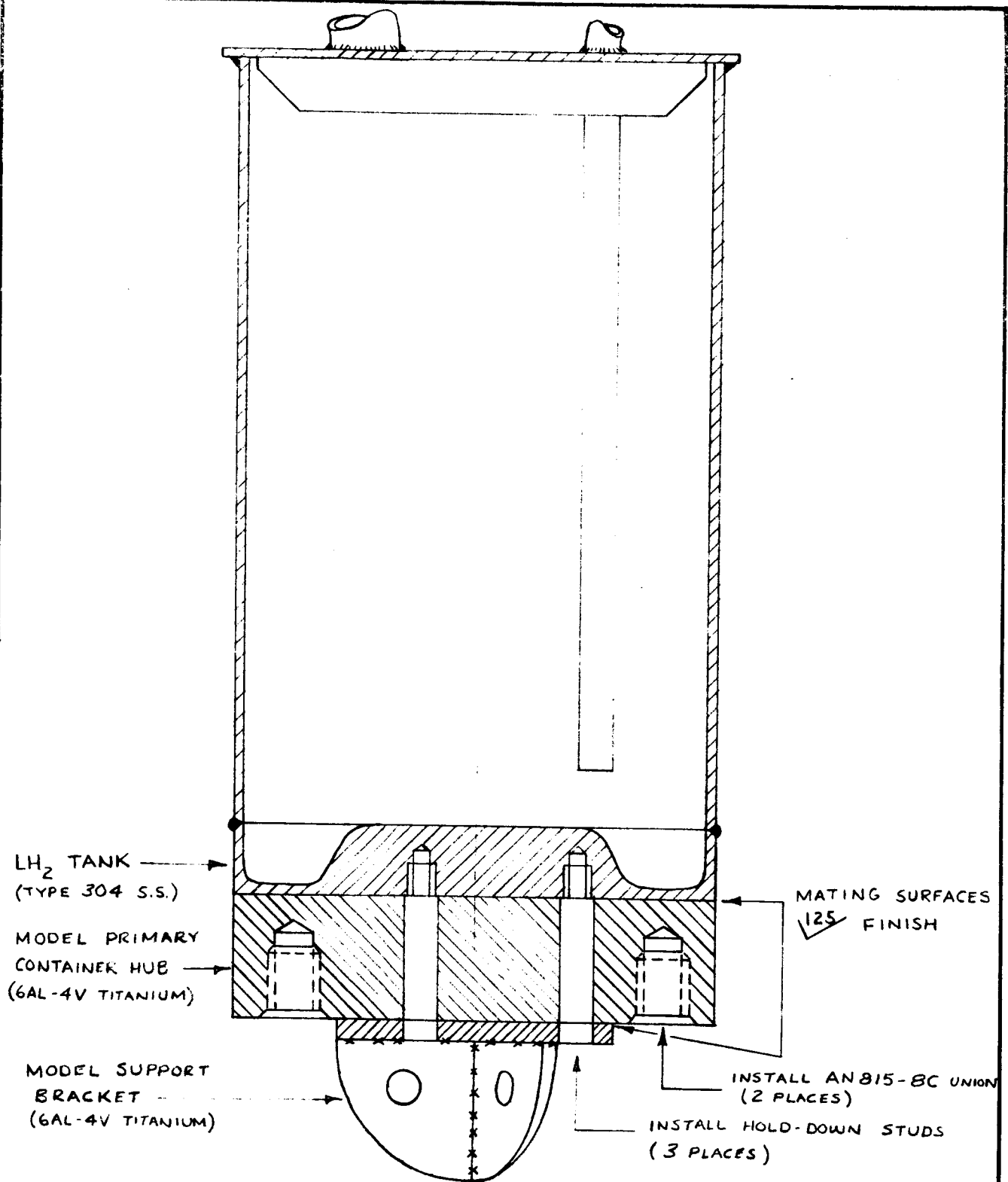
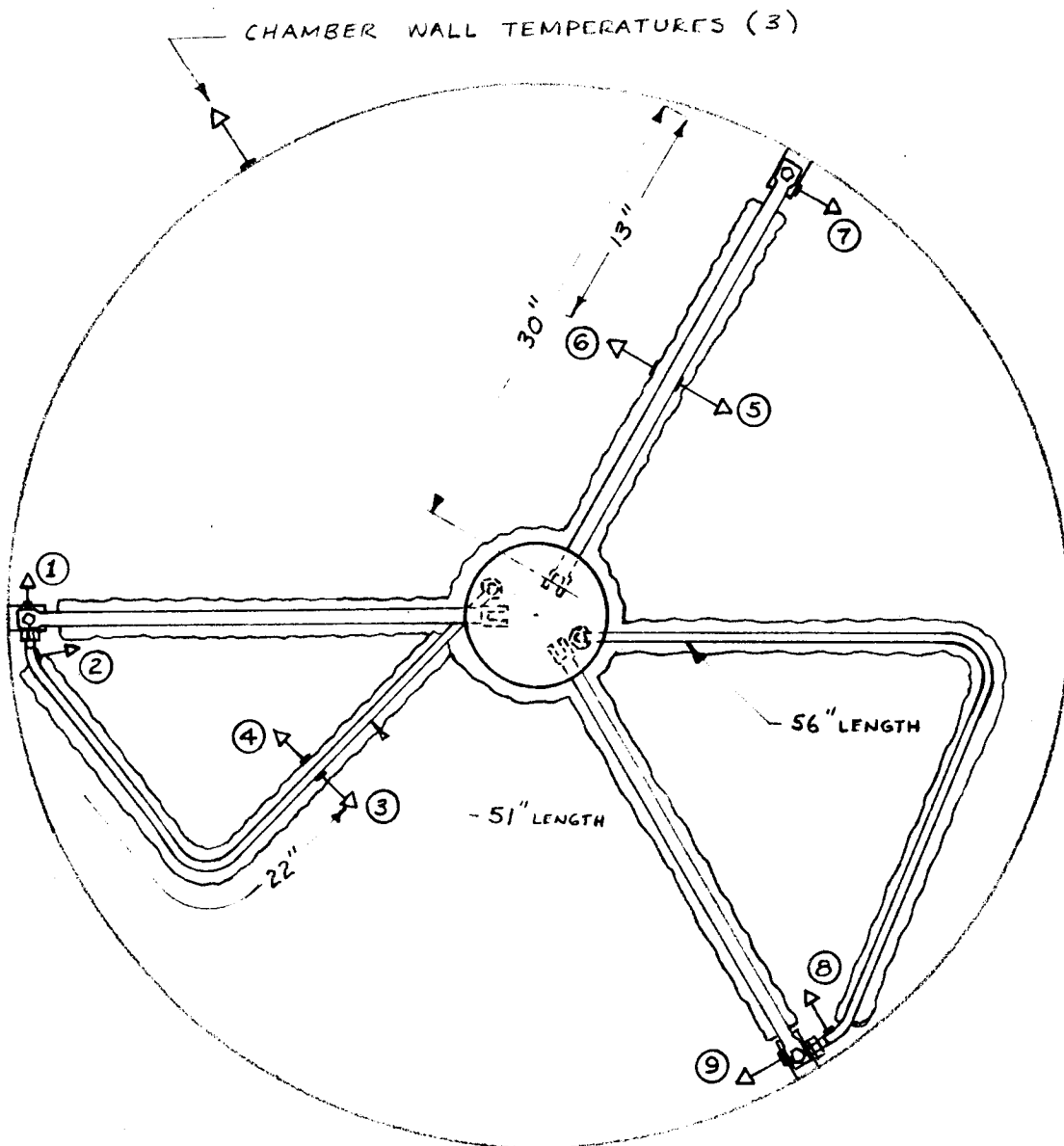


FIGURE 98

TITLE: PRIMARY TANK SUPPORT STRUCTURE ~ ASSEMBLY DETAILS		NUMBER SCALE: $\frac{1}{2}" = 1"$	
MODEL:	THE MARTIN COMPANY DENVER	PAGE	CHG.

# PRIMARY SUPPORT MODEL HEAT LEAK RATE INVESTIGATION

## THERMOCOUPLE LOCATIONS FIGURE 99



### LEGEND:

- ①, ⑦, ⑨ SUPPORT (ANCHOR) TEMPERATURES
- ②, ⑧ DUMMY TUBE TEMPERATURE ~ ANCHOR END [0/0 STATION]
- ③ DUMMY TUBE TEMPERATURE ~ 22/51 STATION
- ④ INSULATION OUTER SURFACE TEMP. ~ 22/51 STATION
- ⑤ SUPPORT TUBE TEMPERATURE ~ 13/30 STATION
- ⑥ INSULATION OUTER SURFACE TEMP. ~ 13/30 STATION

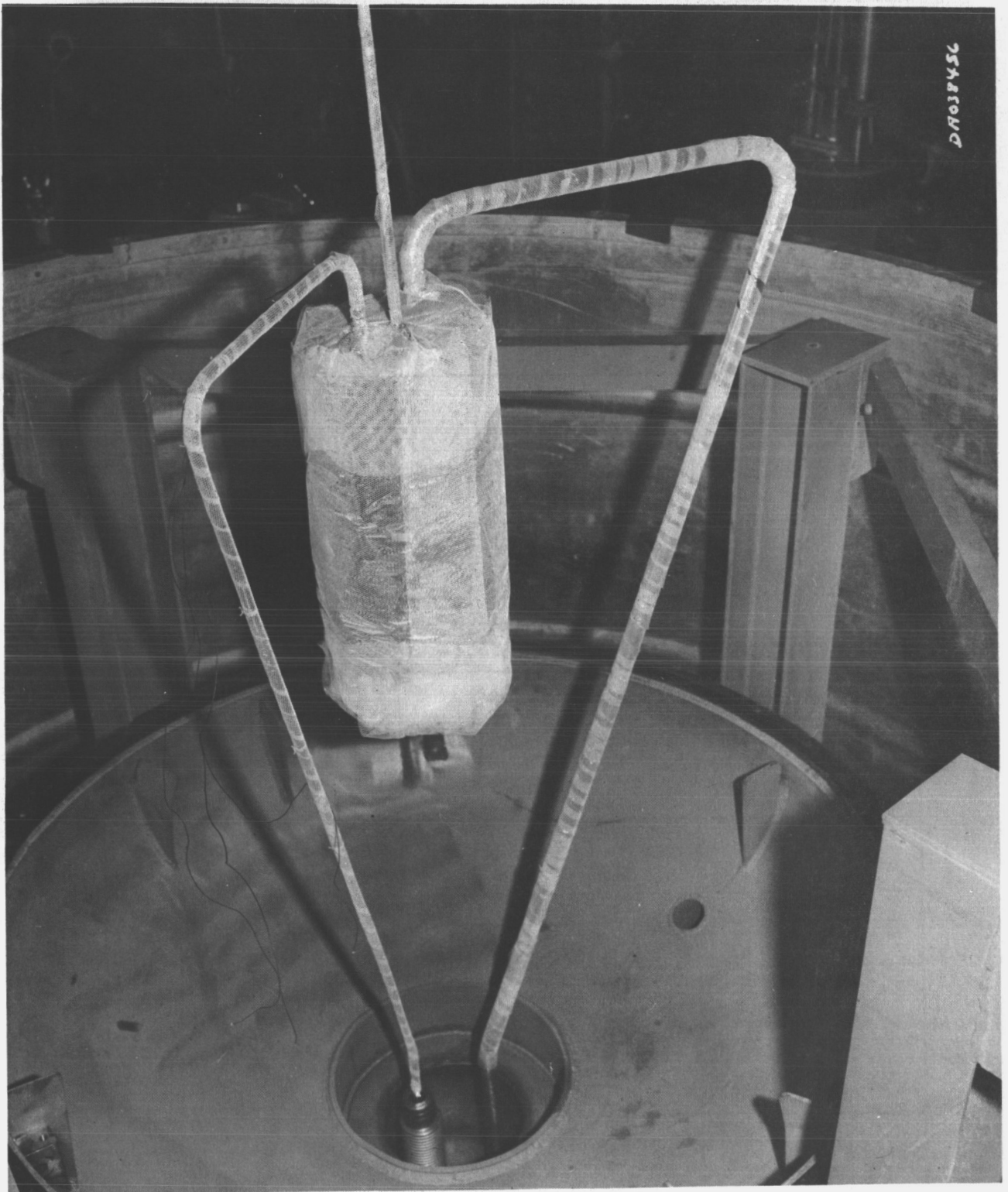
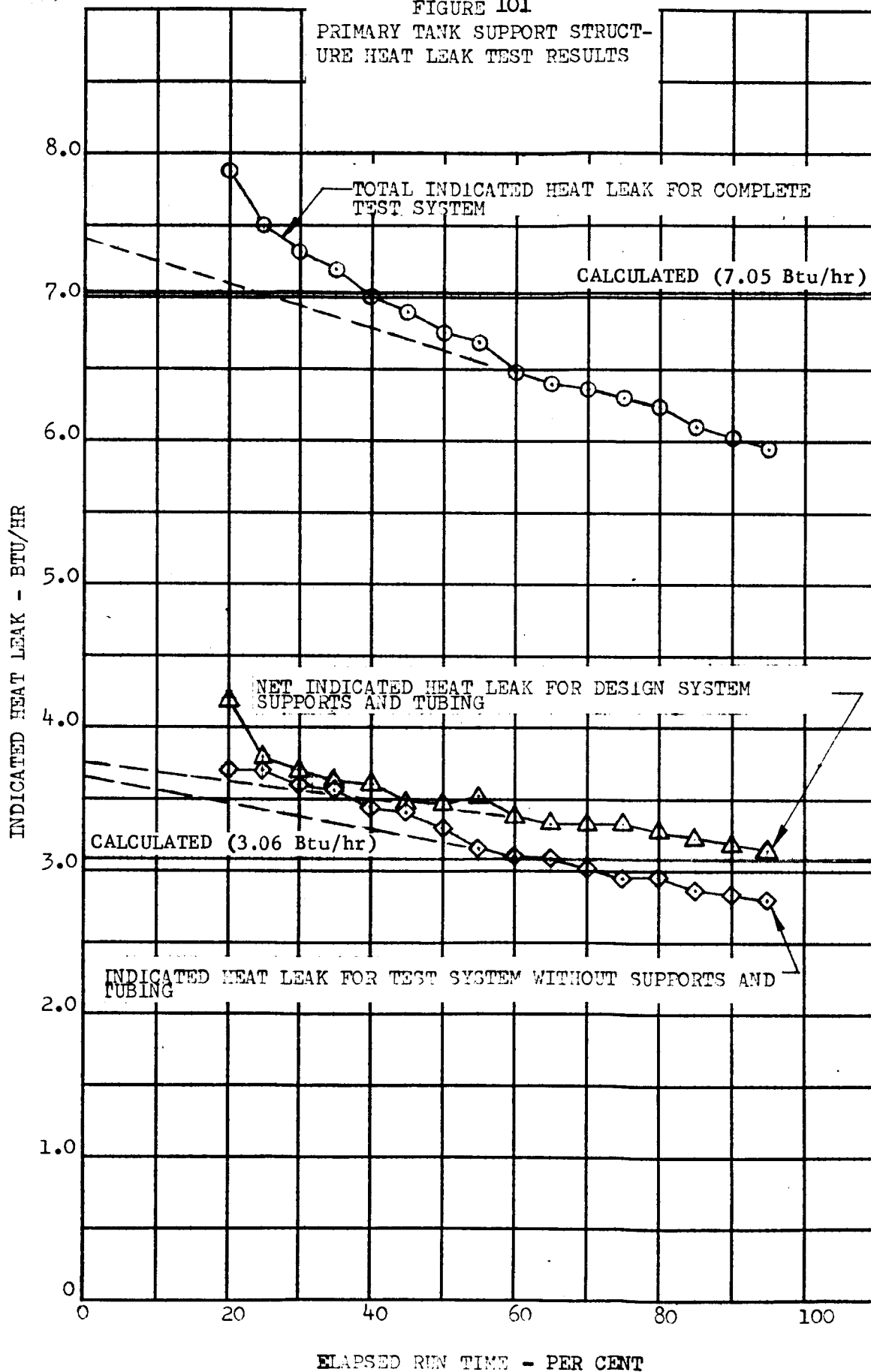
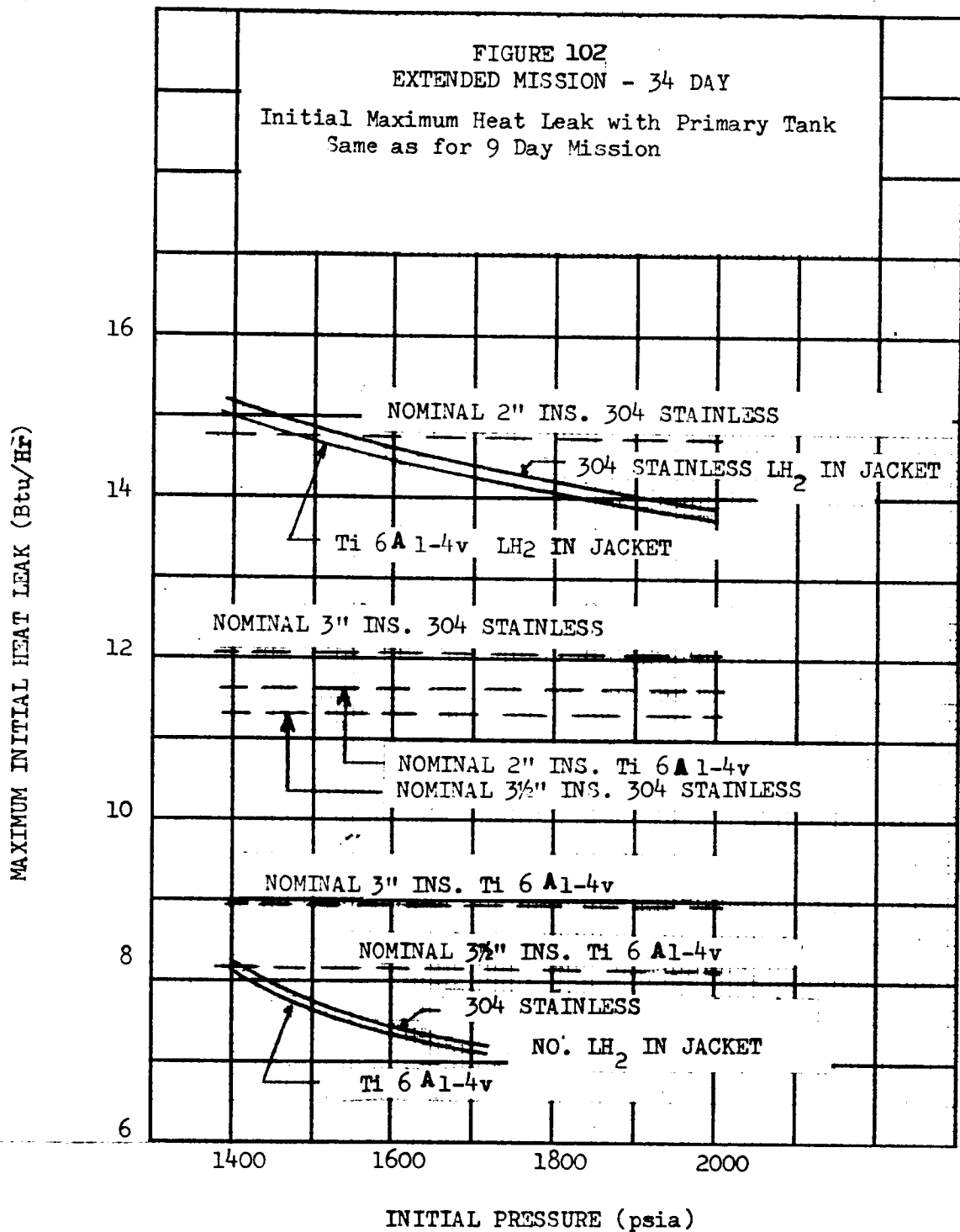
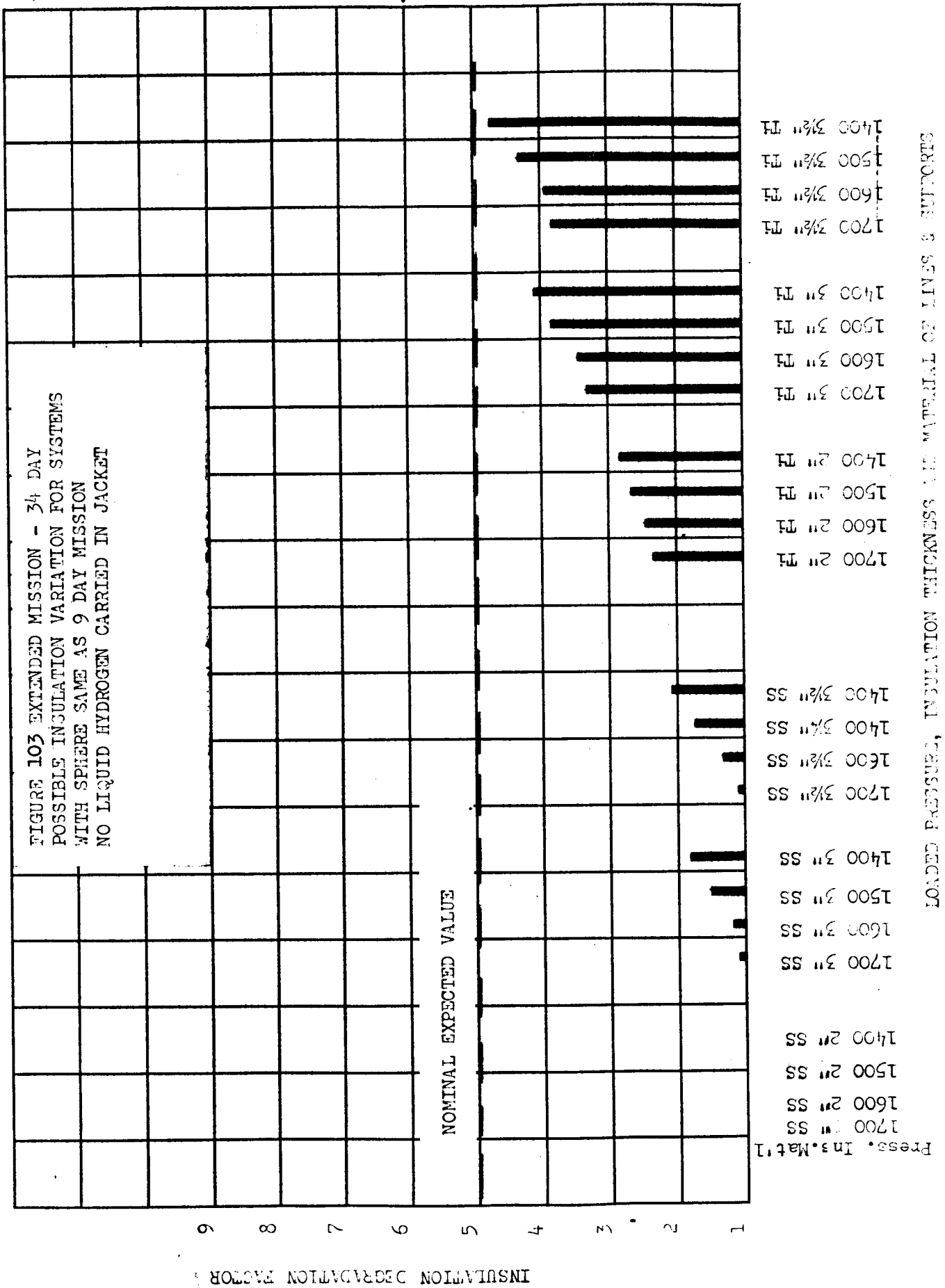


FIGURE 100 SUPPORT HEAT LEAK TEST MODEL AFTER REMOVAL OF SUPPORTS AND DUMMY TUBES

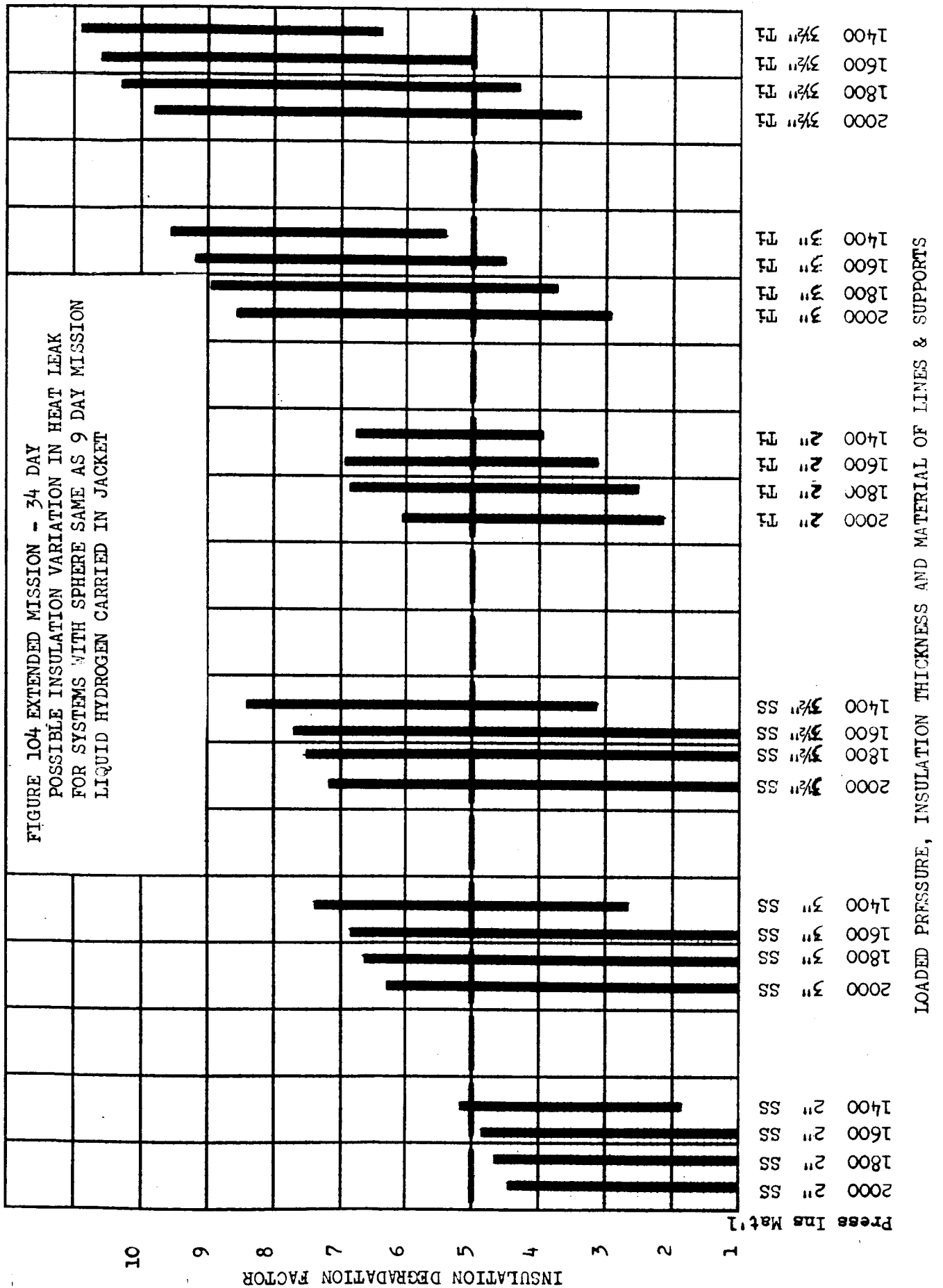
FIGURE 101  
PRIMARY TANK SUPPORT STRUCTURE  
HEAT LEAK TEST RESULTS

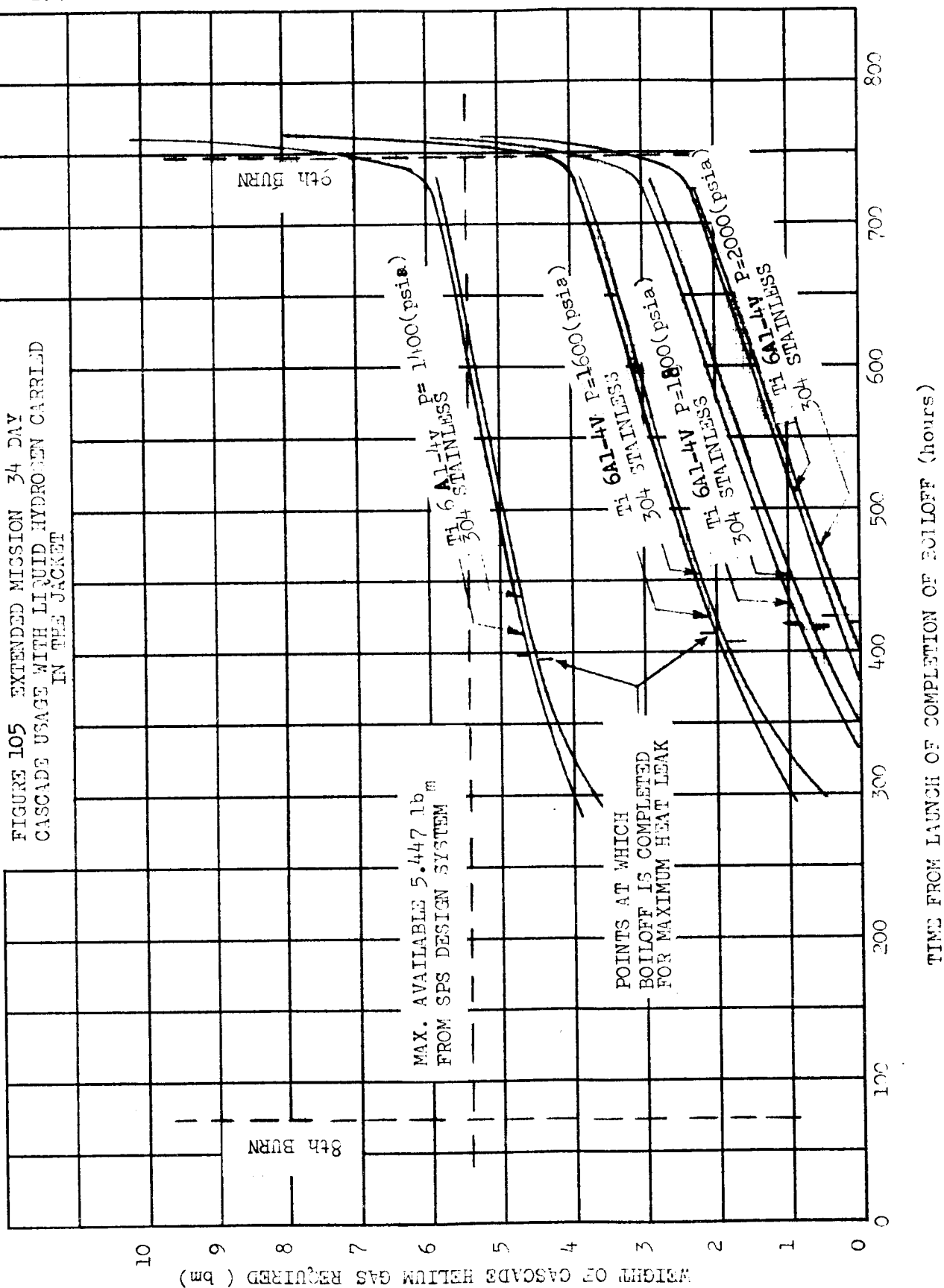


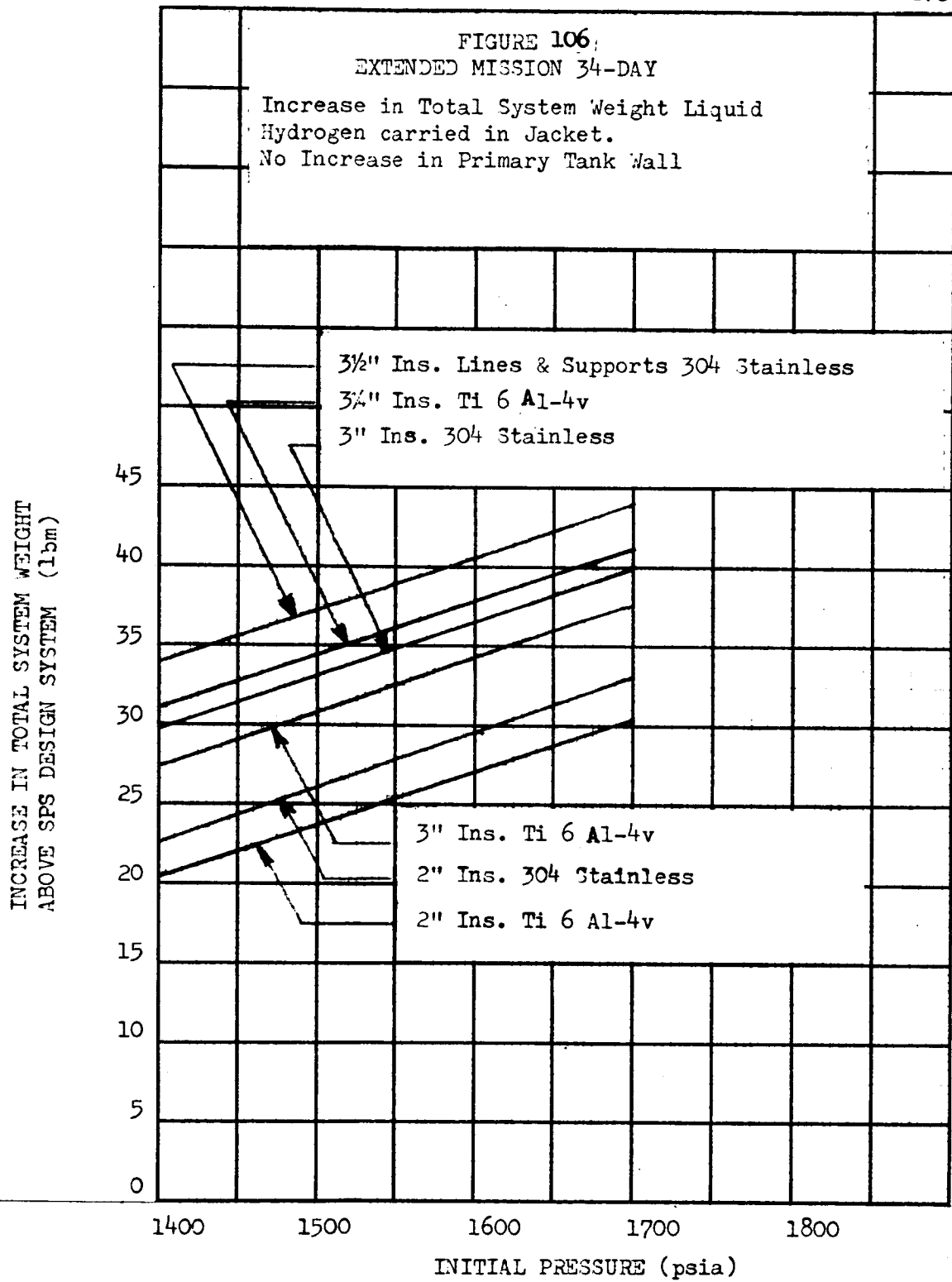


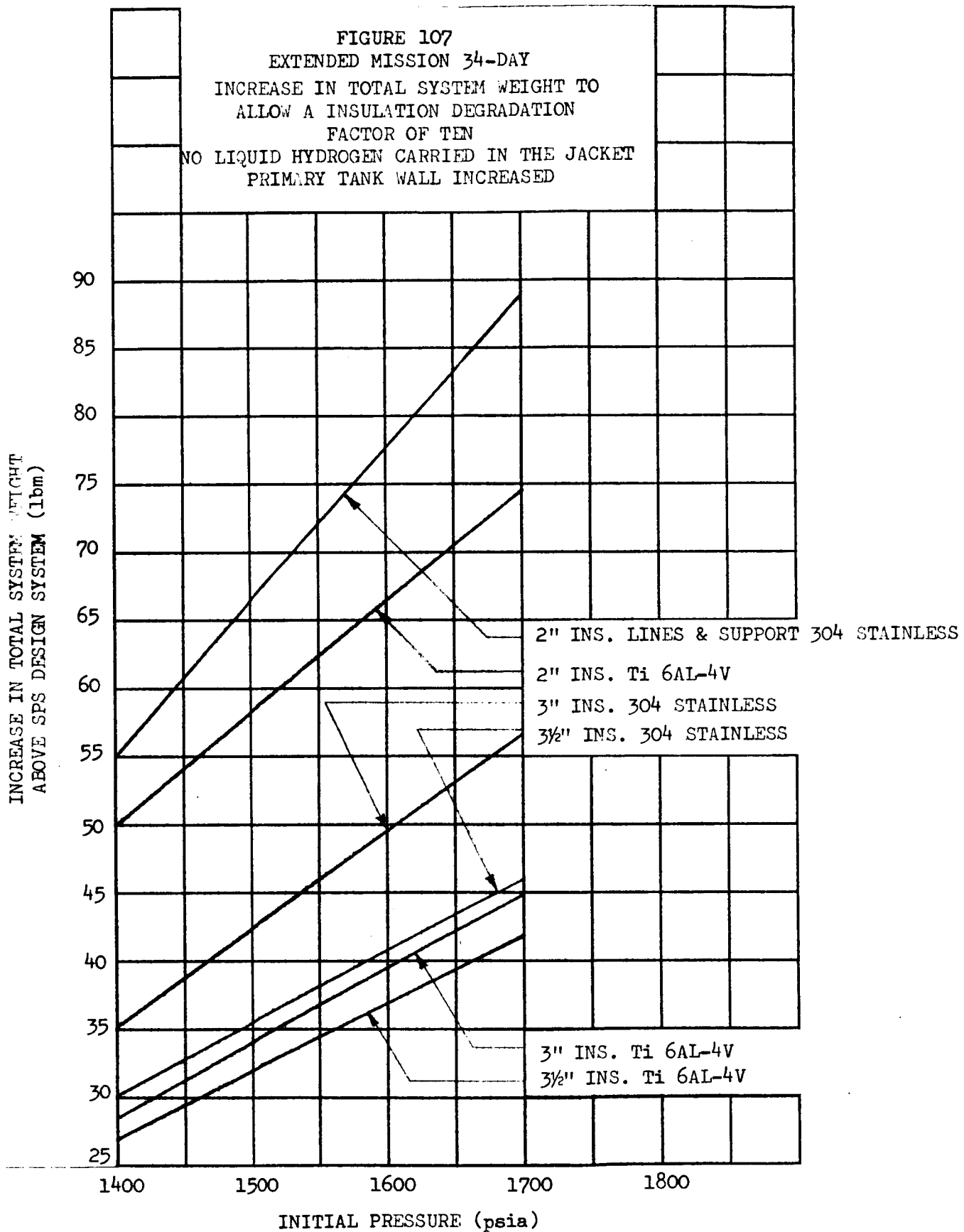


Martin-CR-66-44









Martin-CR-66-44

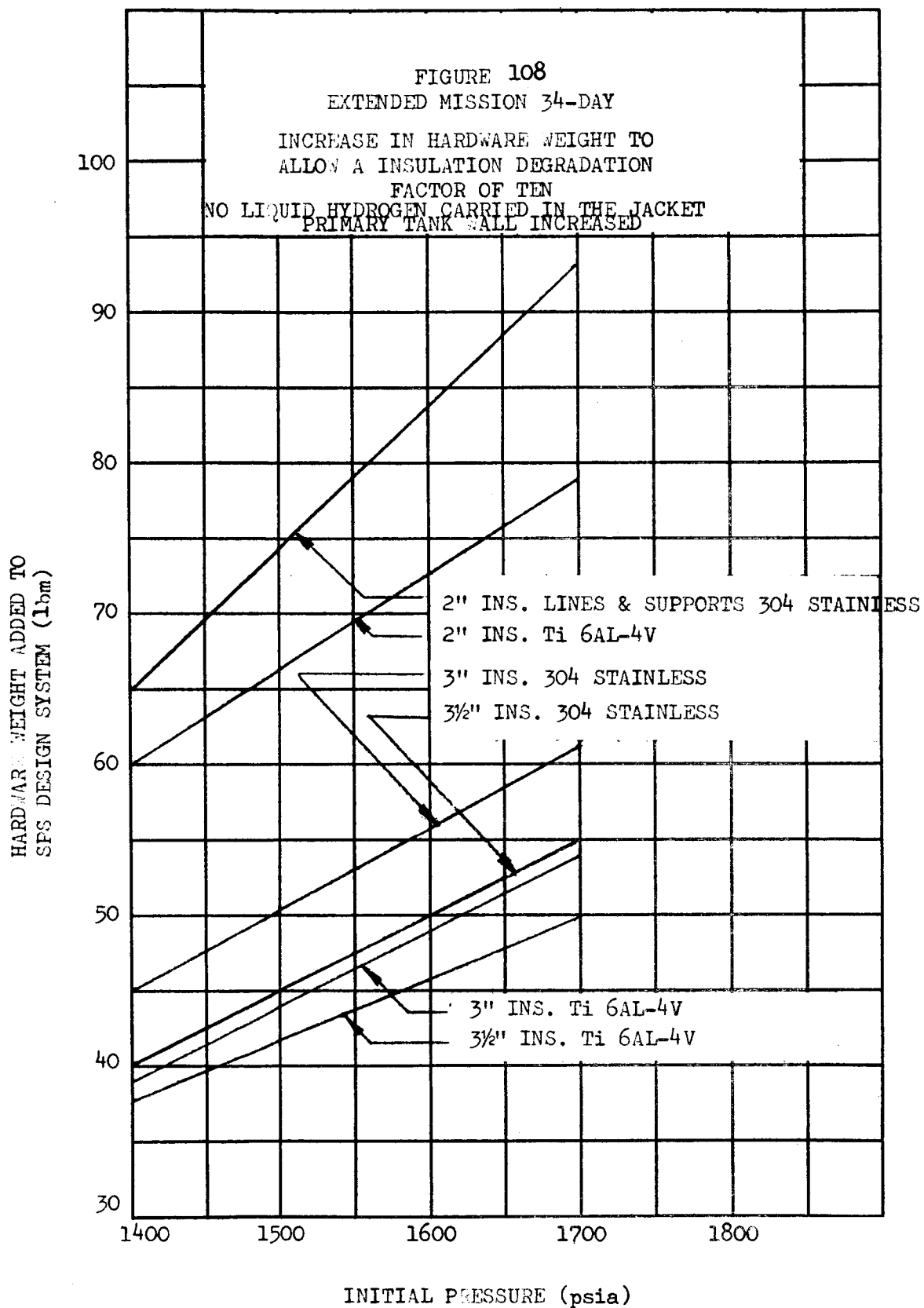
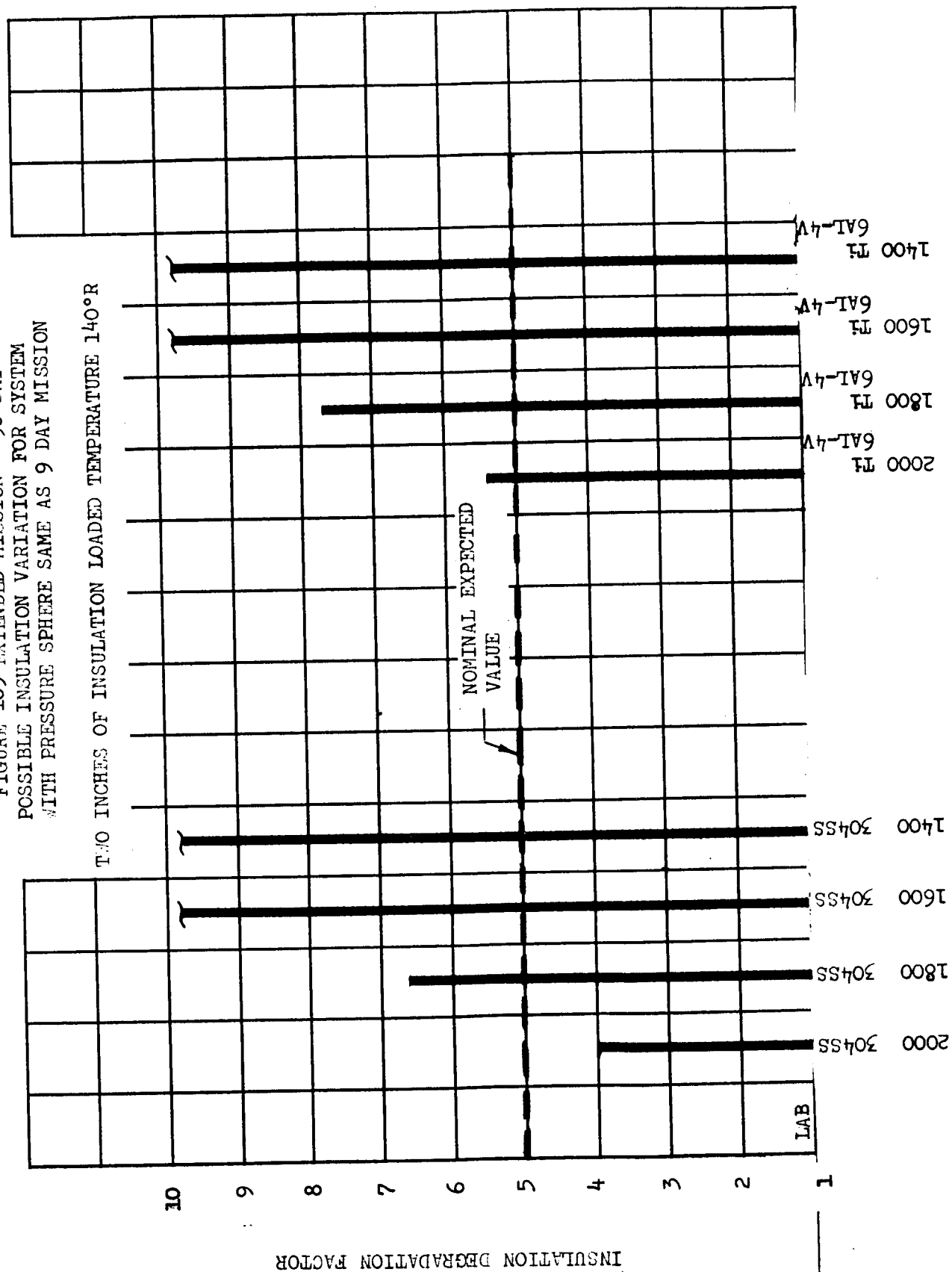


FIGURE 109 EXTENDED MISSION - 90 DAY  
POSSIBLE INSULATION VARIATION FOR SYSTEM  
WITH PRESSURE SPHERE SAME AS 9 DAY MISSION



LOADED PRESSURE & MATERIAL FOR LINES & SUPPORTS

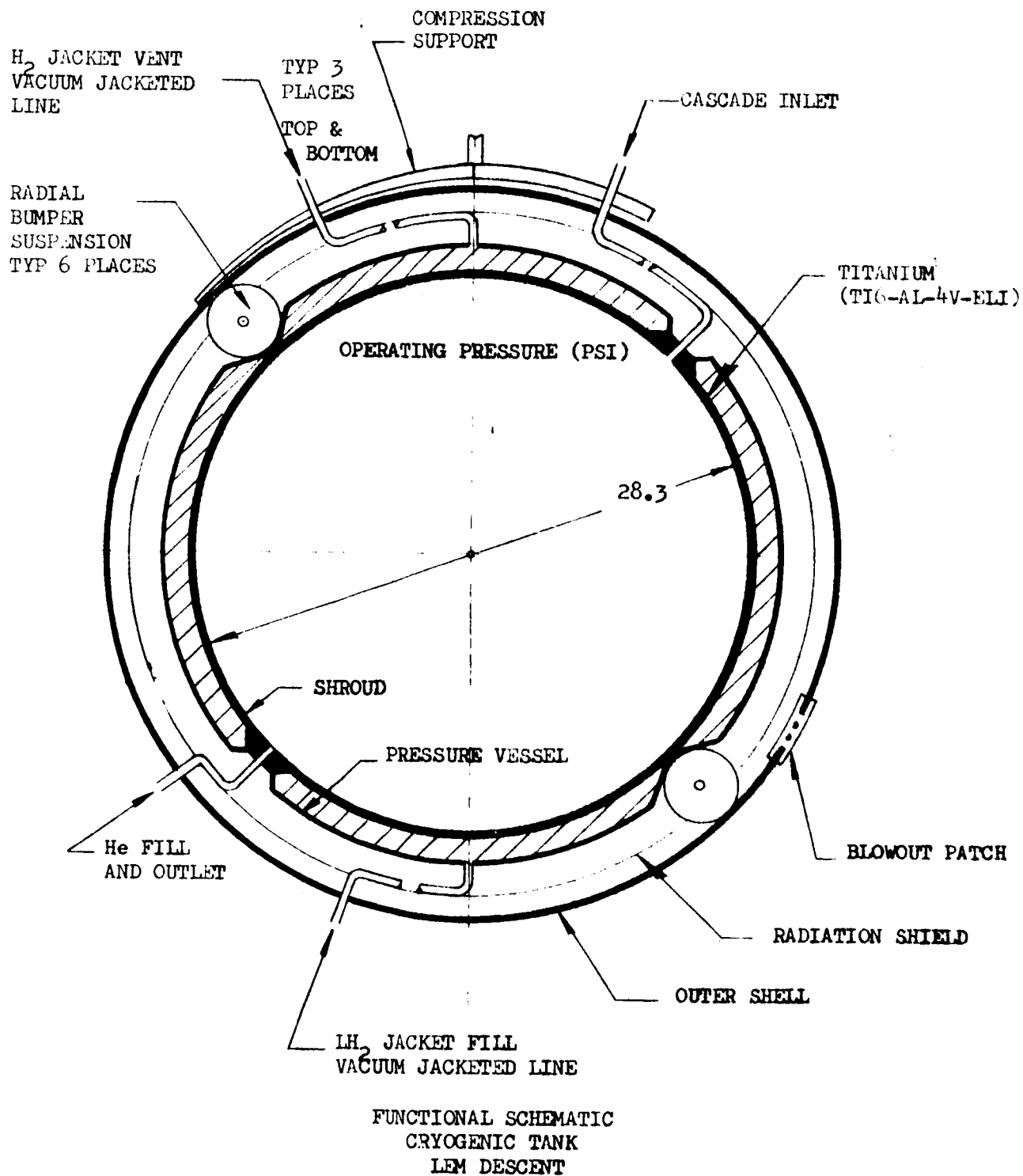


FIGURE 110  
PRIMARY HELIUM TANK DESIGN

Tubing Passes  
Through Radial  
Bumpers